Analysis of Transient
Seepage Through Levees

Matthew David Sleep

Dissertation submitted to the faculty of the Virginia Polytechnic Institute and State University in partial fulfillment of the requirements for the degree of

Doctor of Philosophy
In
Civil and Environmental Engineering

<u>Committee</u>
J. Michael Duncan, Chairman
Thomas L. Brandon, Co-Chair
Matthew Mauldon
George M. Filz
M.P. Singh

October 25, 2011
Blacksburg, VA

Keywords: levee, transient, seepage, stability, dam, unsaturated, soil-water

Analysis of Transient
Seepage Through Levees

by Matthew David Sleep

Dr. J. Michael Duncan, Chairman
Charles E. Via, Jr. Department of Civil and Environmental Engineering

ABSTRACT

Levees are a significant part of the United States flood protection infrastructure. It is estimated that over 100,000 miles of levees exist in the United States. Most of these levees were designed many years ago to protect farmland and rural areas. As growth continues in the United States, many of these levees are now protecting homes and other important structures. The American Society of Civil Engineers gave the levees in the United States a grade of D- in 2009. To bring flood protection up to modern standards there requires adequate methods of evaluating levees with respect to seepage, erosion, piping and slope instability. Transient seepage analyses provide an effective method of evaluating seepage through levees and its potentially destabilizing effects.

Floods against levees usually last for days or weeks. In response to a flood, pore pressures within the levee will change from negative (suction) to positive as the phreatic surface progresses through the levee. These changes can be calculated by finite element transient seepage analyses. In order for the transient seepage analysis to be valid, appropriate soil properties and initial conditions must be used. The research investigation described here provides simple and practical methods for estimating the initial conditions and soil properties required for transient seepage analyses, and illustrates their use through a number of examples.

DEDICATION

This work is dedicated to my mother and father. No matter where life takes me, I will always be able to find my way home.

ACKNOWLEDGEMENTS

Dr. J. Michael Duncan has taught me many things while I have been a student at Virginia Tech. Most importantly Professor Duncan has taught me the meaning of integrity and responsibility. None of this would have been possible without his unwavering support through the entirety of my dissertation research. He is a man rich with awards for his amazing work in geotechnical engineering and they are all well deserved. Few have had the opportunity to work as closely with Professor Duncan as I have and for that I feel truly blessed. Apart from my dissertation, I am a much better person for being able to work with such a magnificent man.

I also wish to acknowledge my committee members, Dr. Thomas L. Brandon, Dr. Matthew Mauldon, Dr. George M. Filz and Dr. M.P. Singh for all of their valuable support and suggestions. A special thanks to Dr. Thomas L. Brandon for all of his valuable insight on levee design and stability. All of your dedication to my education is sincerely appreciated.

The students in the Geotechnical program at Virginia Tech are some of the brightest and genuine people I have ever been able to call my friends. Special thanks go to Todd LaVielle and Manuel Ochoa-LaVergne for their support and friendship. Mike and Tish McGuire have treated me like family and for that I am very grateful. Kate Gunberg has been there for me throughout this long process and has been amazingly supportive.

I also wish to acknowledge my family. As this dissertation has taken some time they have questioned what I am doing, but always have loved and supported me. Thank you.

COPYRIGHT INFORMATION

All tables and figures reprinted with permission of the publishing company or determined fair use.

Table of Contents

List of Figures

List of Tables

Chapter 1
Introduction

The objective of this research is to investigate methods of performing transient analyses of seepage in levees subjected to floods, and to develop practical methods for performing these analyses. The studies included evaluating methods for evaluating the soil properties used in the analysis, the numerical procedures, the initial conditions, and the influence of floods on levee stability and erosion. The methods developed were validated by comparison of computed results with measurements of performance of a half-scale levee experiment performed in Germany.

In many cases steady state seepage analyses have been used to investigate safety against erosion and instability in levees, assuming that the highest water level reached during a flood event persists indefinitely. However, this approach is likely to be excessively conservative when the hydraulic conductivity of the levee soil is low, because steady seepage conditions correspond to high pore pressures within the levee, and relatively low factors of safety against slope instability and internal erosion. Transient seepage analyses provide a more realistic evaluation of conditions. Where Steady state seepage analyses may indicate that a levee is unsafe, Transient seepage analyses may show that the levee would be safe under any foreseeable flood condition.

Transient seepage analyses are becoming more common in practice. With few resources and many miles of levees to maintain, it is important that time, energy and money be focused on the levees that are in most need. Transient seepage analyses provide a more realistic means of assessing seepage within levees that can improve engineering evaluations and avoid unnecessary expense.

Research Studies
The goal of this research is to provide guidance for engineers performing transient seepage analyses. To provide guidance the following studies were undertaken:

1. Investigate transient seepage phenomena and practical methods of analysis.

1

2. Verify the most promising methods of analysis through comparison with results from an instrumented levee test.

3. Provide guidance on the practical methods of estimating soil properties for transient seepage analyses, and develop a new set of charts for this purpose.

4. Review published measurements of initial conditions in riverbanks and slopes, and use these to develop guidance for estimating initial conditions for transient seepage analyses. Show how initial conditions affect the results of transient seepage analyses

5. Provide examples showing how transient seepage can affect the stability of a levee, and the possibility of seepage and piping within levees and levee foundations.

Chapter 2
Transient Seepage Phenomena

Introduction

As water flows into or out of unsaturated soil, the flow conditions and the properties of the soil change with time. Because the flow conditions change with time, the flow is called "transient." This time-dependant flow is governed by the constitutive relationship shown in Eq. 2-1, which was derived by Fredlund and Rahardjo 1993.

$$q = -k_w(u_a - u_w)\left(\frac{\partial h}{\partial y}\right)$$
Eq. 2 - 1

Where: q = water flow rate (cm/sec)

$-k_w(u_a - u_w)$ = conductivity as a function of matric suction (cm/sec)

$\left(\frac{\partial h}{\partial y}\right)$ = gradient (dimensionless)

As unsaturated soils become wetter due to inflow, the amount of water in the voids increases, the amount of air in the voids decreases, and the degree of saturation increases. As unsaturated soils dry, water flows out of the void spaces, replaced by air, and the degree of saturation decreases.

Properties of Unsaturated Soils

Unsaturated soil is three-phase material composed of soil grains, water and air, as shown in Figure 2-1. The degree of saturation (S) is defined as:

Eq. 2 - 2

$$S = \frac{V_w}{V_v} \bullet 100\%$$

Where V_w is the volume of water and V_v is the volume of voids. The degree of saturation defines the percentage of a soil that is filled with water. Unsaturated soils

can also be described by the volumetric moisture content, defined as the volume of water (V_w) divided by the total volume of the soil (V_T)
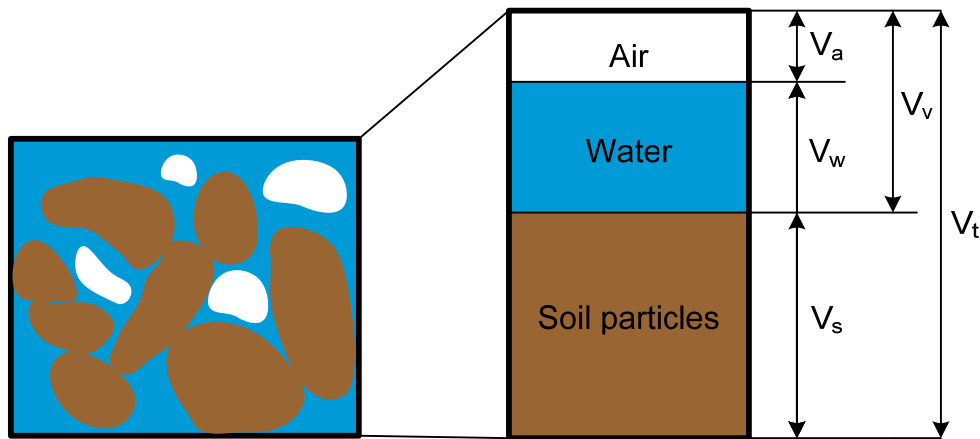
Figure 2-1 – Three phases of an unsaturated soil

Soil Suction

The water in unsaturated soil is under tension, or suction, as a result of the surface tension that exists in the water at the interfaces between air and water. Soil suction is the negative pore water pressure that is present in soil when the degree of saturation is less than 100%. As the amount of air in the soil changes, the soil suction changes, and the properties of the soil that depend on soil suction also change.

Total suction:

Total soil suction has two components, osmotic suction and matric suction.

$$\Psi = (u_a - u_w) + \pi \qquad \text{**Eq. 2 - 3**}$$

Where: Ψ = total suction (kPa)

u_a = air pressure (kPa)

u_w = water pressure (kPa)

π = osmotic suction (kPa)

Osmotic soil suction is controlled by changes in ionic concentrations within the pore water of a soil. The concept of osmotic suction is illustrated in Figure 2-2.
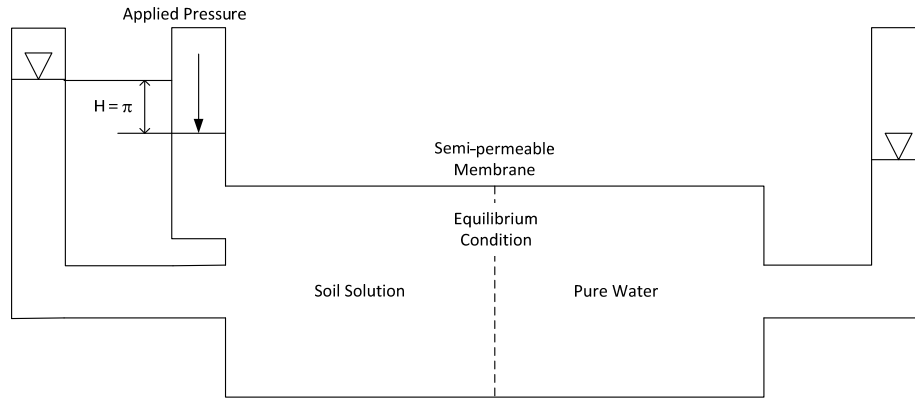
Figure 2-2 – Illustration of how osmotic suction develops in soils due to the presence of dissolved ions

Pure water flows into the soil solution due to the presence of dissolved ions. However when sufficient pressure is applied on the soil solution the flow of pure water into the soil solution is stopped. The applied pressure for the equilibrium condition is equal to the osmotic pressure.

Osmotic pressure can be important in certain geotechnical applications where there is a difference in ionic concentrations within a soil mass. Malusis et al. (2003) found this to be true in many clay and shale liners for waste impoundment. Graham et al. (1992) found that high osmotic suction in clays with low porosities and high ionic exchange capacity can contribute significantly to strength. High osmotic suction can also influence the shrink/swell capacities of some clays (Rao and Shivananda 2002). Outside of these cases, osmotic suction has negligible contribution to flow unless there is a significant change in ionic concentration within the soil mass. In levees and dams this is unlikely to occur, and osmotic suction is not taken into account when solving transient flow problems.

Matric suction:

Matric suction is defined as the difference between the air and water pressure within a soil matrix.

$$\Psi_m = u_a - u_w \qquad\qquad\qquad\qquad \textbf{Eq. 2 - 4}$$

Where: Ψ_m = matric suction (kPa)

u_a = air pressure (kPa)

u_w = water pressure (kPa)

When the soil is partly saturated, the air pressure is usually zero and the matric suction is equal to the negative water pressure in the soil mass. Partly saturated soils can support negative soil pressures from matric suction due to the surface tension properties of water. In partly saturated soils the water forms menisci between soil grains as shown in Figure 2-3a. The menisci form as a result of the tendency of the water to wet the surfaces of the soil grains. The space between two soil grains in a partly saturated soil can be illustrated with a capillary tube model. In an equilibrium condition, the forces can be resolved for the matric suction where:

$$h = \frac{2T_s}{\rho_w g R} = \frac{T_s}{\rho_w g r} \qquad \text{For } \beta =$$

Eq. 2 - 5

0

A.

B. $2\pi r T_s \cos \beta = \pi r^2 h \rho_w g$
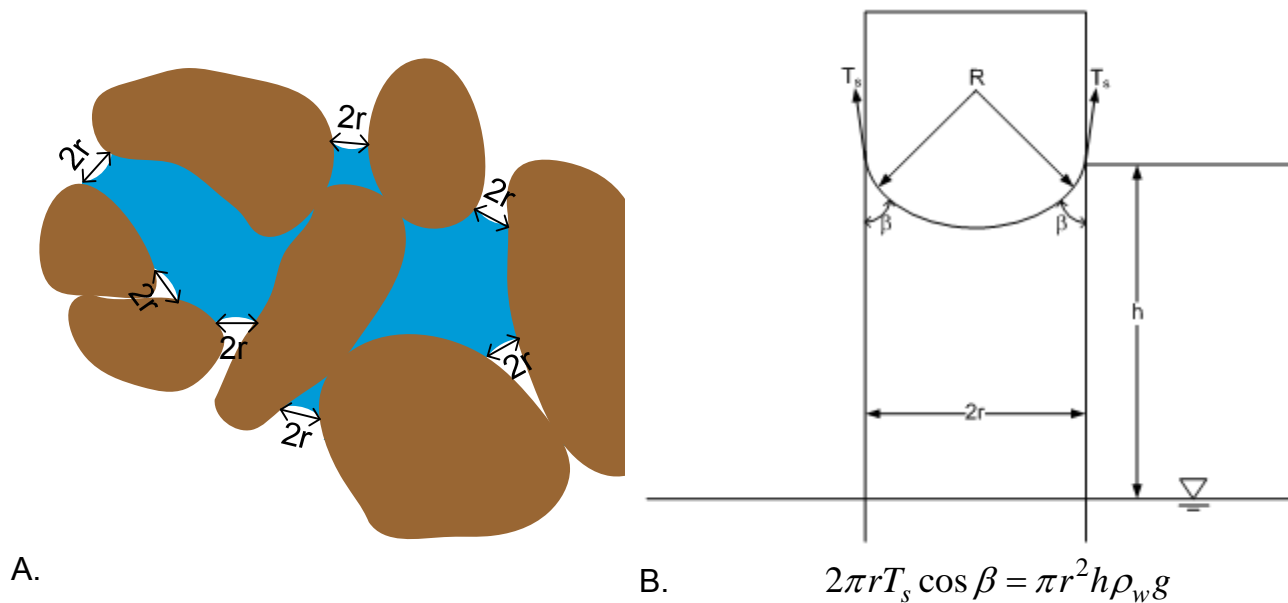
Figure 2-3 – Matric suction in soil and the capillary model

Where T_s is the surface tension between the tube wall and water (F/L), ρ_w is the density of water (m/V), *g* is the (m²/sec), and R is the radius of the tube (L). The strength of the tendency to wet the surface of the soil grains determines the magnitude of the angle β. If the tendency for wetting is very strong, as it is for common soil minerals such as quartz and feldspar, β is equal to zero, and the height of capillary rise can be expressed as:

$$h = \frac{T_s}{\rho g r}$$

Eq. 2 - 6

It can be noted that as the radius of the capillary tube decreases, the matric suction increases. Thus matric suction is larger (more negative) for soils with small particles and small voids. Likewise if the matric suction increases (becomes more negative) the water within the soil matrix will retreat into smaller pore spaces that have smaller radii.

Soil Column

Because during transient seepage the soil can be wetting or drying, the soil suction, water content, degree of saturation and hydraulic conductivity will change as the soil becomes more or less saturated. A simple finite element model that was analyzed using the computer program SEEP/W illustrates how these properties change with time as water flows into a soil column.

The soil column analyzed was 3 feet high and 1 foot across. At the start of the analysis, the water level was raised to 3 feet, the top of the column. Because the sides of the column were modeled as no flow boundaries, water infiltrated the column from the bottom to the top.

Figure 2-4 shows the results of this analysis for two different soils. The soil on the left is silty sand with a saturated hydraulic conductivity of 1×10^{-4} cm/sec and the soil on the right is a clay soil with a saturated hydraulic conductivity of 1×10^{-7} cm/sec. As shown in

the figure, the line of zero pressure (the water table) rises faster in the the silty sand, as would be expected.
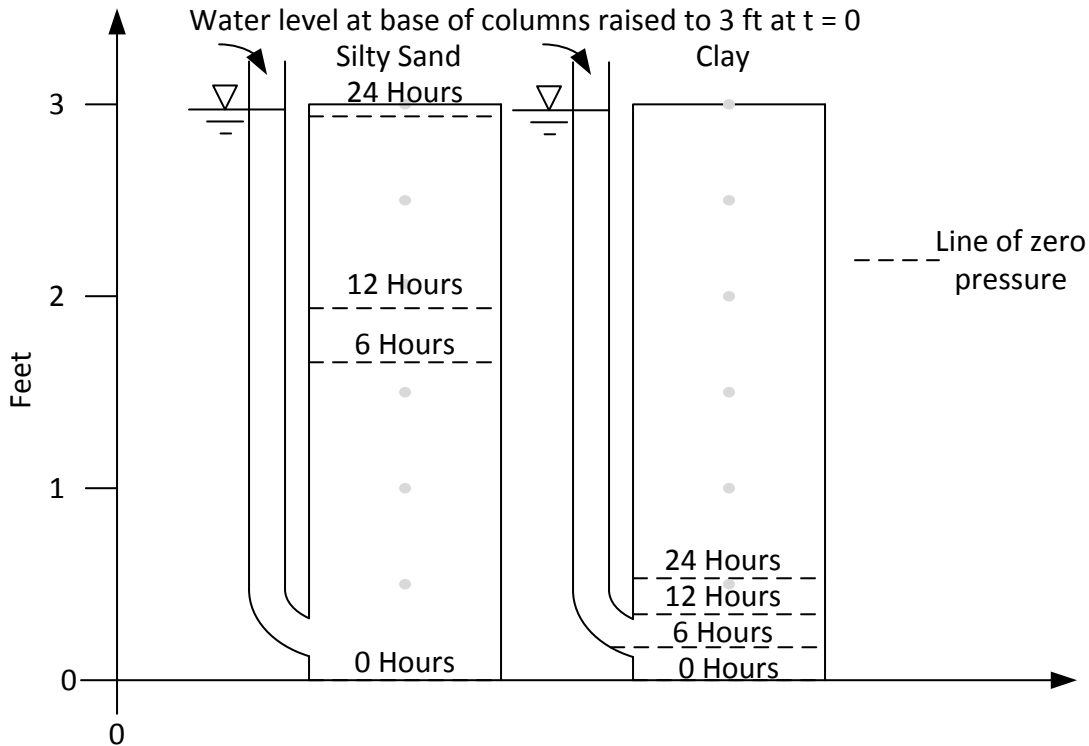
Figure 2-4 – Finite element transient seepage analysis of two soil columns with water infiltrating from bottom of the columns

The soil column comprised of silty sand was studied further. For this soil column, 6 nodes were chosen in the middle of the column at elevations 0.5, 1, 1.5, 2, 2.5, and 3 feet. At each of these nodes, the changes in water content, degree of saturation, hydraulic conductivity, and pore water pressure were plotted with time. These results are shown in Figures 2-5, 2-6, 2-7 and 2-8.
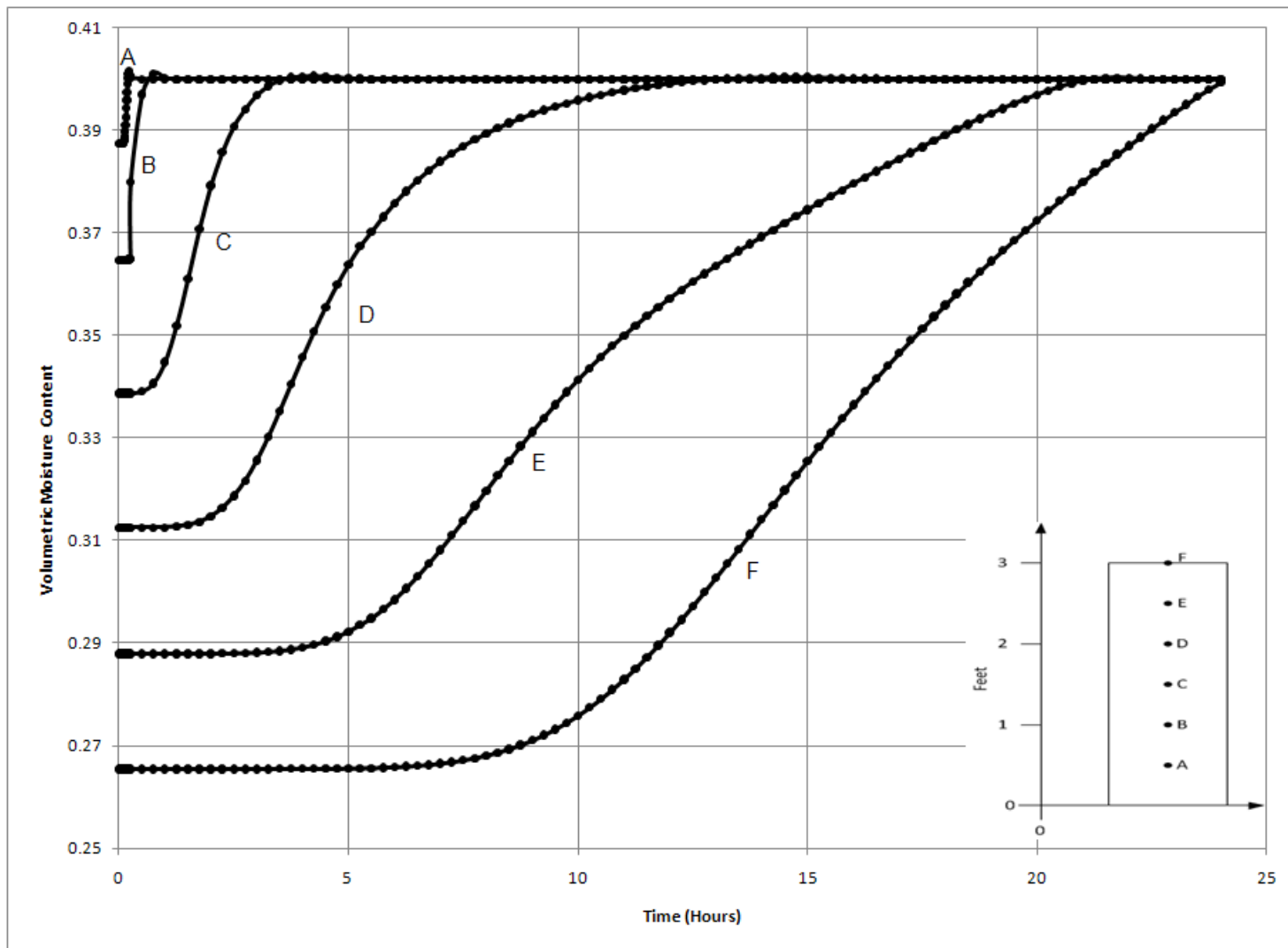
Figure 2-5 – Volumetric moisture content versus time for the finite element analysis of the silty sand column shown in Figure 2-4
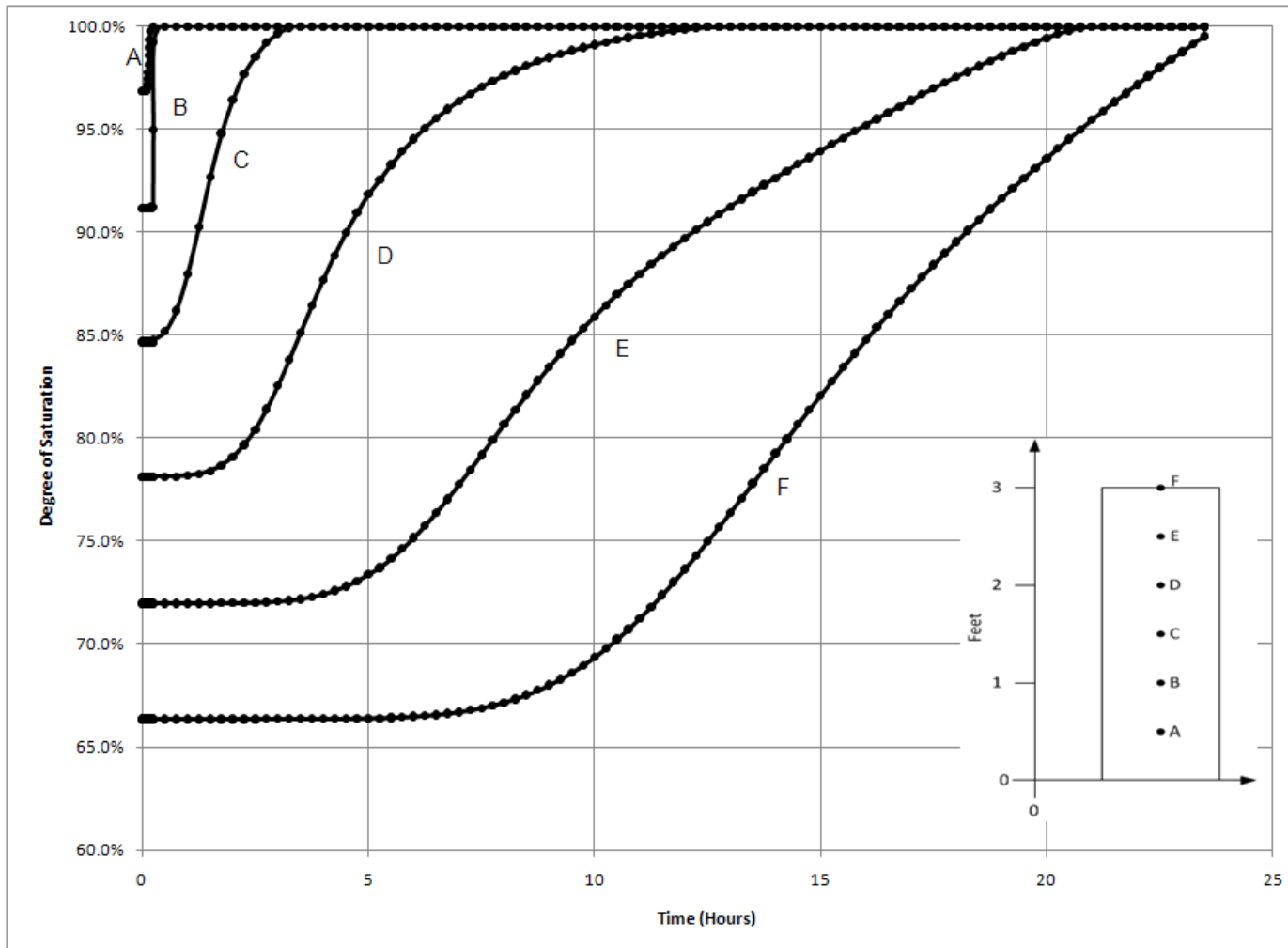
Figure 2-6 – Degree of saturation versus time for the finite element analysis of the silty sand column shown in Figure 2-4
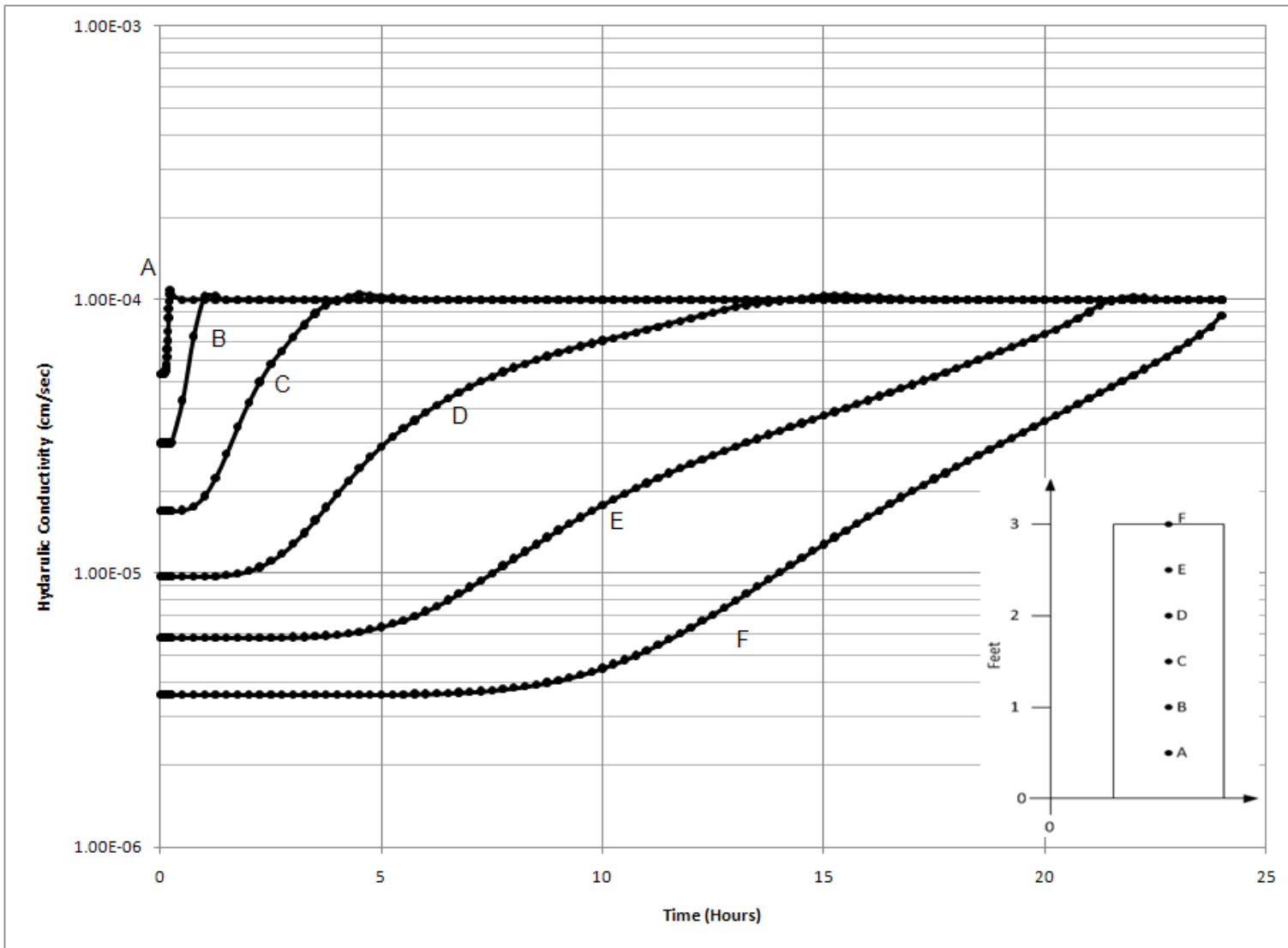
Figure 2-7 – Hydraulic conductivity versus time for the finite element analysis of the silty sand column shown in Figure 2-4
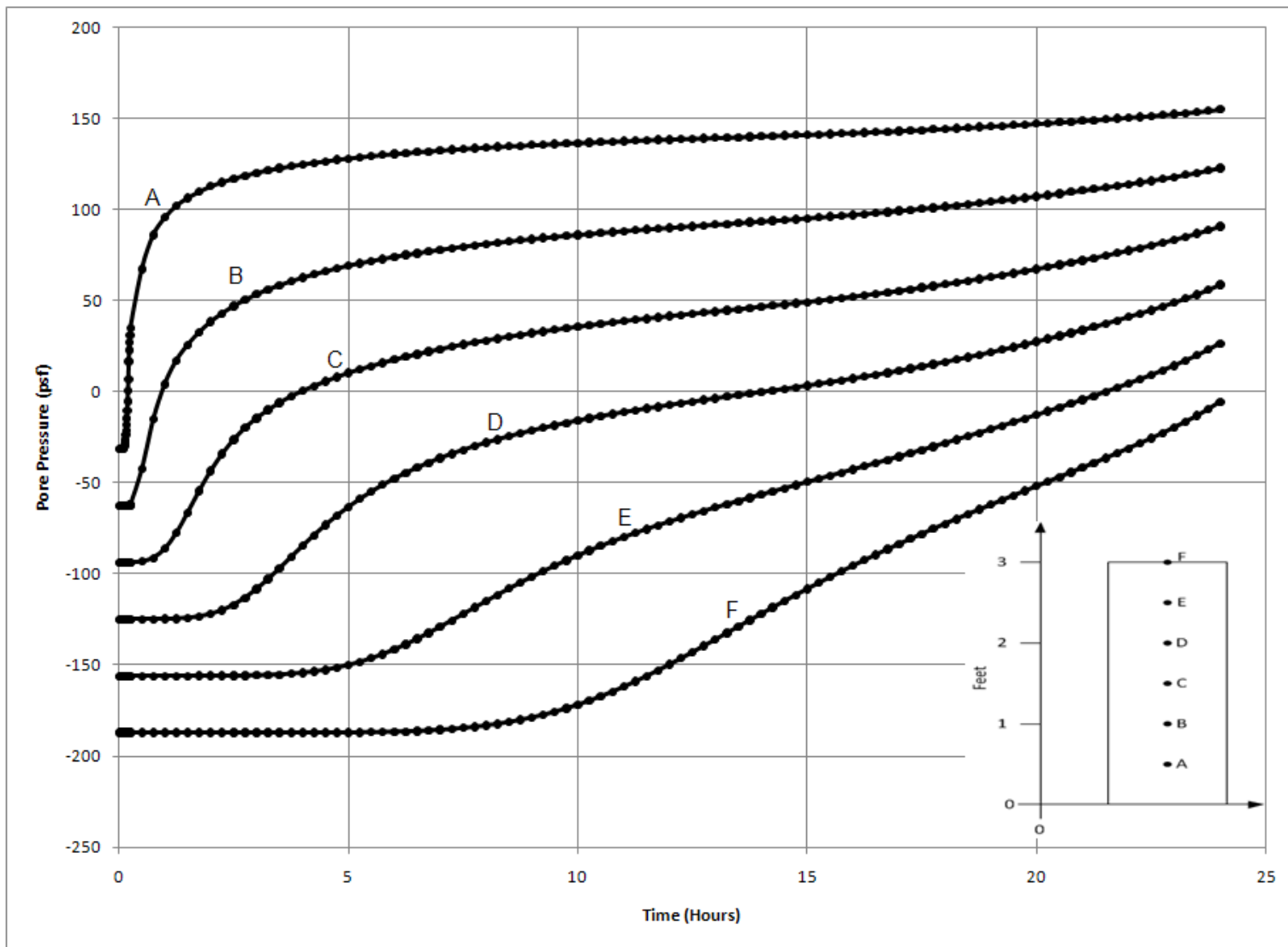
Figure 2-8 – Pore water pressure versus time for the finite element analysis of the silty sand column shown in Figure 2-4

As the water level in the silty sand and clay columns rose from the bottom to the top, the voids in the soil that were filled with air gradually became filled with water, increasing the volumetric moisture content as shown in Figure 2-5. At the start of the analysis each point, A through F, started at a different water content with the highest water content at A and the lowest at F. During the transient analysis, point A reaches the maximum value of volumetric moisture content first followed by B, C, D, E and F. As moisture content of the six points increased in the soil column so does the degree of saturation (Figure 2-6).

Also as the amount of water within the voids increased, the hydraulic conductivity of the soil increased (Figure 2-7). Water can only move through the portions of the voids that are filled with water, and as these water-filled parts of the voids become larger, the water moves more easily through the voids. Thus, as the degree of saturation increases, the hydraulic conductivity increases.

As the amount of water in the voids increased, the soil suction decreased (became more positive), as can be seen in Figure 8.

Figures 5, 6, 7 and 8 all have the same x-axis, time. Therefore it is possible to relate the values on the y-axis to one another. For example, the volumetric moisture content, degree of saturation and hydraulic conductivity can all be plotted on the y-axis with the x-axis as the pore water pressure. Because the degree of saturation bears a simple relationship to volumetric moisture content (degree of saturation is volumetric moisture content divided by porosity), the degree of saturation and volumetric moisture content versus pore water pressure will have the same shape.

When the degree of saturation is plotted versus pore water pressure for points A through F on the same graph, the soil-water characteristic curve is drawn, as is shown in Figure 2-9. The soil-water characteristic curve is the relationship between the degree of saturation and soil suction. Because the silty sand column is homogeneous, the soil-water characteristic curve applies to the entire column. Similarly when the hydraulic conductivity is plotted versus pore water pressure for points A through F on the same graph, the hydraulic conductivity function is drawn, as shown in Figure 2-10. The

hydraulic conductivity function is the relationship between the hydraulic conductivity and pore water pressure (or suction).

As shown in Figure 2-9, when pore water pressures are positive, the soil is fully saturated and all of the voids are filled with water. As shown in Figure 2-10, when the pore water pressure is positive, and the soil is completely saturated, the hydraulic conductivity is the maximum value for the soil. As the pore water pressure becomes negative and air enters the voids of the soil, less space is available for water to move through the soil and the hydraulic conductivity decreases.

These relationships among soil suction, degree of saturation and hydraulic conductivity can be used as the model of soil behavior for finite element analyses of transient seepage through levees. Methods for establishing these methods are discussed in Chapters 6 and 7.
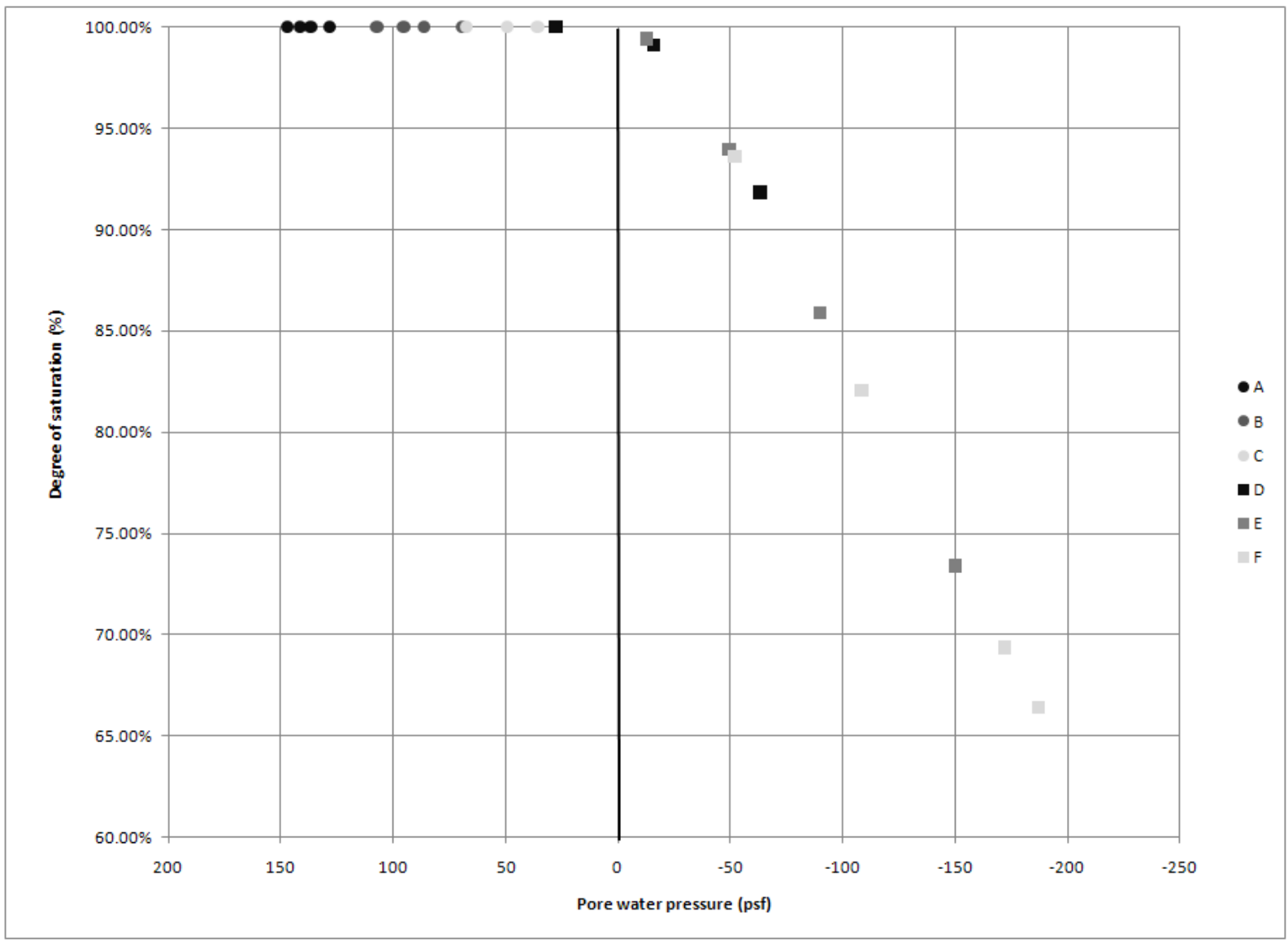
Figure 2-9 – Soil-water characteristic curve for the silty sand material in the column
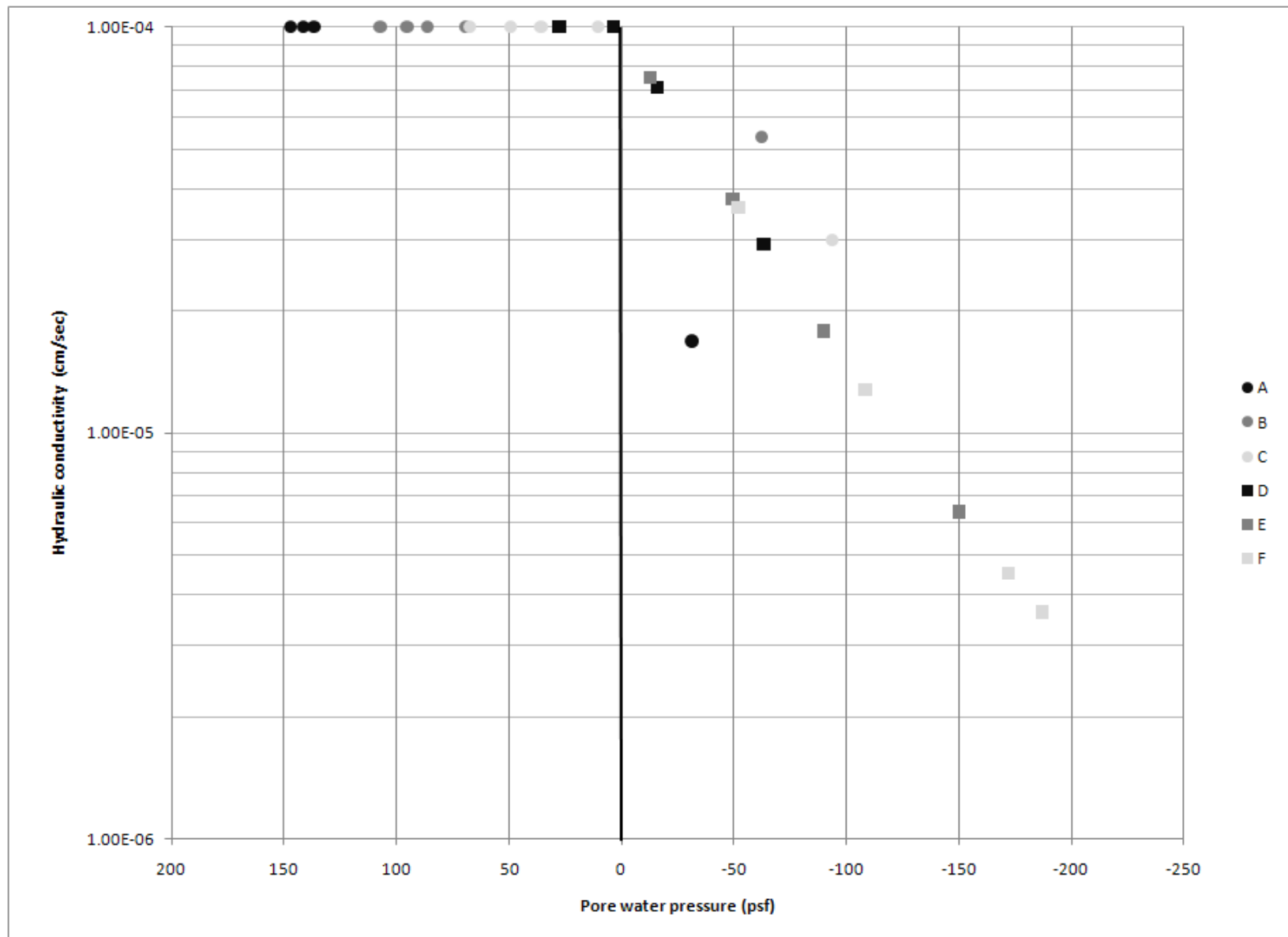
Figure 2-10 – Hydraulic conductivity function for the silty sand material

Chapter 3
Soil Properties for Analysis

Introduction

Meaningful analyses of transient seepage are only possible when the properties of the soil are realistically represented. It is thus essential to model the behavior of the unsaturated soil as accurately as possible. As described in the following sections of this chapter, the properties of unsaturated soils are most often represented using relationships between soil suction and water content, and between soil suction and degree hydraulic conductivity. These relationships, called the soil moisture characteristic curve (SMCC) and the hydraulic conductivity function (HCF) are the subject of this chapter.

During transient seepage through levees, as in the example shown in Figure 3-1, the hydraulic heads, the pore pressures, the amount of flow, and the position of the phreatic surface all change with time. The properties of the soil within the seepage region also change with time as water flows into the levee and fills more of the void space in the soil[1].

Results of an analysis of transient seepage through a 30-ft high levee are shown in Figure 3-1. After the water level outside the levee was raised from 0 feet to 30 feet, the phreatic surface moved upward, gradually saturating a larger region within the levee. After 175 hours, the soil in element A was just slightly above the phreatic surface, and therefore still within the partly saturated zone. The lower part of Figure 3-2 shows how the amount of water in Element A increased with time after the water outside the levee rose. Eventually, when the phreatic surface rises above point A, the soil in this element will be completely saturated, the voids completely filled with water.

---

[1] The transient seepage results shown in Figure 3-1 were calculated using the finite element computer program SEEP/W, developed by Geo-Slope International.

As the amount of water within the voids increases, the hydraulic conductivity of the soil increases. Water can only move through the portions of the voids that are filled with water, and as these water-filled parts of the voids become larger, the water moves more easily through the voids. Thus, as the degree of saturation increases, the hydraulic conductivity increases.
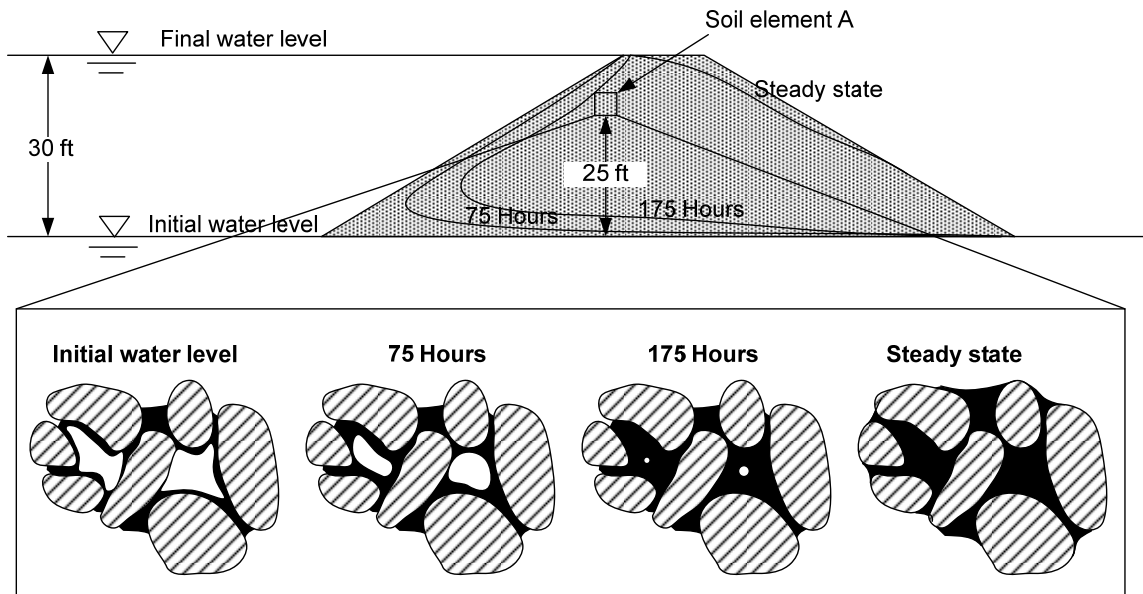
Figure 3-1 – Transient analysis of a levee constructed of silty sand and the changes in the degree of saturation for a soil element after a flood event

The relationship between degree of saturation and soil suction is called the "soil-water characteristic curve." A soil-water characteristic curve for a silty sand is shown in the upper part of Figure 3-2. The use of soil-water characteristic curves to characterize the variation of degree of saturation with soil suction originated within soil science and agricultural soil studies. As used in those studies, the soil-water characteristic curve is represented as the relationship between volumetric moisture content (θ) and soil suction (ψ). Volumetric moisture content is equal to the volume of water divided by the total volume. Degree of saturation (S) bears a simple relationship to volumetric moisture content: degree of

saturation is volumetric moisture content divided by porosity. For a saturated soil, the volumetric water content is equal to the porosity.

A second relationship that is needed for analysis of transient seepage is the relationship between hydraulic conductivity and soil suction. An example for a silty sand in shown in the lower part of Figure 3-2.

(a) Soil-water characteristic curve

Steady state

100 — 50 — ●————————————●175 Hours

●75 Hours

80 — 40 —

← | →

Saturated | Partly Saturated

Initial condition in soil element A

60 — 30 —

Air entry value

40 — 20 —

Wetting

20 — 10 —

0   10   100   1000   10000

Soil Suction (kPa)

Degree of saturation (%)

Volumetric moisture content (%)

(b) Unsaturated hydraulic conductivity function

Steady state

10^{-4} — ●————————————●175 Hours

●75 Hours

← | →

Saturated | Partly Saturated

10^{-5} —

Initial condition in soil element A

10^{-6} —

Air entry value

Wetting

10^{-7} —

10^{-8} —

0   10   100   1000   10000

Soil Suction (kPa)

Hydraulic conductivity (cm/sec)

Figure 3-2 – (a) Soil-water characteristic curve and (b) hydraulic conductivity function used in the transient seepage analysis of the levee shown in Figure 3-1

20

In order to analyze transient seepage it is necessary to know how these things are related:

- soil suction
- degree of saturation or volumetric water content
- hydraulic conductivity

As described earlier, the relationship between the degree of saturation and soil suction is represented by the soil-water characteristic curve. The relationship between the hydraulic conductivity and soil suction is represented by the unsaturated hydraulic conductivity function.

A summary of the required soil properties for a transient analysis is shown in Table 3-1. In most cases the soil-water characteristic curve and the unsaturated hydraulic conductivity function are estimated rather than measured for transient seepage analyses. Fredlund (1998) and Fredlund and Houston (2009) suggested that it is sufficiently accurate for most purposes in transient analyses to estimate the soil-water characteristic curve and the unsaturated hydraulic conductivity function based on tests on similar soils. It appears that this can be done with about the same degree of accuracy as the saturated conductivity can be estimated or measured.

Table 3-1 – Soil properties required for a transient seepage analysis and methods to obtain them

Property	Methods for obtaining:
Saturated hydraulic conductivity	- Estimate based on visual description - Estimate based on grain size or grain size distribution - Measure in the laboratory - Measure in the field
Soil-water characteristic curve (variation of degree of saturation with soil suction)	- Estimate based on visual description (SEEP/W)[*] - Estimate based on grain size or grain size distribution (SEEP/W) - Estimate based on similar soils - Measure in the lab
Hydraulic conductivity function (variation of conductivity with soil suction)	- Estimate based on the soil-water characteristic curve and the saturated hydraulic conductivity (SEEP/W) - Measure in the laboratory

* SEEP/W has 6 generalized soil classes that can be used to estimate the SWCC and the hydraulic conductivity function; clay, silty clay, silt, silty sand, sand, gravel

A common procedure is to measure or estimate the saturated hydraulic conductivity and use an estimated or measured soil-water characteristic curve as a basis for estimating the unsaturated hydraulic conductivity function. Several procedures, such as the Van Genuchten (1980) or Fredlund and Xing (1994) techniques, are available to perform this estimation. These two techniques are available as options in the computer program SEEP/W by GeoSlope.

The hydraulic conductivity function should be consistent with the soil-water characteristic curve. The soil-water characteristic curve shows at what value of soil suction air will begin to enter the soil as the soil dries. This is called the "air entry value." For the silty sand soil moisture characteristic curve shown in Figure 3-2, this is a value of approximately 10 kPa. The conductivity function should begin to show a decrease in conductivity for values of soil suction higher than 10 kPa, because it is at this value that air begins to enter the soil. Air within the

voids of the soil reduces the area for water flow, and the hydraulic conductivity decreases, as noted earlier.

Soil-Water Characteristic Curves

The SWCC is a non-linear soil property. It is defined as the relationship of soil moisture to soil suction (Williams 1983). Soil moisture can be defined as the gravimetric water content, the volumetric water content, or the degree of saturation (Fredlund 2002).

Called the soil-water characteristic curve in this report, the relationship has been given the following names by Fredlund (2002) and others:

1. Water-suction relationship
2. Retention curves
3. Moisture retention curves
4. Soil moisture retention curves
5. Water retention curves
6. Numerous other terms

The soil-water characteristic curve is a function of soil type, adsorption or desorption, volume change characteristics and stress states. Idealized SWCCs are shown in Figure 3-3.
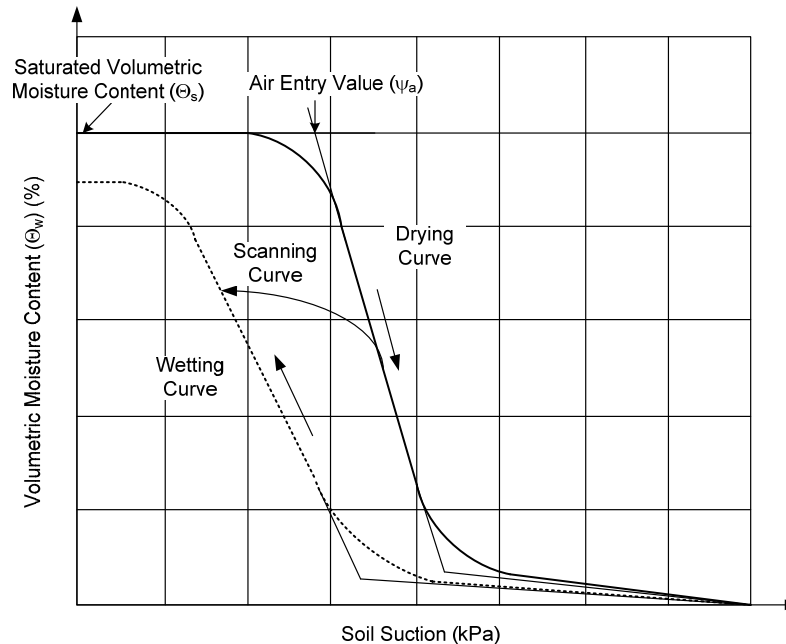
Figure 3-3 – Idealized SWCCs after Yang et al. (2004) (with permission from CGJ)

Hysteresis of Soil-Water Characteristic Curves

Laboratory tests have shown that soil-water characteristic curves and hydraulic conductivity functions are hysteretic. As shown in Figure 3-3, water contents follow a path for wetting that is different from the path for drying. This fact complicates the process of evaluating the soil-water characteristic curve for use in analyses, especially considering the fact that it is almost never certain whether the initial conditions at a given site were established by wetting or by drying.

The difference in the drying and wetting SWCCs can be attributed to the following, as reported by Pham et al. (2005):

1. Irregularities in the cross sections of the void passages (this is commonly referred to as the "ink bottle effect")

2. Contact angles are greater as the meniscus advances as opposed to a receding meniscus

3. Entrapped air will have a different volume depending on whether the soil is wetting or drying

4. Aging effects due to wetting and drying result in gradual adjustments in suction

Hysteresis in the SWCC produces an infinite set of scanning curves bounded by the primary drying and primary wetting curves, as indicated in Figure 3-3 (Fredlund 2006). This effect makes it difficult to predict soil suction values in situ from the SWCC.

To select an appropriate SWCC for a seepage analysis, it is necessary to decide if the process being modeled is a wetting or drying process and then the appropriate SWCC is used for the analysis (Fredlund 2006).

Tami et al. (2004) studied the effects of hysteresis on steady-state infiltration in unsaturated slopes. Comparisons were made between laboratory measurements of water content and soil suction and numerical models based on finite element theory. They found that while it is important to use the correct wetting or drying SWCC, more elaborate hysteresis and scanning curve models may not be needed for geotechnical analyses.

Factors Affecting Soil-Water Characteristic Curves

Soil Type

The shape of the SWCC is controlled by the soil type. Figure 3-4 shows sketches of SWCCs for clay, silty, and sandy soils. Clay soils have small pore spaces. The small pore spaces take a long time to drain because of large surface tension forces between the water and clay particles. In sandy soils, there are large pore spaces. The large pore spaces drain quickly resulting in a sharp break in the slope of the SWCC.
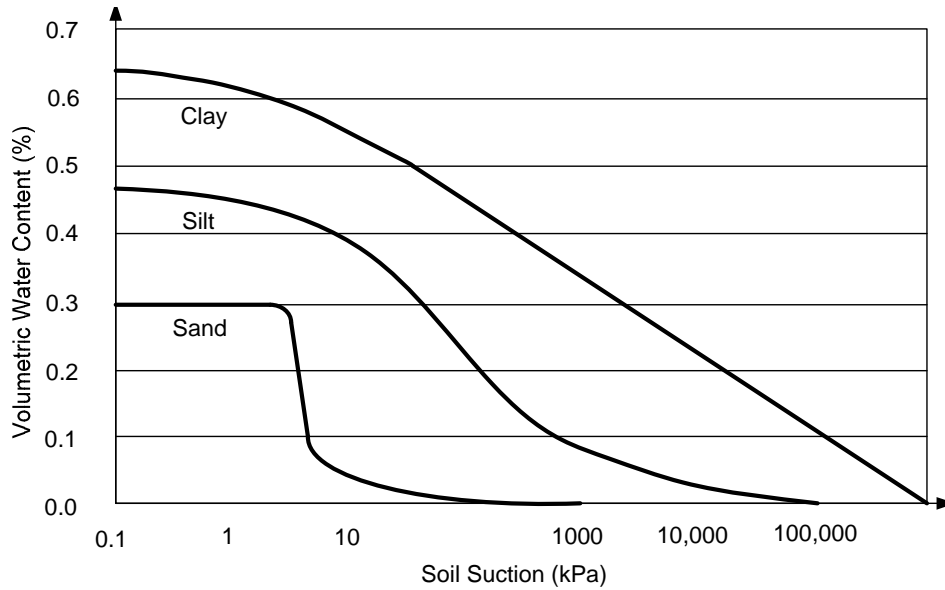
Figure 3-4 – SWCCs for different soil types after Sillers et al. (2001) (with permission from CGJ)

In Situ Stresses

Stress states have a significant influence on the shape of the SWCC (Fredlund 2006). The effect of in situ stresses has been examined by Ng and Pang (2000). Tests were performed on samples of sandy, silty clay. Initial stresses were placed on the samples during laboratory testing to determine the SWCC. The effect of placing loads on the samples before the measurement of the SWCC was similar to testing soils with different initial densities. Stresses were applied to the top of the sample under K_0 conditions. As shown in Figure 3-5 for remolded soil and Figure 3-6 for undisturbed soil, as the load increased for a particular value of soil suction, the degree of saturation increased. The load decreases the void ratio of the soil, increasing the air entry value and decreasing the slope of the soil-water characteristic curve.
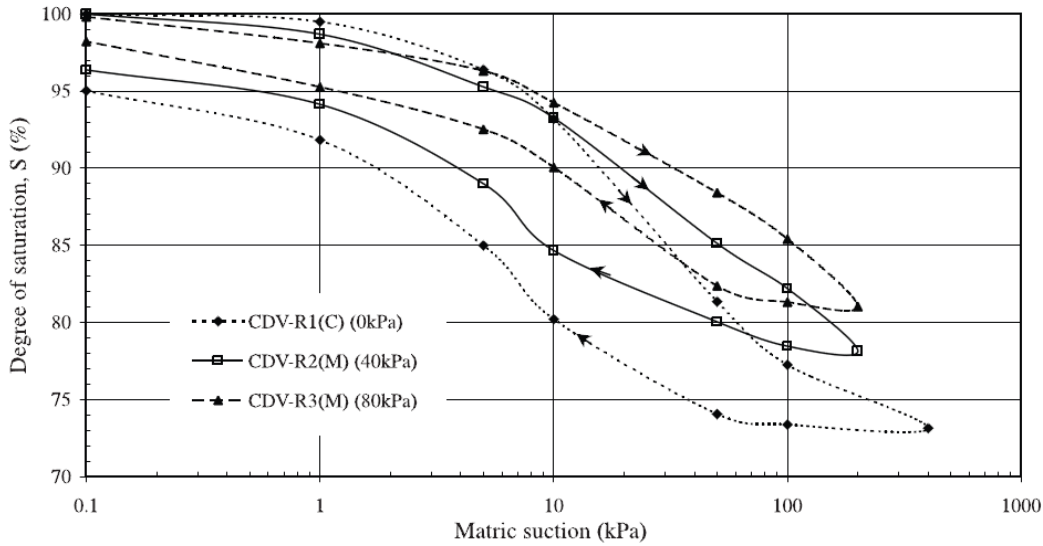
Figure 3-5 – SWCCs for a remolded test specimen with three different applied stresses, from Ng and Pang (2000) (with permission from CGJ)
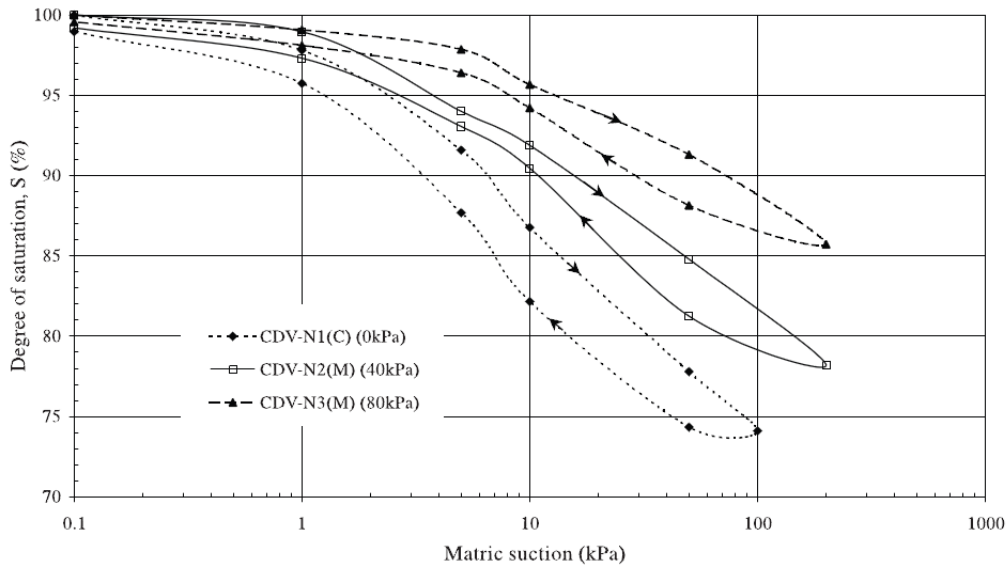
Figure 3-6 – SWCCs for an undisturbed test specimen with three different applied stresses, from Ng and Pang (2000) (with permission from CGJ)

Undisturbed or Remolded Samples

The difference between SWCCs for undisturbed and remolded samples has also been investigated by Fredlund (2004) and Fredlund (2000). The difference is significant as shown in Figure 3-7. It was suggested by Fredlund (2006) that all

27

SWCCs be identified as undisturbed or remolded. Figure 3-7 shows SWCCs measured in the laboratory for slurried, undisturbed, and compacted specimens of the same soil, a silty clay. It can be seen that the method of specimen preparation has a large effect on the SWCC. These effects may not be as significant in sandy soils as they are in clayey soils (Fredlund 2000).
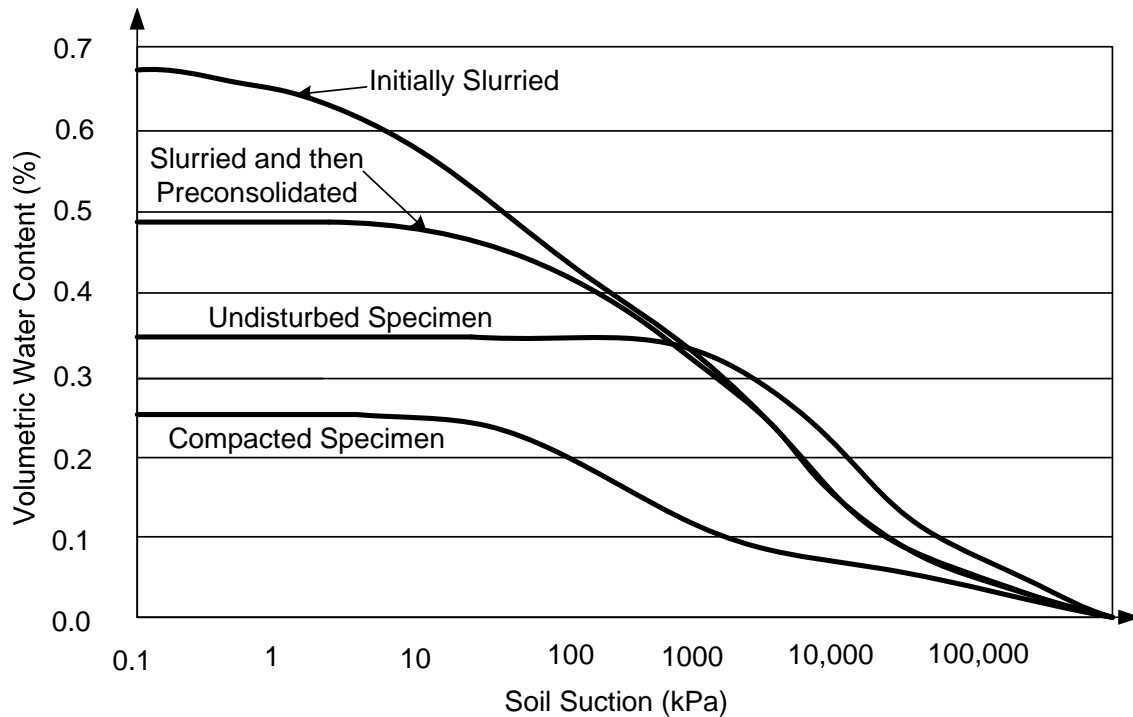
Figure 3-7 – Influence of initial state on the SWCC after Fredlund (2000) (with permission from CGJ)

Volume Change

Soils compress or swell in response to changes in soil suction. This change in volume is not likely to be significant in sandy and silty soils, but it is for clay soils (Fredlund 2004). Volume changes complicate transient seepage modeling because the SWCC will change as the soil swells or compresses. A recent model for the SWCC of a soil exhibiting significant volume change due to changes in suction has been introduced by Pham and Fredlund (2008).

SWCCs measured for a natural soil by Ng and Pang (2000) are shown in Figure 3-8. Taking volume change into account when measuring the SWCC results in an increased degree of saturation for a given value of soil suction.
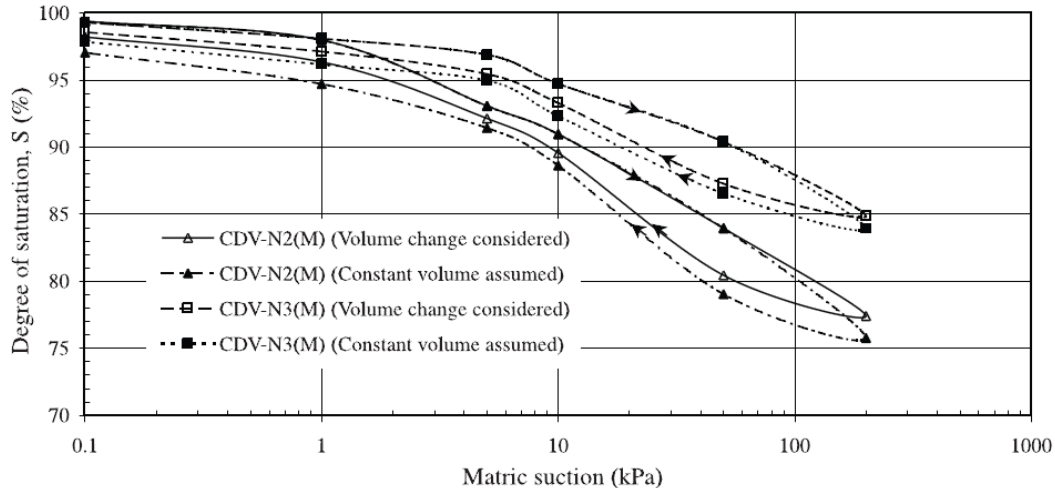
Figure 3-8 – Influence of volume change on the SWCC, from Ng and Pang (2000) (with permission from CGJ)

Fitting the Soil-Water Characteristic Curve

Laboratory or field measurement of the SWCC results in a number of discrete values of soil moisture versus soil suction. To perform a transient seepage analysis, a continuous function is necessary. Many researchers have proposed equations to fit SWCCs (Fredlund and Xing (1994); Gitirana Jr and Fredlund (2004); Leong and Rahardjo (1997b); Pham and Fredlund (2008); Rojas and Rojas (2006)).

SWCCs can be characterized by the saturated volumetric water content, θ_s, the air-entry value, ψ_a, the residual volumetric water content, θ_r, and the residual air content, θ_a.

A generic form for the SWCC can be represented by the following equation (Leong and Rahardjo 1997b):

$$a_1\theta^{b1} + a_2\exp(a_3\theta^{b1}) = a_4\psi^{b2} + a_5\exp(a_6\psi^{b2}) + a_7 \qquad \textbf{Eq. 3-1}$$

29

Where: a_1, a_2, a_3, a_4, a_5, a_6, a_7, b_1, and b_2 are empirical constants determined by curve fitting

ψ = suction pressure (kPa)

θ = normalized volumetric water content i.e. $(\theta_w - \theta_r)/(\theta_s - \theta_r)$

θ_w = volumetric water content (%)

θ_r = residual volumetric water content (%),

θ_s = saturated volumetric water content (%)

Table 3-2 lists various equations that have been used to fit equations to water content-suction data. These equations are all forms of the more generalized equation presented above (Leong and Rhardjo 1997).

The method used to fit an equation to the SWCC is limited by the modeling software. A comparison of the fitting equations has been performed by Leong and Rahardjo (1997) and Sillers and Fredlund (2001). These researchers found that the Fredlund and Xing model (1994) approximates the SWCC the best.

Table 3-2 – SWCC fitting equations after Fredlund (2006) and Leong and Rahardjo (1997)(with permission from ASCE)

Reference	Equation	Coefficients
Gardner 1958	$$\theta_d = \frac{1}{1 + \alpha_g \psi^{n_g}}$$	α_g = soil parameter which is primarily a function of the air entry value of the soil and n_g = soil parameter which is primarily a function of the rate of water extraction from the soil, once the air entry value of the soil has been exceeded
Brooks and Corey 1964	$$\theta_n = 1, \psi \le \psi_a$$ $$\theta_n = \left(\frac{\psi}{\psi_{aev}}\right)^{-\lambda_{bc}}, \psi > \psi_a$$	ψ_a = air entry value of the soil and λ_{bc} = pore size distribution index
Brutsaert 1967	$$\theta_n = \frac{1}{1 + \left[\dfrac{\psi}{a_b}\right]^{n_b}}$$	a_b = soil parameter which is primarily a function of the air entry value of the soil and n_b = soil parameter which is primarily a function of the rate of water extraction from the soil, once the air entry value has been exceeded
Laliberte 1969	$$\theta_n = \frac{1}{2} erfc\left[a_1 - \frac{b_1}{c_1 + \left(\dfrac{\psi}{\psi_{aev}}\right)} \right]$$	The parameters a_1, b_1, and c_1 are assumed to be unique function of the pore-size distribution index, λ
Farrel and Larson 1972	$$w = w_s - \frac{1}{a_f} \ln \frac{\psi}{\psi_a}$$	a_f = medium parameter

Table 3-2 Cont. – SWCC fitting equations after Fredlund (2006) and Leong and Rahardjo (1997)(with permission from ASCE)

Reference	Equation	Coefficients
Van Genuchten 1980	$$\theta_n = \dfrac{1}{\left[1+\left(\dfrac{\psi}{a_v}\right)^{n_v}\right]^{m_v}}$$	a_v = soil parameter primarily a function of air entry value of the soil (1/kPa); n_v = soil parameter which is primarily a function of the rate of water extraction from the soil, once the air entry value has been exceeded; and m_v = soil parameter which is primarily a function of the residual water content
McKee and Bumb 1987	$$\theta_n = \dfrac{1}{1+\exp\left(\dfrac{\psi - a_m}{n_m}\right)}$$	a_m and n_m = curve fitting parameters
Fredlund and Xing 1994	$$w(\psi) = C(\psi)\dfrac{w_s}{\left\{\ln\left[e+\left(\dfrac{\psi}{a_f}\right)^{n_f}\right]\right\}^{m_f}}$$ $$C(\psi) = 1 - \dfrac{\ln\left(\dfrac{1+\psi}{\psi_r}\right)}{\ln\left[1+\left(\dfrac{1,000,000}{\psi_r}\right)\right]}$$	a_f = soil parameter which is primarily a function of the air entry value of the soil; n_f = soil parameter which is primarily a function of the rate of water extraction from the soil, once the air entry value has been exceeded; m_f = soil parameter which is primarily a function of residual water content; and $C(\psi)$ = correction which is primarily a function of the suction at which residual water content occurs

Notes (Table 3-2): $\theta_n = (w - w_r) / (w_s - w_r)$ = normalized water content; w = gravimetric water content; w_r = residual gravimetric water content; w_s = gravimetric water content at saturation; $\theta_d = w / w_s$ = dimensionless water content; w_s and w_r = saturation and residual gravimetric water contents, respectively; and ψ = soil suction.

Hydraulic Conductivity Functions

The relationship between the hydraulic conductivity of a soil and the soil suction or water content, usually abbreviated as the HCF, is also needed for transient seepage analyses.

The conductivity of a soil increases as the degree of saturation increases, and at 100% saturation, the conductivity reaches a maximum value. As the amount of water in the voids decreases, the amount of air in the pore spaces increases, and the spaces through which water can flow are reduced. As a soil dries, water us lost first from the largest, most conductive pore spaces. As a result, soils with large voids have a sharp decrease in conductivity as suction increases. Soils with smaller pore spaces have more gradual decrease in conductivity with increasing soil suction Hillel (1971). This is shown by the HCFs for a clay soil and a sandy soil in Figure 3-9.

The difference in the shapes of the HCFS has an important effect on transient seepage. Soils with the largest voids (such as sandy soils) are the most conductive when fully saturated. Soils with small pore spaces (such as clayey soils) have much lower conductivity values when fully saturated. However, during unsaturated flow, the soils with the larger pore spaces quickly desaturate and their conductivity decreases sharply. The smaller pore spaces of clay soils desaturate more slowly and their conductivity does not decrease as sharply as that of sandy soils. At greater suction values the conductivity of the clay soil can be larger than the conductivity of the sandy soil. Sandy layers can impede flow

relative to clay layers until the water level rises above the sandy layer Hillel (1971).

Little hysteresis is seen in the UHCF when plotted against volumetric water content or degree of saturation, as shown in Figure 3-10 (Fredlund and Rahardjo (1993). However this is not the case when the conductivity is plotted against soil suction. Because there is hysteresis in the volumetric water content when plotted against the soil suction (the SWCC), there will be hysteresis when plotting the conductivity versus soil suction (Figure 3-9) Fredlund and Rahardjo (1993).
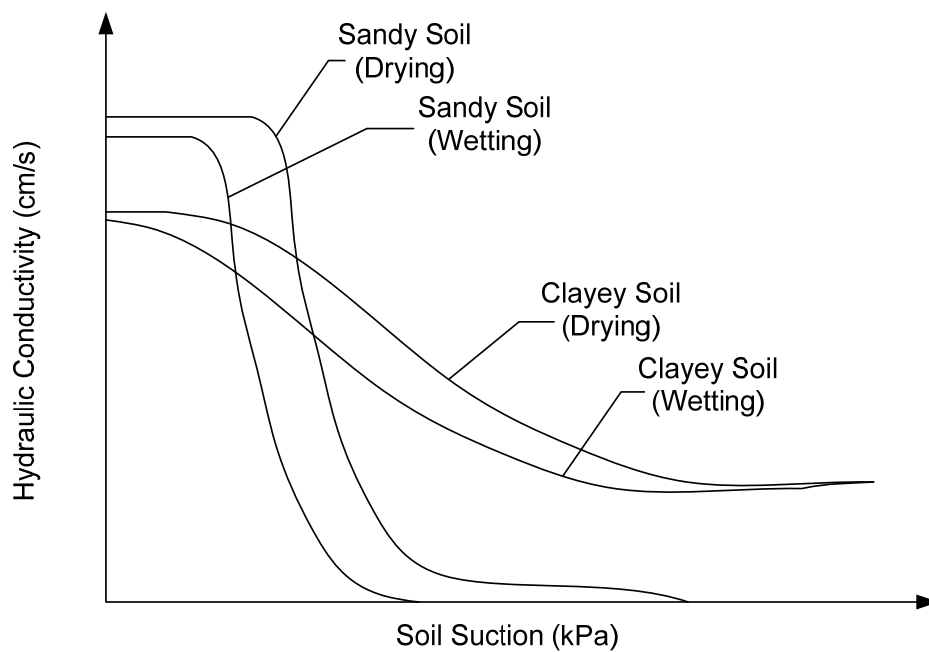
Figure 3-9 – Hydraulic conductivity functions for different soil types after Lu and Likos (2004) (with permission from John Wiley & Sons)
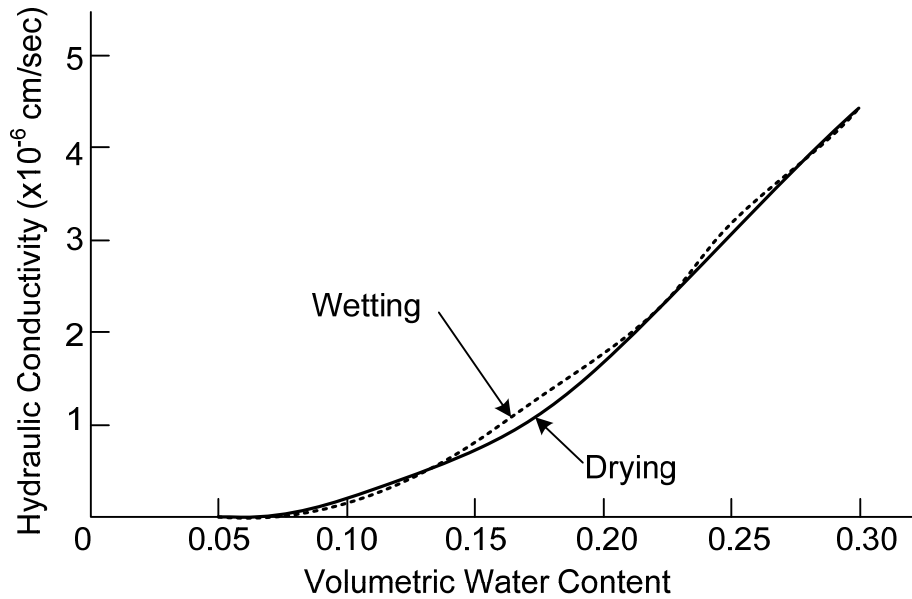
Figure 3-10 – Relationship between hydraulic conductivity and volumetric water content, after Fredlund and Rahardjo (1993) (with permission from John Wiley & Sons)

The HCF is a continuous curve representing hydraulic conductivity values over a range of water contents or soil suction values. If data for the HCF is from laboratory experiments, fitting equations are used to fit a curve to the data. Many researchers have made summaries of these hydraulic conductivity models (Fredlund et al. 1994; Leong and Rahardjo 1997a; Mualem 1986). In the empirical fitting models, the hydraulic conductivity of the soil is a function of the moisture content or soil suction. Table 3-3 is a summary of the fitting models used for the UHCF (Fredlund et al. 1994; Leong and Rahardjo 1997a; Lu and Likos 2004).

Table 3-3 – Empirical HCFs after Fredlund et al. (1994), Leong and Rahardjo (1997a), Lu and Likos (2004)

Form	Equation	Notes	Reference
$k = f(\theta)$	$k(\theta) = k_s \theta_s$	k_s = saturated conductivity $\theta_n = \dfrac{\theta - \theta_r}{\theta_s - \theta_r}$ =normalized water content; θ = volumetric water content θ_r = residual volumetric water content θ_s = volumetric water content at saturation	Averjanov 1950
$k = f(\theta)$	$k(\theta) = k_s \exp(a(\theta - \theta_s))$	k_s =saturated conductivity a= constant θ_s = saturated water content θ = water content	Davidson et al. 1969
$k = f(\theta)$	$k(\theta) = k_s \left(\dfrac{\theta}{\theta_s} \right)^n$	k_s =saturated conductivity n = constant based on pore size distribution θ_s = saturated water content θ = water content	Campbell 1973
$k = f(\theta)$	$k(\theta) = a\theta^b$	θ = water content a, b = constants	Gardner 1958
$k = f(\psi)$	$k(\psi) = a\psi + b$	ψ = soil suction a, b = constants	Richards 1931

Summary

In order to perform transient seepage analyses, it is necessary to define the variations of water content and hydraulic conductivity with changes in soil suction, the Soil Water Characteristic Curve (SWCC) and the Hydraulic Conductivity function (HCF). Both the SWCC and the HCF are hysteretic (they vary depending on whether the soil is wetting or drying).

Many studies have been made to measure SWCCs and HCFs for different soils, and a large number of fitting equations have been proposed for use in analyses. It does not appear that any one of the proposed fitting methods is significantly more accurate than the others. Considering the fact that the behavior being modeled is complex, and is affected by many variables, some of which can only be estimated for a particular soil and seepage condition, and considering the fact that even saturated hydraulic conductivity can only be evaluated within one or two orders of magnitude, it appears unlikely that the soil properties required for transient seepage analyses can be estimated with high accuracy, no matter how sophisticated are the fitting relationships that are used.

Chapter 4
Numerical Analyses of Transient Seepage

Introduction

Numerical analyses of transient seepage are prone to problems because transient seepage through soil is governed by highly nonlinear relationships. Fortunately, these difficulties have been largely resolved in the 2007 version of SEEP/W. This chapter provides guidance for designing finite element meshes for use with SEEP/W and selecting time steps for analyses to achieve accurate results with minimal solution time.

Equations Governing Transient Seepage

Unsaturated flow problems, such as the transient flow of water through a levee in response to rise in river level, can be calculated numerically using the finite element method. Many computer programs are available that can solve unsaturated flow problems using the finite element method, including SEEP/W by GeoStudio, SLIDE by Rocsciense, and SVFlux by SoilVision.

When pore pressures in unsaturated flow problems no longer change with time, they have reached steady state conditions. Until steady state conditions are reached the flow is transient. The computer programs cited above can solve both steady state and transient flow problems. Steady state seepage conditions are governed by the Laplace equation for conditions of isotropic hydraulic conductivity:

$$\frac{\partial^2 h}{\partial x^2} + \frac{\partial^2 h}{\partial y^2} + \frac{\partial^2 h}{\partial z^2} = 0$$

Eq. 4 - 1

Where h = hydraulic head (ft) and x, y, z = coordinates (ft).

During steady flow the net flow is equal to zero with inflow equal to outflow.

Transient flow is governed by the following partial differential equation:

$$\frac{\partial}{\partial x}\left(k_{wx}\frac{\partial h}{\partial x}\right) + \frac{\partial}{\partial y}\left(k_{wy}\frac{\partial h}{\partial y}\right) + \frac{\partial}{\partial z}\left(k_{wz}\frac{\partial h}{\partial z}\right) = m_2^w \gamma_w \frac{\partial h}{\partial t}$$

Eq. 4 - 2

Where k_{wx}, k_{wy}, and k_{xz} are hydraulic conductivities (cm/sec), m_2^w = slope of the soil-water characteristic curve (ft^2/lb), and γ_w = unit weight of water (lb/ft^3).

Both the hydraulic conductivity function and the soil-water characteristic curve are needed to solve transient flow problems. These soil properties are highly nonlinear, as discussed in Chapter 3. The nonlinearity of these soil properties can create numerical problems including numerical oscillations and slow or non-convergence. When transient flow problems do not converge, the calculated pore pressures are likely to be inaccurate. This can be significant in slope stability problems where the pore pressures along potential slip surfaces affect soil strength. These problems are discussed here briefly to give guidance on how to develop numerical models of transient seepage that converge with minimal computing time, and also to indicate which conditions cause convergence to be slow. When transient flow problems do not converge, it is also likely that calculated values of hydraulic gradient will be inaccurate, affecting analyses of the safety against erosion and piping.

Numerical Oscillations

Karthikeyan et al. (2001) studied the effects of numerical oscillations on the solutions to transient seepage problems. Numerical oscillation is the phenomena where computed quantities (pore pressures or seepage quantity) oscillate around the correct solution at successive time steps. This can have significant effects on the position of the wetting front and should be prevented (Karthikeyan et al. 2001).

Karthikeyan et al. (2001) found that these oscillations were produced by time steps that were too small for particular element sizes. They found through numerical simulations that applying the minimum time step criteria of Thomas and Zhou (1997), who suggested minimum time step criteria for finite element analyses of heat diffusion, that oscillations could be prevented for seepage problems. For two dimensional finite

element analyses of seepage, the minimum time step criterion to prevent oscillations with four-noded elements (the default in SEEP/W) is defined as:

$$\Delta t \geq L^2 \lambda / 2k \qquad\qquad \textbf{Eq. 4 - 3}$$

Where Δt = time step (sec), L = element size (width or length measured in the direction of flow) (ft), λ = slope of the soil-water characteristic curve (ft^2/lb) • unit weight of water (62.4 lbs/ft^3) and k = hydraulic conductivity (ft/sec).

The slope of the soil-water characteristic curve and the hydraulic conductivity used in Eq. 4 - 3 should be from the driest point (largest soil suction) that the unsaturated soil being modeled will experience during the transient seepage analysis. An example for soil suction of 300 psf (approximately 5 feet of negative pressure head) is shown in Figure 4-1. The element size for this example is 2 feet. This example illustrates how it is possible have very large minimum time steps for highly nonlinear soil properties. To reduce the minimum time step it is necessary to reduce the element size. The consequence of reducing the element size is greater computational time.

Soil-Water Characteristic Curve

$y = -2E-08x^3 + 7E-05x^2 - 0.0836x + 40.31$

Slope of line at 300 psf = 0.047 (ft^{-1})

Δu

Δw

300 psf

Hydraulic Conductivity Function

2.84E-06 (ft/sec)

300 psf
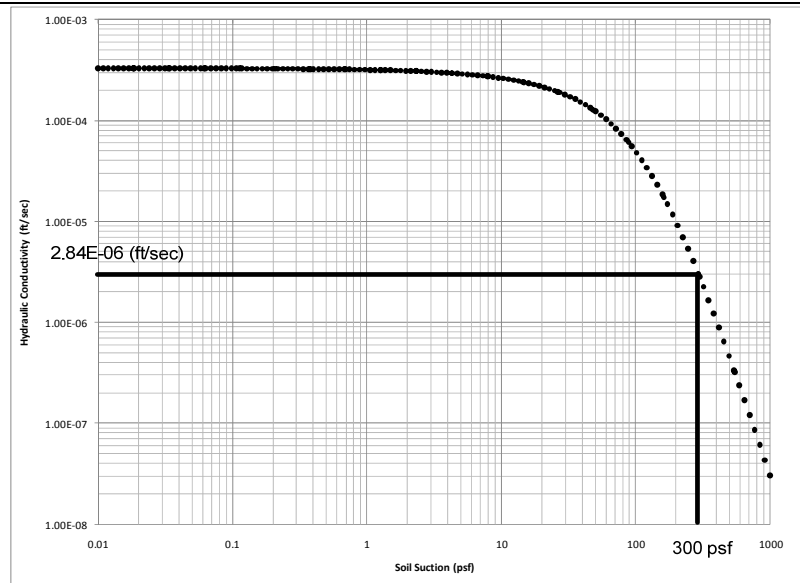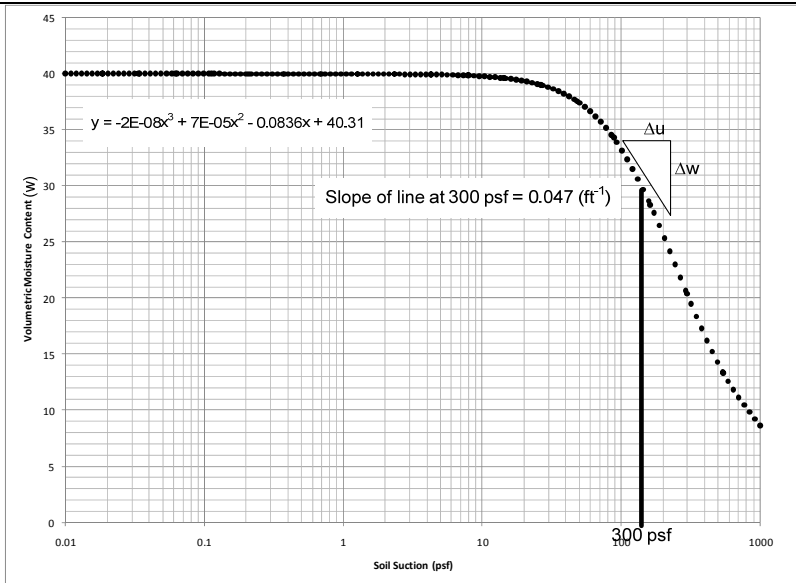
$\lambda = 0.047$ (ft^2/lb) * 62.4 (lb/ft^3) = 2.93 (ft^{-1})

$k = 2.84 \times 10^{-6}$ (ft/sec)

$L = 2$ (ft) (for example)

$$\Delta t = L^2 \lambda / 2k = \frac{2^2 \left(ft \right) \ * \ 2.93 \left(ft^{-1} \right)}{2 * (2.64 * 10^{-6})(ft / \sec)} = 2.16 \times 10^6 \text{ sec} =$$

25 days

Flow

2 ft
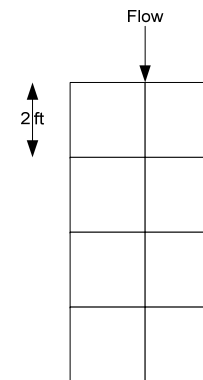
Figure 4-1 – Example of a minimum time step calculation based on criteria by Karthikeyan et al. (2001)

41

Both Karthikeyan et al. (2001) and Tan et al. (2004) performed numerical experiments to show that the criteria established by Thomas and Zhou (1997) for minimum time step criteria were valid for transient seepage problems using the computer program SEEP/W. The analysis of Tan et al. (2004) is repeated here using the most up-to-date version of SEEP/W available (2007). The numerical experiment involves a 1 m tall column of soil, 0.01 m wide. The soil column and associated soil-water characteristic curve and hydraulic conductivity function are shown in Figure 4-2. At the start of the analysis there is a uniform pressure head of -8 m throughout the column. At t > 0, a total head of 1 m is imposed at the top boundary while the h = -8 m boundary condition is maintained at the bottom. This causes one dimensional vertical infiltration of water into the soil column from the top to the bottom.

The results from Tan et al. (2004) and SEEP/W (2007) are shown in Figure 4-3.   Tan et al. (2004) calculated the minimum time step to be approximately 12 hours. As shown in Figure 4-3, time steps less than 12 hours produced numerical oscillations. However these numerical oscillations are not observed in the results calculated during this study using the new version of SEEP/W (2007). This is because the current version of SEEP/W uses default meshes of 3-noded triangles and 4-noded quadrilaterals, and the matrix system of equations is solved using a mass-lumped scheme. Even for time steps significantly less than the minimum time step criteria of Thomas and Zhou (1997), numerical oscillations are not observed in the results as shown in Figure 4-2.

h = -8 m for t < 0, h = +1 m for t ≥ 0

Soil Column

1 m

◄0.01m►

h = -8 m for t ≥ 0
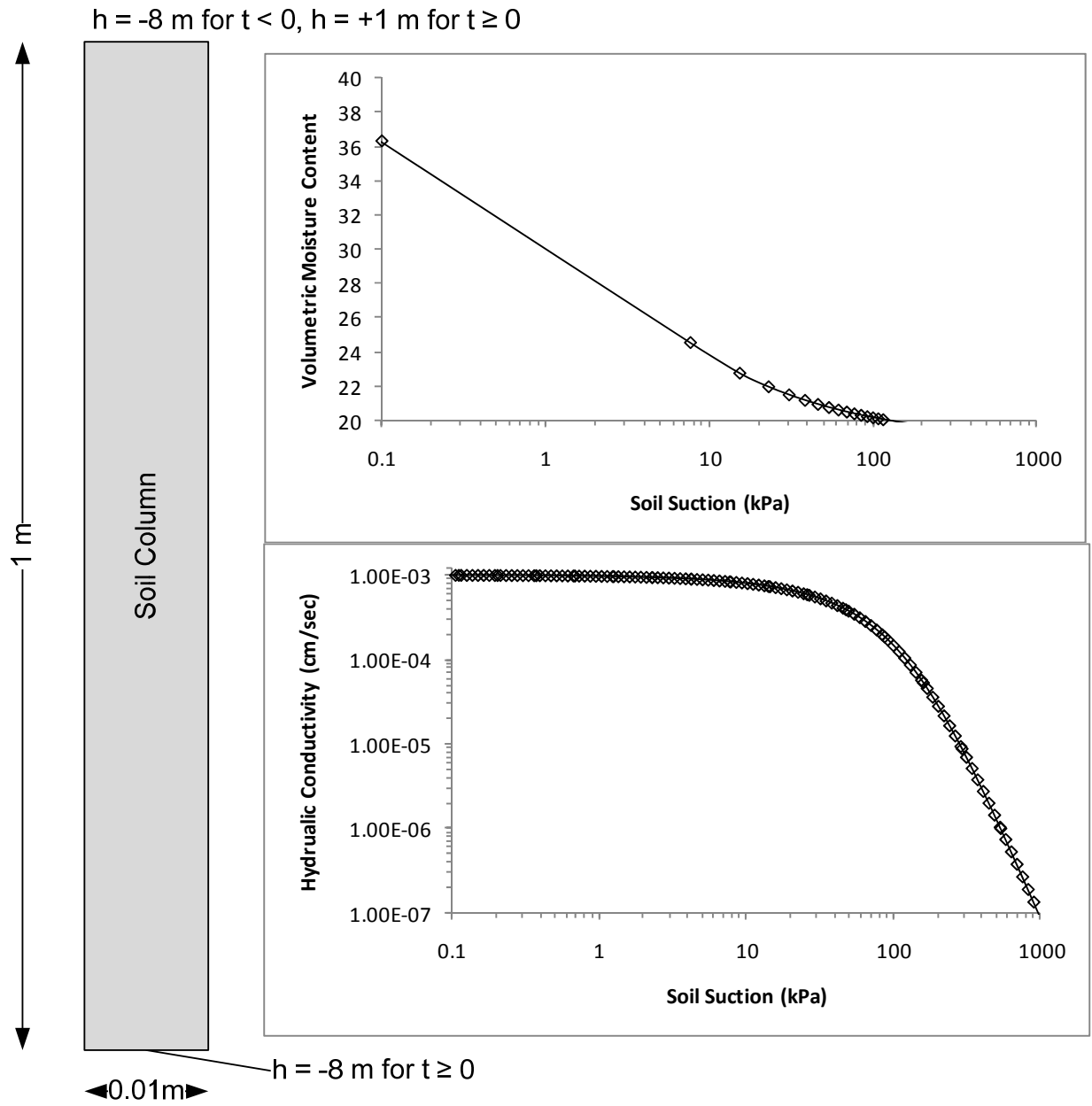
Figure 4-2 – Numerical study of a soil column from Tan et al. (2004)
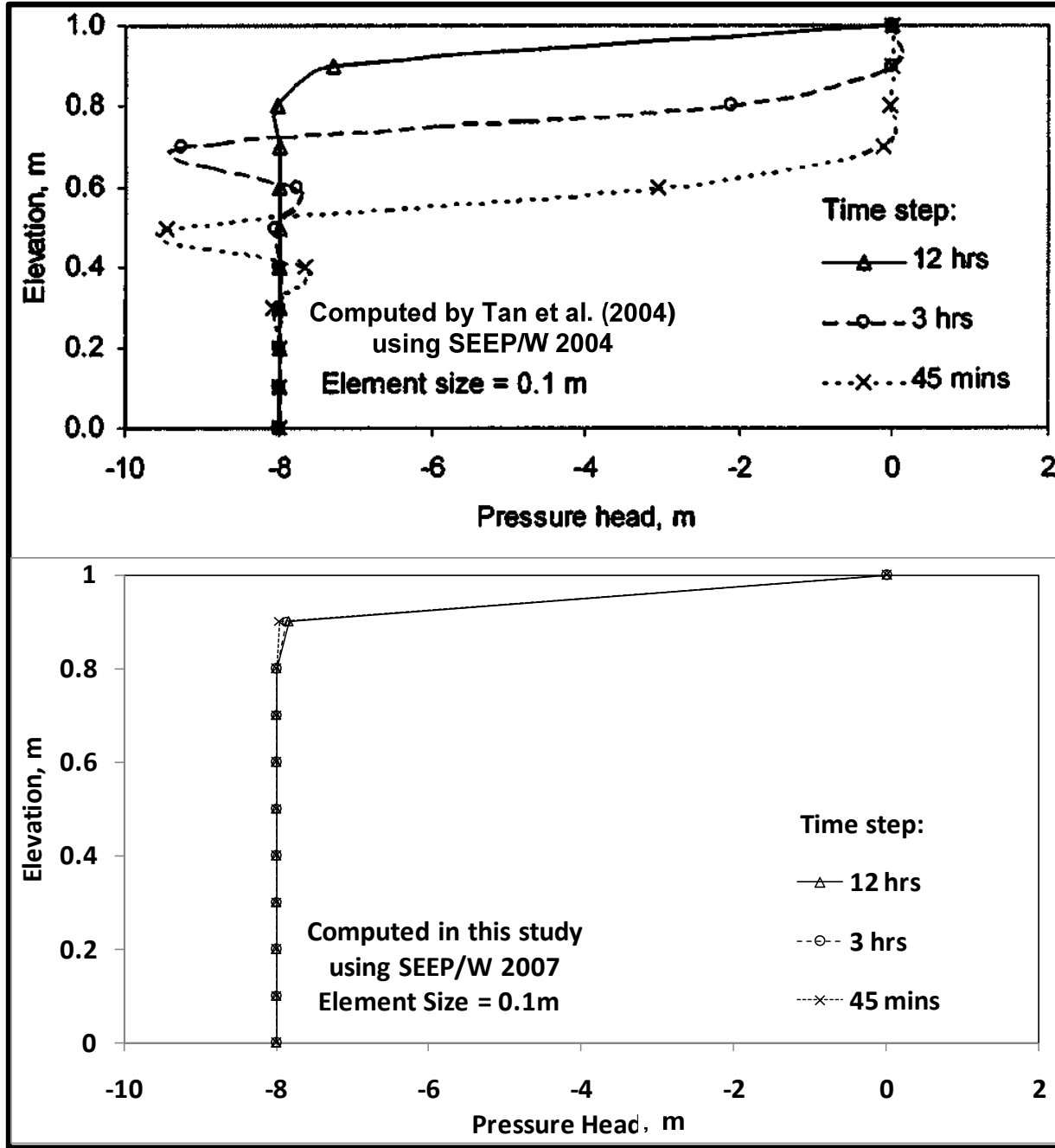
Figure 4-3 –Tan et al. (2004) results (top) and SEEP/W 2007 results (bottom) for 0.1 m elements after 12 hours of the model run for different time steps (with permission from ASCE)

Using higher-order elements in SEEP/W (2007), it is possible that numerical oscillations will occur. Using higher 8-noded quadrilaterals for example, results in numerical oscillations in the results. These numerical oscillations can be avoided if 3-noded triangular and 4-noded quadrilaterals are used in SEEP/W (2007).

Study of Numerical Problems with Calculated Pore Pressure Changes and Exit Gradients in Levees

The one dimensional numerical study by Tan et al. (2004) was performed to observe the effects of element size and time step on numerical oscillations. During the course of this research study, it was found that by using the default 3-noded and 4-noded elements in SEEP/W analyses, numerical oscillations could be avoided. A study of two dimensional transient seepage was conducted to examine the effects of element type, element size and time step magnitude on calculated pore pressures and exit gradients for a transient seepage analysis.

Pore pressures

The first phase of the study examined the effects of element type, element size and time step magnitude on the calculated pore pressures calculated in a transient seepage analysis of seepage through a levee. The conditions analyzed are shown in Figure 4-4. A 15 ft high silty sand levee with a 10 ft wide crest and 2.5 to 1 slopes has been constructed on top of a 10 ft thick layer of fine sand. The soil-water characteristic curve and the hydraulic conductivity function for the levee material is shown in Figure 4-4. The initial pore pressures within the levee corresponded to a hydrostatic condition with the water table at the base of the levee. At the start of the transient seepage analysis the water level was raised 15 ft to the top of the levee. For different element types, element sizes and time step magnitudes the pore pressures were calculated along a vertical line through the center of the levee 14 days after the water level was raised.

The first analysis examined the effects of the four different mesh types shown in Figure 4-5 on the calculated pore pressures. The four different mesh types were "quadrilaterals and triangles" (default), "triangles only", a "rectangular grid" of quadrilaterals, and a "triangular grid" of quadrilaterals, as shown in Figure 4-5. These

are the four names for finite element meshes that can be generated automatically for SEEP/W. The results of the numerical analysis for the four different mesh types are shown in Figure 4-6.
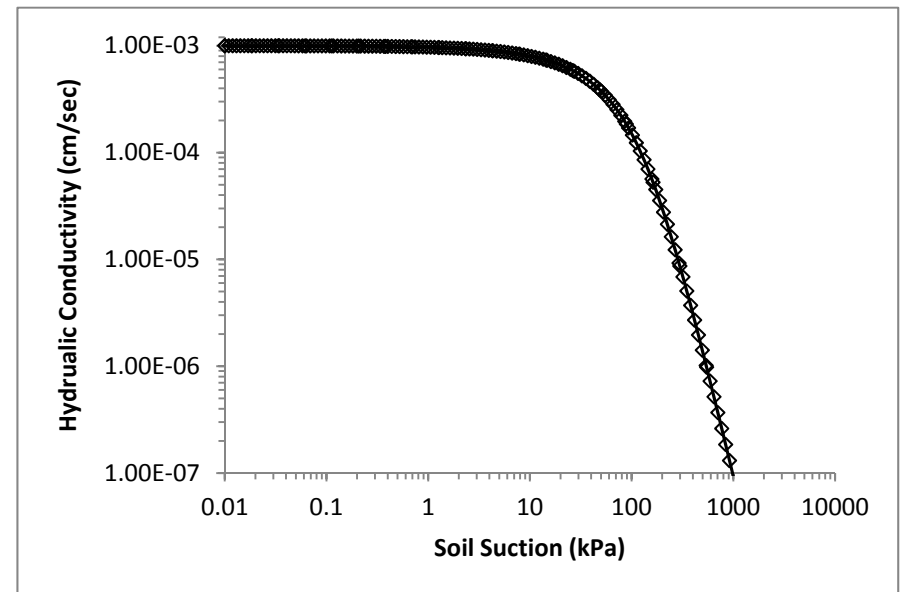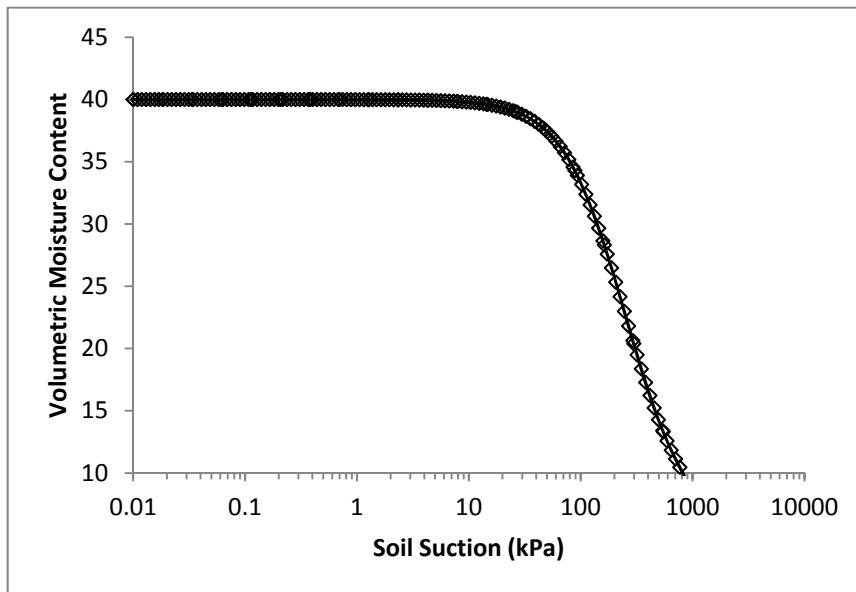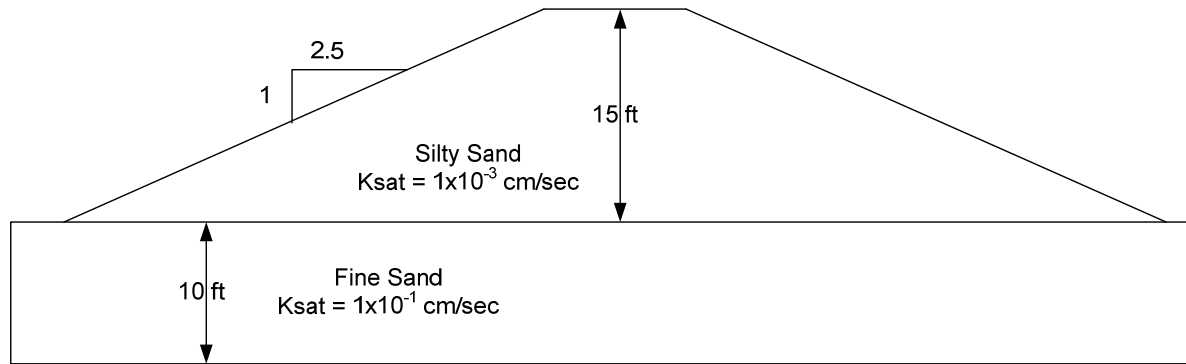
Figure 4-4 – Levee used for numerical model case study of changes in pore pressures within the levee along the centerline
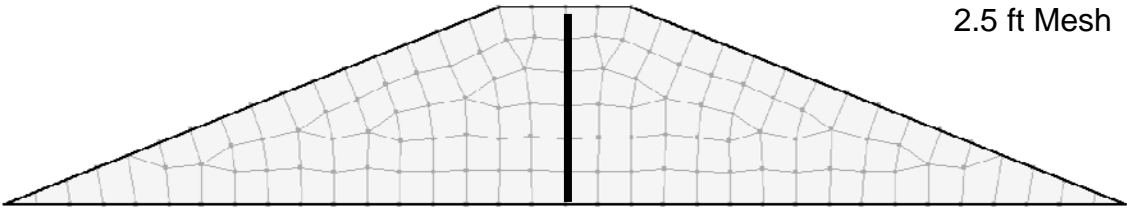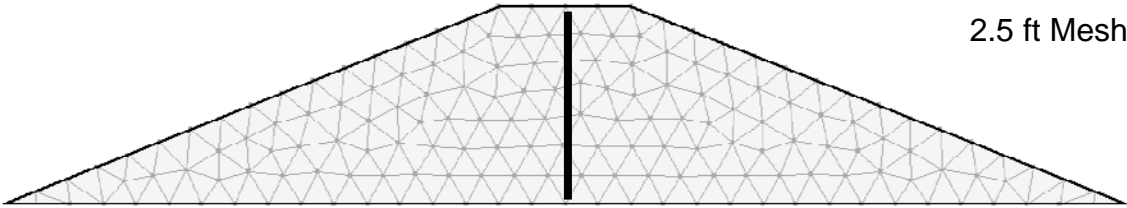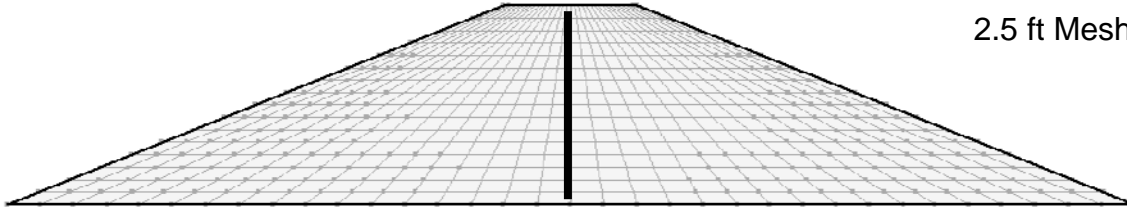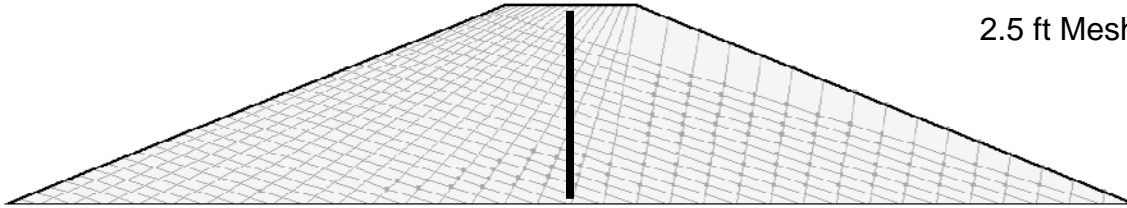
Mesh Illustration	Mesh Name
2.5 ft Mesh	Quadrilaterals and Triangles
2.5 ft Mesh	Triangles Only
2.5 ft Mesh	"Rectangular" Grid of Quadrilaterals
2.5 ft Mesh	"Triangular" Grid of Quadrilaterals

Figure 4-5 – Mesh types and associated names available in SEEP/W
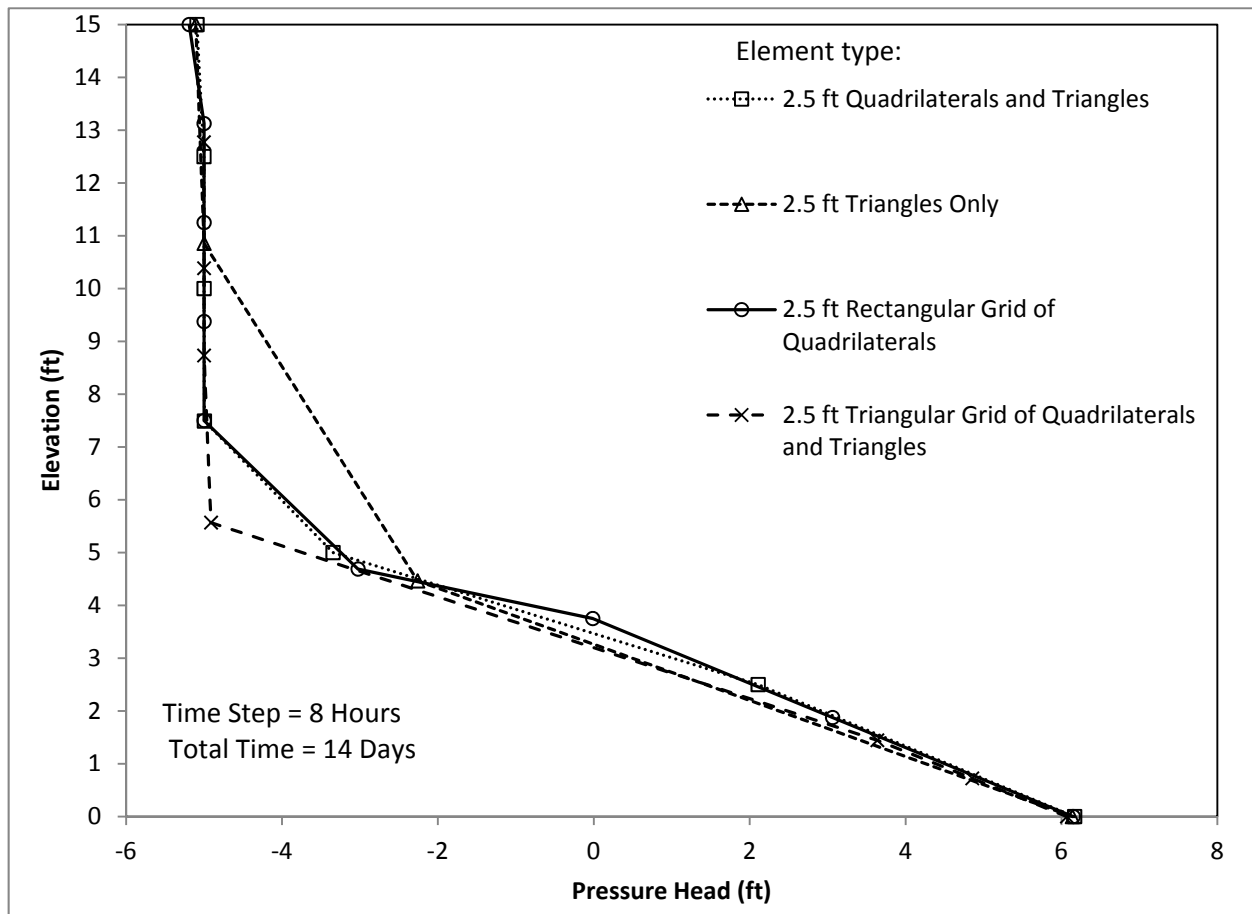
Figure 4-6 – Calculated pore pressures along centerline of levee after 14 days

The meshes produced different results for pore pressures in the portion of the levee where the pore pressures were changing most rapidly, the negative pore pressure zone. The differences were caused by the number of nodes that fell along the centerline of the levee for each different mesh. More nodes along the centerline produced more places that the pore pressure was calculated and a smoother transition between negative and positive pore pressures.

The effect of element size is further illustrated by the results shown in Figure 4-7. These results are for elements of the same type, quadrangles and triangles, but of different sizes. The three analyses shown in the figure all used the same time step of 8 hours.
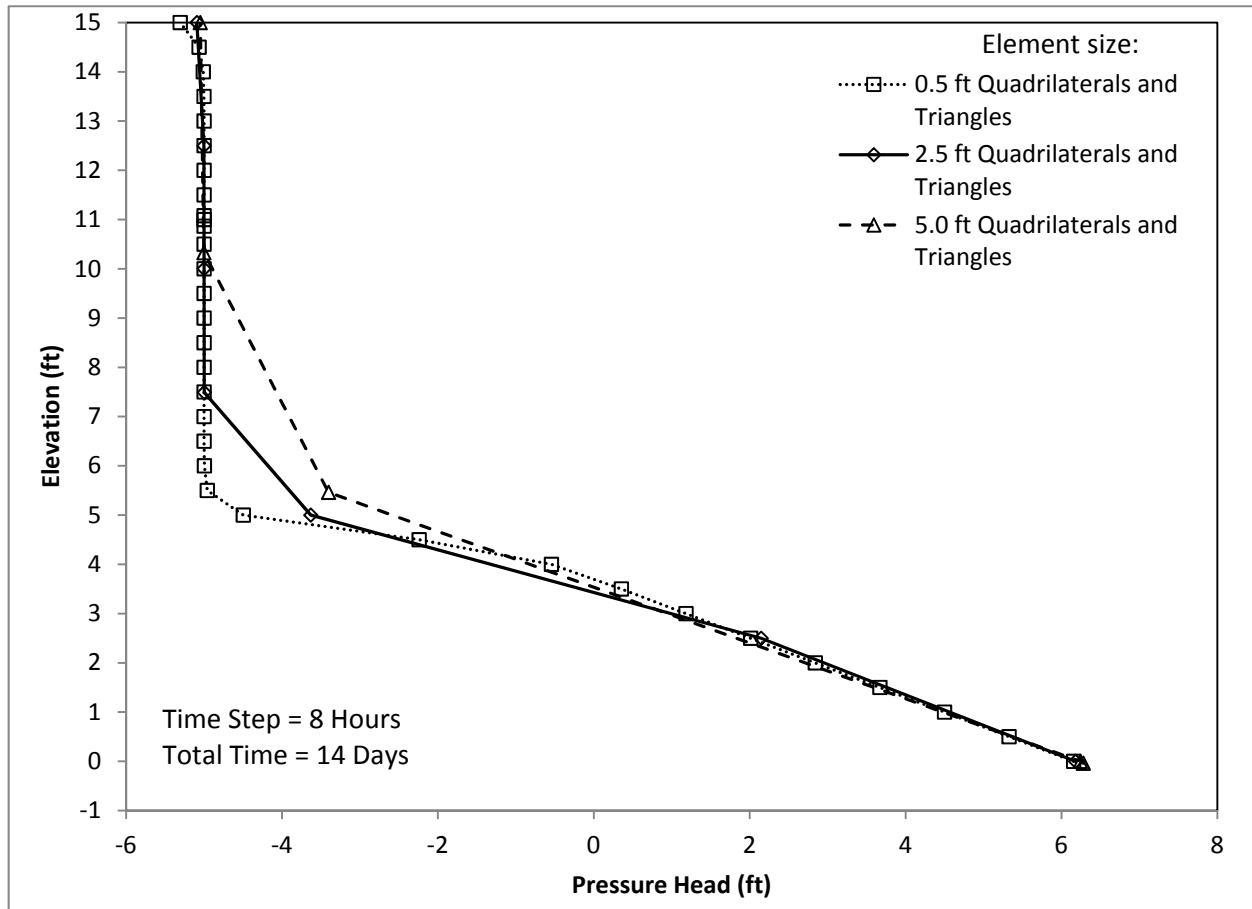
Figure 4-7 – Calculated pore pressures along centerline of levee after 14 days

Differences in pore pressures can be seen in the negative pore pressure zone. With smaller elements there are more points along the centerline of the levee, and the result is a smoother transition from negative to positive pore pressures. Smaller elements should be used in transient seepage analyses for stability if negative pore pressures are being used to determine the shear strength of the soil. More accurate estimates of negative pore pressures are achieved when the element size is small. Using smaller elements comes at the cost of computational time.

The entire line of zero pressure is shown in Figure 4-8 and Figure 4-9. There is no significant difference in the position of the line of zero pressure for different element types (Figure 4-8). As shown in Figure 4-9 for elements of different sizes, there is no difference in the position for 0.5 ft and 2.5 ft elements, and only a small difference between those and the result calculated using 5.0 ft elements.

50

2.5 ft Quadrilaterals and Triangles
2.5 ft Triangles Only
2.5 ft Rectangular Grid of Quadrilaterals
2.5 ft Triangular Grid of Quadrilaterals and Triangles
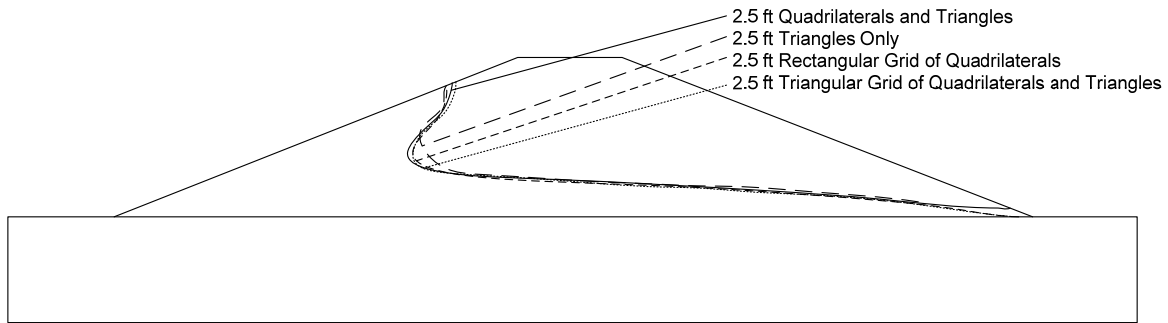
Figure 4-8 – Calculated line of zero pressure in levee after 14 days for different element types

0.5 ft Quadrilaterals and Triangles
2.5 ft Quadrilaterals and Triangles
5.0 ft Quadrilaterals and Triangles

Time Step = 8 Hours
Total Time = 14 Days
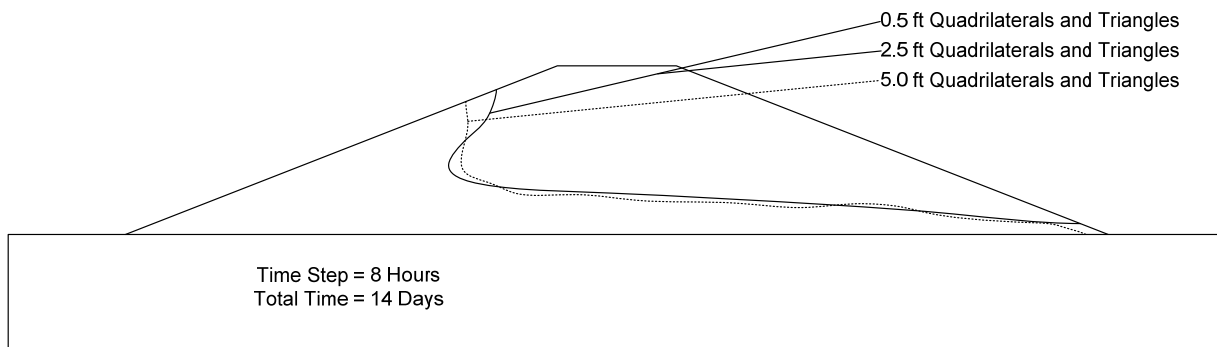
Figure 4-9 – Calculated line of zero pressure in levee after 14 days for different element sizes

Exit gradient

To examine the effects of element type, element size and time step magnitude on the calculated exit gradient for a levee, a numerical model was created of a levee on a layered foundation. The model is shown in Figure 4-10. A 15 ft high silty sand levee with 2.5 on 1 side slopes and a 10 ft crest has been constructed on a foundation of fine sand. The fine sand is differentiated into two layers based on saturated hydraulic conductivity. The upper 2 ft of the fine sand has a conductivity one order of magnitude lower than the 10 ft thick layer of fine sand below. The soil properties for the levee are the same as those shown in Figure 4-4. For different combinations of element type, element size and time step magnitude the exit gradient was calculated at the toe of the

levee using the average gradient across the top 2 ft layer and the calculated point value of the exit gradient from SEEP/W. The initial pore pressures within the levee corresponded to a hydrostatic condition with the water table at the base of the levee. At the start of the transient seepage analysis, the water level on the upstream side of the levee was raised to 15 feet. Exit gradients were calculated after 14 days of the raised water level.
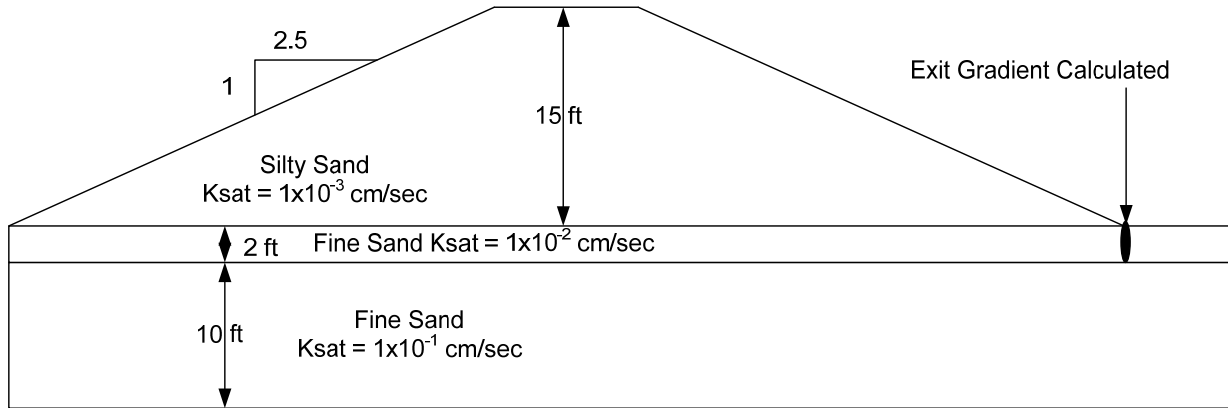
Figure 4-10 – Levee used for the numerical model case study of exit gradient

The exit gradient calculated at the toe of the levee is affected significantly by the size of the elements. The four different element sizes used in this study are shown in Figure 4-11. As the elements become smaller, the value of the point exit gradient from SEEP/W increases, because the toe of the levee is a singular point numerically, with a theoretically infinite value of hydraulic gradient. Larger values of point gradient are shown in Table 4-1 for elements of different sizes and the dame time step (2 hours). The point value of the exit gradient will continue to increase as the element size decreases. This is a correct result analytically, but is not very useful from a practical point of view. It is recommended to calculate the gradient across the entire capping, rather than using the point value, in order to avoid this difficulty.

| 5.0 ft | 2.5 ft | 0.5 ft | 0.25 ft |
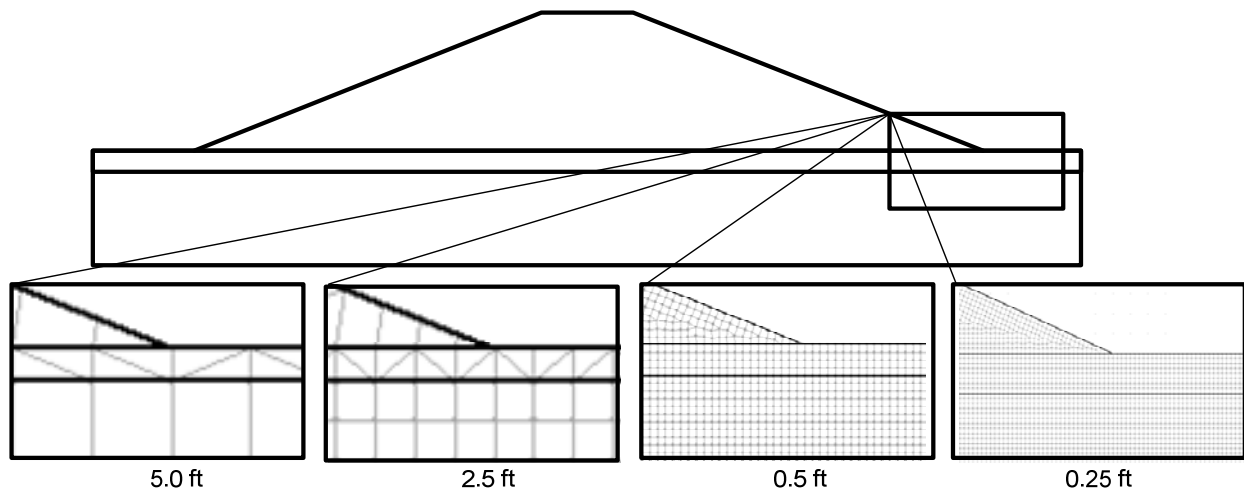
Figure 4-11 – Four different mesh sizes used to compute exit gradients at the toe of the levee

Table 4-1 – Calculated exit gradients after 14 days

Element Type	Element Size (ft)	Time Step (hours)	Calculated Gradient Across Top Layer	Calculated Point Gradient
Quads and Triangles	5	2	0.6	0.41
Quads and Triangles	2.5	2	0.68	0.48
Quads and Triangles	0.5	2	0.64	1.31
Quads and Triangles	0.25	2	0.64	1.4

The size of the elements should be appropriate for the thickness of the layer in which the gradient is calculated. When the elements used are too large, the calculated exit gradient across the layer is unstable. This is shown in Table 4-2 which shows different values of hydraulic gradient across the 2-ft thick layer depending on the time step used in the analysis. Not only is using 5-ft or 2.5-ft elements to represent a 2-ft thick layer illogical, it produces results that vary depending on the magnitude of the time step. The calculated exit gradient should be the same independent of the time step used to solve the problem. It is suggested that the maximum element size should be no more than one fourth of the thickness of the layer. This is verified in Table 4-2 as the exit gradient across the two foot thick layer does not change with time step for 0.5-ft elements.

53

Table 4-2 – Calculated gradients across the top layer after 14 days

Element Type	Element Size (ft)	Time Step (hours)	Calculated Gradient Across Top Layer
Quads and Triangles	5	1	0.68
Quads and Triangles	5	2	0.6
Quads and Triangles	5	8	0.68
Element Type	Element Size (ft)	Time Step (hours)	Calculated Gradient Across Top Layer
Quads and Triangles	2.5	1	0.6
Quads and Triangles	2.5	2	0.68
Quads and Triangles	2.5	8	0.6
Element Type	Element Size (ft)	Time Step (hours)	Calculated Gradient Across Top Layer
Quads and Triangles	0.5	1	0.64
Quads and Triangles	0.5	2	0.64
Quads and Triangles	0.5	8	0.64

Conclusions

The following conclusions from this study of transient seepage through levees provide guidance for using SEEP/W to analyze this type of problem:

- Numerical oscillations can be avoided if SEEP/W (2007) is used, with 3-node triangles and/or 4-node quadrilaterals. While it might seem likely that higher-order elements would produce more accurate results, the fact is that they produce numerical problems and less accurate results.

- The position of the line of zero pressure, the phreatic surface, within a levee is not significantly affected by element type, element size or time step magnitude, provided that the elements are no more than one-fourth the height of the levee.

- Smaller elements increase the accuracy with which negative pore pressures within a levee are calculated, but it appears that elements can be as large as one-fourth of the size of the soil region they model.

- Exit gradients should be calculated as the average across the thickness of the capping layer, using elements no larger than one fourth the thickness of the layer. In cases where there is no capping layer, the exit gradient should be calculated for the top foot of the foundation using 0.25-ft elements.

Chapter 5

Analysis of transient seepage through a half-scale levee

Introduction

Transient seepage analyses can be used to calculate the movement of water through soil with time. An important practical application of these analyses is to estimate the time required for pore pressures and hydraulic gradients to increase within a levee after rise in river level, which are needed to anticipate the likelihood that seepage through the levee may result in slope instability, erosion or piping. As the river level rises, the levee will begin to saturate from the river side toward the land side slope. Important questions regarding the possibility of stability and seepage problems due to the flood are these:

- "How far will the seepage progress during the flood?" and

- "Is it likely that a steady seepage condition will be reached during the duration of the flood?"

While these questions can be addressed through transient seepage analyses, it remains to be determined with what accuracy these analyses can be performed. The best means of examining this accuracy is by comparing calculated results with experimental results. The test performed by Worsching et al. (2006) provides the data required for such a comparison.

Worsching et al. (2006) performed tests on a 1.4-meter high silty sand levee constructed in the laboratory, raising the water level against the upstream slope and measuring the response as seepage progressed through the levee. This levee test has been modeled numerically using the finite element computer program SEEP/W, by GeoStudio (2007). Comparison of the calculated and measured results examined the effects of the initial conditions, the unsaturated

hydraulic conductivity function and the soil-water characteristic curve on the results of the analysis.

Worsching's model Levee

Worsching et al. (2006) conducted their tests on a model levee constructed in the Theodor Rehbock Laboratory at the Institute for Water and River Basin Management at the University of Karlsruhe, Germany. The levee model was 1.4m high, with 2.5 on 1 side slopes and a 1m wide crest, as shown in Figure 5-1. The model was constructed in a concrete trough with low angle sides to maintain firm contact with the trough walls (Preko et al. 2009). The experimenters were able to control the upstream water level within the trough to simulate a flood event on the upstream slope of the levee.
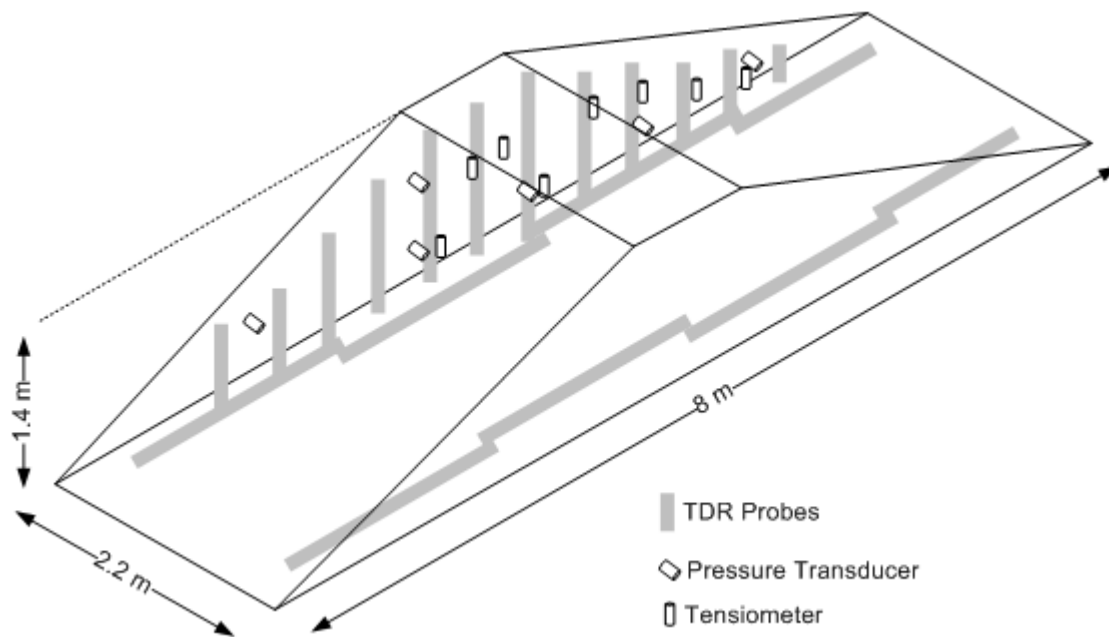
Figure 5-1 –Worsching's model levee

The simulated flood began by raising the upstream water level to 0.5m where it was held for 9 days. The water level was briefly lowered to 0.0m to correct a technical problem and afterwards was raised to 1m and held for 10 days. The water level was then slowly lowered to 0.0m over a period of 3 days. The flood hydrograph for this experiment is shown in Figure 5-2.

57
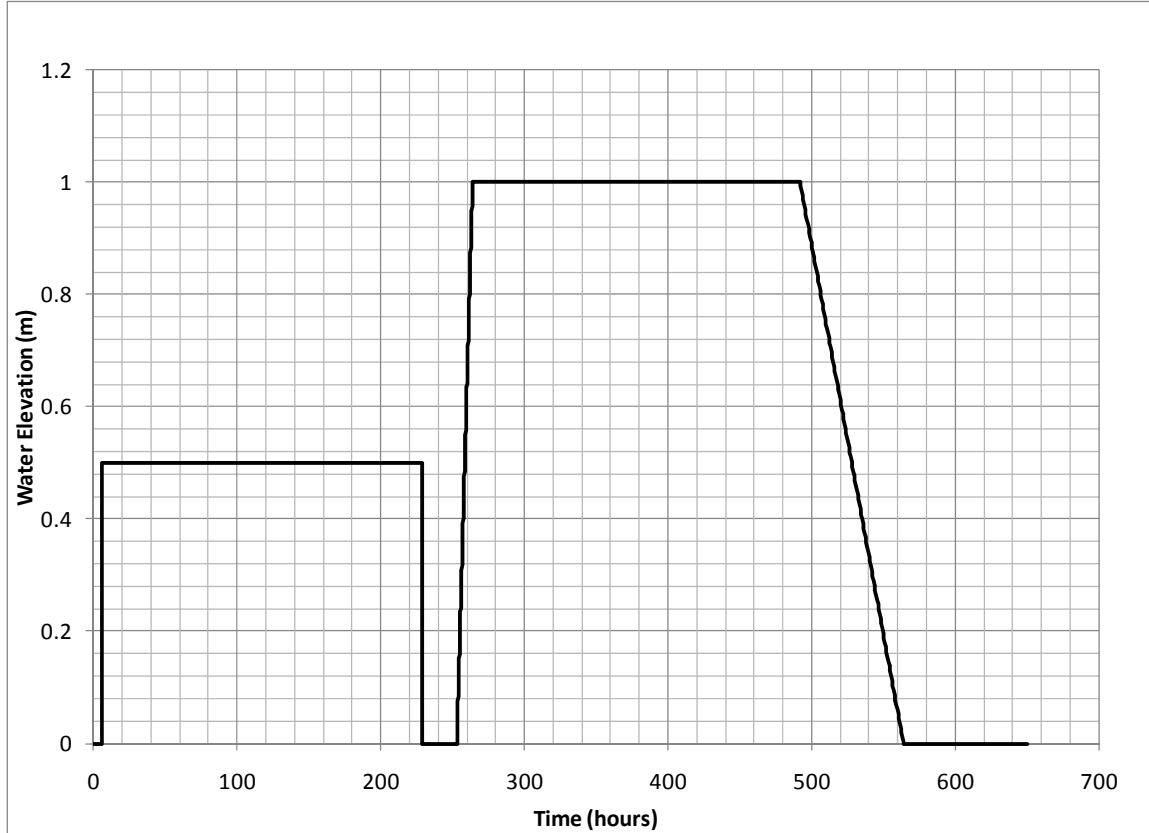
Figure 5-2 – Flood hydrograph for the levee test performed by Worsching et al. (2006)

The model levee was constructed of silty sand (Preko et al. 2009). Standard Proctor compaction tests showed that the material had a maximum dry density of 119.9 pcf with an optimum moisture content of 10.2%. The material was compacted in 13 lifts of different thicknesses, as shown in Table 5-1.

The values of relative compaction by the Standard Proctor compaction test ranged from 84% to 91%. Agrawal and Altschaeffl (1991) reported measured values of saturated hydraulic conductivity for the material as 1.4×10^{-4} cm/sec when compacted to 80% of the Standard Proctor maximum dry density, and 1×10^{-5} cm/sec when compacted to 100%.

Worsching et al. (2006) reported an average porosity of 44% for the levee fill. However, Preko et al. (2009) calculated porosity values using a measured specific gravity of solids of 2.71 by taking cylindrical samples from the levee after construction. These calculated values of porosity from Preko et al. (2009) varied from 35% to 41%, and are judged to be more reliable than the value of 44% reported by Worsching et al. (2006)

Table 5-2 shows calculated values of porosity and values of hydraulic conductivity for the levee fill from Preko et al. (2009).

Soil-water characteristic curves for the material were measured by Preko et al. (2009) on samples compacted to 92% and 100% of the Standard Proctor maximum dry density. These curves are shown in Figure 5-3. The starting point for the soil-water characteristic curve, corresponding to a soil suction = 0.01 kPa is the saturated value of volumetric moisture content, which is equal to the porosity The average relative compaction for the 13 layers of the levee is 88%, which corresponds to a porosity of 38%. Because the average porosity of the levee fill was higher than the porosities for the two experimentally derived soil-water characteristic curves, neither of the experimental curves is precisely representative of the fill as compacted in the levee, and it was necessary to estimate the soil water characteristic curve shown in Figure 5-3 for the as-compacted condition.

The soil-water characteristic curve for the as-compacted condition was estimated based on three considerations:

 (1) The saturated volumetric moisture content of the soil-water characteristic curve at zero soil suction (actually 0.01 kPa) is equal to the value of porosity, 38%.

(2) From the starting point at zero soil suction, the shape of the soil-water characteristic curve was estimated as shown in Figure 5-3, using the shape for silty sand, from the database for different soil types available in SEEP/W.

59

(3) At high values of soil suction the soil-water characteristic curve reaches a residual moisture content. At a soil suction of approximately 40 kPa. Both of the soil-water characteristic curves from Preko et al. (2009) reach a residual moisture content of about 0.07, and the estimated soil water characteristic curve was drawn through this point. The final estimated curve is shown in Figure 5-3.

Table 5-1 – Thicknesses and properties of soil layers in the model levee (after Preko et al. 2009)

Soil layer	Soil layer thickness (m)	Depth from crest (m)	Dry unit weight (pcf)	Proctor Relative Compaction	Porosity
1 (crest)	0.115	0.115	100.5	84%	0.41
2	0.11	0.225	100.5	84%	0.41
3	0.105	0.33	104.2	87%	0.39
4	0.11	0.44	104.8	88%	0.38
5	0.11	0.55	103.6	86%	0.39
6	0.12	0.67	105.5	88%	0.38
7	0.115	0.785	107.3	90%	0.36
8	0.11	0.895	104.8	88%	0.38
9	0.1	0.995	108.6	91%	0.35
10	0.085	1.08	108.0	90%	0.36
11	0.12	1.2	108.0	90%	0.36
12	0.085	1.285	105.5	88%	0.36
13	0.115	1.4	102.3	85%	0.40
		Average	104.9	88%	0.38

Table 5-2 – Densities, porosities and hydraulic conductivity values for the model levee fill

Proctor Relative Compaction (%)	γ_d (g/cm^3)	γ_d (pcf)	Porosity	k (cm/sec)
100%	1.92	119.8	0.29	1.00E-05
95%	1.82	113.8	0.33	
92%	1.77	110.2	0.35	
90%	1.73	107.8	0.36	
88%	1.69	105.4	0.38	1.00E-04 (estimate for model)
85%	1.63	101.8	0.40	
80%	1.54	95.8	0.43	1.40E-04
75%	1.44	89.9	0.47	
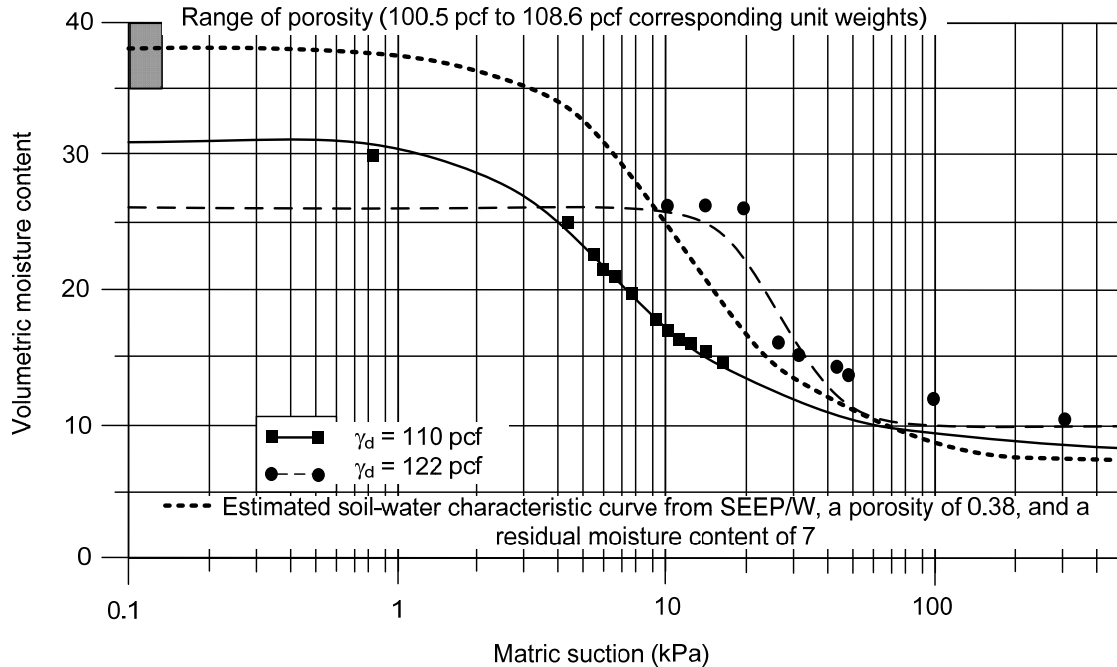
Figure 5-3 – Soil-water characteristic curves measured by Preko et al. (2009), together with the estimated curve for porosity of 38%.

Instruments installed in the model levee

Twenty insulated flat-ribbon time-domain refloctometry (TDR) probes were placed in the levee to measure changes in volumetric moisture content with time as the levee was subjected to the flood events,. These probes were installed during placement and compaction of the levee fill, and each new layer was compacted around the TDR probes. TDR probes measure the water content of soils indirectly, using the principle that the dielectric number of water is much larger than the dielectric number of the soil (Worsching et al. 2006). If the dielectric number of the soil's solid constituents is known, then the water content of the soil can be calculated from the measured dielectric number.

The position of the phreatic surface during the flood was monitored with tensiometers and pressure transducers installed within the levee at the locations shown in Figure 5-1.

SEEP/W analysis of the model levee test

The levee test was analyzed numerically using the finite element computer program SEEP/W from GeoStudio (2007). The finite element mesh used in the analyses is shown in Figure 5-4. The mesh contains 658 elements and 713 nodal points. The mesh was generated in SEEP/W by specifying that it should draw "global" (or average) element sizes of 0.1 m using a combination of quadrilaterals and triangles. The nodes along the base are no-flow nodes, consistent with the fact that the model was built on a concrete base.

The external boundaries of the finite element mesh are the same as those of the physical model. In the physical model the water level was raised on the upstream slope of the levee to simulate two flood events. To model this numerically using SEEP/W, a boundary function was used along the upstream slope of the levee. This function is the flood hydrograph shown in Figure 5-2. In SEEP/W this type of function is called a total head versus time function.
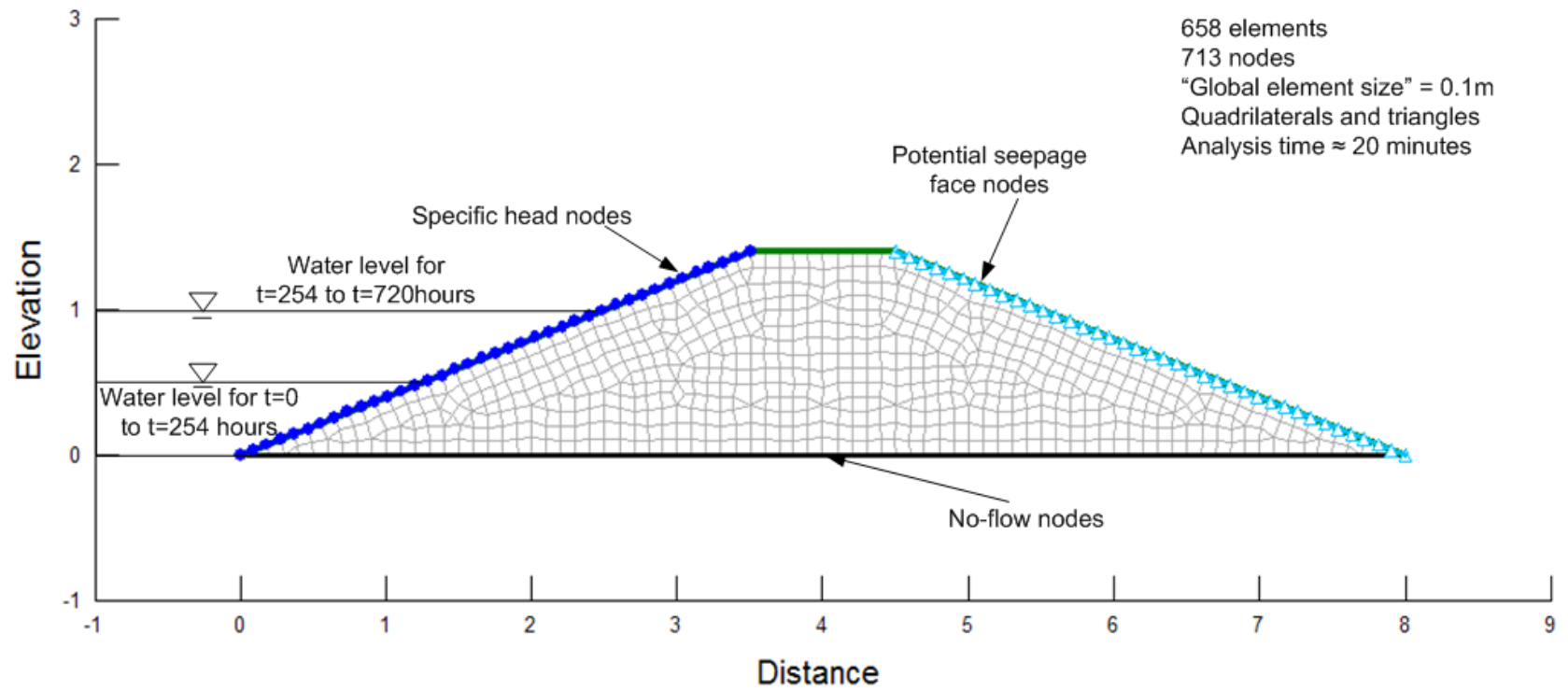
Figure 5-4 – Finite element mesh used for the SEEP/W model of the scaled levee test

The soil properties used in the transient seepage analysis are shown in Table 5-3. This table also shows the methods used to calculate or estimate the properties. The saturated hydraulic conductivity measured in the laboratory by Preko et al. (2009) was reported as 1×10^{-5} cm/sec when the material was compacted to 100% relative compaction and 1.4×10^{-4} cm/sec when the material was compacted to 80% relative compaction. As discussed previously the average value of relative compaction for the 13 layers of the levee fill was 88%. The conductivity value used in the first analysis was 1.0×10^{-4} cm/sec, which is between the values of conductivity measured at 80% and 100% relative compaction. This is also the value of conductivity reported by Worsching et al. (2006).

Using the estimated soil-water characteristic curve, the unsaturated hydraulic conductivity function shown in Figure 5-4 was estimated using the Van Genuchten (1980) transformation available in SEEP/W. SEEP/W has two different transformations that can be used to develop unsaturated hydraulic conductivity functions: the Van Genuchten (1980) transformation, and the Fredlund and Xing (1994) transformation. These transformations estimate the shape of the unsaturated hydraulic conductivity function based on the value of saturated hydraulic conductivity and the shape of the soil-water characteristic curve. The soil-water characteristic curve and the unsaturated hydraulic conductivity function are closely related because both are functions of the pore space distribution within a soil. One hydraulic conductivity function was constructed for the estimated saturated hydraulic conductivity and two more were estimated for values of saturated hydraulic conductivity one order of magnitude higher and lower. These three hydraulic conductivity functions are shown in Figure 5-4.

Table 5-3 – Soil properties used in the SEEEP/W model of Worsching's levee test

Soil Parameter	Value	Method
Saturated hydraulic conductivity	See Table 5-2	Estimated from measured values of hydraulic conductivity at 80% and 100% relative compaction. Levee soil was compacted to 88% relative compaction.
Soil-water characterisitc curve	See Figure 5-3	1. Starting point at zero soil suction is equal to the calculated value of porosity at 88% relative compaction (0.38)
		2. Shape of curve from silty sand in SEEP/W database
		3. End of curve at high soil suction values is equal to the residual moisture content from the two measured curves by Preko et al. (2009)
Unsaturated hydraulic conductivity function	See Figure 5-4	Estimated using the Van Genuchten (1980) transformation model and the saturated hydraulic conductivity
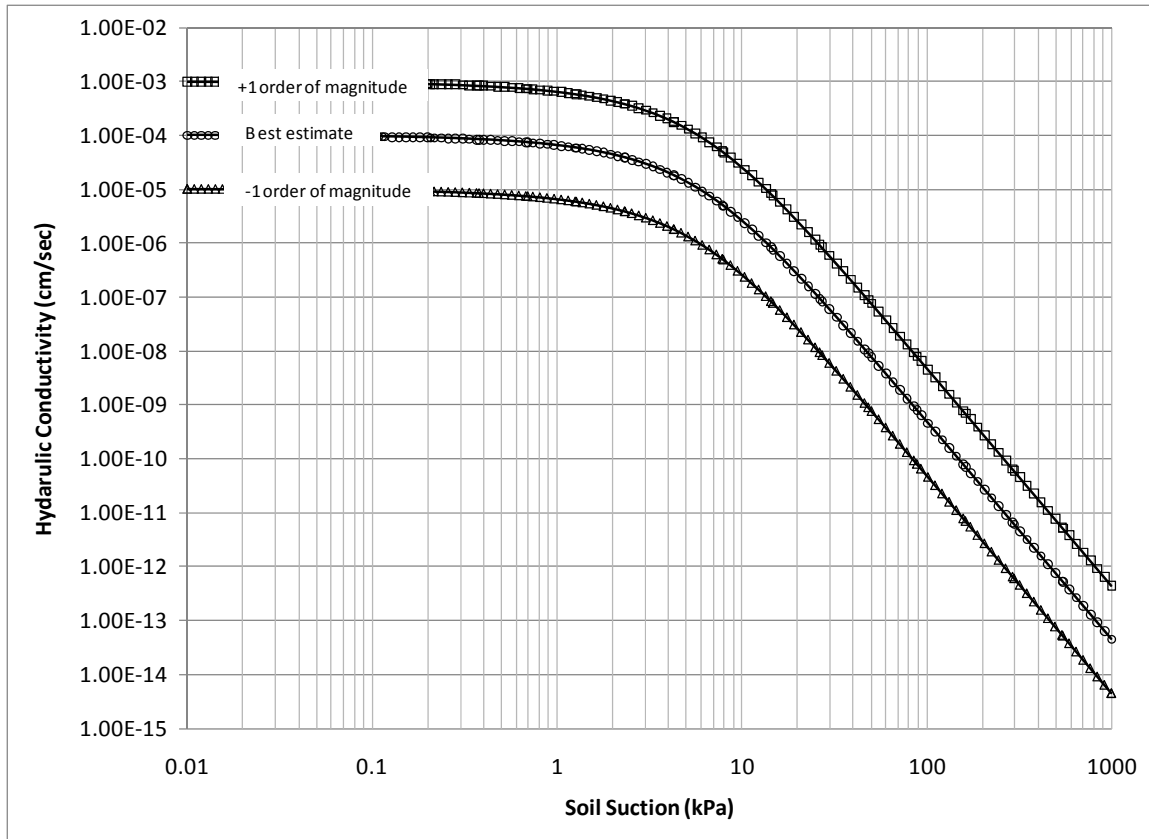
Figure 5-5 –Estimated unsaturated hydraulic conductivity function for the model levee fill

Transient seepage through the model levee was analyzed using the finite element mesh, the properties of the levee fill, and the boundary conditions discussed earlier. Time steps of 6 hours were used for analysis of the two flood events, which lasted 28 days (672 hours) in total. The analysis took 20 minutes on a Dell Latitude laptop computer.

Comparison of measured and calculated results

Figure 5-6 shows the initial conditions within the model levee before the flood. The measured initial volumetric moisture contents within the levee varied between 0.08 and 0.17 with an average value of 0.14. These initial moisture contents were replicated in the SEEP/W model using a spatial pressure distribution, or point-by-point distribution of soil suction values.

From the soil moisture characteristic curve shown in Figure 5-3, the values of soil suction corresponding to each measured value of volumetric moisture content was determined, and these values were used as the initial conditions for the analysis.

To compute the values of volumetric water content shown in Figure 5-6, the data for the estimated soil-water characteristic curve from SEEP/W was exported to the computer program RETC (US Soil Salinity Laboratory 2009), a code for calculating hydraulic functions for unsaturated soils. The program used the following equation from VanGenuchten (1980) to calculate values of degree of saturation for the specified values of soil suction:

$$S_e = \left[1 + \left(\alpha h \right)^n \right]^{-m}$$ **Eq. 5-1**

Where: S_e = degree of saturation (%), h = soil suction in terms of pressure head (m), α = a fitting parameter with units of m^{-1}, and n and m = dimensionless fitting parameters. The values of α, n and m were determined by RETC based on the shape of the soil-water characteristic curve. These values are shown in Table 5-4.

Table 5-4 – Values of a, n and m determined by the computer program RETC

VanGenuchten fitting equation constants	Values determined by RETC for the soil-water characteristic curve
α	0.0079 meters^{-1}
n	1.5239
m	1.2194

The VanGenuchten equation for the soil-water characteristic curve was used to determine the values of soil suction corresponding to the spatial pressure

distribution, resulting in the same initial volumetric moisture content values as in the levee test. Linear interpolation between the point values of the spatial pressure distribution produced initial conditions very similar to those in the levee test, as may be seen in Figure 5-6.

The water level on the upstream side of the model levee was raised and lowered and raised again to simulate the flood hydrograph shown in Figure 5-2. The results of both the levee test and numerical model after 354 hours of the simulated flood event are shown in Figure 5-7.

As shown in Figure 5-7, the SEEP/W results agree reasonably well with measured behavior, especially considering the fact that it was necessary to estimate the hydraulic conductivity and the soil water characteristic curve for the analysis. The calculated results differ from the measurements in these regards:

1. The measured position of the phreatic surface indicated by the tensiometers and the pressure transducers is farther downstream than the calculated position of the zero pressure line, and

2. The TDR measurements indicated a zone of complete saturation at elevation 0.3 meters even farther downstream than shown by either the tensiometer and pressure transducers or the calculations.

Although there is reasonable agreement between the results of the analysis and the measurements, it is of interest to determine through back analysis what property values would result in better agreement. Such results will provide better understanding of the sensitivity of the analysis to changes in values of the input parameters. To examine these factors, six additional analyses were performed, varying the hydraulic conductivity and the initial volumetric moisture content before the flood loading. These six parametric analyses were:

1. Saturated hydraulic conductivity increased by a factor of 1.5, and a corresponding change in the hydraulic conductivity function.
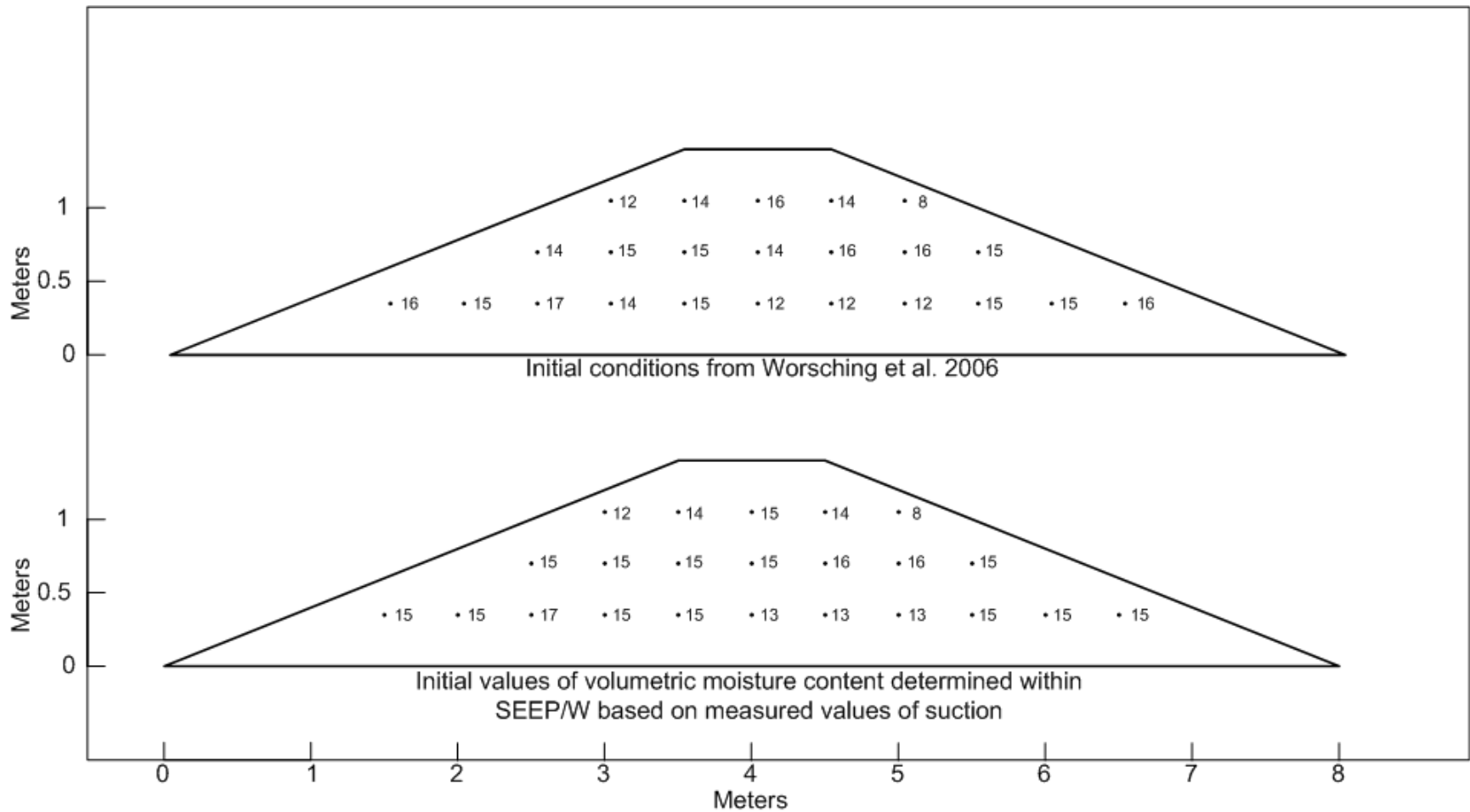
Figure 5-6 – Initial volumetric water contents from Worsching et al. (2006) and those calculated in SEEP/W using point-by-point measured values of soil suction
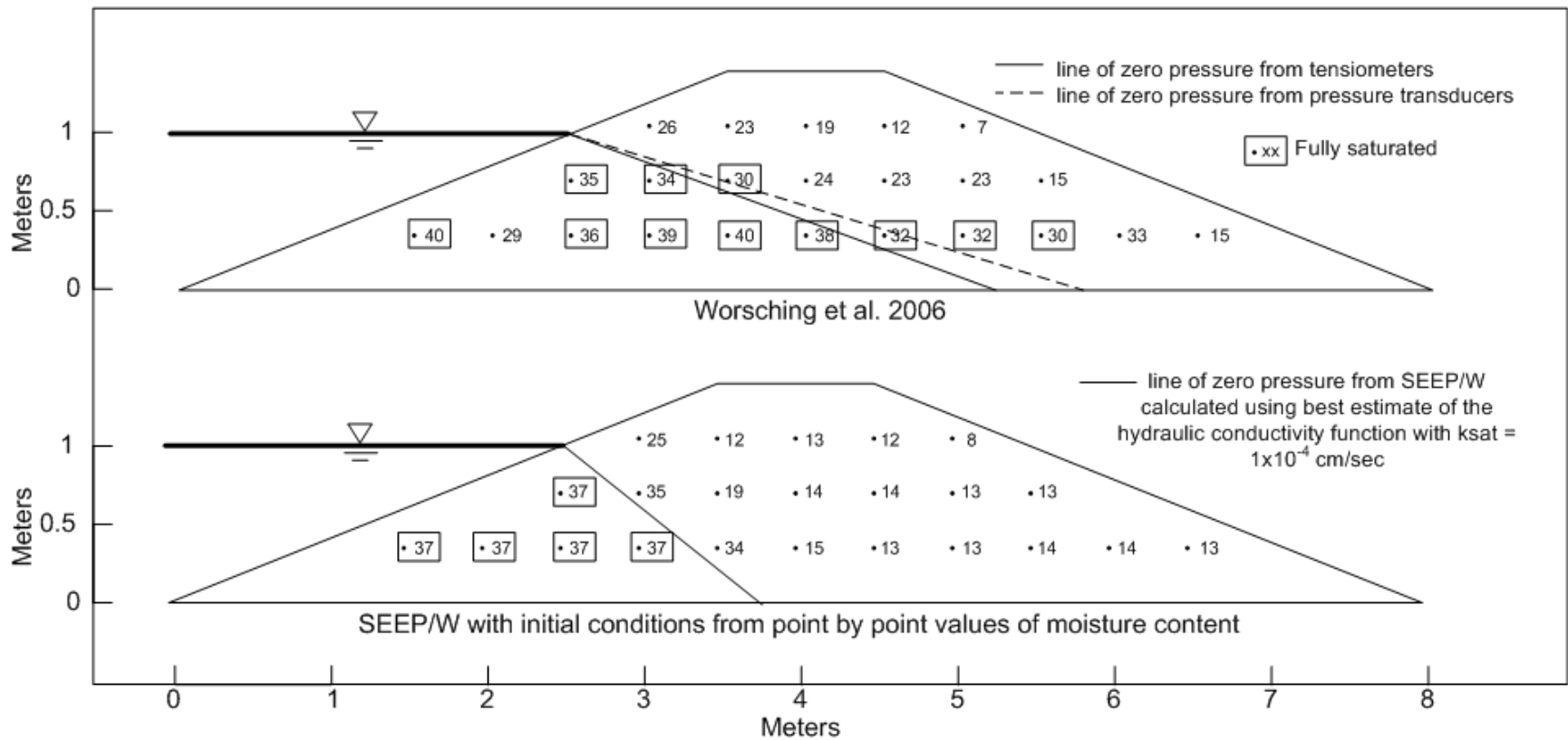
Figure 5-7 – Volumetric water contents and lines of zero pressure after 354 hours from the model test and the finite element analysis

2. Saturated hydraulic conductivity increased by a factor of 3.0, and a corresponding change in the hydraulic conductivity function.

3. Saturated hydraulic conductivity increased by a factor of 5.0, and a corresponding change in the hydraulic conductivity function.

4. Higher volumetric water contents in a zone at elevation 0.6 m.

5. Assigned layer of higher hydraulic conductivity at elevation 0.3 meters.

6. Uniform initial volumetric moisture content equal to 14% rather than point by point initial values of volumetric moisture content.

The results of these parametric variations in parameter values are shown in Figure 5-8 through Figure 5-14, and are discussed in the following paragraphs.

Effects of increased hydraulic conductivity

The variations in parameters involved increasing the saturated and the unsaturated hydraulic conductivity of the levee fill. Three such analyses were performed, increasing the saturated hydraulic conductivity by factors of 1.5, 3.0, and 5.0. The results of these analyses are shown in Figure 5-8, 5-9, and 5-10. It can be seen that to achieve a close match between the calculated and the measured positions of the phreatic surface, it was necessary to increase the hydraulic conductivity by a factor of 5.0.

Considering the fact that it is seldom possible to estimate values of hydraulic conductivity with accuracy better than an order of magnitude, this result seems reasonable. This result also indicates what accuracy can be expected of transient seepage analyses, which inevitably involve values of hydraulic conductivity that cannot be expected to be more accurate than an order of magnitude.
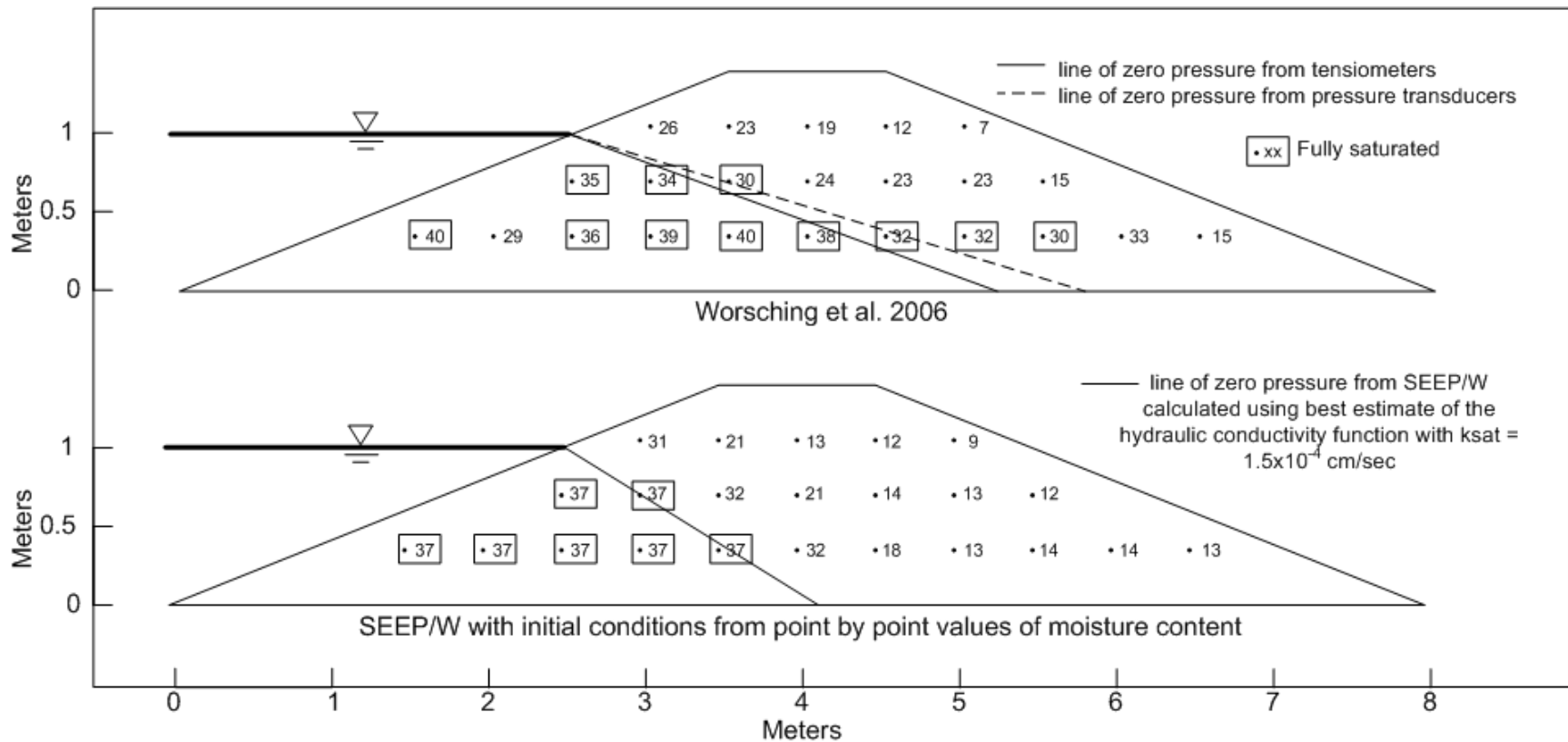
Figure 5-8 – Volumetric water contents and lines of zero pressure after 354 hours from the model test and the finite element analysis after increasing the saturated hydraulic conductivity by 1.5 x to 1.5 x 10^{-4} cm/sec
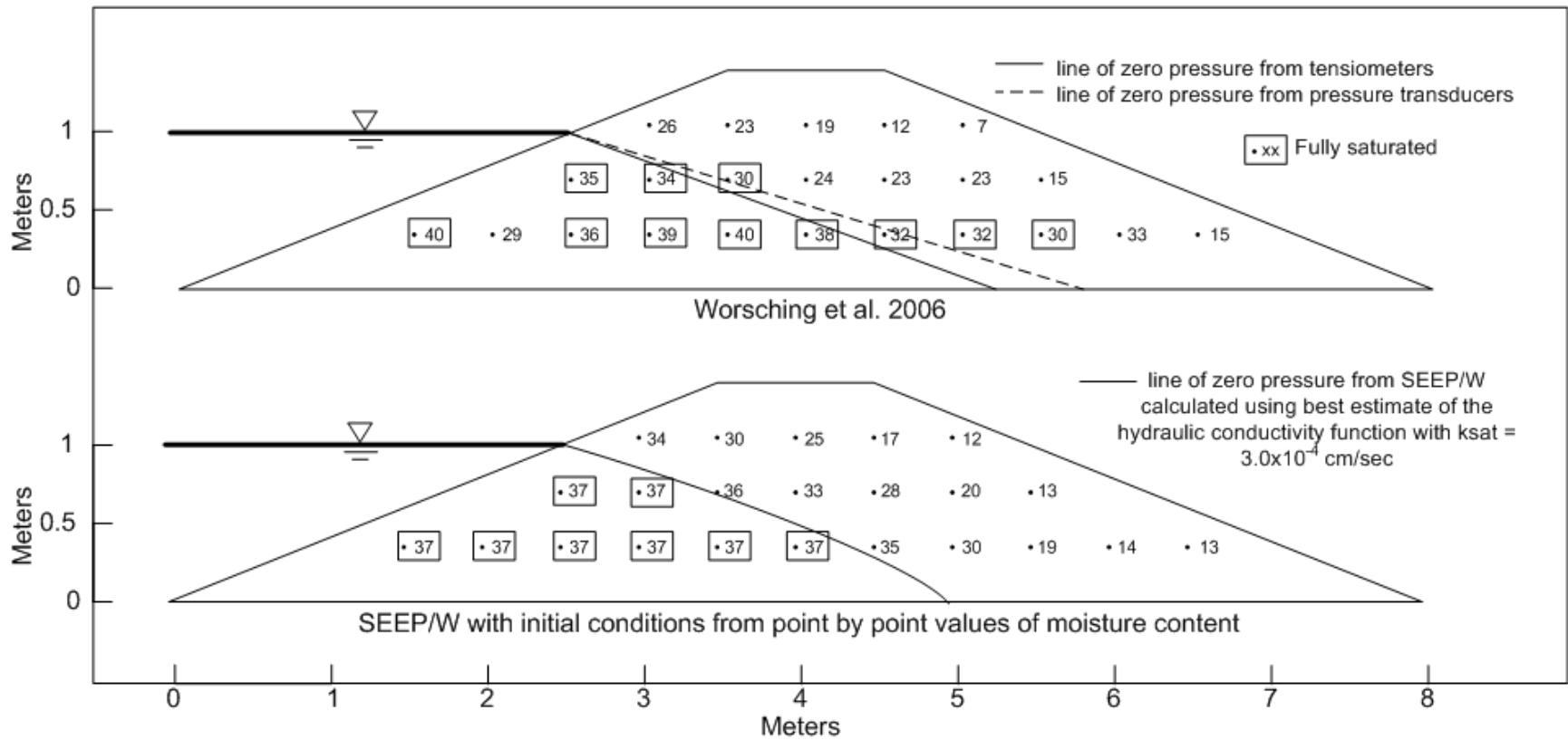
Figure 5-9 – Volumetric water contents and lines of zero pressure after 354 hours from the model test and the finite element analysis after increasing the saturated hydraulic conductivity by 3.0 x to 3.0 x 10^{-4} cm/sec
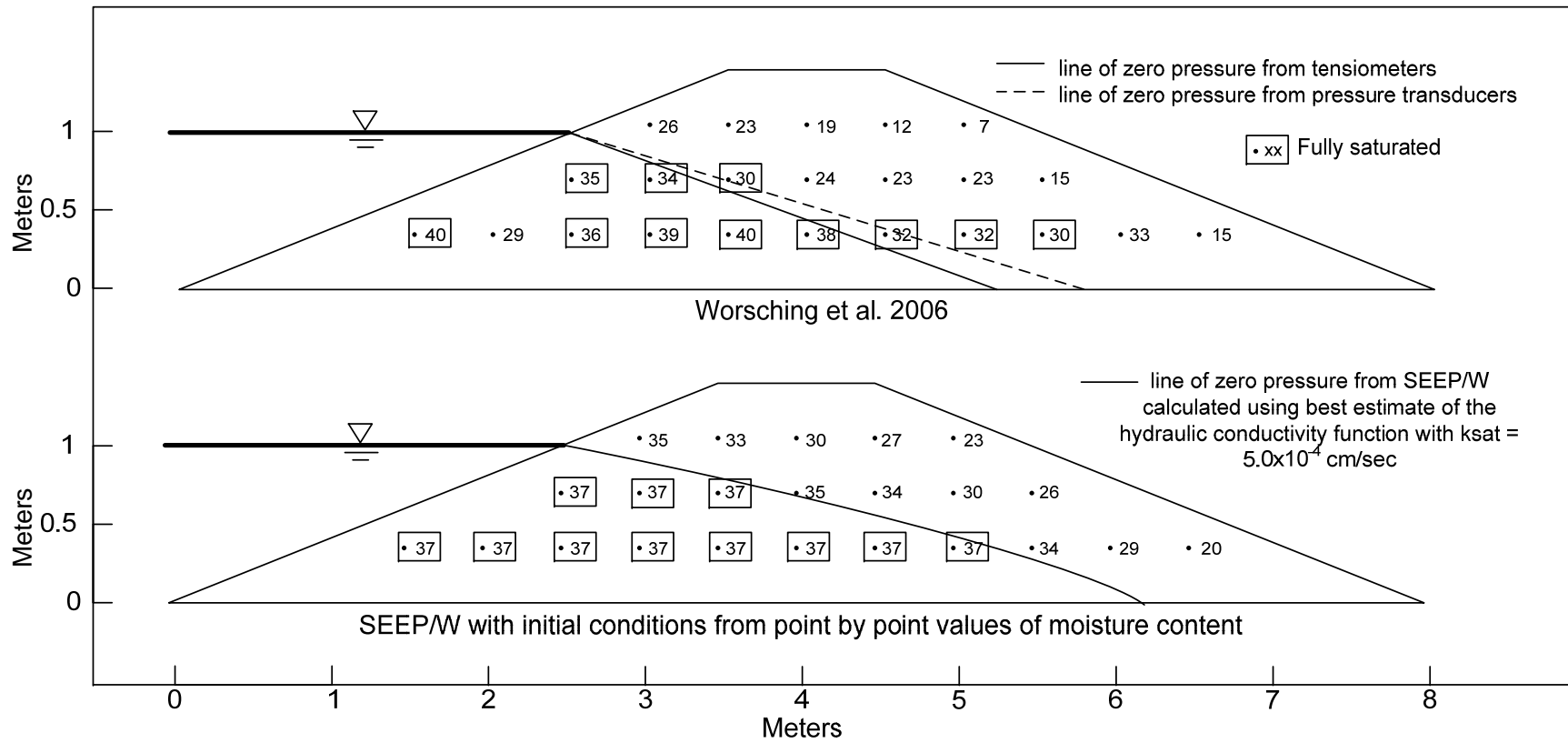
Figure 5-10 – Volumetric water contents and lines of zero pressure after 354 hours from the model test and the finite element analysis after increasing the saturated hydraulic conductivity by 5.0 x to 5.0 x 10^{-4} cm/sec

Effects of higher volumetric water contents in a zone at elevation 0.6 meters

An evaluation was conducted with a 'seeded' zone of higher volumetric moisture content for the initial condition at an elevation of 0.6m (Figure 5-11). The zone was assigned a volumetric moisture content of approximately 25.0% for the initial condition while the other assigned moisture contents remained the same as those reported by Worsching et al. (2006).

The zone of higher moisture content (25%) in the levee has an unsaturated conductivity of $2.7X10^{-6}$ cm/sec. The surrounding levee material with an average moisture content of 0.14 has a significantly lower conductivity, $8.7X10^{-8}$ cm/sec. When the transient seepage analysis is conducted, the zone of high moisture content will be able to move water faster than the surrounding material.

The transient seepage analysis was conducted for this model to see if the results would replicate the horizontal propagation of the wetting front found in the half-scale levee test. The results are shown in Figure 5-12 after 354 hours of the simulated flood.

As soon as the analysis was started in the numerical model, unsaturated flow occurred from the zone of higher moisture content to the adjacent zones of lower moisture content. By the time that the flood wave had risen on the upstream slope and began to enter the levee, the hydraulic conductivity within the high moisture content zone had decreased due to the unsaturated flow out of this zone. At the decreased moisture content the hydraulic conductivity of the zone is no longer significantly higher than the surrounding materials, resulting in no concentrated horizontal flow. Comparing the 'seeded' model and the model without the 'seeded' zone of higher moisture content, the wetting front is in nearly the same position. If there are suspected zones in levees with higher moisture contents than the surrounding soil, modeling by increasing the initial value of moisture content is not likely to have much effect because as the model starts to run, the zone of high moisture content will dissipate.
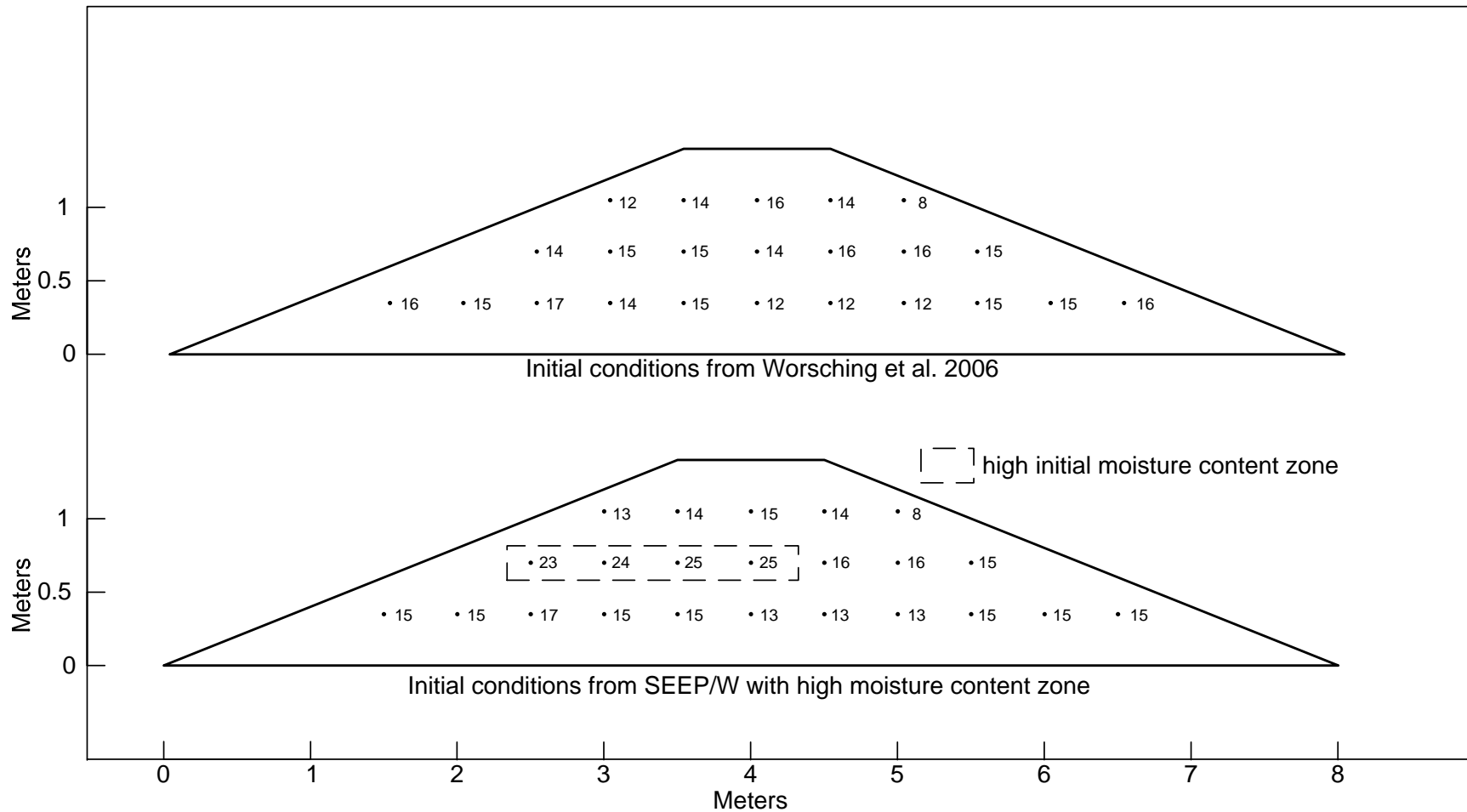
Figure 5-11 – Initial volumetric moisture contents from Worsching et al. (2006) and those calculated in SEEP/W using point-by-point measured values of soil suction with arbitrarily higher volumetric water contents in a zone at elevation 0.6 m
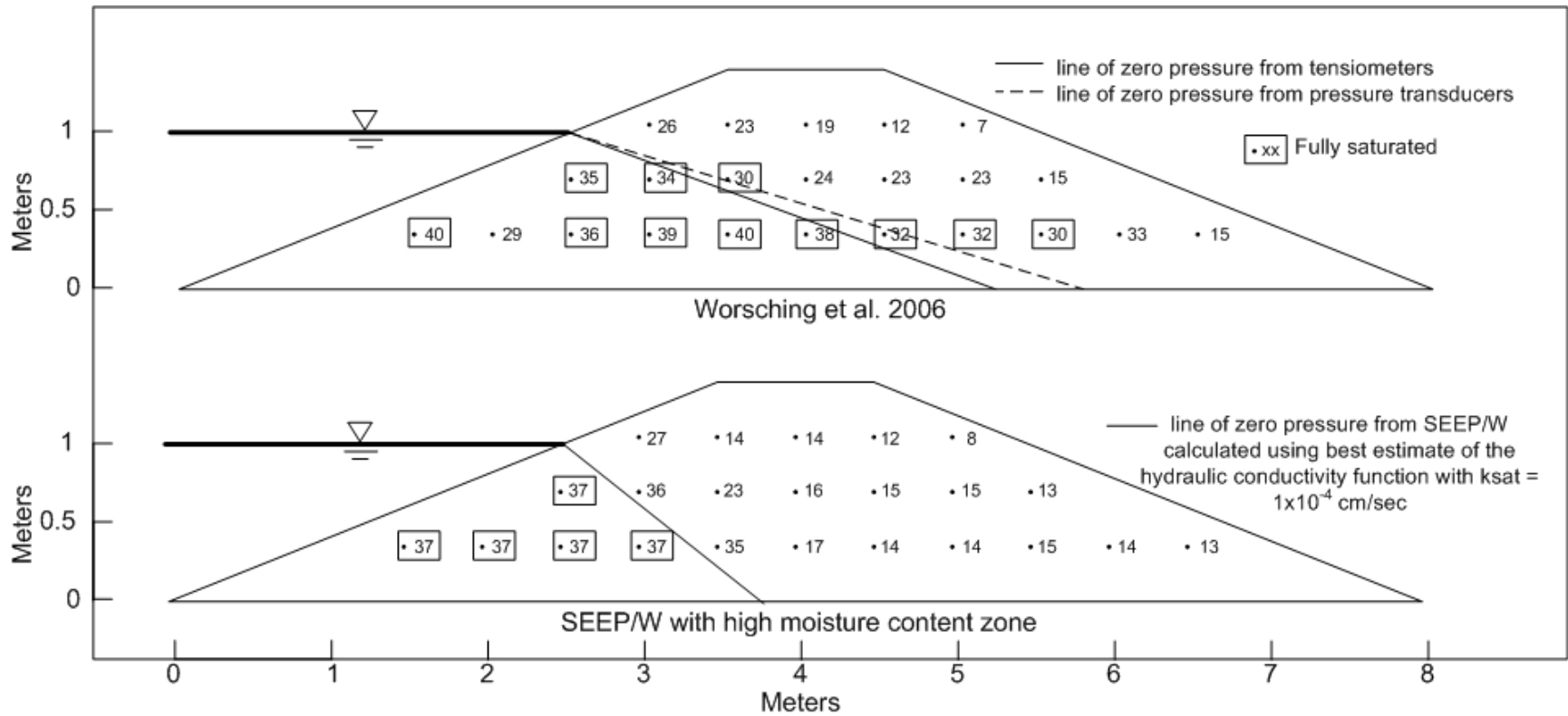
Figure 5-12 – Volumetric moisture contents after 354 hours from Worsching et al. (2006) and those calculated in SEEP/W using point-by-point measured values of soil suction for initial values with arbitrarily higher volumetric water contents in a zone at elevation 0.6 m

Effects of higher hydraulic conductivity in a zone at elevation 0.3 meters

A numerical model was created using a 0.1m thick layer with a higher saturated hydraulic conductivity placed at 0.3m above the base of the levee. The saturated hydraulic conductivity of the levee soil was 1×10^{-4} cm/sec. The hydraulic conductivity value of the layer is one order of magnitude greater than the surrounding soil, 1×10^{-3} cm/sec. This model was run to see if the analysis would replicate the horizontal progression of the wetting front observed in the half-scale levee test conducted by Worsching et al. (2006). The results of this model after 354 hours of the simulated flood are shown in Figure 5-13.

By comparison with Figure 5-7, it can be seen that even a thin layer of higher hydraulic conductivity can results in appreciable faster rate of saturation within a levee. Steady state conditions will be reached faster in levees which contain layers with high conductivity. If there is high variability in borrow material, steady state seepage conditions may be reached faster than if the levee was of homogeneous.
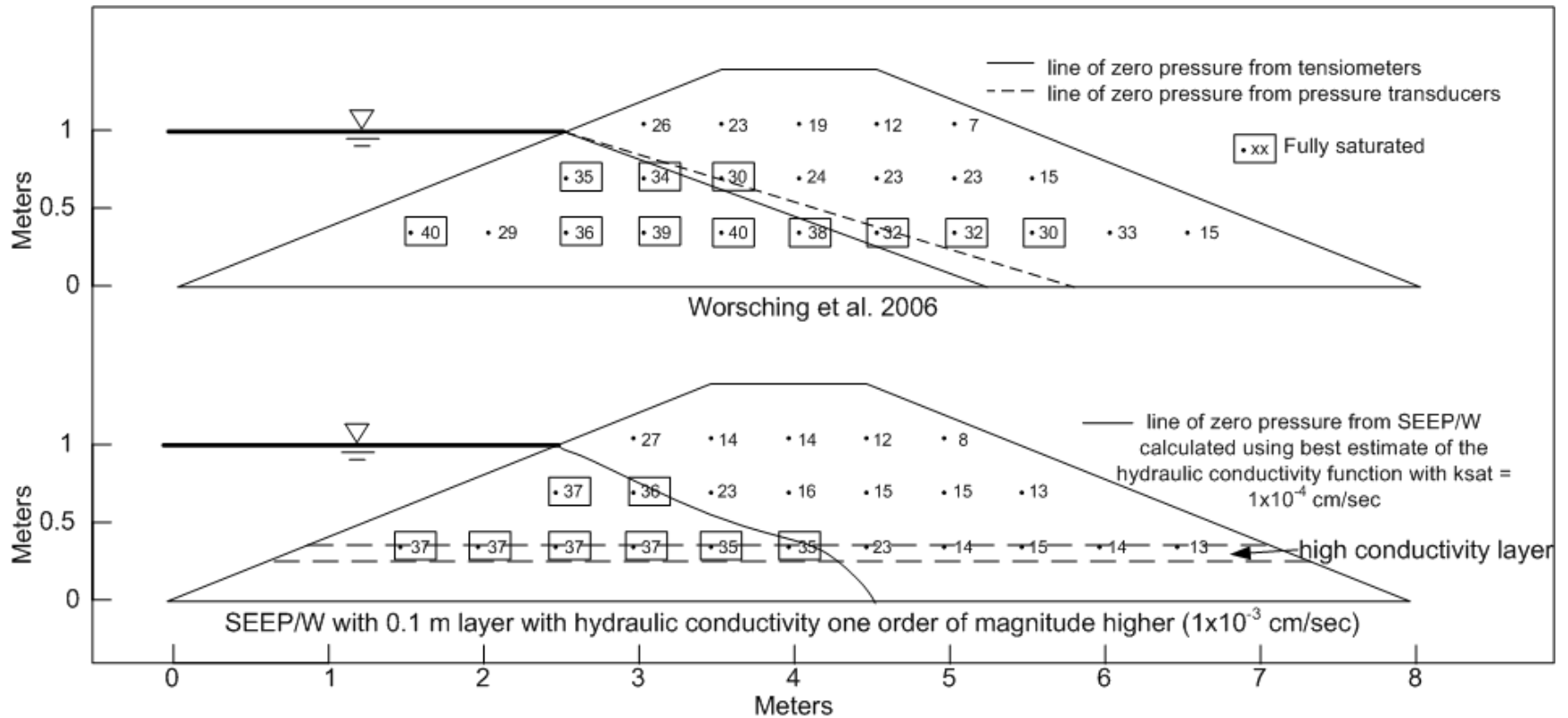
Figure 5-13 – Volumetric moisture contents after 354 hours from Worsching et al. (2006) and those calculated in SEEP/W using point-by-point measured values of soil suction for initial values with an arbitrarily assigned layer of higher hydraulic conductivity at elevation 0.3 m

Effects of uniform initial volumetric moisture content rather than point by point initial values of volumetric moisture content.

The half-scale levee was constructed in lifts with the soil near the optimum moisture content. The initial moisture contents measured in the levee before the start of the test varied from 8% to 17% corresponding to -2% and +7% of optimum moisture content of 10%. Levees constructed in the field will have similar or greater variability of moisture content after construction. Accurately predicting the variation of the moisture content to produce such a detailed initial condition as shown in Figure 5-6 would be very difficult or impossible. To model levees without the in situ measurements of moisture content, a uniform value of moisture content is likely to be the only practical alternative.

The average value of volumetric moisture content from the half-scale levee test was 14%. A numerical model was constructed in SEEP/W using 14% as the initial value of volumetric moisture content throughout the cross section to see if the results would vary significantly from the results using the point by point measurements of moisture content. As shown in Figure 5-14, a uniform value of moisture content does not significantly affect the results of the numerical model, and it still closely matches the results from Worsching et al. (2006). For transient seepage analyses of levees recently constructed in the field, using a uniform value of volumetric moisture content estimated from the compaction moisture content for the initial condition would be expected to produce results similar to those obtained using point by point measurements of moisture content.
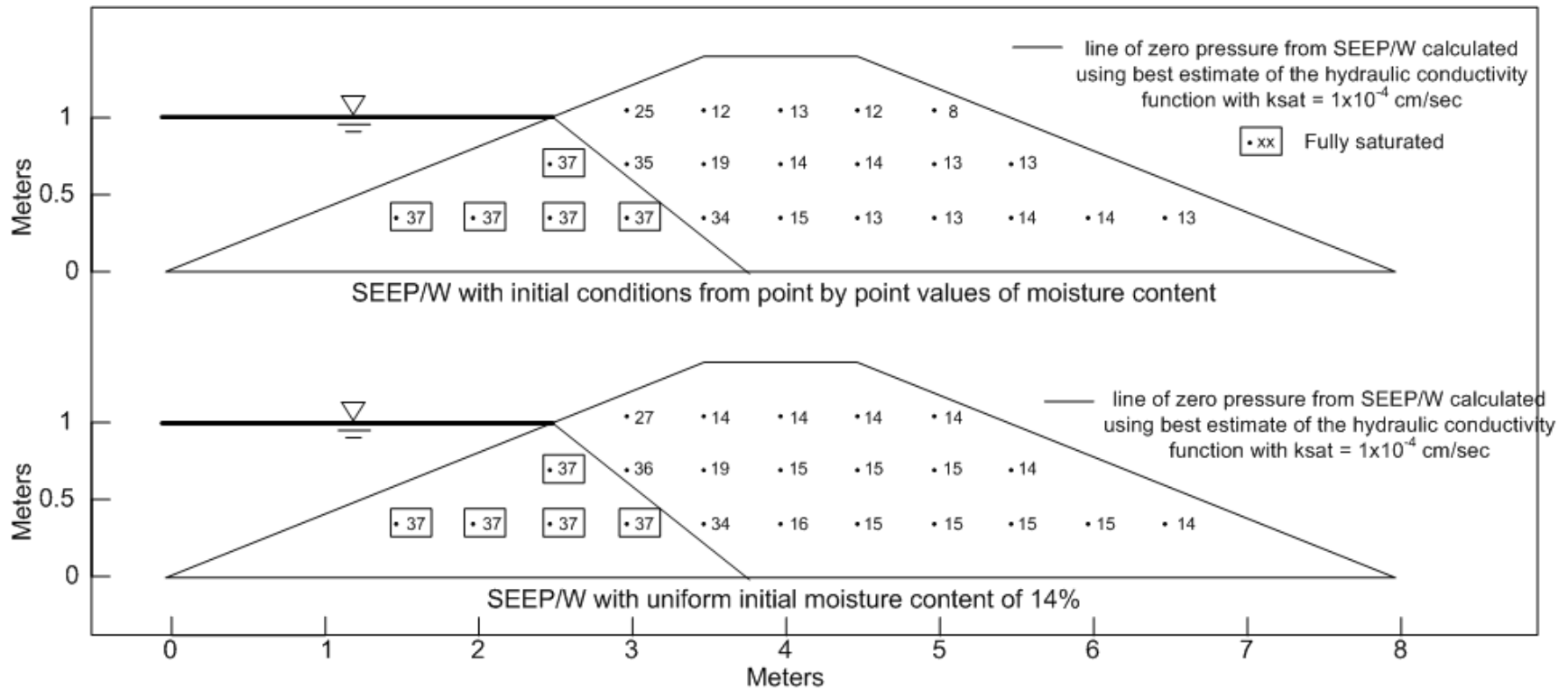
Figure 5-14 – Comparison of the half-scale levee test and the SEEP/W numerical model using a uniform value of volumetric moisture content of 14% for the initial condition and using point by point values of the volumetric moisture content after 354 hours of the simulated flood test

Conclusions

The physical model test performed by Worsching et al. (2006) was replicated numerically using the finite element computer program SEEP/W by GeoStudio using reasonable estimates of the soil properties. It was found that the results of the numerical analyses compared well with the numerical results. The largest contributing factor to the rate of propagation of the phreatic surface during the transient seepage analysis was the value of saturated hydraulic conductivity.

From the parametric study conducted it was found that:

- By increasing the value of the saturated hydraulic conductivity by a factor of 5.0 from the value based on laboratory testing, the results of the physical and numerical models were nearly the same.

- Increasing the initial volumetric moisture content for a zone within the levee did not significantly affect the results of the numerical analysis.

- Small zones of high saturated hydraulic conductivity can significantly affect the rate of propagation of the phreatic surface.

- It is appropriate to use an average value of initial volumetric moisture content of a levee as the initial condition, rather than attempting to estimate point by point variations.

Chapter 6

Proposed methods of determining soil-water characteristic curves and hydraulic conductivity functions

Introduction

The soil-water characteristic curve is a non-linear, highly variable curve that depends on a number of properties and conditions. There are numerous laboratory and empirical methods to determine the soil-water characteristic curve. These methods are described here briefly before the introduction of a new method to determine the soil-water characteristic curve in Chapter 7

The soil-water characteristic curve

Numerous researchers have presented methods of measuring or predicting the soil-water characteristic curve. A summary of the methods that can be used to determine the soil-water characteristic curve are shown in Figure 6-1.
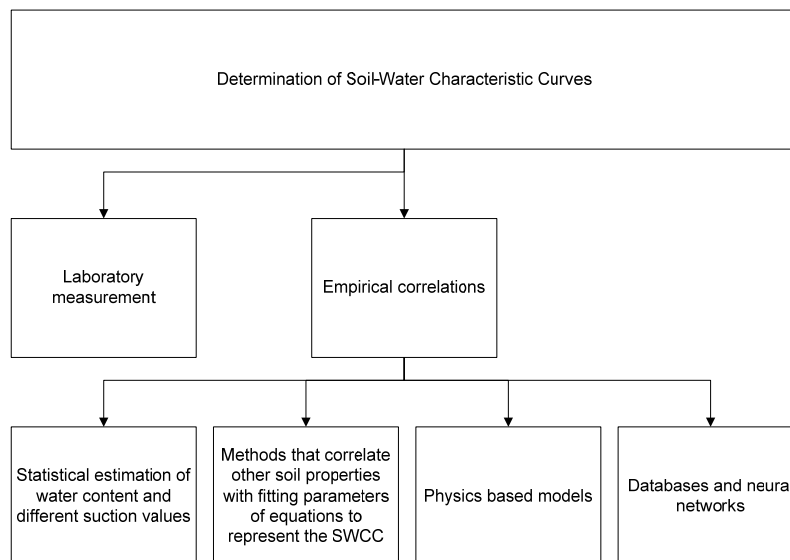
Figure 6-1 – Methods to determine the soil-water characteristic curve after Fredlund (2006) and Zapata (1999)(with permission from ASCE)

Laboratory measurement

Numerous laboratory methods exist for the measurement of the soil-water characteristic curve. These methods were mostly developed in the soil science discipline and are not commonly used in geotechnical laboratories. Fredlund (2006) describes the desired characteristics of laboratory equipment to measure the soil-water characteristic curve as follows:

1. Soil suction values should range up to 1500 kPa (217 psi)
2. Total stresses should be applied to soils
3. Both water volume change and change in the volume of the soil should be measured
4. Any air that flows out through the high air entry disk should be measured
5. Individual soil specimens should be tested
6. Both drying and wetting procedures should be measured

Laboratory measurements of the soil-water characteristic curve are costly because they require difficult measurements and long test durations. In addition, the soil-water characteristic curve is highly variable and dependent on past stress states (Pham and Fredlund 2008). The following are descriptions of available laboratory methods to measure the soil-water characteristic curve (Table 6-1). These are discussed further subsequently.

Table 6-1 – Laboratory methods to measure the soil-water characteristic curve from Lins et al. (2009) (determined fair use)

Equipment	Technique	Type	Measurement Range (kPa)
Pressure plate apparatus	Axis translation	Matric suction	0 to 1500
Tempe pressure cell	Axis translation	Matric suction	0 to 1500
Filter paper	--	Matric or total suction	All
Thermal conductivity sensor	--	Matric suction	10 to 1000

High air entry disks

Laboratory measurements of the soil-water characteristic curve require high-air entry disks. These disks separate the air and water phases in unsaturated soils and are an integral part of laboratory tests on unsaturated soils. A brief

description of these disks is provided along with an example from Lu and Likos (2004).

High-air entry disks have very small, uniform pores. The disks are placed in a testing apparatus and act as a membrane between the air and water (Fredlund and Rahardjo (1993). The disks can be made of ceramic or cellulose (Lu and Likos 2004). When the disk is saturated, the small pores prevent the movement of air through the disk because of the surface tension of the water. Air will not pass through the disk until the air-entry pressure, u_{wa}, is reached. This property allows the high-air entry disk to be used in laboratory measurements of soil suction. The disk is placed at the interface of the unsaturated soil and the measuring system. The pore water pressure in the soil is linked to the measuring system by the water in the high-air entry disk and as long as the air-entry pressure is not reached, air will not enter the measuring system which would cause erroneous results (Fredlund and Rahardjo 1993). The maximum air-entry pressure is defined by:

$$u_{wa} = (u_a - u_w) = \frac{2T_s}{R_s}$$

Eq. 6-1

Where u_a = air pressure (F/L^2), u_w = water pressure (F/L^2), T_s = surface tension at the interface (F/L), and Rs = maximum effective radius of the pores of the HAE material (L).

Pressure plate apparatus

Pressure plates use "axis translation" to measure the soil-water characteristic curve. Axis translation is a method used to measure negative water pressures. When measuring negative pore water pressures in the laboratory using an apparatus like that shown in Figure 6-2, errors can occur because water will fail in tension resulting in air bubbles in the measurement system. Axis translation is the process through which the air pressure in the chamber is raised so that the

negative water pressure within the soil remains in a measureable range (Fredlund and Rahardjo 1993). If for example the soil sample had a negative water pressure of -300 kPa, after placing the soil on the high-air entry disk the soil would draw up water and eventually the pressure measured would be -300 kPa. However the water would fail in tension in the measurement system before -300 kPa was measured. To prevent this, the air pressure in the chamber is raised until an equilibrium condition is reached and water does not flow into or out of the soil sample. The air pressure might be 310 kPa and the pressure in the water compartment would be 10 kPa. The difference between the air pressure in the chamber and the water pressure in the soil specimen is then the value of soil suction or matric suction:

$$\psi = u_a - u_w = 310 - 10 = 300 kPa \qquad \text{Eq. 6-2}$$
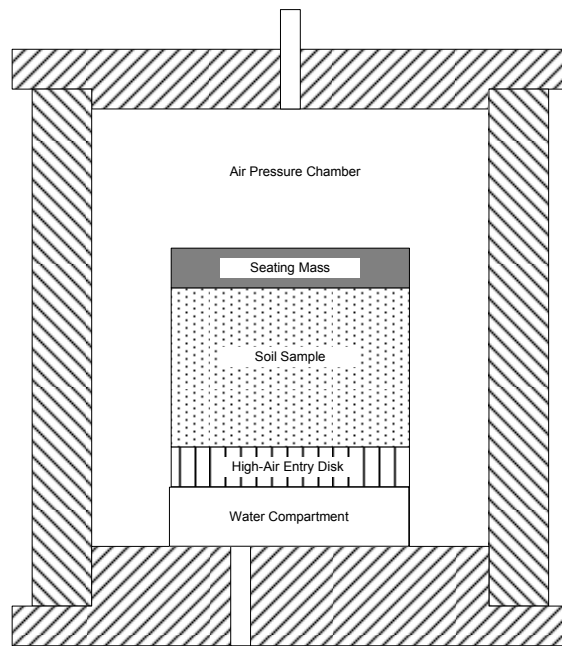
Figure 6-2 – Pressure plate for measuring the soil-water characteristic curve

The procedure for using the pressure-plate device is described in Fredlund and Rahardjo (1993). It starts with a saturated soil sample placed within the pressure

cell on top of a high-air entry disc. The air pressure within the pressure chamber is raised to the desired matric suction value and the amount of water that is removed from the soil is measured. This process is repeated for different values of matric suction to obtain a complete soil-water characteristic curve. After the highest value of matric suction desired is obtained, the soil sample is removed and weighed before and after drying to determine the water content. Then the water content measurements for different values of matric suction can be calculated based on the measured amount of water that was removed from the soil sample in response to increases in matric suction.

Tempe cell
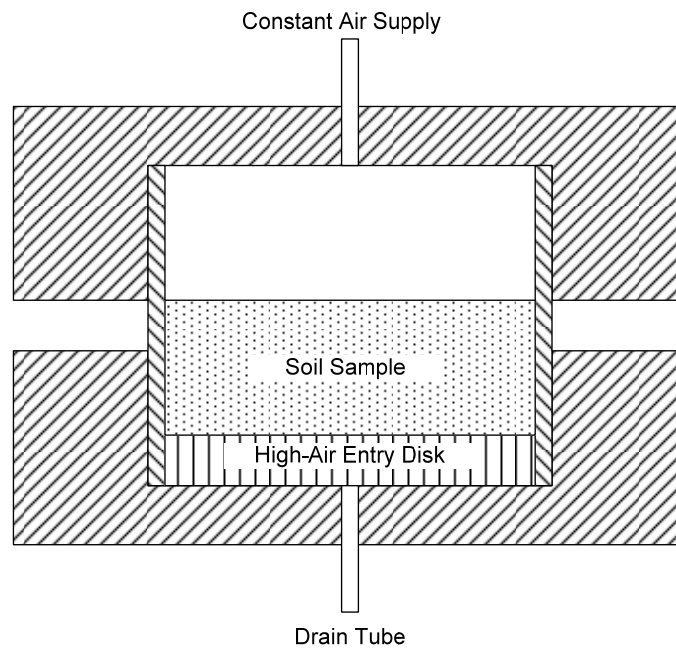
Figure 6-3 – Tempe cell apparatus for measuring the soil-water characteristic curve

The tempe cell is similar to the pressure-plate for measuring the soil-water characteristic curve and the procedure for measurement is described in Fredlund and Rahardjo (1993). A saturated soil sample is placed on top of a high-air entry disk. The air pressure in the chamber is raised to the desired value of soil suction. Water is allowed to drain from the sample and after equilibrium

conditions are reached the whole apparatus is weighed.   After the highest desired value of air pressure is applied to the sample, the device is disassembled and the water content of the soil sample is determined.   Based on this water content and the weights from previous measurements the soil-water characteristic curve can be constructed.

Filter paper

Filter paper can be used to measure the soil-water characteristic curve.   Using filter paper to measure the soil-water characteristic curve is described in Bulut et al. (2001) and ASTM D 5298, Measurement of Soil Suction Using Filter Paper. To construct a soil-water characteristic curve using the filter paper method, a sample of soil is placed in a sealed container and a piece of filter paper is placed in contact with the soil.   Moisture from the soil will enter the filter paper until an equilibrium condition is reached.   At that point, the filter paper is removed and weighed before and after drying to determine the moisture content of the filter paper.   The moisture content of the soil is determined at this time as well.   By using a calibration curve specific to the filter paper, the soil suction can be determined based on the moisture content of the filter paper.   This process is repeated for different moisture content levels of the soil to obtain a soil-water characteristic curve.

Thermal conductivity sensors

Using thermal conductivity sensors to measure the soil-water characteristic curve is described in Fredlund and Wong (1989). A thermal conductivity sensor has a temperature sensor and small heater surrounded by a porous ceramic tip. The porous tip is calibrated so that the water content is dependent on the soil suction surrounding the tip.   To measure the soil-water characteristic curve, the tip is placed into a soil test specimen.   The moisture content of the tip comes into equilibrium with the moisture content of the soil over a period of time.   The moisture content of the tip is then determined by the thermal conductivity measured across the tip by the temperature sensor using the heater in the

sensor. The moisture content of the porous tip is dependent on the soil suction applied to the tip. The moisture content of the soil is then measured. This process is repeated for different values of soil moisture content to determine the soil-water characteristic curve.

Empirical methods

Due to the cost and uncertainty of laboratory methods, many empirical methods have been developed to predict soil-water characteristic curves. Levee analyses typically cover large areas where the spatial variability of the soil-water characteristic curve may be high and simpler empirical methods would therefore be preferred to detailed and relatively expensive laboratory methods.

The empirical methods described here have been grouped into four categories by Zapata (1999) and Johari (2006).

- Category 1 – water contents at each suction value are correlated to soil properties
- Category 2 – fitting parameters of equations for the soil-water characteristic curve are correlated to soil properties
- Category 3 – physics-based models are used to estimate soil-water characteristic curve
- Category 4 – database models and genetic programming/neural networks are used to estimate the soil-water characteristic curve

Category 1 – water content suction correlations

McQueen and Miller (1974)

McQueen and Miller (1974) proposed a method to determine the entire soil-water characteristic curve from limited data. To use this method laboratory data must be available for values of moisture content and the corresponding soil suction value. This procedure is useful because data from the soil science discipline often contains a few data points for the soil-water characteristic curve. The

procedure to construct an entire soil-water characteristic curve from limited data is as follows and shown in Figure 6-4:

1. Plot any available data in the 250 – 500 kPa range.
2. Draw a straight line through the point (625, 0) and the plotted data points.
3. Draw a line from the point (700, 0) to intersect with the line of step 2 at 500 kPa.
4. Draw a line from point (290, 0) to intersect the line drawn in step 2 at soil suction = 250 kPa. This line should be modified for any existing data.
5. Sketch by hand a curve connecting the line from step 4 to the moisture content at saturation.

In the example shown the solid lines represent the final soil-water characteristic curve and the dashed lines are used in the construction. The saturated water content of the soil in the example shown in Figure 6-4 is 50%.
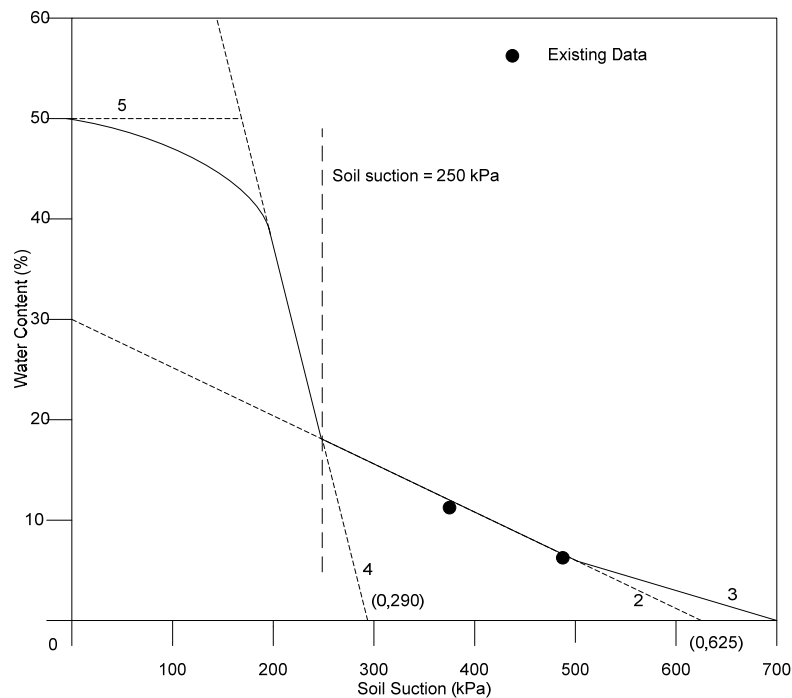
Figure 6-4 – Graphical method for the soil-water characteristic curve from limited soil data after McQueen and Miller (1974) (Example soil is saturated at 50% water content) (determined fair use)

Gupta and Larson (1979)

Gupta and Larson (1979) developed a predictive model for the soil-water characteristic curve based on the particle size distribution, organic matter percent and bulk density of a soil. They performed pressure plate tests on soils from ten different geographical regions and performed a regression analysis for the soil-water characteristic curve and the aforementioned soil properties. The generalized form of their regression equation is:

$$\theta_p = a \cdot sand(\%) + b \cdot silt(\%) + c \cdot clay(\%) +$$

$$d \cdot organic\ matter(\%) + e \cdot bulk\ density(g/cm^3)$$

Eq. 6-3

Where θ_p = predicted water content for a given matric suction potential and a, b, c, d, and e are regression coefficients. For a specific value of soil suction there are accompanying values for the regression coefficients. These are shown in Table 6-2. They found good agreement between their predictive model and tests performed on 61 soils from Missouri. Using the method they were able to obtain an R^2 value between the predicted and measured water contents for the 61 Missouri soils of 0.95, 0.96, and 0.95 for suction values of 4, 33, and 700 kPa respectively.

Table 6-2 – Regression coefficients for the Gupta and Larson (1979) soil-water characteristic curve predictive equation (determined fair use)

Soil Suction (kPa)	a x10^3	b x10^3	c x10^3	d x10^3	e x10^3
4	7.053	10.242	10.07	6.333	-32.12
7	5.678	9.228	9.135	6.103	-26.96
10	5.018	8.548	8.833	4.966	-24.23
20	3.89	7.066	8.408	2.817	-18.78
33	3.075	5.886	8.039	2.208	-14.34
60	2.181	4.557	7.557	2.191	-9.276
100	1.563	3.62	7.154	2.388	5.759
200	0.932	2.643	6.636	2.717	-2.214
400	0.483	1.943	6.128	2.925	-0.204
700	0.214	1.538	5.908	2.855	1.53
1000	0.076	1.334	5.802	2.653	2.145
1500	-0.059	1.142	5.766	2.228	2.671

Rawls et al. (1982)

Rawls et al. (1982) developed a similar model to that of Gupta and Larson (1979) by fitting empirical data to an equation for the entire soil-water characteristic curve based on the percent sand, silt and clay, bulk density and organic content. Their regression analysis included 2,541 different measured soil-water characteristic curves. The generalized form of their equation is:

$$\theta_p = a + b \cdot sand(\%) + c \cdot silt(\%) + d \cdot clay(\%) + \qquad \textbf{Eq. 6-4}$$

$$e \cdot organic\ matter(\%) + f \cdot bulk\ density(g/cm^3)$$

Where θ_p = predicted water content for a given matric suction potential and a, b, c, d, e and f are regression coefficients. A summary of their regression coefficients is shown in Table 6-3. .

Table 6-3 – Regression coefficients for various values of soil suction from Rawls et al. (1982) (determined fair use)

Soil Suction (kPa)	Intercept (a)	% Sand (b)	% Silt (c)	% Clay (d)	% Organic matter (e)	Correlation coefficient (R^2)
10	0.4118	-0.003		0.0023	0.0317	0.81
20	0.3121	-0.0024		0.0032	0.0314	0.86
33	0.2576	-0.002		0.0036	0.0299	0.87
60	0.2065	-0.0016		0.0040	0.0275	0.87
100	0.0349		0.0014	0.0055	0.0251	0.87
200	0.0281		0.0011	0.0054	0.0220	0.86
400	0.0238		0.0008	0.0052	0.0190	0.84
700	0.0216		0.0006	0.0050	0.0167	0.81
1000	0.0205		0.0050	0.0049	0.0154	0.81
1500	0.0260			0.0050	0.0158	0.80

De Jong et al. (1983)

De Jong et al. (1983) developed an equation to determine the soil-water characteristic curve based on the organic content and the grain size distribution. They performed regression analyses for measured soil-water characteristic curves for 64 soils from Canada that were sampled from shallow depths (<30cm). They used two polynomial equations in their regression and characterized the soil-water characteristic curve as two straight lines on a semi-log plot (Figure 6-5):

$$\theta_w = \left[a + \left(b_1(\log S - t)\right)\right]10, \; for \; S \leq 1000 kPa \qquad \text{Eq. 6-5}$$

$$\theta_w = \left[a + \left(b_2(\log S - t)\right)\right]10, \; for \; S > 1000 kPa \qquad \text{Eq. 6-6}$$
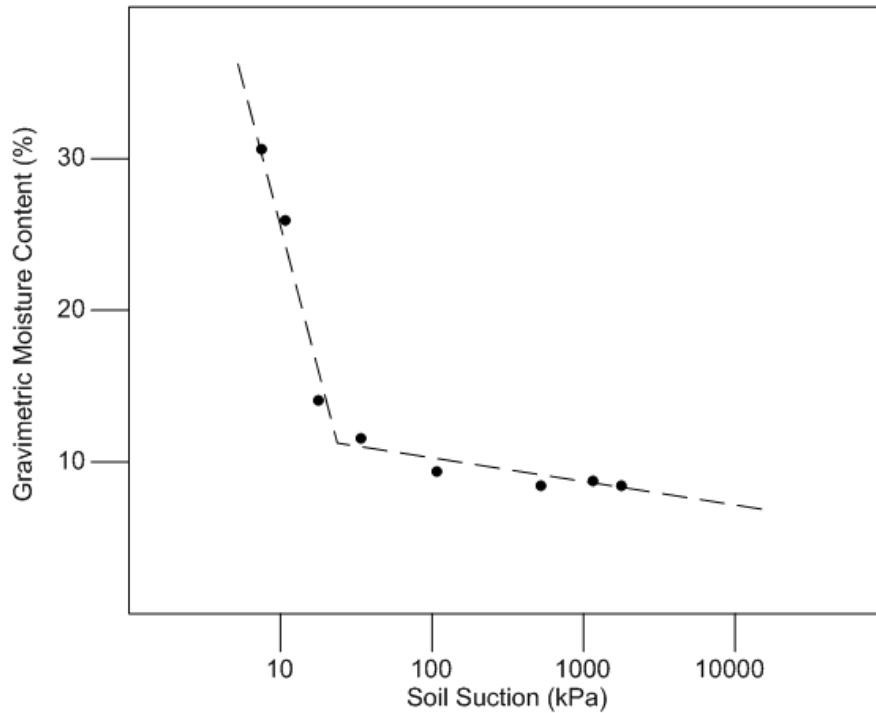
Figure 6-5 – Two-line soil-water characteristic curve fitted to data from De Jong et al. (1983) (determined fair use)

Where θ_w = gravimetric moisture content (%), S = soil suction (kPa) and *a, b₁, b₂* and *t* are constants. Through their regression analysis they found that *a, b₁, b₂* and *t* can be found from the following equations:

$$a = 6.40 + 2.78(\%organic) + 0.24(\%clay) \qquad \text{Eq. 6-7}$$

$$b_1 = -42.90 + 0.55(\%clay) \qquad \text{Eq. 6-8}$$

$$b_2 = -1.56 - 0.028(\%silt + \%clay) - 0.24(\%organic) \qquad \text{Eq. 6-9}$$

$$t = -1.12 + 0.029(\% clay)$$ **Eq. 6-10**

Cosby et al. (1984)

Cosby et al. (1984) used multiple linear regression to derive the soil-water characteristic curve based on grain size distribution using a database of 1448 soil samples. They used a power function to fit the soil-water characteristic curve:

$$\psi = \psi_s (\theta_v / \theta_s)^b$$ **Eq. 6-11**

Where ψ = soil suction (cm of water), ψ_s = soil suction at saturation (cm of water), θ_v = volumetric moisture content (cm^3/cm^3), θ_s = saturated volumetric moisture content (cm^3/cm^3) and b = dimensionless fitting parameter. The results of their regression were:

$$\psi_s = (\% sand \cdot -0.0095) + 1.54$$ **Eq. 6-12**

$$b = (\% clay \cdot 0.157) + 3.01$$ **Eq. 6-13**

$$\theta_s = (\% sand \cdot -0.142) + 50.5$$ **Eq. 6-14**

Category 2 – fitting parameter correlations

Saxton et al. (1986)

Saxton (1986) extended the work of Rawls et al. (1982) to create an equation for a continuous soil-water characteristic curve based on the regression coefficients that are shown in Table 6-3. Saxton et al. (1986) used the general fit of the Brooks and Corey (1964) equation for the soil-water characteristic curve which is:

$$\Psi = A\theta^B$$ **Eq. 6-15**

Where $A = \psi_e \theta_s^{-B}$, ψ_e = the soil suction value at the air entry value (kPa), θ_s = the saturated volumetric moisture content (cm^3/cm^3) and B = dimensionless fitted

value. Saxton et al. (1986) divided the soil-water characteristic curve into three sections: saturation to the air entry value, the air entry value to 10 kPa, and soil suction greater than 10 kPa. For the portion of the curve greater than 10 kPa they found that A and B from Eq. 6-15 are:

$$A = 100 \exp \begin{bmatrix} -4.396 - 0.0715(\% clay) - 4.880 \times 10^{-4}(\% sand)^2 \\ -4.285 \times 10^{-5}(\% sand)^2 \bullet (\% clay) \end{bmatrix}$$

Eq. 6-16

$$B = -3.140 - 0.00222(\% clay)^2 - 3.484 \times 10^{-5}(\% sand)^2(\% clay)$$

Eq. 6-17

For soil suction values less than 10 kPa, they represented the soil-water characteristic curve as a constant value from saturation to the air entry value, and a straight line from the air entry value to 10 kPa. To estimate the saturated water content and the air entry value they suggested:

$$\theta_s = 0.332 - 7.251 \times 10^{-4}(\% sand) + 0.1276 \log_{10}(\% clay)$$

Eq. 6-18

$$\psi_e = 100.0 \left[-0.108 + 0.341(\theta_s) \right](kPa)$$

Eq. 6-19

They found their proposed equation to be valid when tested against measured soil-water characteristic curves, except when clay content was above 60% or below 10%.

Zapata et al. (2000)

Zapata et al. (2000) proposed a method to determine the soil-water characteristic curve based on soil index properties. For their study they used a database of 190 soils. The data consisted of 70 plastic soils and 120 non-plastic soils. They used multiple regression and the Fredlund and Xing (1994) equation to fit the soil-water characteristic curve data:

$$\theta_w = C(h) \left[\frac{\theta_s}{\left[\ln\left[\exp(1) + \left(\frac{h}{a}\right)^b \right] \right]^c} \right]$$

Eq. 6-20

$$Where \; C(h) = \left[1 - \frac{\ln\left(1 + \frac{h}{h_r}\right)}{\ln\left(1 + \frac{10^6}{h_r}\right)} \right]$$

Eq. 6-21

Where θ_w = volumetric moisture content (cm^3/cm^3), h = matric suction (kPa), h_r is the residual soil suction (kPa) and a, b, c are dimensionless fitting parameters. For plastic soils they correlated the fitting parameters to *wPI* which is the product of the percent passing the #200 sieve expressed as a decimal (*w*) multiplied by the plasticity index, (*PI*).

$$wPI = \text{Passing \#200 x PI}$$

Eq. 6-22

PI = Plasticity Index (%) = Liquid Limit – Plastic Limit

Eq. 6-23

For soils with PI > 0 they found:

$$a = 0.00364(wPI)^{3.35} + (wPI) + 11$$

Eq. 6-24

$$\frac{b}{c} = -2.313(wPI)^{0.14} + 5$$

Eq. 6-25

$$c = 0.0514(wPI)^{0.465} + 0.5$$

Eq. 6-26

$$\frac{h_r}{a} = 32.44e^{0.0186(wPI)}$$

Eq. 6-27

For non-plastic soils they correlated the fitting parameters of the soil-water characteristic curve to D_{60} from the grain size distribution curve.

$$a = 0.8627(D_{60})^{-0.751}$$ **Eq. 6-28**

$$b = 7.5$$ **Eq. 6-29**

$$c = 0.1772\ln(D_{60}) + 0.7734$$ **Eq. 6-30**

$$\frac{h_f}{a} = \frac{1}{D_{60} + 9.7e^{-4}}$$ **Eq. 6-31**

Where the units of D_{60} are (mm).

Vanapalli and Catana (2005)

Vanapalli and Catana (2005) proposed a correlation for the soil-water characteristic curve of coarse grained soils using one measured point of soil suction and degree of saturation, and simple soil properties. They correlated the fitting parameters of the Fredlund and Xing (1994) equation for the soil-water characteristic curve (Eq. 6-20) to the grain size distribution and dominant particle size, and found (as described by Chin et al. 2010):

$$a = \frac{1.33}{(d_e)^{0.86}}$$ **Eq. 6-32**

$$b = \frac{7.78}{\left[(D_{60}/D_{10})e\right]^{1.14}}$$ **Eq. 6-33**

$$c = x$$ **Eq. 6-34**

Where D is the soil particle diameter (mm) corresponding to the percent passing on the grain size distribution curve, e is the void ratio and x is the adjusted variable for the soil-water characteristic curve to pass through or close to the

measured soil-water characteristic point. The dominant particle (d_e) size can be found from Vukovic and Soro (1992):

$$\frac{1}{d_e} = \sum_{i=1}^{i=n} \Delta g_i \frac{\ln(d_i^g / d_i^d)}{(d_i^g - d_i^d)}$$

Eq. 6-35

Where Δg_i is the fraction weight in parts of the total weight (g), d_i^g is the maximum grain diameter of the corresponding fraction (mm), and d_i^d is the minimum grain diameter of the corresponding fraction (mm).

Perera et al. (2005)

Perera et al. (2005) used multiple regression and the Fredlund and Xing (1994) equation with a database of 154 non-plastic and 63 plastic soils to derive equations for the soil-water characteristic curve based on the grain size distribution and the plasticity index. Their work was an extension of the work by Zapata et al. (2000). The form of the Fredlund and Xing (1994) equation used by Perera et al. (2005) was:

$$S = C(h) \left[\frac{1}{\left[\ln\left[\exp(1) + \left(\frac{h}{a_f} \right)^{b_f} \right] \right]^{c_f}} \right]$$

Eq. 6-36

$$Where \; C(h) = \left[1 - \frac{\ln\left(1 + \frac{h}{h_{rf}} \right)}{\ln\left(1 + \frac{10^6}{h_{rf}} \right)} \right]$$

Eq. 6-37

Where S = volumetric moisture content (cm^3/cm^3), h = matric suction (kPa), h_{rf} is the residual soil suction (kPa) and a_f, b_f, c_f are dimensionless fitting parameters.

The results of their multiple regression were two different correlation equations, one for plastic soils and one for non-plastic soils. For plastic soils:

$$a_f = 32.835\{\ln(wPI)\} + 32.438$$

Eq. 6-38

$$b_f = 1.421(wPI)^{-0.3185}$$

Eq. 6-39

$$c_f = -0.2154\{\ln(wPI)\} + 0.7145$$

Eq. 6-40

$$h_{rf} = 500(kPa)$$

Eq. 6-41

Where *wPI* = weighted plasticity index, equal to the product of P_{200} (%passing the No. 200 sieve expressed as a decimal) and the PI. For non-plastic soils the derived correlation equations were:

$$a_f = 1.14a - 0.5$$

Eq. 6-42

$$a = -2.79 - 14.1\log(D_{20}) - 1.9 \times 10^{-6} P_{200}^{4.34} + 7\log(D_{30}) + 0.055 D_{100}$$

Eq. 6-43

$$D_{100} = 10^{\left[\frac{40}{m_1} + \log(D_{60})\right]} (mm)$$

Eq. 6-44

$$m_1 = \frac{30}{\left[\log(D_{90}) - \log(D_{60})\right]}$$

Eq. 6-45

$$b_f = 0.936b - 3.8$$

Eq. 6-46

$$b = \left\{5.39 - 0.29\ln\left[P_{200}\left(\frac{D_{90}}{D_{10}}\right)\right] + 3D_0^{0.57} + 0.021P_{200}^{1.19}\right\}m_1^{0.1}$$

Eq. 6-47

$$D_0 = 10^{\left[\frac{-30}{m_2} + \log(D_{30})\right]}$$

Eq. 6-48

$$m_2 = \frac{20}{\left[\log(D_{30}) - \log(D_{10})\right]}$$

Eq. 6-49

$$c_f = 0.26e^{0.758c} + 1.4D_{10}$$

$$c = \log(m_2^{1.15}) - \left(1 - \frac{1}{b_f}\right)$$

$$h_{rf} = 100(kPa)$$

Using these equations they obtained R^2 values or 0.58 for the non-plastic soil equation and 0.51 for the plastic soil equation when comparing measured and predicted values of soil suction. Houston et al. (2006) reported that better estimates of the soil-water characteristic curve can be made if the Perera et al. (2006) equations are used in conjunction with one measured soil suction and degree of saturation point. The curve is first derived using the equations of Perera et al. (2006) and then the entire curve is shifted to go through the one measured point. There are no provided ranges for this one soil suction point.

Chin et al. (2010)

Chin et al. (2010) proposed a method to determine the soil-water characteristic curve for a soil based on index properties and one measured soil suction and degree of saturation point for the soil-water characteristic curve in the 10 to 500 kPa range. They correlated the fitting parameters of the Fredlund and Xing (1994) equations (Eq. 6-20) for 30 plastic and 30 non-plastic soils and tested their proposed method against 62 measured soil-water characteristic curves. For fine grained soils (>30% passing the No. 200 sieve), the correlated equations for the Fredlund and Xing (1994) fitting parameters were found to be:

$$a = -2.4(x) + 722$$

$$b = 0.07(x)^{0.4}$$

$$c = 0.015(x)^{0.7}$$

$$h_r = 914\exp[-0.002(x)]$$ <div align="right">**Eq. 6-56**</div>

The parameter *x* is to be adjusted to allow the soil-water characteristic curve to pass through the measured point. An example of how *x* affects the soil-water characteristic curve for fine grained soils is shown in Figure 6-6.
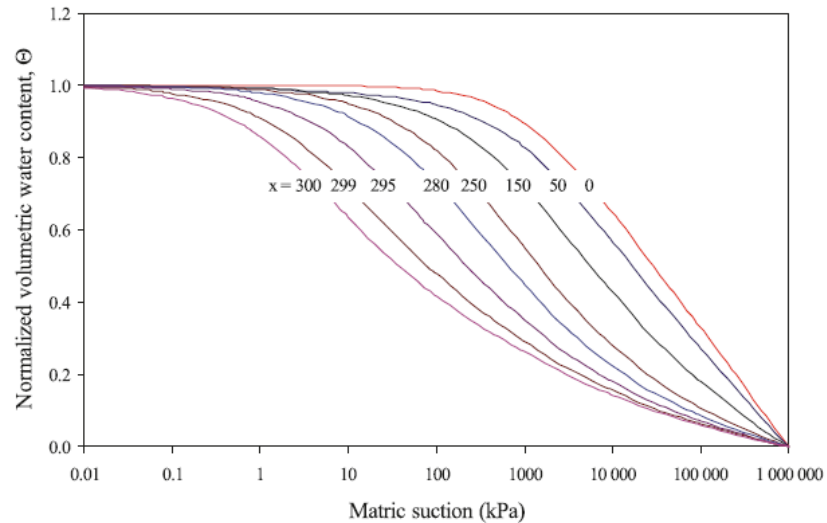
Figure 6-6 – Soil-water characteristic curves with variation in the parameter *x* for fine grained soils (with permission from CGJ)

For coarse grained soils they found the following correlations for the Fredlund and Xing (1994) fitting parameters:

$$a = 0.53(D_{50})^{-0.96}$$ <div align="right">**Eq. 6-57**</div>

$$b = x$$ <div align="right">**Eq. 6-58**</div>

$$c = -0.23\ln(x) + 1.13$$ <div align="right">**Eq. 6-59**</div>

$$h_r = 100 kPa$$ <div align="right">**Eq. 6-60**</div>

Where *x* can be changed to adjust the soil-water characteristic curve to pass through the measured point.

Category 3 – physics-based models

Arya and Paris (1981)

Arya and Paris (1981) proposed a model to derive the soil-water characteristic curve based on the grain size distribution, the bulk density and the particle density of a soil. The model translates the grain size distribution to a distribution of pore sizes. The pore volumes and pore radii are found by dividing the grain size distribution curve into segments. For each segment the pore volume is found from:

$$V_i = (W_i / \rho_p)e \qquad\qquad \textbf{Eq. 6-61}$$

Where V_i = pore volume per unit sample mass associated with the solid particles in the i_{th} grain size range, W_i = solid mass per unit sample mass in the i_{th} grain size range, ρ_r = particle density, e = void ratio. The pore volume divided by the sample bulk density give the volumetric moisture content. The size of the pore radii for each segment is found from:

$$r_i = R_i [4en^{1-\alpha} / 6]^{1/2} \qquad\qquad \textbf{Eq. 6-62}$$

Where r_i = mean pore radius of the ith grain size segment, R_i = mean grain size radius of the ith segment, e is the void ratio, n is the number of particles, and α is empirically derived to be 1.38 for most cases. The number of particles n, can be found from:

$$V = n4\pi R^3 / 3 \qquad\qquad \textbf{Eq. 6-63}$$

Where V is the volume of a cylinder a single particle radius, $R,$ in size.

The corresponding soil suction is found from the pore radii size for each segment based on the equation for capillarity:

$$\psi_i = 2\gamma\cos\theta / \rho_w g r_i \qquad\qquad \textbf{Eq.6- 64}$$

Where ψ_i = soil suction, γ = surface tension of water, θ = contact angle, ρ_w = density of water, g is the acceleration due to gravity and r_i = pore radius. For their research they assumed a contact angle of 0 degrees.

Fredlund et al. (1997)

Fredlund et al. (1997) proposed a predictive model for the soil-water characteristic curve based on grain-size distribution and volume-mass properties of the soil. They first fitted the soil-water characteristic curve with the Fredlund and Xing (1994) fitting equation:

$$\theta = \theta_s \left[\frac{1}{\ln\left[e + (\psi / a)^n \right]} \right]^m \qquad\qquad \textbf{Eq. 6-65}$$

Where θ_s = volumetric moisture content at saturation (cm^3/cm^3), ψ = soil suction (kPa) and a, n and m are fitting parameters. They proposed that the grain size distribution curve could be discretized into a number of small linear segments. Each segment would have an average grain size. For each grain size there is a unique soil-water characteristic curve. The entire soil-water characteristic curve would be superimposed from these small individual soil-water characteristic curve segments based on the grain size distribution.

Tomasella and Hodnett (1998)

Tomasella and Hodnett (1998) derived two expressions for the soil-water characteristic curve using the Brooks and Corey (1964) fitting equation and the fractal dimension for a soil. The fractal dimension is a measure of how the soil particles fill space as defined by fractal theory. They derived an expression for the fractal dimension of a soil based on the grain size distribution. The fractal dimension can be found by the slope of particle mass versus particle radii. After

finding the fractal dimension *D*, they found that the Brooks and Corey equation could be written as:

$$\theta_h = \theta_r + (\theta_0 - \theta_r)(h_0 / h)^{3-D}$$

Eq. 6-66

Where θ_h =volumetric moisture content at a specific soil suction, *h*, θ_r = residual moisture content, θ_0 = saturated volumetric moisture content, h_0 = air entry value.

The value of *D*, was found based on the textural class of the soil and the grain size distribution. The values of *D* found in their study based on textural class are shown in Table 6-4.

Table 6-4 – Values of D based on soil texture for the Brooks and Corey equation from the study by Tomasella and Hodnett (1998) (determined fair use)

Soil Texture	D
Sand	2.505
Loamy Sand	2.778
Sandy Loam	2.864
Sandy Clay Loam	2.899
Loam	2.909
Silt Loam	2.913
Clay Loam	2.931
Silty Clay Loam	2.930
Sandy Clay	2.937
Silty Clay	2.955
Clay	2.959

Category 4 – database models, genetic programming and neural networks

Pachepsky et al. (1996)

Pachepsky et al. (1996) used artificial neural networks to predict the soil-water characteristic curve based on soil texture and bulk density. Artificial neural networks are similar to the best non-linear regression techniques where there is an "input-output" relationship. For their study the input was six particle size fractions and one bulk density. The output was the residual moisture content, θ_r

α and *n* of the Van Genuchten (1980) equation for the soil water characteristic curve:

$$\theta = \frac{\theta_s - \theta_r}{\left[1 + |\alpha \psi|^n\right]^{1-1/n}}$$

<div align="right">**Eq. 6-67**</div>

Where θ is the volumetric moisture content (cm^3/cm^3), θ_s is the saturated volumetric moisture content, θ_r is the residual moisture content, ψ is the soil suction (kPa), and α and *n* are fitting parameters. They compared the results of the artificial neural network with polynomial regression and found that the artificial neural network better predicted the measured soil-water characteristic curve better than polynomial regression.

Schaap and Leij (1998)

Schaap and Leij (1998) also used artificial neural networks to predict the soil-water characteristic curve from grain size distribution and bulk density. They used data from the UNSODA (Nemes et al. 2001) database for soil-water characteristic curve data based on soil texture and bulk density. They found that artificial neural networks were able to predict the soil-water characteristic curve with grain size distribution and bulk density data well. The accuracy of the prediction increased if one or two suction versus moisture content data points were added to the neural network for prediction. Figure 6-7 shows the 90% confidence limit for the soil-water characteristic curve for loamy sand and clay textural classes.
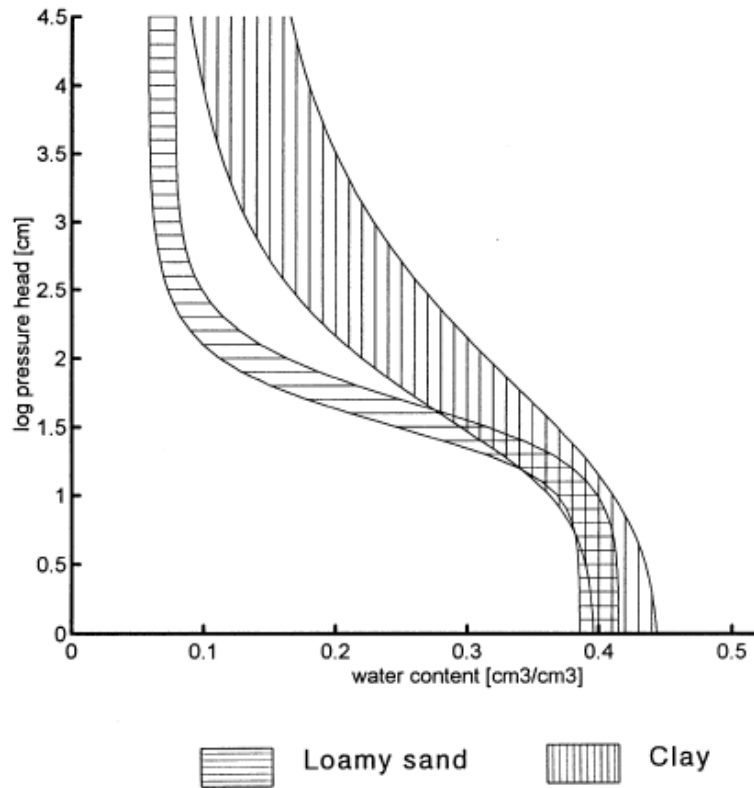
Figure 6-7 – 90% confidence limits for soil-water characteristic curves for loamy sand and clay textural classes using the UNSODA database and artificial neural networks from Schaap and Leij (1998) (determined fair use)

Nemes et al. (2001)

Nemes et al. (2001) describe the latest version of the unsaturated soil hydraulic database (UNSODA). UNSODA is a database that contains measured soil-water characteristic curves for soils along with several other measured soil parameters such as bulk density, particle size distribution and organic content. There are 137 field measured drying soil-water characteristic curves, 730 laboratory measured drying soil-water characteristic curves, 2 field measured wetting soil-water characteristic curves and 33 measured laboratory wetting soil-water characteristic curves. Queries can be created to find data in the database for soils that are similar to the soil that the soil-water characteristic curve is needed.

Schaap et al. (2001)

Schaap et al. (2001) described Rosetta, a computer program that can be used to predict the soil-water characteristic curve of soils based on minimal input data. Rosetta uses the soil data found in the UNSODA database along with other soil data to predict the soil-water characteristic curve. There are five different hierarchal models that can be used as input data for the prediction of the soil-water characteristic curve:

- Soil textural class
- Sand, silt and clay percentages
- Sand, silt and clay percentages and bulk density
- Sand, silt and clay percentages, bulk density
  and a water retention point at 330 cm (33 kPa).
- Sand, silt and clay percentages, bulk density
  and water retention points at 330 and 15000 cm (33 and 1500 kPa)

The Hydraulic Conductivity Function

The hydraulic conductivity function is a non-linear curve relating hydraulic conductivity to soil suction. It depends on a number of soil properties and conditions. A number of laboratory and empirical methods have been proposed to determine hydraulic conductivity functions. These are described briefly in the following paragraphs.

Laboratory measurement

Several types of laboratory methods are available for measurement of the hydraulic conductivity function (Benson and Gribb (1997); Dirksen (2001); Fredlund and Rahardjo (1993); Klute (1972); Klute (1986). Two types of methods exist in the laboratory (sometimes called direct measurements), the steady state and unsteady state methods (Masrouri et al. (2009)). Laboratory methods for the determination of the hydraulic conductivity function are summarized in Table 6-5.

Table 6-5 – Laboratory methods for measuring the hydraulic conductivity function from Masrouri et al. (2009) (with permission from Springer)

Test Methods		Advantages	Disadvantages	Relative Cost
Steady state methods (SS)	Conventional constant head (CCH)	Simplicity	Costly, tedious and lengthy in low permeability materials	Low
		Can control stress state		
	Constant flow	Simplicity	Flow pump required	Moderate initial cost (equipment)
		Can control stress state		
		Faster and higher resolution than CCH		
		Yields conductivity and the soil-water characteristic curve		
	Centrifuge	Short time for measuring low conductivity	Centrifuge required	High initial cost (equipment)
			Only for dense, stiff soil specimens	
			High net normal stress	
			Considerable operator attention	
Unsteady state methods (USS)	Outflow-inflow	Quicker than SS	Few reliable and favorable comparisons with other methods	Low
		Good control on mass		
		Simplicity (equipment)		
	Instantaneous profile	Simplicity	Poor mass control	Moderate to high initial cost (equipment)
		Yields conductivity and the soil-water characteristic curve	No control on stress state	
		Good for clays (30%-90% saturation) and sands (<50% saturation)	Possibility of errors when 100% saturation is approached	

Steady state

Steady state methods measure hydraulic conductivity with a constant flow rate or hydraulic gradient across an unsaturated sample. The matric suction and water content are held constant during the test. Steady state is assumed to have been reached in laboratory tests when the flow into and out of the sample is equal. At this point the hydraulic conductivity for the specific value of matric suction is computed (Fredlund and Rahardjo 1993); (Masrouri et al. 2009). Different magnitudes of soil suction are used to establish the hydraulic conductivity function. Steady state methods can be accomplished using triaxial cells (Bjerrum 1957), flow pumps (Aiban 1998); (Likos 2005); (Masrouri et al. 2009); (Olsen 1985), or a combination of triaxial cells and flow pumps (Bicalho 2005). In low permeability soils, steady state methods can be difficult to accomplish accurately because of low flow rates. Centrifuges can be used to impart a driving force on the water in the soil (Nimmo et al. 1987); (Nimmo et al. 1992); (Conca and Wright 1992); (McCartney and Zorenberg 2005). These methods can be accomplished faster and with more precision for low permeability soils than standard steady state tests (Masrouri et al. 2009).

The "standard method"

It has been found that it is difficult to prepare soil test specimens for measurement of the unsaturated hydraulic conductivity. In addition, wetting and drying samples to the same water content does not produce the same unsaturated hydraulic conductivity (Dirksen 2001). For these reasons any measurement of hydraulic conductivity functions involves variability and uncertainty. What Benson and Gribb (1997) and Dirksen (2001) describe as the "standard method" is an attempt to develop a method that reduces the uncertainties as much as possible. Dirksen (2001) states that to reduce uncertainties of measurements the standard method should:

1. Use only Darcy's Law as an assumption
2. Should have steady flow

3. The hydraulic head gradient should be measured in the soil directly
4. Water contents should be measured simultaneously at different points in the soil column
5. Flow should be induced by gravity and not by excess pressure

A diagram showing the standard method is shown in Figure 6-8. The method is sometimes called a constant-head test procedure. A head difference is applied to the sample using Mariotte bottles. Two tensiometers in the sample measure the pore water pressure across the sample. A time domain reflectometry (TDR) probe is used to measure of the soil moisture content.

The method takes considerable time because steady state conditions must be reached. For low conductivity (fine grained) soils, the flow rates may be very small. This increases the length of time required. When this method is employed, the unsaturated hydraulic conductivity can be computed from:

$$K_\psi = q_{s,\psi} \left[\frac{L}{\Delta H_s} \right]$$

Eq. 6-68

Where: K_ψ = hydraulic conductivity (L/T) or (cm/sec), $q_{s,\psi}$ = steady state volumetric water flux at applied matric suction (L/T) or (m/sec), L = specimen length (L) and ΔH_s = drop in total head across the specimen (L)
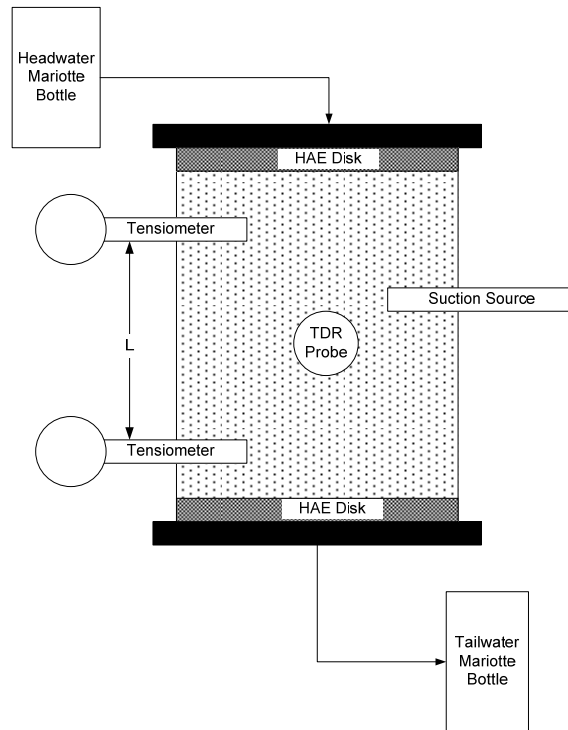
Figure 6-8 – Steady state, standard test method for hydraulic conductivity function measurements after Benson and Gribb (1997) (with permission from ASCE)

Constant flow method

The standard method described by Dirksen (2001) uses a constant head difference to induce flow through the soil specimen. Another steady state method to measure the hydraulic conductivity function is the constant flow method. This method is becoming much easier to implement since modern laboratory equipment can maintain very small, constant flow rates (Lu and Likos 2004). The new laboratory equipment provides a very controlled flow rate that reduces seepage-induced disruption of the soil fabric. Some constant flow methods are also capable of measuring the soil-water characteristic curve concurrently with the hydraulic conductivity function (Lu et al. 2004). The constant flow method is much faster than the standard constant head method.

Constant flow methods induce flow across a soil specimen to measure the hydraulic conductivity. The flow rate is induced in soil under a constant value of water content or matric suction. The hydraulic conductivity for that particular

value of water content or matric suction is determined by measuring head loss across the sample (Lu et al. 2004).

Centrifuge modeling

Unsaturated hydraulic conductivity measurements can also be made using a centrifuge (Conca and Wright 1992); (McCartney and Zorenberg 2005); (Nimmo et al. 1992); (Nimmo et al. 1987). Centrifuges impart a driving force inducing flow through the unsaturated sample. The advantage of the centrifuge method is that the forces imposed on the soil induce steady state flow much more rapidly than constant head or constant flow methods (Lu and Likos 2004). Figure 6-9 shows results of centrifuge tests on Oakley sand together with results from steady state, constant head tests. The method is only applicable to dense soils, as the body forces imparted by the centrifuge can change the soil fabric and density and thus the hydraulic conductivity of the soil (Benson and Gribb 1997).
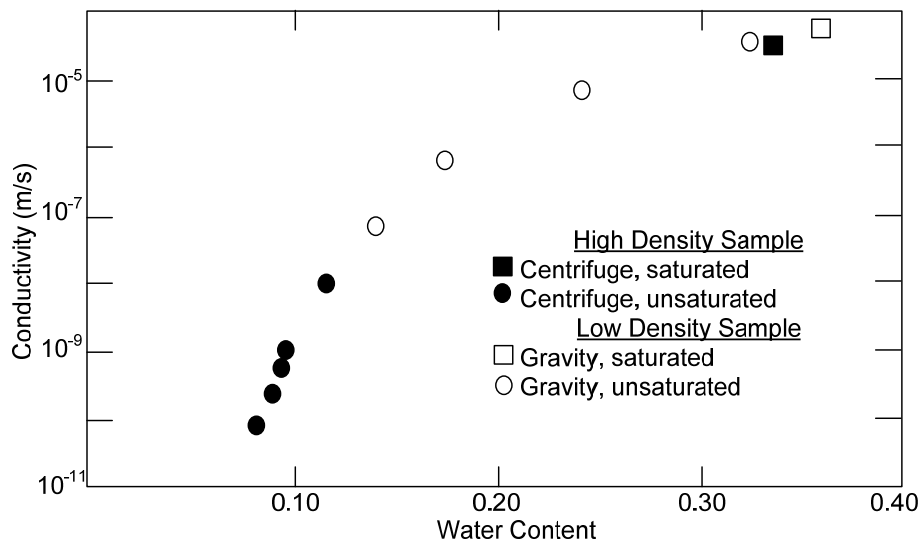
Figure 6-9 – Centrifuge and gravity methods for unsaturated hydraulic conductivity after Nimmo et al. (1987) (with permission from AGU)

Unsteady flow methods

Unsteady flow laboratory tests for determination of the hydraulic conductivity function involve changes in the flow rate or hydraulic head with time (Fredlund and Rahardjo 1993). These methods are sometimes divided into outflow-inflow

methods and instantaneous profile methods (Masrouri et al. 2009). The original outflow method was proposed by Gardner (1958). These methods have disadvantages in terms of accuracy compared to steady state methods, but they are often faster than steady state methods (Masrouri et al. 2009).

Unsteady flow methods use measurements of hydraulic diffusivity to calculate the hydraulic conductivity. Lu and Likos (2004) and Dirksen (2001) describe the relationship of diffusivity to conductivity. Hydraulic diffusivity is defined as the ratio of hydraulic conductivity to specific moisture capacity:

$$D(\theta) = \frac{k(\theta)}{C(\theta)}$$

Eq. 6-69

Where: $D(\theta)$ = diffusivity as a function of moisture content (L^2/T) or (m^2/sec), $C(\theta)$ = specific moisture capacity (1/L) or (1/m) and is the slope of the soil-water characteristic curve (water content versus soil suction):

$$C(\theta) = \frac{\partial \theta}{\partial \psi}$$

Eq. 6-70

The hydraulic conductivity function can be found from these two equations as:

$$k(\theta) = D(\theta) \left(\frac{\partial \theta}{\partial \psi} \right)$$

Eq. 6-71

If diffusivity is measured in the lab and the soil-water characteristic curve is known, then the hydraulic conductivity function can be calculated. One of the disadvantages of using unsteady methods to evaluate the hydraulic conductivity function is that the soil-water characteristic curve must be known to calculate the hydraulic conductivity function.

Outflow-inflow

Outflow methods subject a soil specimen to a small increment of soil suction and measure the total outflow. Outflow methods are usually conducted using the same laboratory equipment as used for the determination of the soil-water

characteristic curve (pressure plates, Tempe cells, etc.) (Lu and Likos 2004). The method assumes that during outflow (as stated by Lu and Likos 2004 and Masrouri et al. 2009):

1. The hydraulic conductivity at that particular soil suction is constant
2. Soil suction and water content are linear over the increment of imposed suction
3. Flow is one dimensional
4. Gravity driven flow is negligible
5. The soil is homogeneous and rigid
6. The HAE disk does not impede fluid flow

The increments of suction must be large enough to generate flows but small enough to meet the assumptions of the tests. The method measures both the hydraulic conductivity function and the soil-water characteristic curve along the drying branch.

Inflow measurements are similar to outflow measurements but instead of measuring the total outflow for a certain matric suction value, water is introduced to one side of a soil column and the water content distribution is measured after time for equilibration (Klute and Dirksen 1986). This laboratory equipment is typically comprised of a long cylinder of soil that contains several segments in which water content is measured after the conclusion of the test. At the start of the test, a water supply of known head is introduced to one side of the column. After some period of time, t, the valve is shut off and the individual segments of the soil column are separated for water content measurements.

The results of inflow tests often have significant scatter in the results (Lu and Likos 2004). This scatter is a result of variations in the water content distribution after the test.

Instantaneous profile

The instantaneous profile method induces a transient flow within a sample and the water content and/or pore pressure is measured at various time intervals (Fredlund and Rahardjo 1993 and Masrouri et al. 2009). These tests can be performed during the wetting or drying process to find the unsaturated hydraulic conductivity. A variation of this method uses temperature gradients across the sample (Benson and Gribb 1997).

Instantaneous profile methods are similar to the inflow method described previously in the steady state section. Figure 6-10 shows a typical, horizontally oriented laboratory apparatus for the measurement of the hydraulic conductivity function and the soil-water characteristic curve using the instantaneous profile method. The soil specimen is initially dry and flow is started from left side of the test apparatus. At specific time intervals, water contents and suction are measured through ports in the sides of the apparatus, using time domain reflectometry (TDR) probes and tensiometers for measurement of the soil suction (Lu and Likos 2004). It is possible to calculate the hydraulic conductivity function and the soil-water characteristic curve from these measurements.
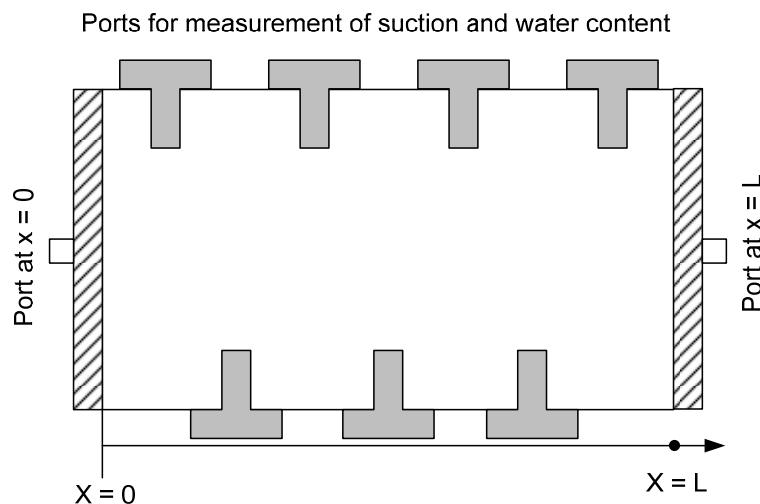
Figure 6-10 – Instantaneous profile method laboratory apparatus after Lu and Likos (2004) (with permission from John Wiley &Sons)

Empirical methods

Several methods are available for estimating the hydraulic conductivity function. This section focuses on methods that predict the hydraulic conductivity function from other soil properties, principally the soil-water characteristic curve.

As seen from the previous section on laboratory methods for determination of the hydraulic conductivity function, measuring the hydraulic conductivity function can be time-consuming and expensive. In lieu of measuring the hydraulic conductivity function, it is often estimated from other soil properties, mostly the soil-water characteristic curve (Lu and Likos 2004). These methods are sometimes called statistical methods. These methods are possible because both the soil-water characteristic curve and the hydraulic conductivity function are defined primarily by pore size distribution (Fredlund et al. 1994).

The most widely used statistical models to predict the hydraulic conductivity function from the soil-water characteristic curve include the models from several researchers (Fredlund et al. 1994; Van Genuchten 1980; Mualem 1976; Kunze 1968). A summary of these models is shown in Table 6-6.

Often the hydraulic conductivity function is estimated from the soil-water characteristic curve because the hydraulic conductivity function should be consistent with the soil-water characteristic curve. The soil-water characteristic curve shows at what value of soil suction air will begin to enter the soil as the soil dries, or at which value the soil becomes saturated upon wetting. This is called the "air entry value." The hydraulic conductivity function should begin to show a decrease in conductivity for values of soil suction higher than the air entry value because it is at this value that air begins to enter the soil. Air within the voids of the soil reduces the area for water flow, and the hydraulic conductivity decreases. The methods listed in Table 6-6 are discussed in the following paragraphs.

Table 6-6 – Statistical models for the hydraulic conductivity function

Reference	Parameters needed to solve for the hydraulic conductivity function
Kunze and Graham 1968	Saturated hydraulic conductivity Soil-water characteristic curve
Mualem 1976	Saturated hydraulic conductivity Soil-water characteristic curve
Van Genuchten 1980	Saturated hydraulic conductivity Van Genuchten fit of the soil-water characteristic curve
Fredlund et al. 1994	Saturated hydraulic conductivity Fredlund and Xing fit of the soil-water characteristic curve

Kunze and Graham 1968

Kunze and Graham (1968) used a modified form of the Millington and Quirk (1959) equation to determine the hydraulic conductivity function from the soil-water characteristic curve. The soil-water characteristic curve is first divided into segments and for each segment the hydraulic conductivity is found from:

$$K(\theta)_i = \frac{K_s 30 \gamma^2 \theta}{K_{sc} \rho g \eta \, n^2} \sum_{j=i}^{n} \left[(2j+1-2i)\frac{1}{h_j} \right] i = 1, 2..n$$

Eq. 6-72

Where $K(\theta)_i$ is the calculated conductivity for specified moisture content (cm/min), K_s / K_{sc} is a matching factor (measured saturated conductivity / calculated saturated conductivity) (dimensionless), γ is the surface tension of water (dynes/cm), ρ is the density of water (g/cm^3), g is the gravitational constant (cm/sec^2), η is the water viscosity (g/cm per sec), θ is the porosity (cm^3/cm^3), n is the number of pore classes and h is the suction (cm of water). The matching factor is the ratio of the measured saturated hydraulic conductivity and that predicted by the equation at 0 soil suction.

Mualem (1976)

Mualem (1976) proposed the following equation to derive the hydraulic conductivity function from the soil-water characteristic curve and the saturated hydraulic conductivity:

$$k_r(\theta) = \Theta^{0.5} \left(\frac{\int_{\theta_r}^{\theta} \frac{d\theta}{\psi(\theta)}}{\int_{\theta_r}^{\theta_s} \frac{d\theta}{\psi(\theta)}} \right)$$

Eq. 6-73

Where Θ is the normalized water content ($\frac{\theta - \theta_r}{\theta_s - \theta_r}$), θ_r is the residual volumetric moisture content (cm^3/cm^3) and θ_s is the saturated volumetric moisture content (cm^3/cm^3).

Van Genuchten (1980)

Van Genuchten (1980) used Mualem's (1976) equation to create a closed form solution for the hydraulic conductivity function from the saturated hydraulic conductivity and the soil-water characteristic curve. Van Genuchten (1980) first proposed an equation for the entire soil-water characteristic curve:

$$\theta = \left[\frac{1}{1 + (\alpha h)^n} \right]^m$$

Eq. 6-74

Where θ is the volumetric moisture content (cm^3/cm^3), h is the soil suction (cm of water) and α, n, m are fitting parameters for the soil-water characteristic curve equations (α has units of 1/cm of water). Using this equation Van Genuchten (1980) showed that the hydraulic conductivity function could be found from:

$$K(h) = \frac{1 - (\alpha h)^{n-2} \left[1 + (\alpha h)^n \right]^{-m}}{\left[1 + (\alpha h)^n \right]^{2m}}$$

Eq. 6-75

Where $K(h)$ is the hydraulic conductivity at a value of soil suction (cm/sec), h is the value of soil suction (cm of water) and α, n, m are the fitting parameters for the soil-water characteristic curve (*α* has units of 1/cm of water). The Van Genuchten (1980) equation for the hydraulic conductivity function is programmed into the 2007 version of SEEP/W by GeoStudio.

Fredlund et al. (1994)

Fredlund et al. (1994) proposed an equation for the hydraulic conductivity function based on the soil-water characteristic curve and the saturated value of hydraulic conductivity. This equation is also programmed into the 2007 version of SEEP/W by GeoStudio:

$$k_w = k_s \frac{\displaystyle\sum_{i=j}^{N} \frac{\Theta(e^y) - \Theta(\psi)}{e^{y_i}} \Theta'(e^{y_i})}{\displaystyle\sum_{i=1}^{N} \frac{\Theta(e^y) - \Theta_s}{e^{y_i}} \Theta'(e^{y_i})}$$

Eq. 6-76

Where k_w is the conductivity at a specific water content (m/sec), k_s is the saturated value of conductivity (m/sec), Θ is the volumetric moisture content (cm^3/cm^3), e is the base of natural logarithm (2.718), y is a dummy variable of integration representing the natural logarithm of negative pore pressure, i is the interval between the range of j to N, j is the least negative pore water pressure to be described by the final function(kPa), N is the maximum negative pore water pressure to be described by the final function (kPa), ψ is the soil suction corresponding to the *jth* interval (kPa) and Θ' is the first derivative of the Fredlund and Xing (1997) equation for the soil-water characteristic curve (Eq. 6-20and Eq. 6-21).

Variability and uncertainty in the soil-water characteristic curve and the hydraulic conductivity function

As discussed in Chapter 3, the soil-water characteristic curve and the hydraulic conductivity function are highly variable, non-linear soil properties that depend on a large number of soil factors. Considering the large areas that levees cover and the limited soil data available for seepage analyses, performing laboratory tests to determine these functions would be costly. However, an examination of laboratory measurements is useful for understanding the inevitable uncertainties in soil-water characteristic curves and hydraulic conductivity functions.

Zapata et al. (2000) and her colleagues at Arizona State University conducted a survey to determine the degree of accuracy with which soil-water characteristic curves could be established by different laboratories. Three different soils, a sand, a silt and a clay were sent to 11 different laboratories. These laboratories performed tests to establish soil-water characteristic curves for the three soils by measuring moisture contents at various values of soil suction. The results are shown in Figure 6-11.
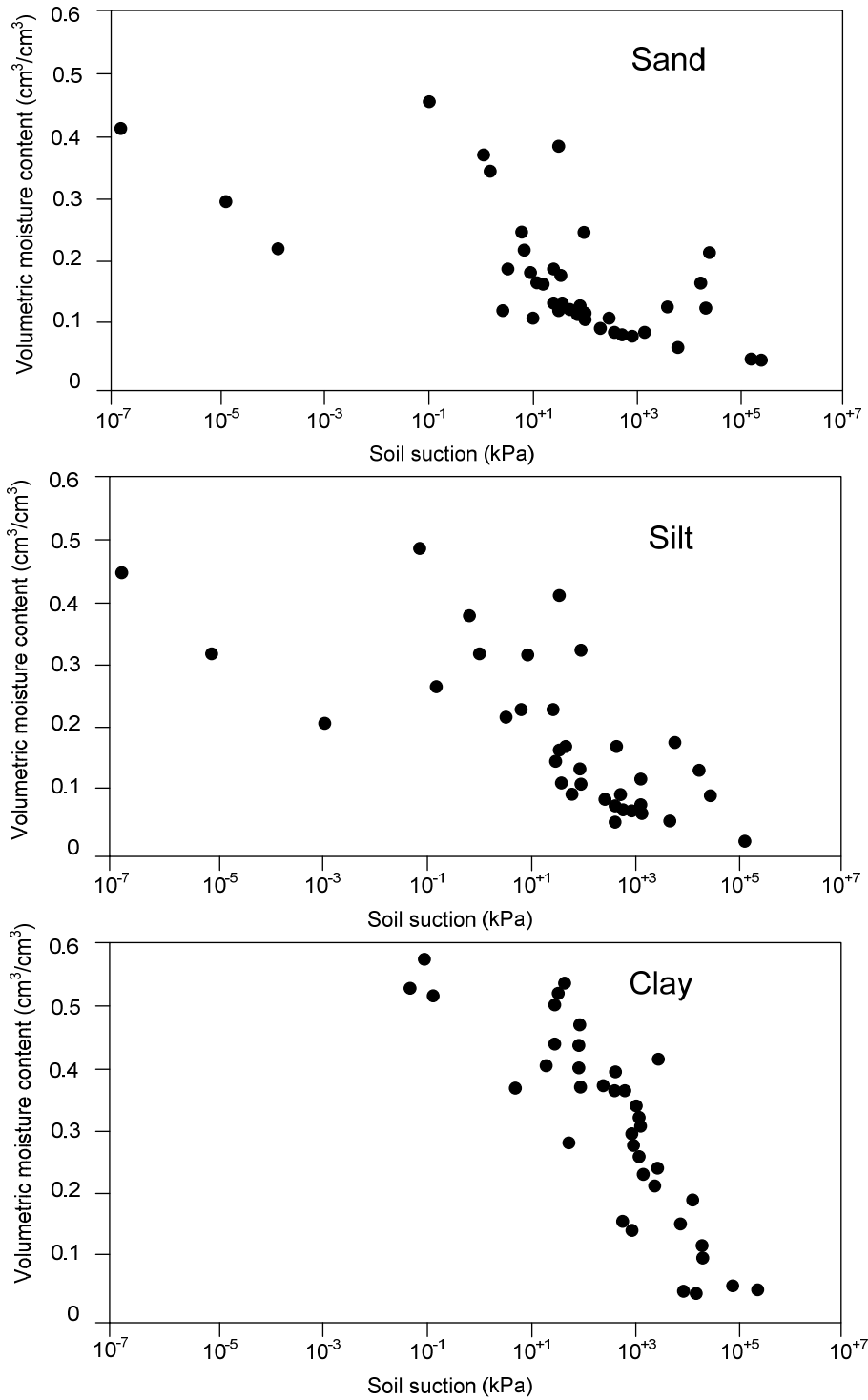
Figure 6-11 – Measurements of soil-water characteristic curves for three soils made by different laboratories (Zappata et al. 2000) (determined fair use)

As the figures show there are very significant differences in the measurements from the various laboratories. Zapata et al. (2000) concluded that it may not be possible to measure soil-water characteristic curves reliably, which seems clear from the results in Figure 6-11.

Conclusions regarding soil-water characteristic curves and hydraulic conductivity functions

Experimental determination of soil-water characteristic curves and hydraulic conductivity functions is difficult, and the results of such tests involve considerable uncertainty. It is at least as accurate to estimate these functions as it is to try to measure them. The estimation techniques described in this chapter can be used in practice to estimate the soil-water characteristic curve and the hydraulic conductivity function. The difficulty in using many of these techniques is that many of the methods use textural classifications or other soil properties that may not be readily available or familiar to geotechnical engineers. As shown in Chapter 5, the most significant soil property affecting the transient seepage analysis is the value of saturated hydraulic conductivity. Considering this, a method has been devised to estimate the soil-water characteristic curve based on the best estimate of the soil's saturated hydraulic conductivity, as described in Chapter 7.

Chapter 7

A new database method of determining soil properties

Introduction

The soil-water characteristic curve and the hydraulic conductivity function are often estimated rather than measured due to the cost and difficulty in measurement. Zapata et al. (2000) showed that laboratory methods of the soil-water characteristic curve can vary significantly depending on the laboratory performing the test. As described in Chapter 6, many of the methods for estimating the soil-water characteristic curve rely on the textural class of the soil which is rarely used in geotechnical engineering. This chapter provides guidance for estimating soil-water characteristic curves based on the estimated or measured value of saturated hydraulic conductivity for the soil.

Previous methods

As discussed in Chapter 6 there are many empirical methods to determine unsaturated soil hydraulic properties. Many of these methods (Gupta and Larson 1979; Rawls et al. 1982; De Jong et al. 1983; Saxton et al. 1986; Pachepsky et al. 1996) were devised in the soil science discipline and require soil properties that geotechnical engineers are unaccustomed to measuring such, as textural class and organic content. In addition the most important soil property in a transient seepage analysis, saturated hydraulic conductivity, can vary significantly within soil textural class. Other methods supply fitting parameters for established soil-water characteristic curve equations (Zapata et al. 2000; Vanapalli and Catana 2005; Perera et al. 2005). These methods require knowledge of the fitting equation and significant calculations to derive the fitting parameters. Methods that derive the soil-water characteristic curve from grain-size distributions (Arya and Paris 1981; Fredlund et al. 1997) have no provision for taking into account the variability of the grain-size distribution of the soil. A

few methods require a laboratory measured value of soil suction at a moisture content (McQueen and Miller 1974; Chin et al. 2010). This reduces laboratory cost and time but not the variability associated with laboratory measurements. Other methods that use neural networks or genetic programming (Schaap and Leji 1998; Nemes et al. 2001; Schaap et al. 2001) require programming knowledge.

New method using a knowledge based system for estimating unsaturated soil properties

Fredlund (1998) describe the broad principles for using a knowledge based system to estimate soil-water characteristic curves and hydraulic conductivity functions as shown in Figure 7-1.
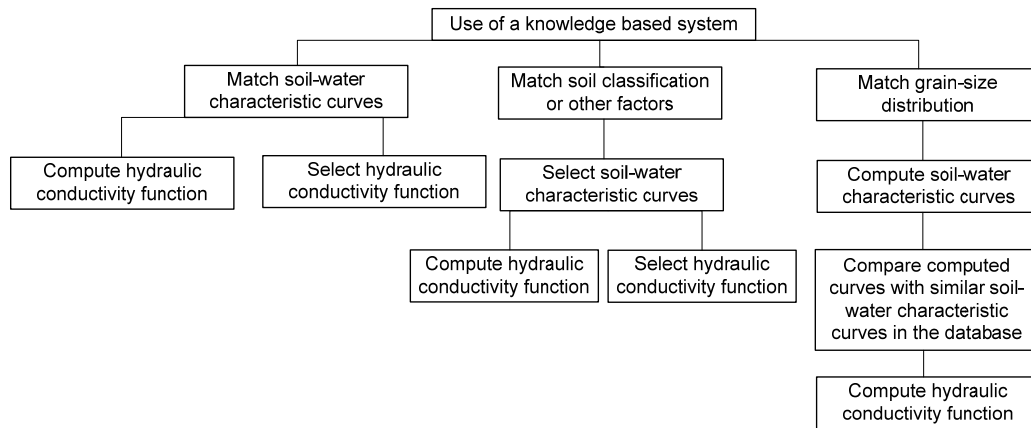
Figure 7-1 – Using a *knowledge based* system to determine soil properties after Fredlund (1998) (with permission from ASCE)

A *knowledge based system* employs one or more databases of measured soil-water characteristic curves and hydraulic conductivity functions. The databases also contain additional information such as grain size distribution, textural class or soil classification.   This information is used to select soils with similar characteristics as a means of estimating the soil-water characteristic curve for the soil of interest.

Several databases common in the soil science and agricultural fields have not been used significantly in geotechnical engineering. Examples include the Rosetta database from the United States Soil Salinity Laboratory, the RETC database from Van Genuchten et al. (1991), the commercially available SoilVision computer program from SoilVision Systems and the Unsaturated Soil Hydraulic Database (UNSODA) from Nemes et al. (2001).

Two difficulties arise when attempting to use these databases as illustrated in Figure 7-1; (1) which soil properties should be matched or compared to produce the most accurate unsaturated soil properties, and (2) common soil properties used in geotechnical engineering, such as the Unified Soil Classification System, are not included in the databases. A method is presented here using the UNSODA database and saturated hydraulic conductivity as the basis for selecting similar soils, to produce a series of charts that can be used to estimate soil-water characteristic curves directly. The UNSODA database was chosen because it includes values of saturated hydraulic conductivity for many soils.

The UNSODA database is a collection of data for 790 soils organized in a Microsoft Access database. The information obtained for these soils came from published sources and a survey of 100 soil scientists (Leij et al. 1996).

The 790 soils in the UNSODA database are not classified according to the Unified Soil Classification System (USCS). It is not possible to classify the soils according the USCS because the database does not contain Atterberg Limits. All of the soils in the database are classified according to the USDA soil textural classification system. This classification system is based on the percentage of clay, silt and sand. This system of classification is rarely used in geotechnical engineering. Attempts have been made to convert the USDA textural classification to the USCS. As shown in Figure 7-2 from Curtis (2005), the USDA and USCS classification systems differ significantly. A highly plastic clay (CH) can be classified as six different textural classes in the USDA system.

127

Each point shows the position within the USDA textural class triangle of highly plastic clay, there is little correspondence
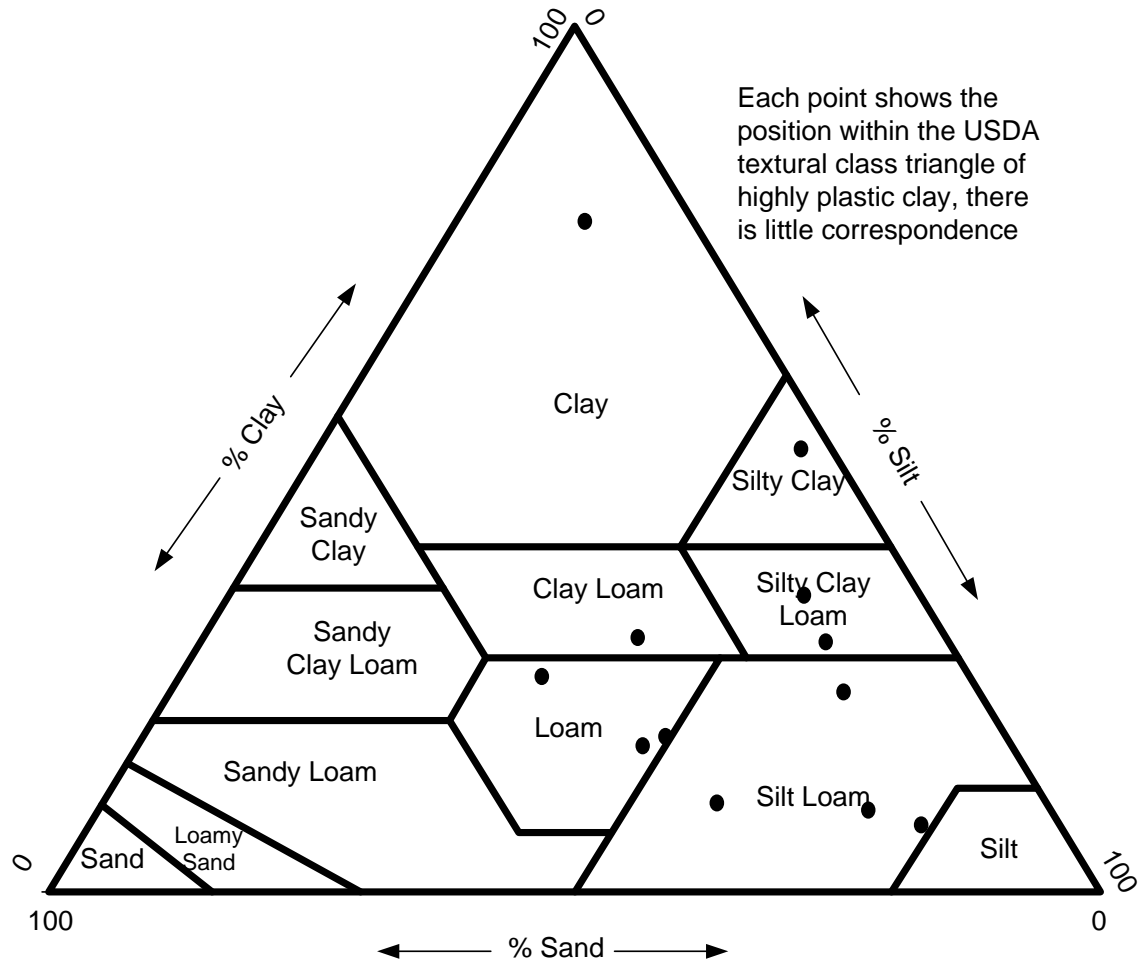
Figure 7-2 – Soils classified as highly plastic clay (CH) according to the USCS plotted on the USDA textural class triangle after (Curtis 2005) (determined fair use)

An attempt was made to correlate the soil-water characteristic curves in the database with the percent passing the No. 200 sieve. The percent passing the No. 200 sieve was chosen because it is a common geotechnical test and the information was available in the database.   This attempt was abandoned because the percent passing the No. 200 sieve is not correlated with the saturated hydraulic conductivity as shown in Figure 7-3 for soils with 10% to 20% passing the No. 200 sieve.
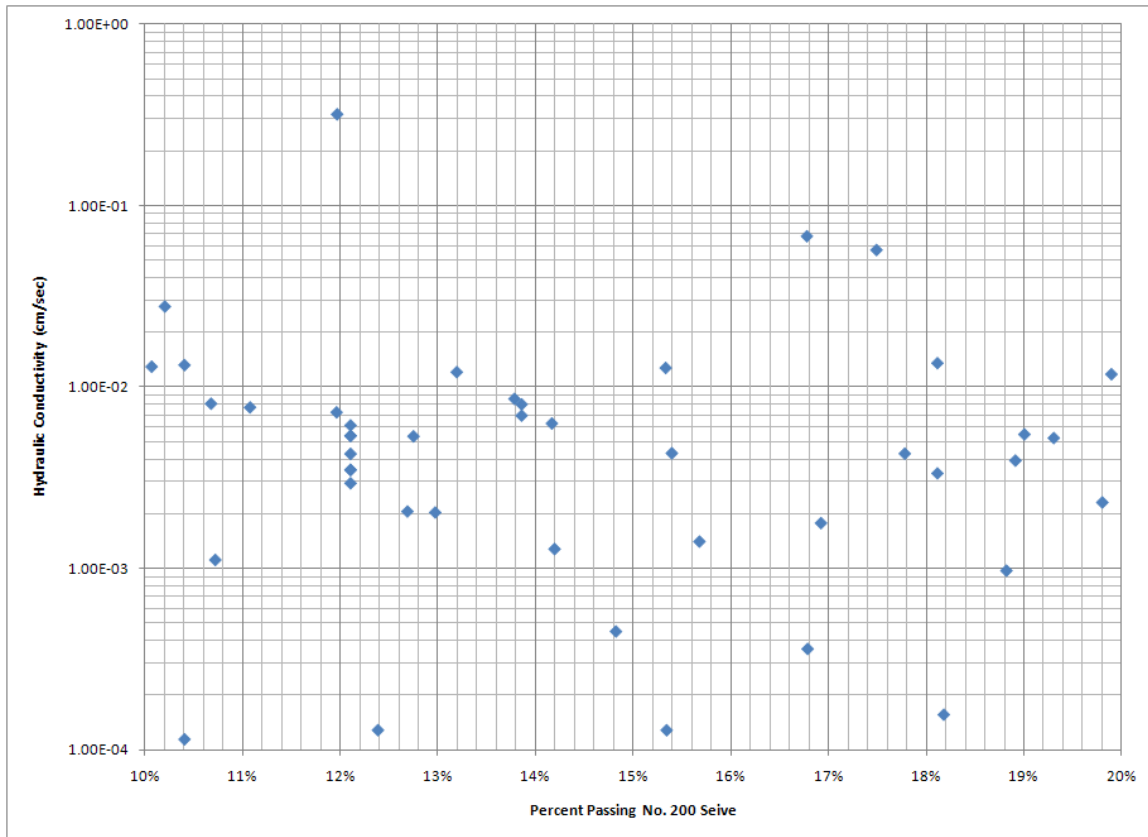
Figure 7-3 – Saturated hydraulic conductivity correlated with the percent passing the No. 200 sieve from the UNSODA database

Soil categorization based on saturated hydraulic conductivity

Because the value of saturated hydraulic conductivity influences the results of a transient seepage analysis very significantly, it was concluded that saturated hydraulic conductivity would provide a suitable factor for grouping soils for the purpose of selecting appropriate soil-water characteristic curves.

Soil-water characteristic curve charts were developed for five groups of soils based on saturated hydraulic conductivity. The five groups were chosen from a simple correlation proposed by Terzaghi et al. (1996) based on soil type shown in Table 7-1.

Table 7-1 – Five soil classifications based on saturated hydraulic conductivity after Terzaghi et al. (1996) (with permission from John Wiley and Sons)

Soil Category	Saturated Hydraulic Conductivity (cm/sec)
Coarse Sand	$> 10^{-1}$
Fine Sand	10^{-1} to 10^{-3}
Silty Sand	10^{-3} to 10^{-5}
Silt	10^{-5} to 10^{-7}
Clay	$< 10^{-7}$

Soil-water characteristic curve charts

The soil-water characteristic curve charts shown in Figure 7-4 through Figure 7-7 were developed by querying laboratory drying tests of soil-water characteristic curve data based on the five soil groups from Table 7-1. The queried data contained volumetric moisture content versus soil suction. The volumetric moisture content values were converted to degree of saturation using measured values of porosity. The data, using degree of saturation as the measure of water content, was plotted on semi-log plot. Best fit lines for the data were developed and labeled as the drying curve.

The standard deviation of this best fit line was calculated using the procedure described in the *Manual for Geotechnical Reliability Calculations* from Sleep and Duncan (2010). Only data between 95% and 40% degree of saturation were used to calculate the standard deviation to prevent very low and very high values of soil suction from increasing the standard deviation of the data. These standard deviations are shown on each of the four soil-water characteristic curve charts in Figure 7-4 through Figure 7-7. Because soil-water characteristic curves have hysteresis between wetting and drying, the wetting curve was constructed based on the finding by Yang et al. (2004) that the hysteresis between the wetting and drying soil-water characteristic curves is variable, but is approximately 1 order of magnitude. To calculate upper and lower bounds for

each group, the 90% confidence limit was constructed using 1.28 times the standard deviation of the dataset to the right of the drying curve and to the left of the wetting curve. The database did not contain data for soils within the clay group ($k < 10^{-7}$ cm/sec) so the clay soil-water characteristic curve was estimated as the shaded area on the silt chart.

Figure 7-4 – Soil-water characteristic curves for coarse sand (k > 10⁻¹ cm/sec) constructed from the UNSODA database using calculated standard deviations to construct the wetting curve and confidence limits
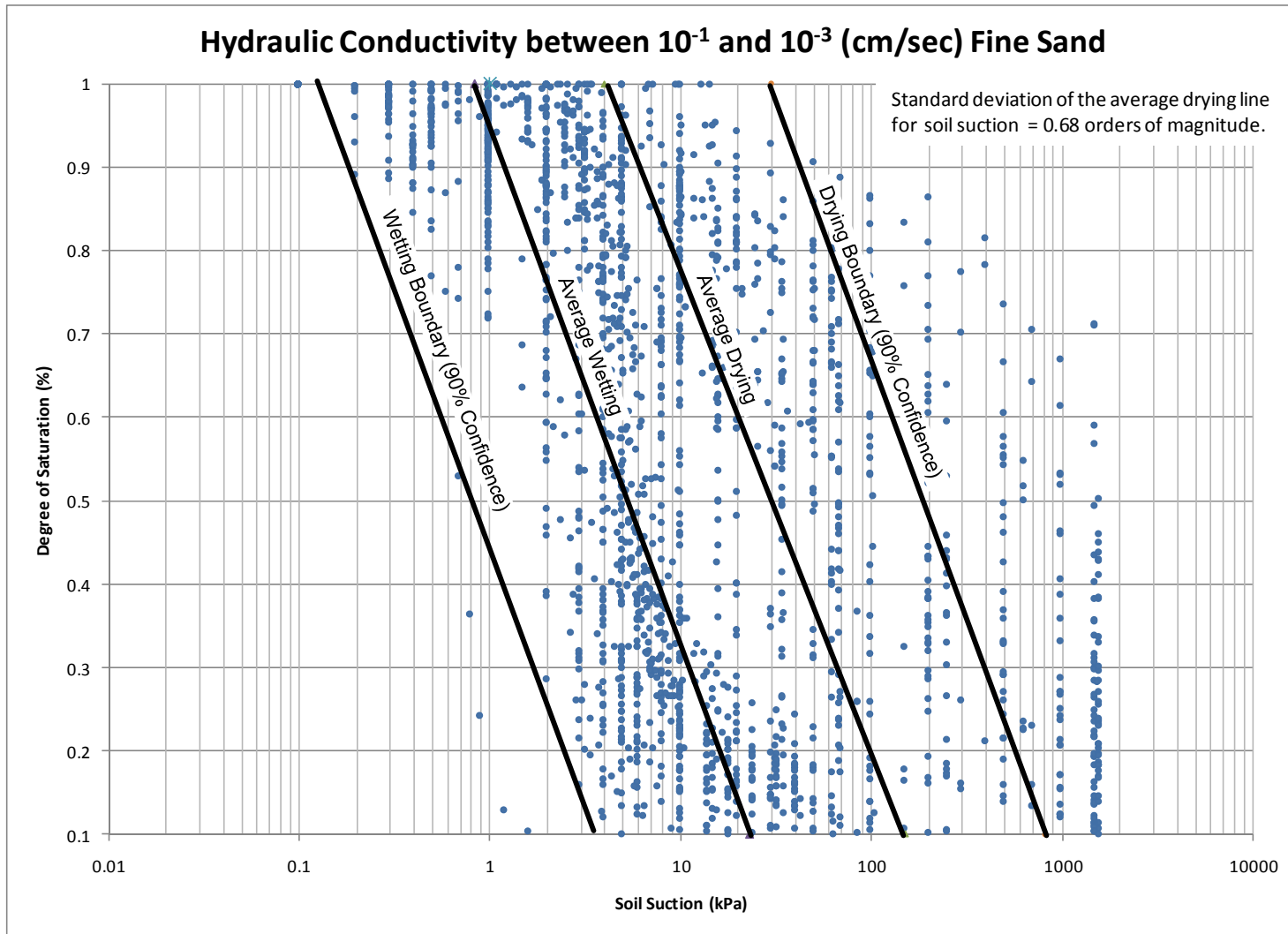
Figure 7-5 – Soil-water characteristic curves for fine sand (k = 10^{-1} to 10^{-3} cm/sec) constructed from the UNSODA database using calculated standard deviations to construct the wetting curve and confidence limits

133
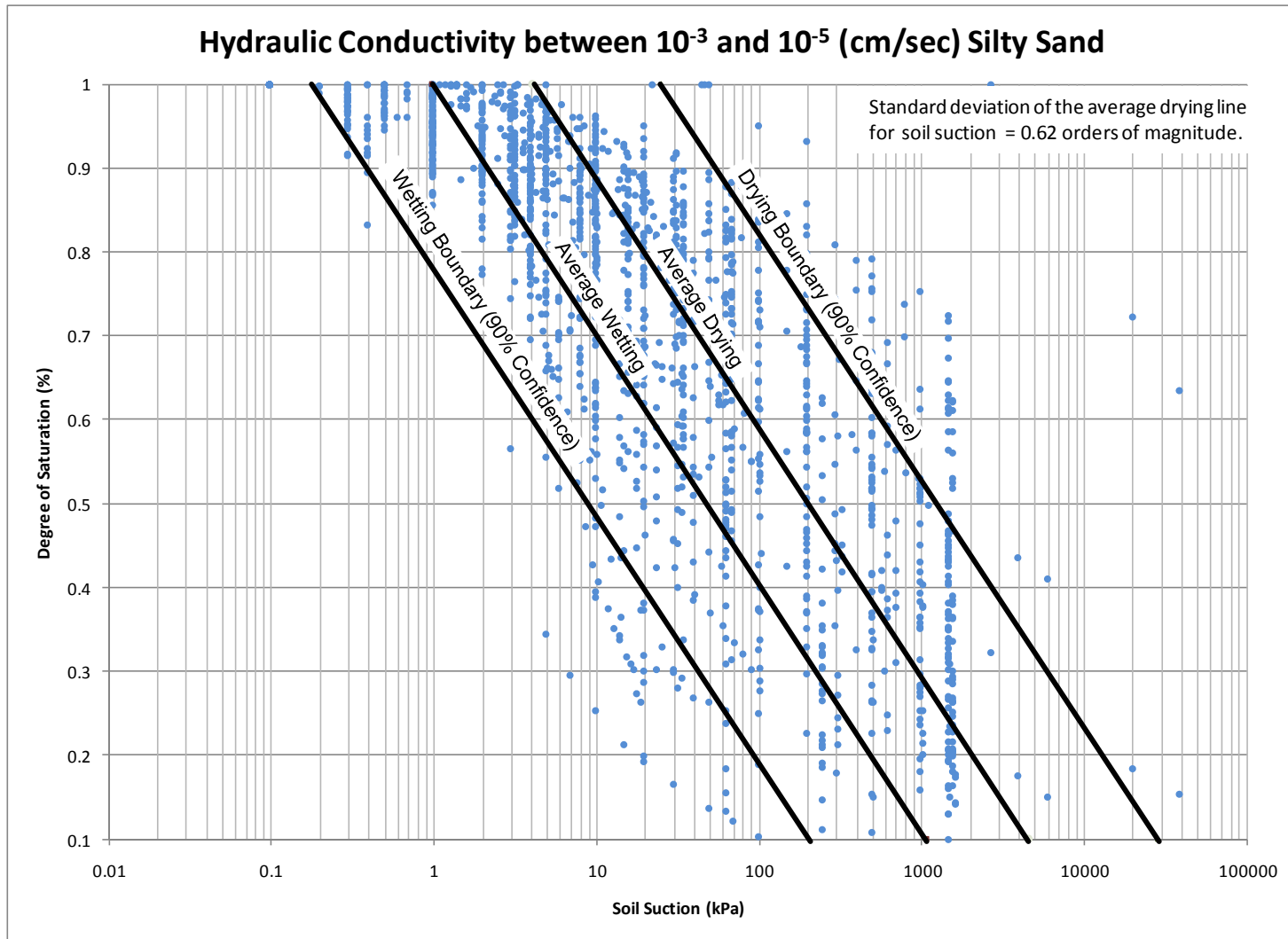
Figure 7-6 – Soil-water characteristic curves for silty sand (k = 10^{-3} to 10^{-5} cm/sec) constructed from the UNSODA database using calculated standard deviations to construct the wetting curve and confidence limits
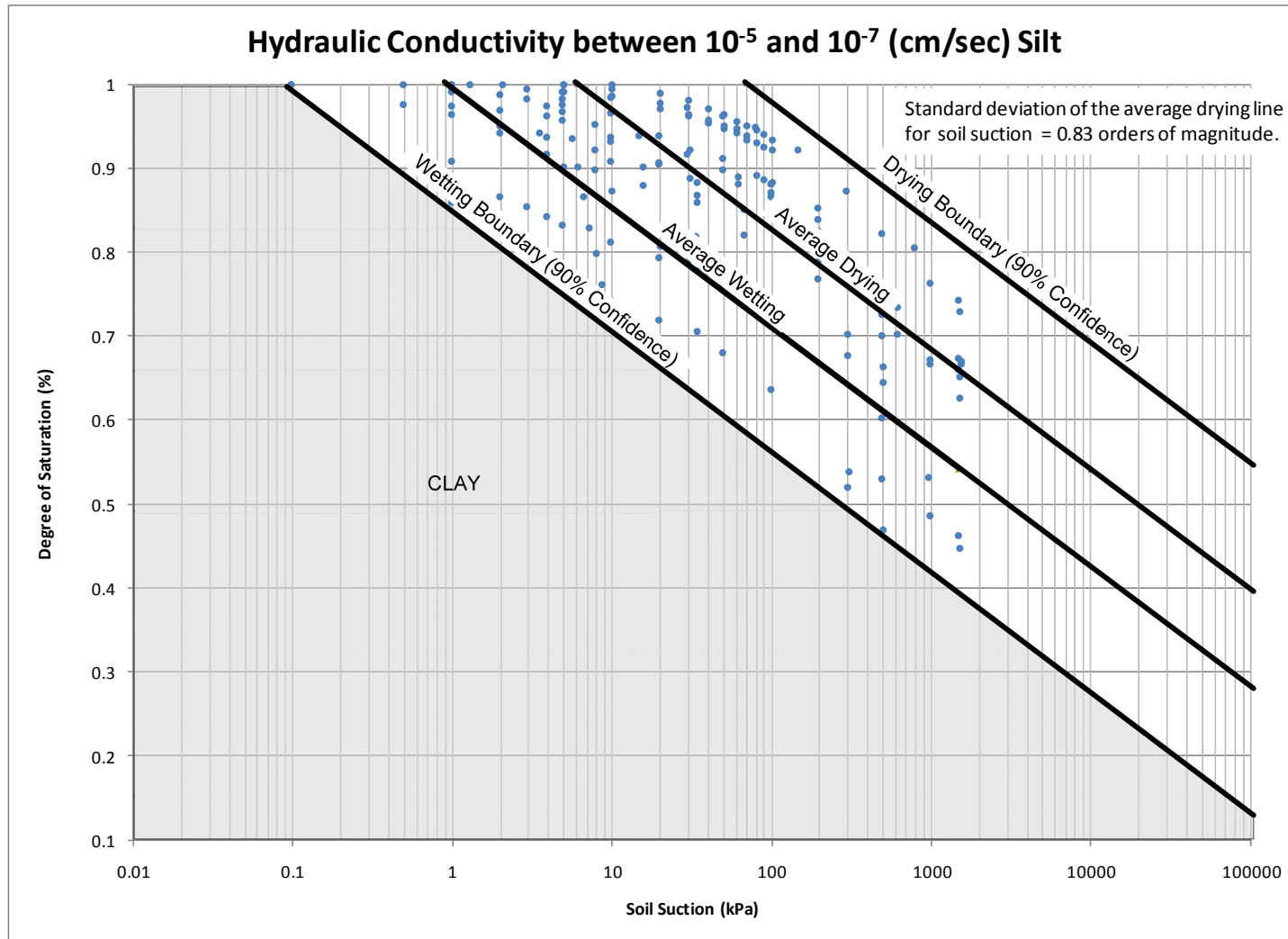
Figure 7-7 – Soil-water characteristic curves for silt (k = 10^-5 to 10^-7 cm/sec) constructed from the UNSODA database using calculated standard deviations to construct the wetting curve and confidence limits

Use of the soil-water characteristic curve charts

Figure 7-4 through Figure 7-7 can be used to estimate the soil-water characteristic curve for levee soils for use in a transient seepage analysis. The following steps are required to determine the soil-water characteristic curve for a soil based on these figures.

1. Estimate or measure the saturated hydraulic conductivity of the soil.
2. Use this value of saturated hydraulic conductivity to determine which figure is appropriate for estimation of the soil-water characteristic curve (Table 7-2).

Table 7-2 – Appropriate figures to use for estimation of the soil-water characteristic curve based on the saturated value of hydraulic conductivity

Soil Category	Saturated Hydraulic Conductivity (cm/sec)	Figure to use to estimate the soil-water characteristic curve
Coarse Sand	$> 10^{-1}$	Figure 7-4
Fine Sand	10^{-1} to 10^{-3}	Figure 7-5
Silty Sand	10^{-3} to 10^{-5}	Figure 7-6
Silt	10^{-5} to 10^{-7}	Figure 7-7
Clay	$< 10^{-7}$	Left of the silt wetting curves in Figure 7-8

3. Determine the appropriate soil-water characteristic curve based on whether the soil is wetting or drying.
4. Input into SEEP/W two points from the shown curve (soil suction at 1.0 and 0.1 degree of saturation are convenient choices).
5. To input these values into SEEP/W it is necessary to convert the degree of saturation to volumetric moisture content.

$$\theta_{100\%} = n \cdot 100\%$$ **Eq. 7-1**

$$\theta_{10\%} = n \cdot 10\%$$ **Eq. 7-2**

Where $\theta_{100\%}$ and $\theta_{10\%}$ are the volumetric moisture contents at 100% and 10% degree of saturation, and *n* is the porosity of the soil.

6. This process should be repeated for curves to the left and right of the original curve to account for likely variability of the soil-water characteristic curve.

As an example, the soil-water characteristic curve of the silty sand in the half-scale levee constructed by Worsching et al. (2004) was estimated using the proposed method. The soil-water characteristic curves measured in the laboratory and the estimated soil-water characteristic curve used in the transient seepage analysis presented in Chapter 5 are shown in Figure 7-8.
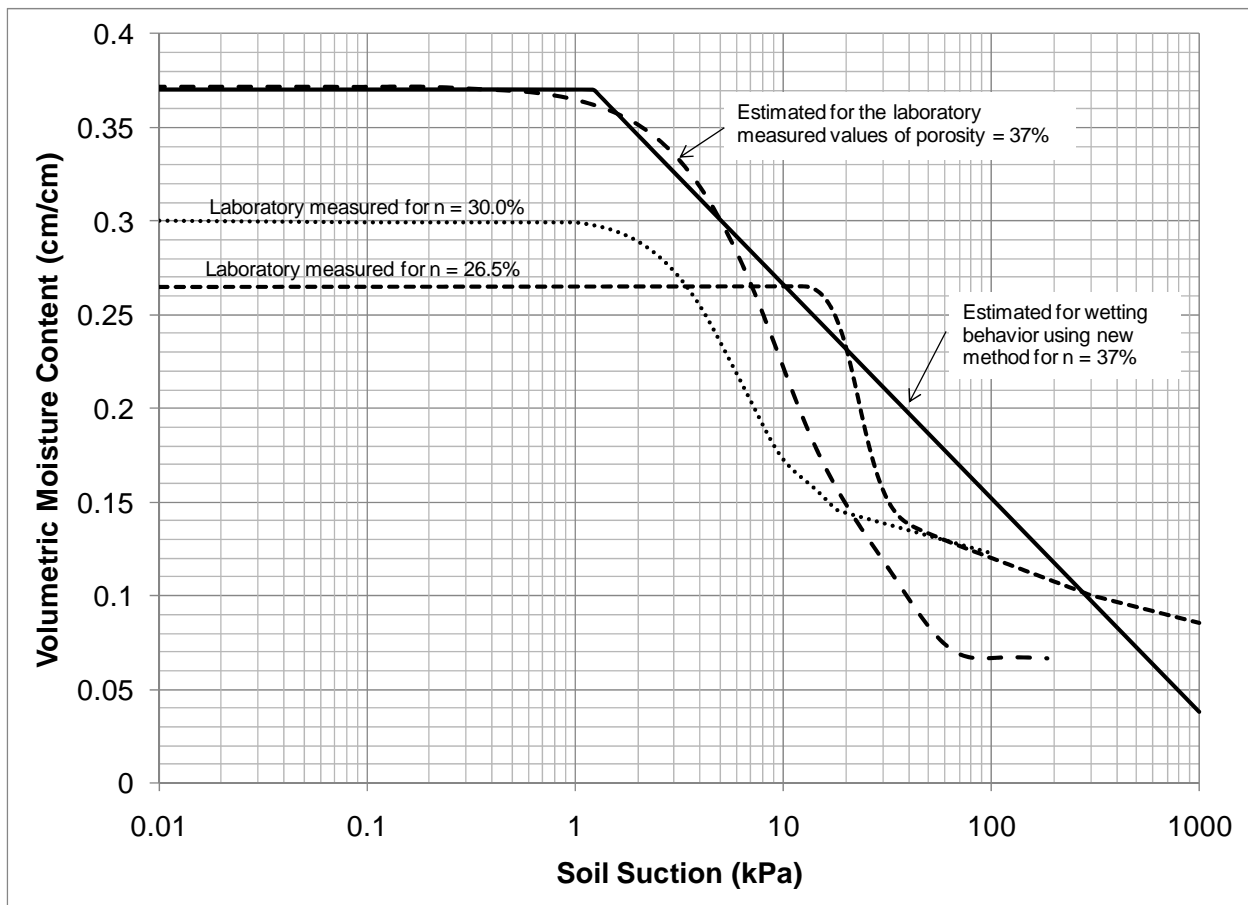
Figure 7-8 – Soil-water characteristic curves measured in the laboratory and estimated for the silty sand of the half-scale levee test

Results of the new method of estimating unsaturated soil properties with the half-scale levee test

The results of the transient seepage analysis of the half-scale levee test using the estimated soil-water characteristic curve from the proposed method is shown in Figure 7-10. For this analysis the same point-by-point values of the initial volumetric moisture content were used from the analysis in Chapter 5. The initial conditions are shown in Figure 7-9. The hydraulic conductivity function was estimated from the soil-water characteristic curve using the Van Genuchten (1980) transformation available in SEEP/W. The results match those of the instrumented half-scale levee test fairly closely.

Step 6 of the proposed method is to use a range for the soil-water characteristic curve to take into account variability of the soil property. The procedure of estimating the soil-water characteristic curve for the silty sand was repeated using the 90% wetting boundary (to the left of the initial estimate) and the drying boundary (to the right of the initial estimate). The results of the analyses using these soil-water characteristic curves are shown in Figure 7-11 and Figure 7-12.

In Chapter 5 the best estimate of the saturated hydraulic conductivity was increased by 5x to match the numerical and physical results of the half-scale levee test. Using the estimate of the soil-water characteristic curve from the new proposed method and 5x the best estimate of the saturated hydraulic conductivity the analysis was repeated. The results are shown in Figure 7-13. The results of the analysis closely match the physical model.
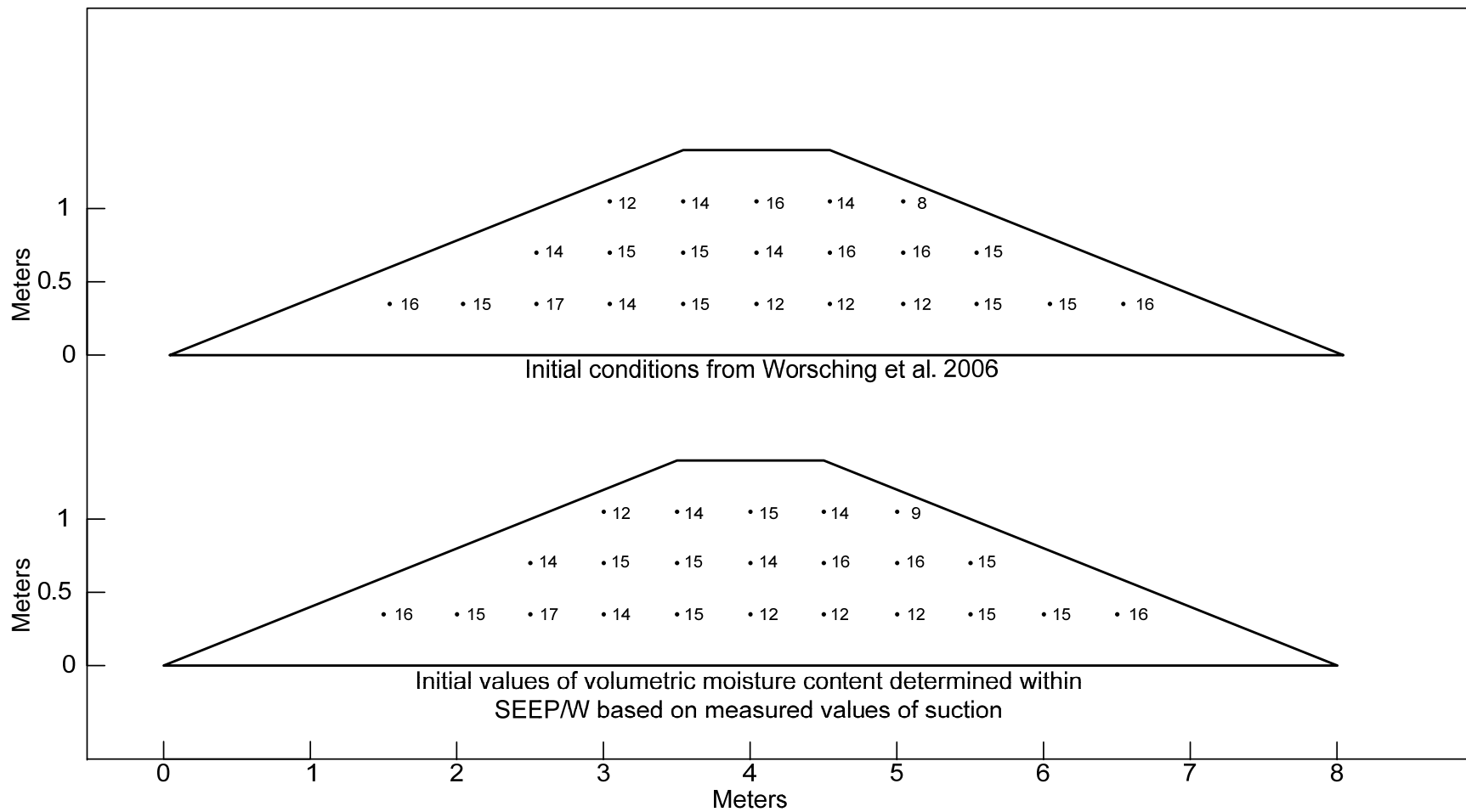
Figure 7-9 – Initial conditions from the half-scale levee test and the initial conditions used with the soil properties estimated from the unsaturated soil property charts
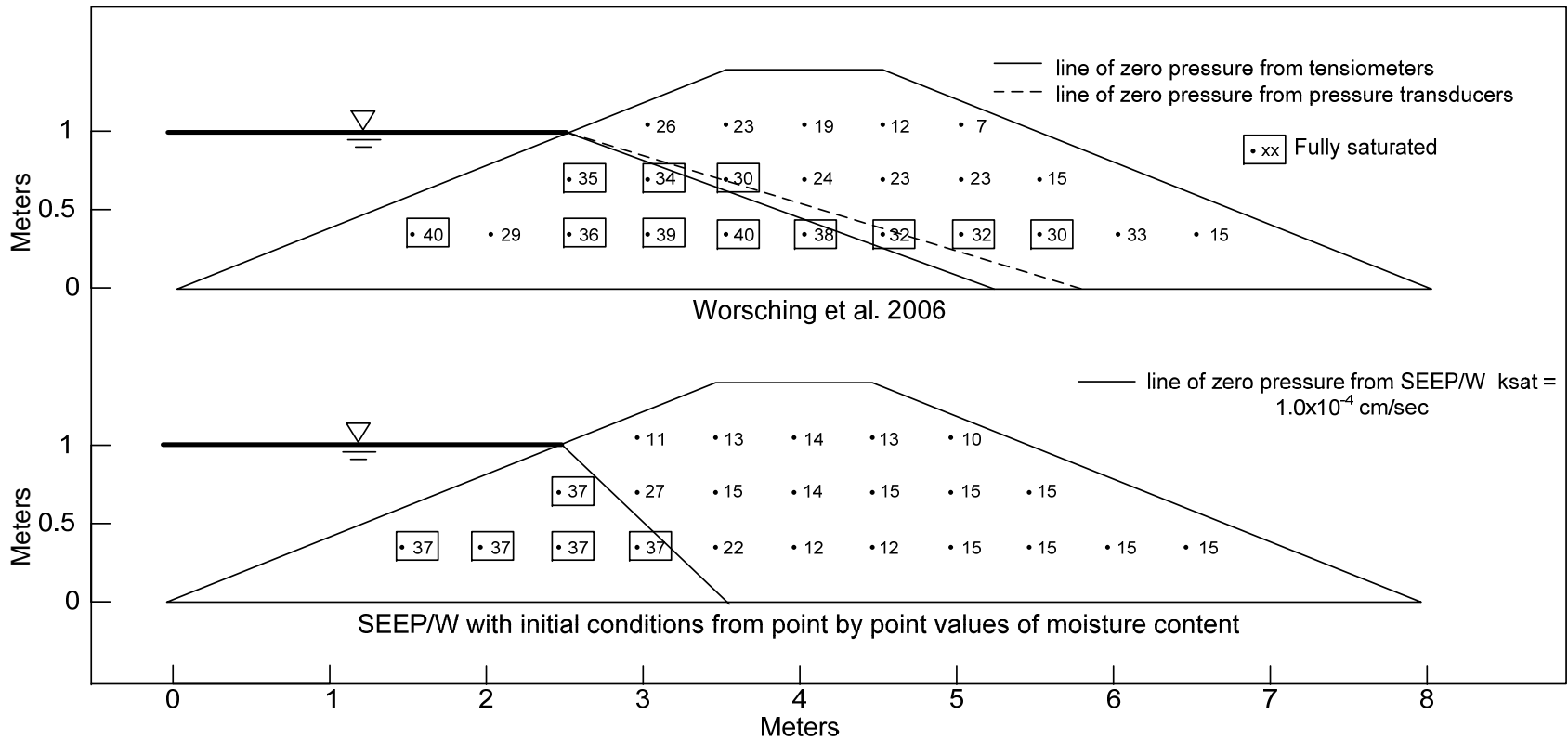
Figure 7-10 – Conditions after 354 hours from the half-scale levee test and the numerical model with the soil properties (the wetting SWCC) estimated from the unsaturated soil property charts and the saturated hydraulic conductivity equal to 1.0x10^{-4} cm/sec
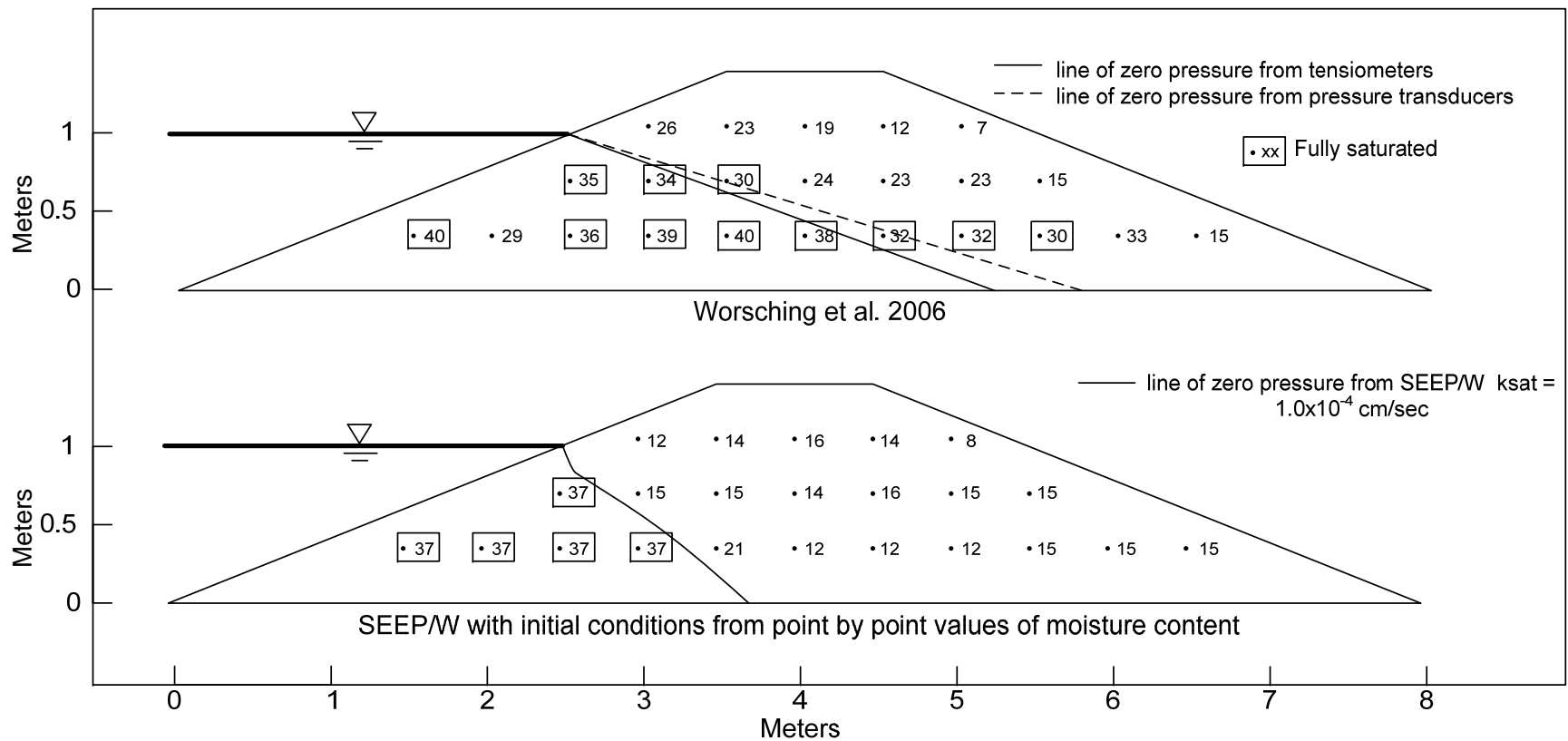
Figure 7-11 – Conditions after 354 hours from the half-scale levee test and the numerical model with the soil properties (the wetting 90% boundary SWCC) estimated from the unsaturated soil property charts and the saturated hydraulic conductivity equal to 1.0x10⁻⁴ cm/sec
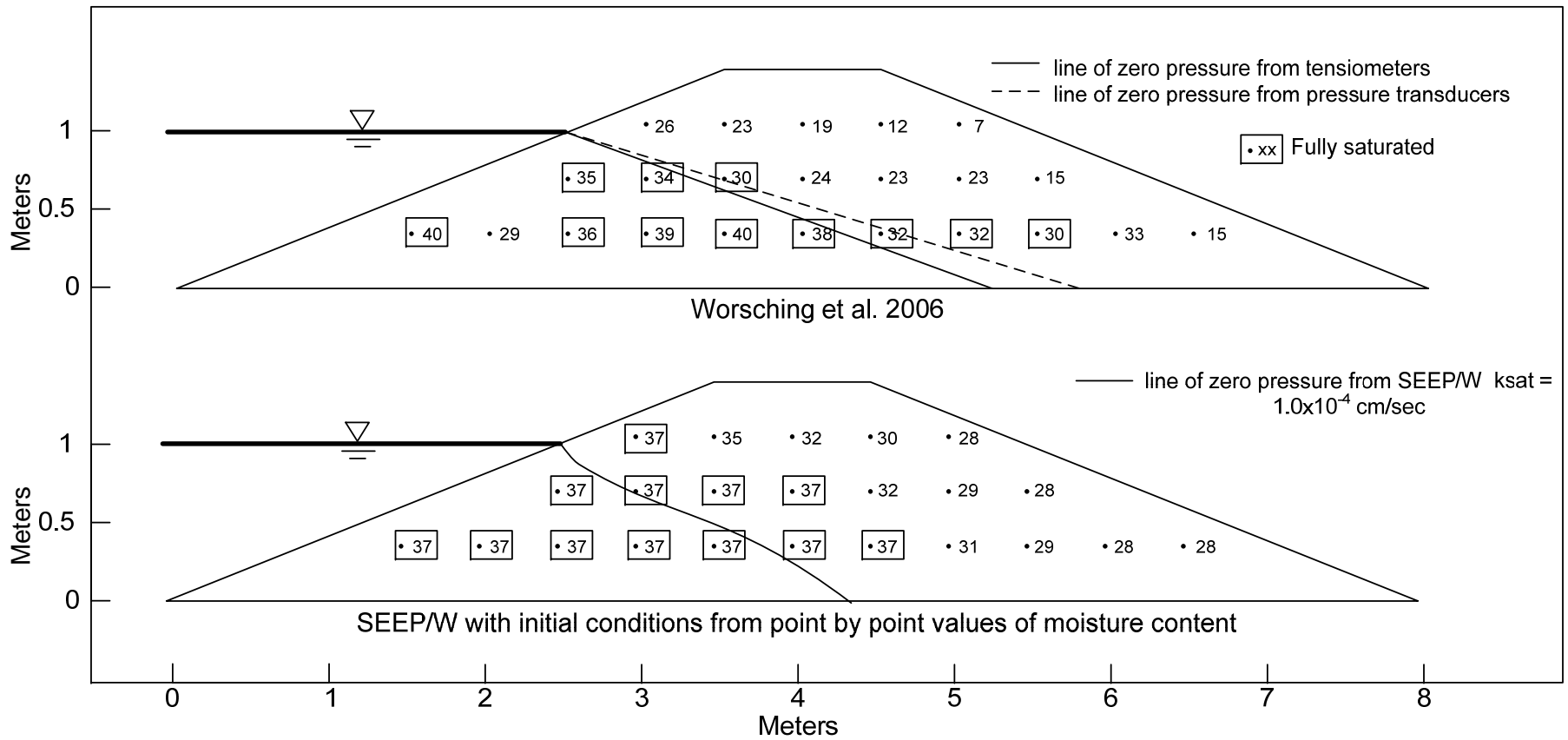
Figure 7-12– Conditions after 354 hours from the half-scale levee test and the numerical model with the soil properties (the drying SWCC) estimated from the unsaturated soil property charts and the saturated hydraulic conductivity equal to 1.0x10⁻⁴ cm/sec
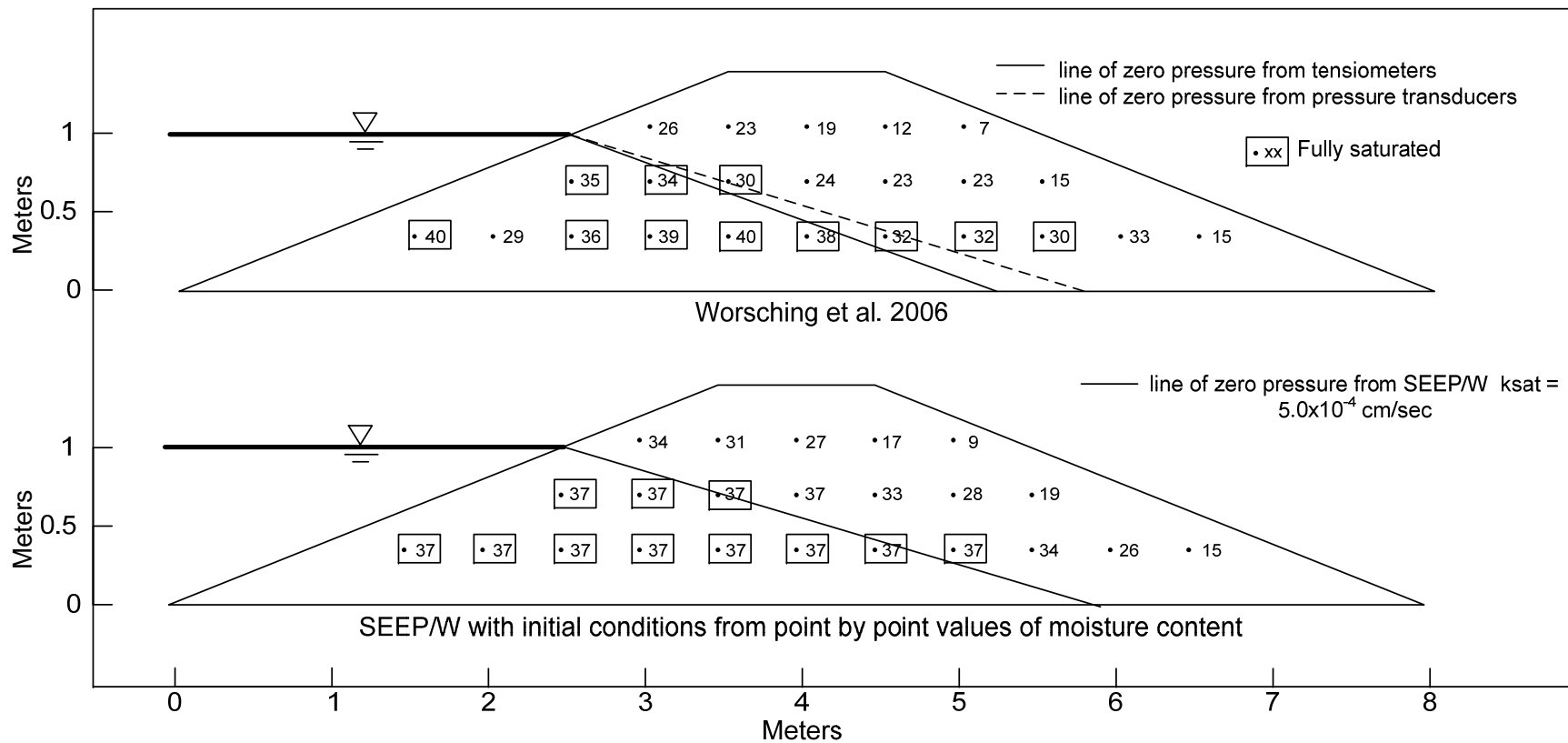
Figure 7-13 – Conditions after 354 hours from the half-scale levee test and the numerical model with the soil properties (the wetting SWCC) estimated from the unsaturated soil property charts and the saturated hydraulic conductivity equal to 5.0x10^{-4} cm/sec

Conclusions

This chapter presents a new method that can be used to estimate the soil-water characteristic curve for use in transient seepage analyses of levees. The method categorizes soils based on the best estimate the saturated hydraulic conductivity. Charts were developed to provide an estimate of the soil-water characteristic curve based on the saturated hydraulic conductivity of the soil.

This method was used to estimate the soil-water characteristic soil for the half-scale levee soils used in the Worsching et al. (2006) experiment. The results of a numerical model using the estimated soil-water characteristic curve from this method match the results of the half-scale model fairly closely.

Chapter 8
Initial Conditions for
Transient Seepage Analyses

Introduction

A transient seepage analysis of a flood event on a levee calculates changes in suction, pore pressure, degree of saturation, and hydraulic conductivity with time in response to a change in the external water level. The pore pressure and suction values within the levee at the beginning of the analysis are called the initial conditions. The hydraulic conductivity and volumetric moisture contents of the unsaturated soils within the levee at the beginning of the transient seepage analysis are determined by the values of suction and the soil-water characteristic curves of the soils. If the initial values of soil suction are small and the degrees of saturation are high, the hydraulic conductivity of the soil will be high (closer to the saturated values), and the time it takes to reach steady state conditions will be relatively small. If the initial values of suction are high, and the degrees of saturation are low, the initial values of hydraulic conductivity will be low, and the time required to reach steady state conditions will be long. Thus it is important to begin transient seepage analyses with reasonable estimates of the initial conditions.

Types of initial conditions

Within the finite element computer program SEEP/W, the initial conditions can be defined in three ways: (1) by specifying the position of a phreatic surface, (2) by performing an initial steady state seepage analysis to establish a phreatic surface, or (3) by specifying a distribution of initial suction values. These three possibilities are shown in Figure 8-1.

The initial conditions defined with a phreatic surface or steady state seepage analyses have similar characteristics. For points above the phreatic surface, values of soil suction increase with increasing elevation above the phreatic surface. Along an

equipotential line (perpendicular to the flow lines for isotropic permeability), the soil suction is equal to the unit weight of water multiplied by the elevation above the phreatic surface, as shown in Figure 8-1. This corresponds to a hydrostatic variation of suction with elevation.

The initial condition for a transient seepage analysis can also be defined by a specified distribution of soil suction values. The soil suction values are input as point values of soil suction, and suction values at intermediate points are generated by interpolation. The values of suction need not increase hydrostatically with elevation above the phreatic surface. Because any distribution of soil suction values can be used, this method offers the greatest flexibility. Use of this method requires an understanding of how initial conditions are affected by soil type, rainfall and evapotranspiration.
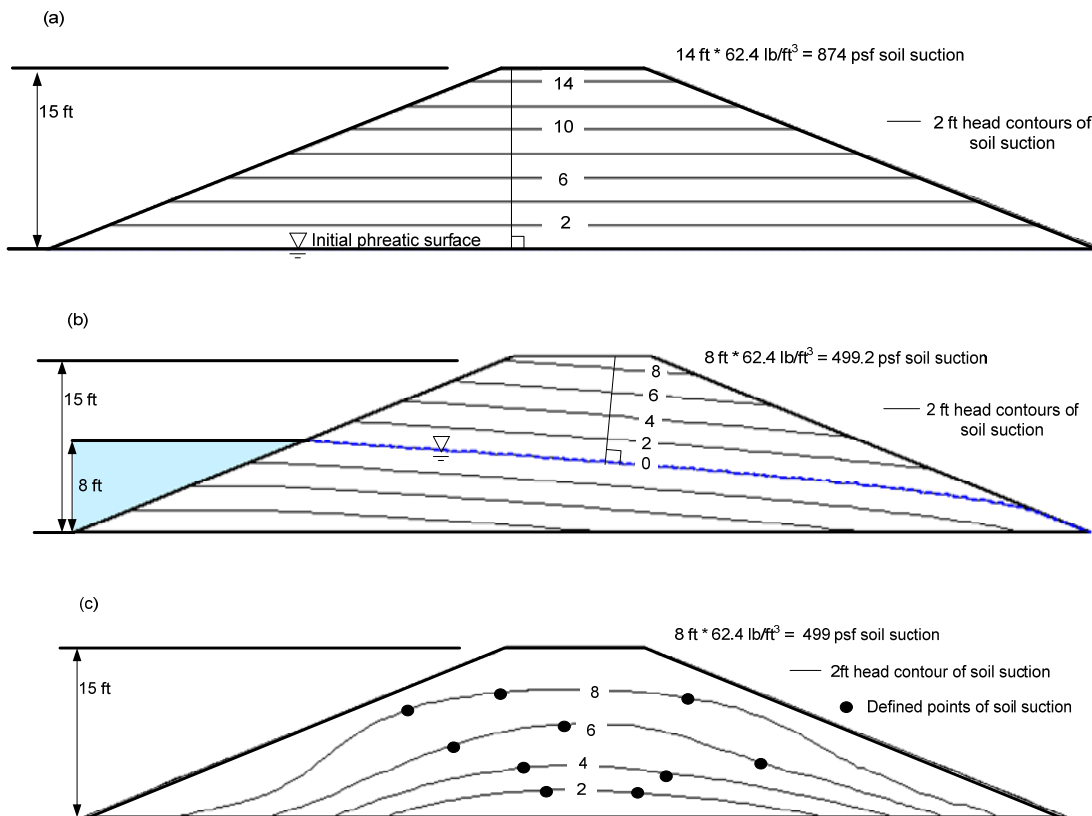
Figure 8-1 – Types of initial conditions to define the distribution of soil suction values, (a) – phreatic surface, (b) – steady state analysis, (c) – defined distribution of soil suction values

Measured soil suction distributions

To establish a basis for estimating realistic initial conditions, measured soil suction values found in the literature were examined. While no measured soil suction values were found specifically for levees, several were found for slopes and river banks that can provide guidance for estimating initial conditions for levees. These measured values of soil suction were compared to hydrostatic values of soil suction in those cases where a phreatic surface was known.

Riverbank soil suction profiles

Rinaldi et al. (2004) and Rinaldi and Casagli (1999) studied the stability of a silty sand riverbank in Italy during periods of rising and falling river levels. As part of their study, they used tensiometers placed in the riverbank to measure how the soil suction varied in response to changes in the river level and climactic conditions, such as precipitation and temperature. As shown in Figure 8-2, tensiometers were placed in the riverbank at depths of 0.6 to 2.8 meters below the ground surface. In colder months, such as January and March, soil suction values within the embankment were low, indicating downward movement of water from precipitation. During the warmer month of May, soil suctions increased due to evaporation at the ground surface. It can be seen that the measured soil suction values were always smaller than those corresponding to hydrostatic condition, which are shown as a dotted line in the figure.
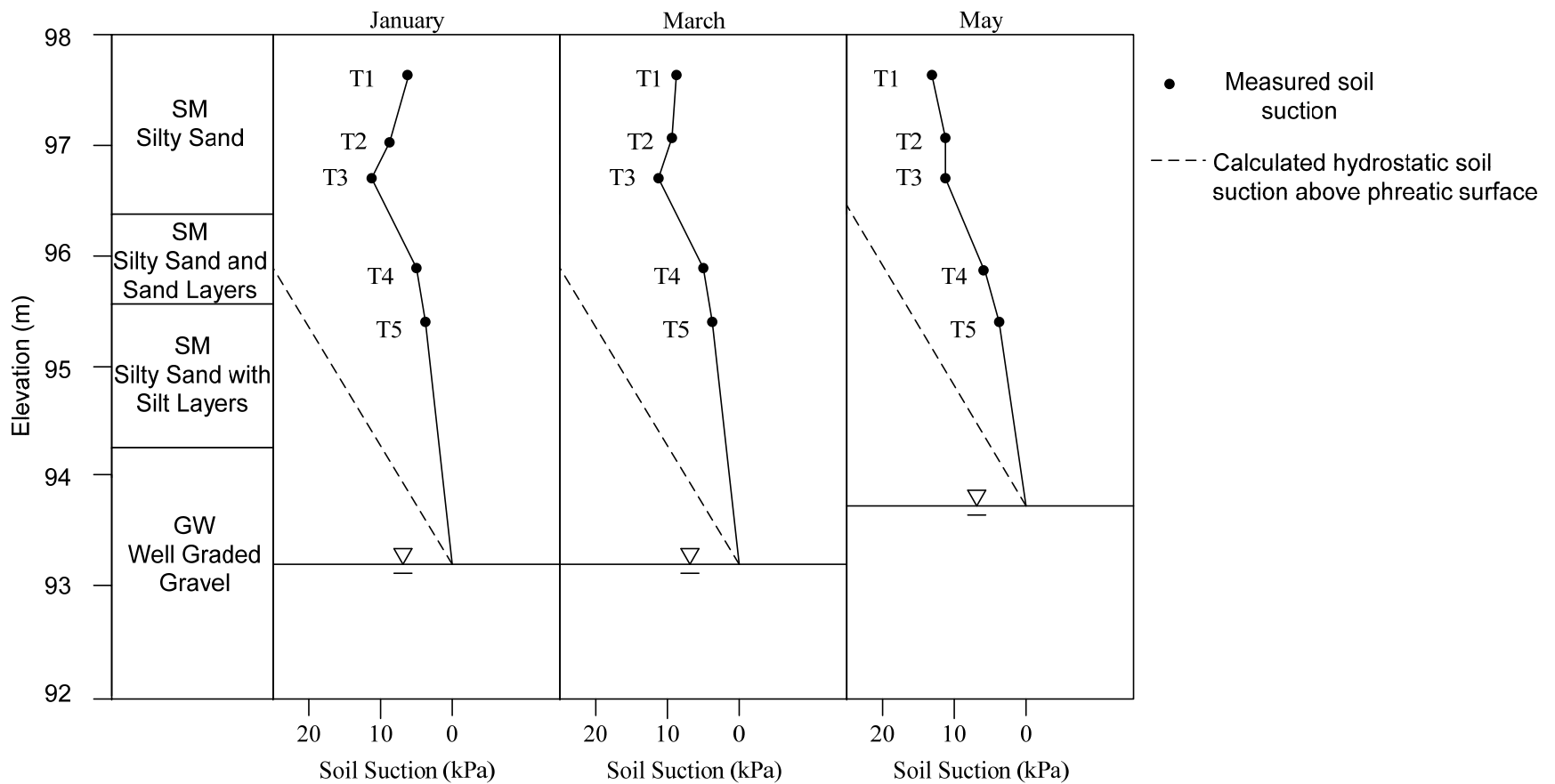
Figure 8-2 – Measured values of soil suction beneath a level ground surface near the Sieve River, in Tuscany, Italy in different seasons, and the hydrostatic soil suction above the phreatic surface (after Rinaldi et al. 2004) (with permission from John Wiley & Sons)

Soil suction profiles within slopes

Gasmo et al. (2000); Gvirtzman et al. (2008); Hughes et al. (2009); Kim et al. (2004); Ng et al. (2008); Ng et al. (2003); Springman et al. (2003); Tami et al. (2004); Toll et al. (2011); Trandafir et al. (2008); Tsaparas et al. (2003); and Tu et al. (2009) have instrumented soil slopes to monitor variations in soil suction with time and changes in climatic conditions. Some of these are shown here to provide guidance for estimating initial soil suctions in levees.

Ng et al. (2003) monitored tensiometers along sections R1, R2 and R3 shown in Figure 8-3 as they applied artificial rainfall on the slope with a sprinkler system. Tensiometers placed at depths up to 1.6 m showed a decrease in soil suction in response to the artificial rainfall with no change in the position of the phreatic surface. This suggests that rainfall is important in determining initial soil suction conditions within levees. It can be seen that the measured values of soil suction before and after the rainfall at tensiometers R1 and R2 are less than those corresponding to a hydrostatic variation with depth. At R3 the measured value of suction before the rainfall was larger than the hydrostatic value. After the rainfall event, the values of suction were reduced considerably, and were zero at R2 and R3.

Tu et al. (2009) monitored a loess slope in China with tensiometers to study changes in soil suction with both natural and artificially induced rainfall. The slope they studied is shown in Figure 8-4. As shown in the figure, the phreatic surface is at great depth beneath the soil slope. Average soil suctions measured at a depth of 2.5 m are significantly less than those that would correspond to a hydrostatic variation of suction with depth. Tu et al. (2009) noted that rainfall events affected the soil suctions of tensiometers at depths as great as 3.0 meters.
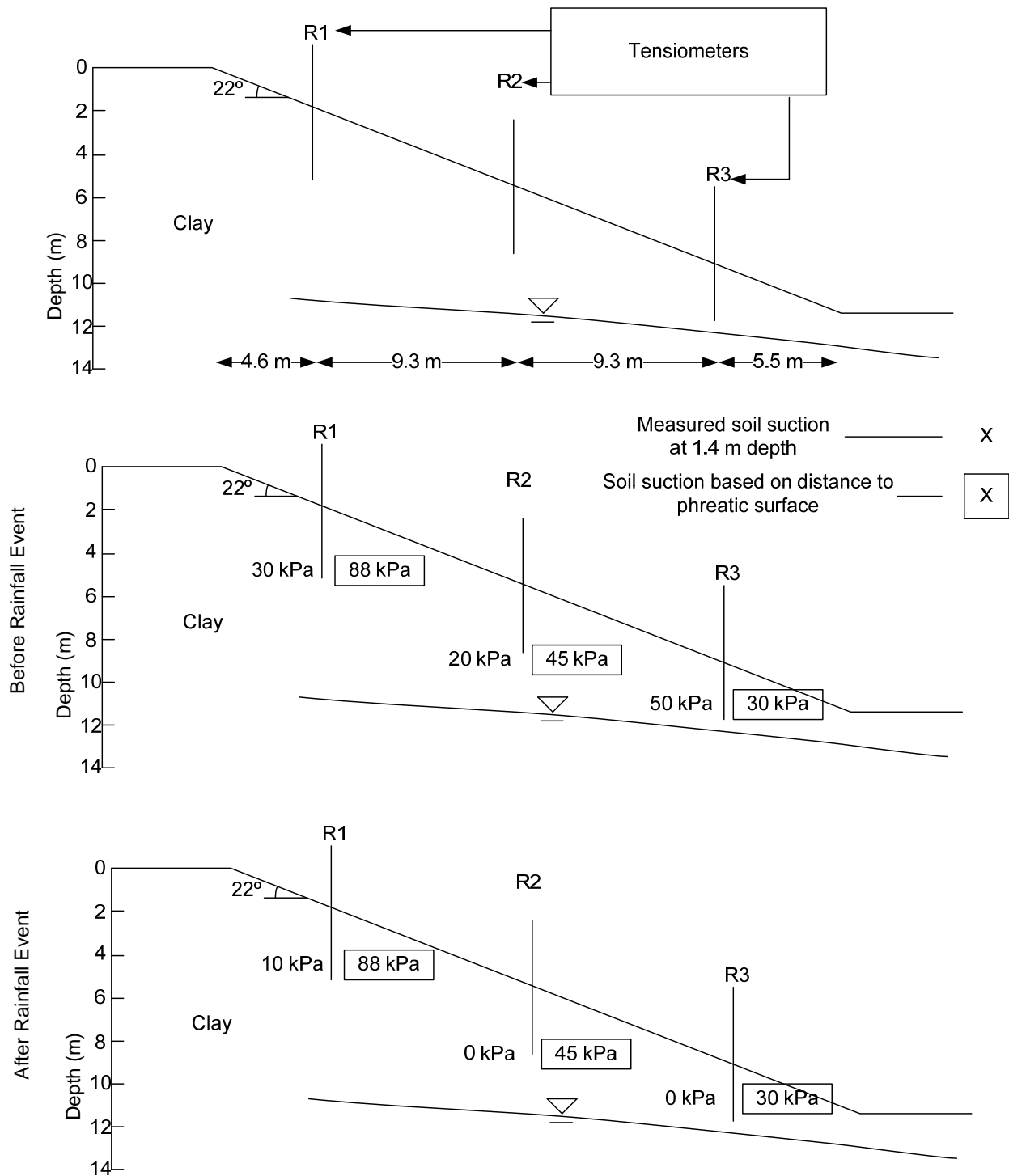
Figure 8-3 – Measured soil suctions for a shallow clay slope in Zaoyang, Hubei, China before a rainfall event and the soil suction based on the distance to the phreatic surface (after Ng et al. 2003) (with permission from ICE Publishing)

Measured average / Value of soil suction corresponding to hydrostatic
soil suction / variation of soil suction with depth
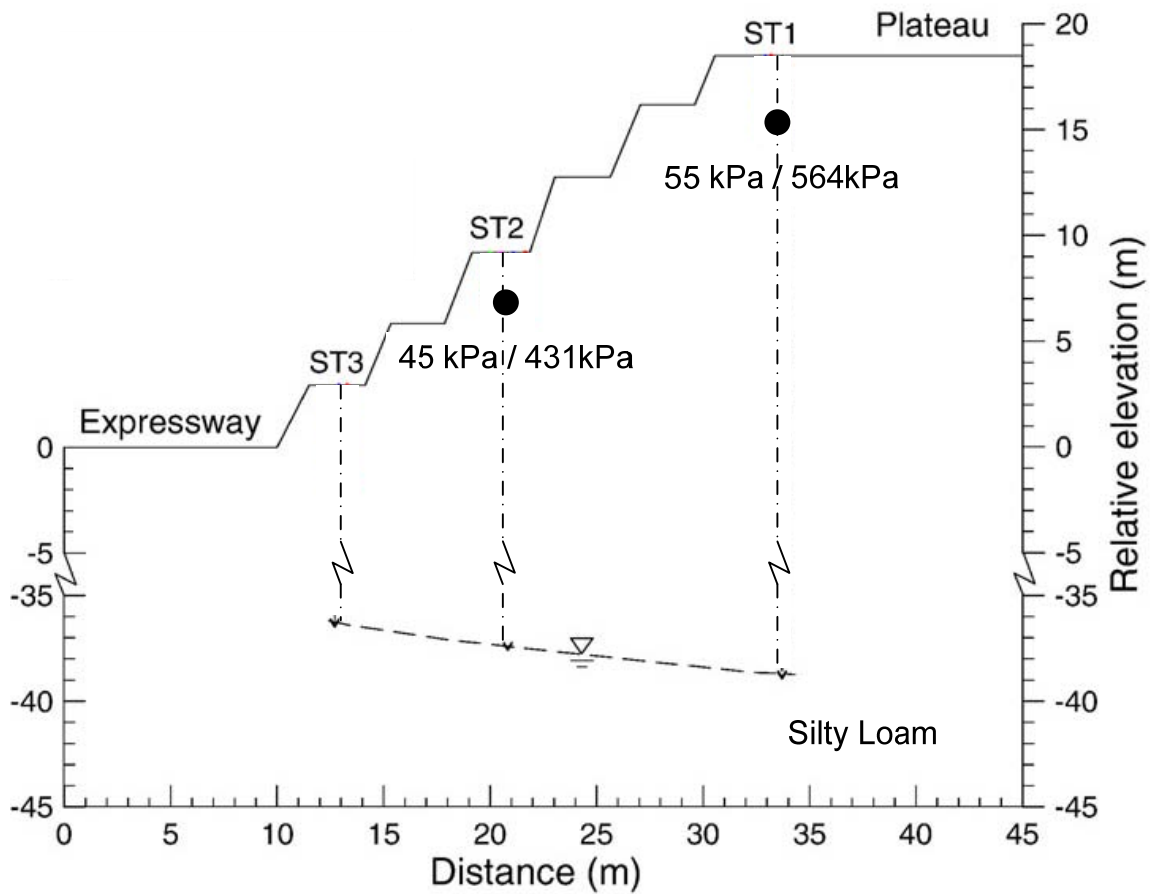
Figure 8-4 – Measured soil suction in a silty loam (loess, ML) slope in northwest China and those based on the distance to the phreatic surface (after Tu et al. 2009) (with permission from Elsevier)

Li et al. (2005) measured values of soil suction in a silty sand slope in Hong Kong, as shown in Figure 8-5. This slope was monitored with vibrating wire piezometers and tensiometers to study the effects of infiltration during rainfall events. Tensiometers placed at 1, 2, 3 and 4 m depth were used to measure changes in soil suction over a period of approximately four months. As shown in the figure, the measured values of soil suction ranged from 8 to 58 kPa during the four-month period. None of the measured values of suctions were as large as those corresponding to a hydrostatic variation with depth, which varied from 69 to 85 kPa.

Figure 8-6 shows measured values of soil suction measured by Gofar et al. (2008) in slopes in sandy gravel, and sandy silt. The position of the phreatic surface is unknown for these slopes, so comparison between the measured and hydrostatic values are not possible. What is shown are the high, low and average measured values of during the 12-month period of measurement. Gofar et al. (2008) attributed these changes in soil suction to rainfall events. This study, like those described previously, shows that soil suction at shallow depths is significantly affected by climatic conditions. Rainfall infiltration can reduce the soil suction to zero at shallow depths as the rainfall infiltrates the slope.
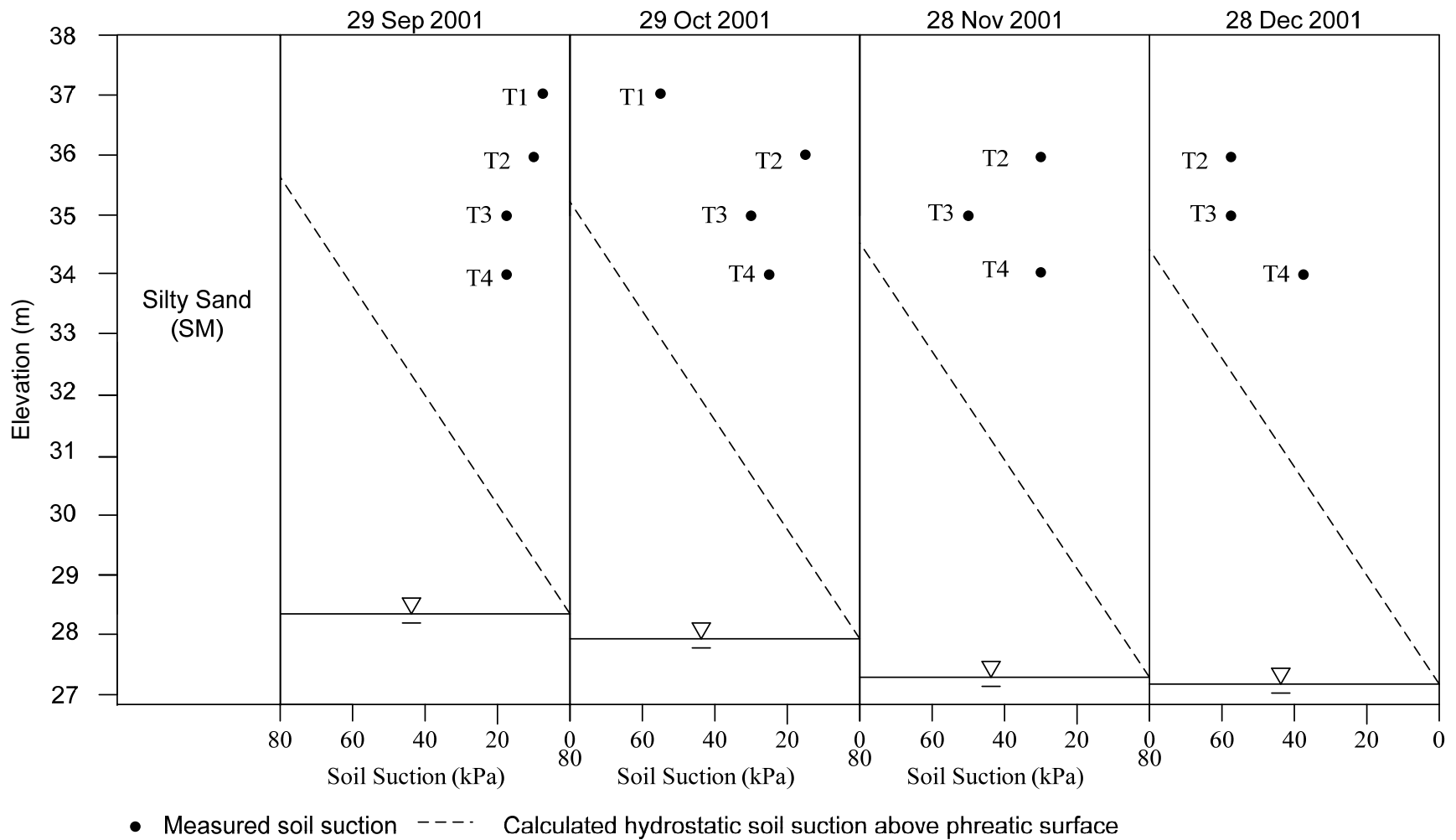
Figure 8-5 – Soil suctions measured in a silty sand slope in Hong Kong from four tensiometers and values based on hydrostatic variation of suction with depth (data from Li et al. 2005) (with permission from ASCE)
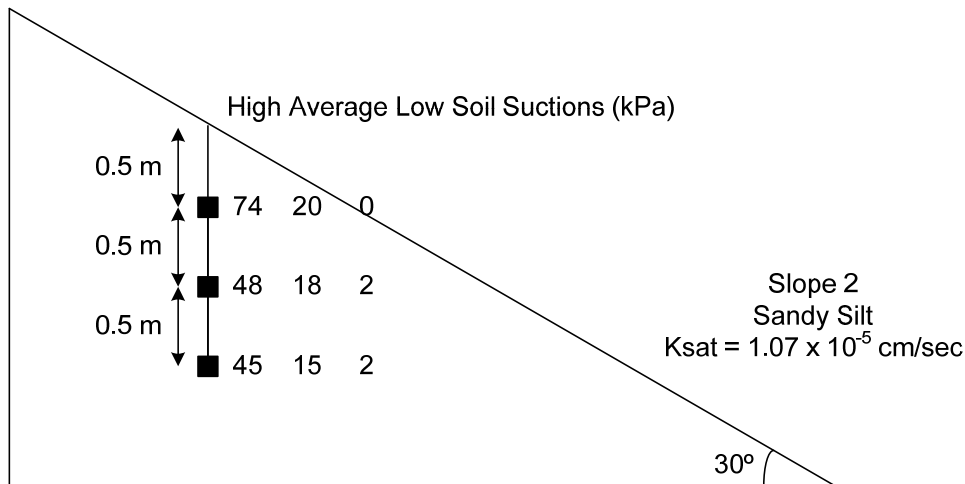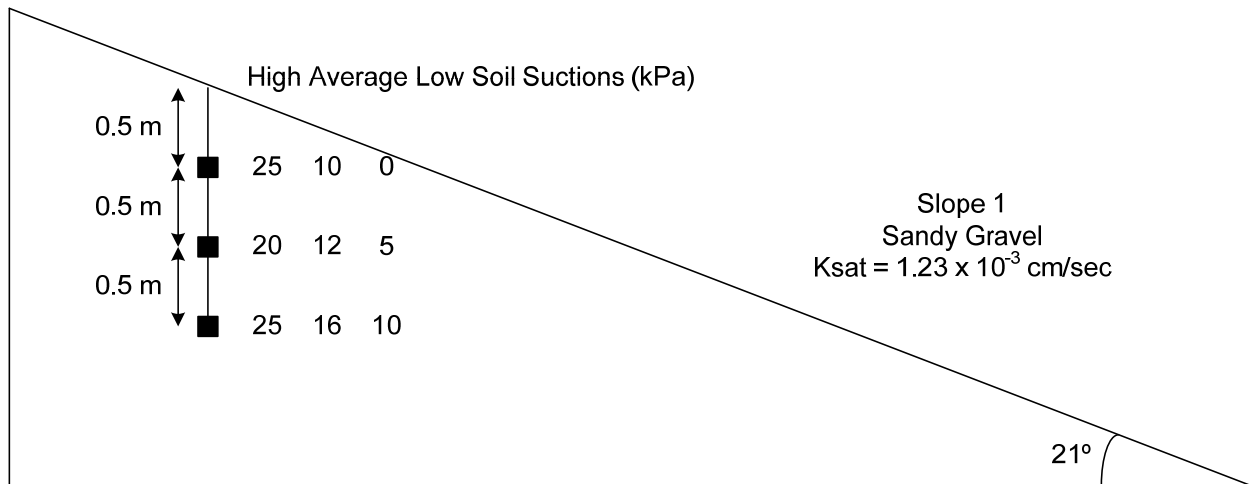
Figure 8-6 – Soil suction values measured in two slopes in Johor, Malaysia over a period of 12 months (position of phreatic surface unknown) (after Gofar et al. 2008) (determined fair use)

Importance of initial conditions

These examples for riverbanks and soil slopes show that rarely if ever do values of soil suction correspond to hydrostatic conditions above the phreatic surface. All of the examples found in the literature showed that the measured soil suctions were less than those corresponding hydrostatic conditions above the phreatic surface, and that soil suction values at shallow depths (approximately less than 3 m) are affected by rainfall and evapotranspiration.

Smaller values of soil suction correspond to higher values of hydraulic conductivity. If the initial values of soil suction assumed in the analysis are too high, the calculated wetting front will move too slow. Assuming hydrostatic variations of suction with depth is likely always to underestimate the rate of progression on the phreatic surface.

To investigate this further, four transient seepage analyses and one steady state seepage analysis were performed for the levee shown in Figure 8-7. The four transient seepage analyses were conducted using initial values of soil suction equal to 100%, 75%, 50%, and 25% of the hydrostatic condition. The positions of the phreatic surface after 2 weeks of the flood event are shown in Figure 8-7 for each of these initial conditions, together with the steady state position of the phreatic surface. All analyses used the same soil properties, estimated for a silty sand with a saturated hydraulic conductivity of 1.0 x 10^{-4} cm/sec.

As shown in Figure 8-7, using lower values of soil suction for the initial condition results in a higher calculated position of the phreatic surface, all other things being equal. In terms of pore pressures, using smaller values of soil suction for the initial conditions results in higher values of pore pressures in the levee for all times during a flood event, and steady state seepage conditions will be reached faster.
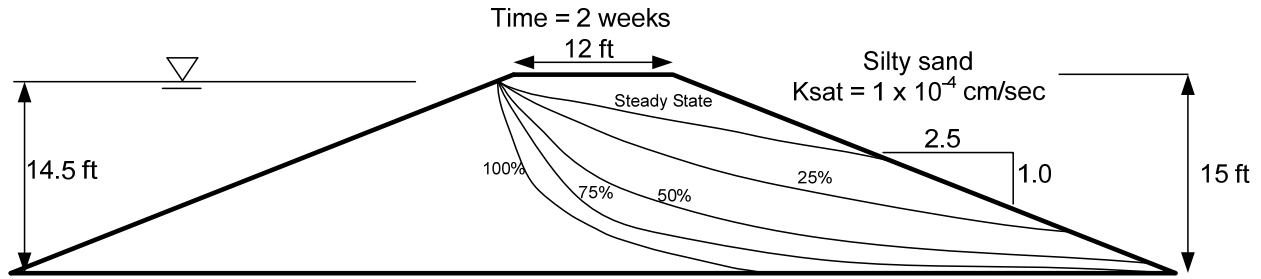
Figure 8-7 – Results of transient seepage analyses for a levee using 100%, 75%, 50% and 25% of the hydrostatic pore pressures for the initial condition and the steady state seepage position of the phreatic surface

Summary

A review of measured soil suction profiles shows that measured values of soil suction are smaller than those corresponding to hydrostatic variations of suction with depth. Measured values vary from a minimum value close to zero at 0.5 meter depth in one case, to a maximum of about 85% of the hydrostatic value in another case. Soil suction values are influenced by soil type (generally smaller suctions for coarse-grained soils), rainfall events (generally smaller suctions during and after rainfall), and depth (generally greater variations at depths less than 10 feet).

The example analysis described above shows that assuming small values of soil suction results in higher calculated positions of the phreatic surface at any time after a rise in water level against a levee, and more rapid development of the steady seepage condition within the levee.

Chapter 9
Implications for Stability and Erosion

Introduction

When levees are analyzed using transient seepage methods, pore pressure changes are calculated with time in response to a flood event. When a flood occurs and does not receed, the pore pressure will increase until steady state seepage conditions are reached. At any time before steady state conditions are reached the pore pressures will be less than those after steady state conditions are reached. This chapter examines the effects of these lower pore pressures on stability and erosion and piping.

Representation of the Flood Hydrograph

Transient seepage analyses can be used to calculate changes in pore water pressures in response to a flood event on the riverside slope of a levee. The flood hydrograph is represented as a time-varying riverside boundary condition. Three methods of representing the flood hydrograph are discussed here, using the flood hydrograph for the Inner Harbor Navigational Canal (IHNC) during the flood associated with hurricane Katrina as an example.

The (IHNC) flood hydrograph is shown in Figure 9-1. The first method for representing the flood hydrograph is to use the complete flood hydrograph as shown. The advantage of this method is that the actual field conditions are represented. The disadvantage is that numerical difficulties may be caused by steeply sloping hydrographs. A way to avoid these numerical difficulties is by representing the flood hydrograph in separate analyses and using very small time steps for the steepest portion of the flood hydrograph. As shown in Figure 9-1, the flood hydrograph was separated into five separate parts. Each segment of the analysis used the pore pressures from the previous segment as the initial conditions. The results using this method are shown in Figure 9-1 for a silty sand levee after 33 and 66 hours of the flood with the initial condition as a water table at the base of the levee.
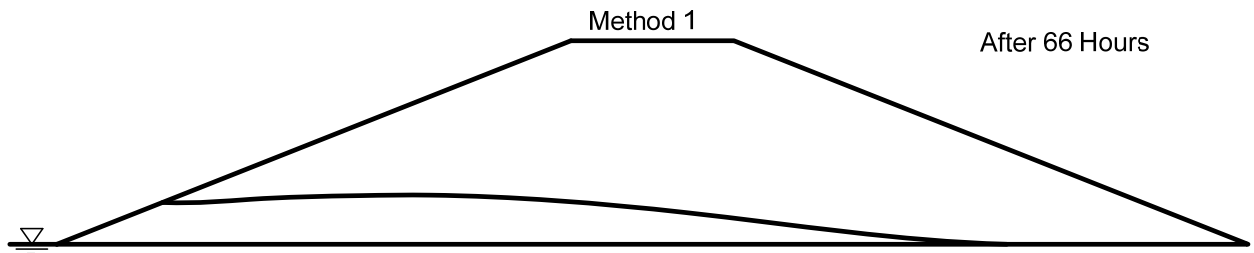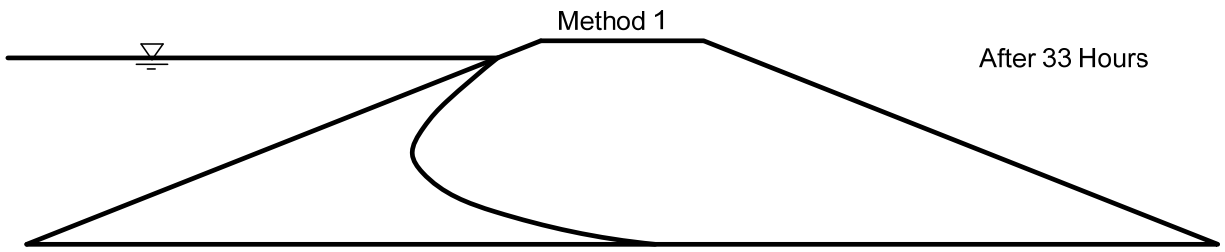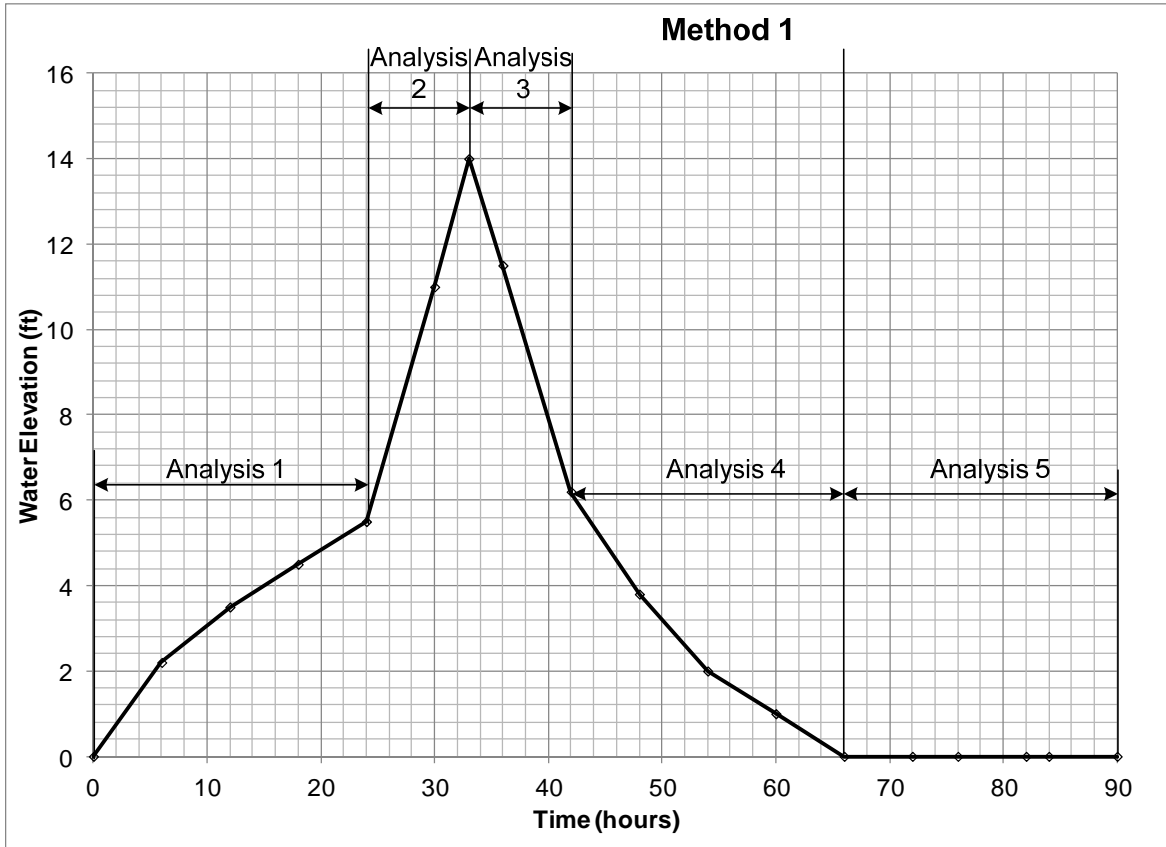
Figure 9-1 – Example 9-1 flood hydrograph and computed positions of the phreatic surface in a silty sand levee at the peak of the flood and at the end of the flood

A second method of representing the flood hydrograph is shown in Figure 9-2. This method uses the same flood hydrograph as method 1 until the peak of the flood event. Then the flood is held at this level. This method is conservative in terms of pore pressures because the flood does not dissipate with time. It can however be used to determine when a flood of a particular level will reach steady state conditions, which is useful information. The results using this method for the same silty sand levee are shown in Figure 9-2. The phreatic surface is much higher after 66 hours than computed using the actual flood hydrograph.

A third method is to disregard the flood hydrograph and use the peak water level for the entire analysis. Using this method for a transient seepage analysis is the most conservative in terms of pore pressures. This hydrograph and the computed positions of the phreatic surface after 33 and 66 hours are shown in Figure 9-3.
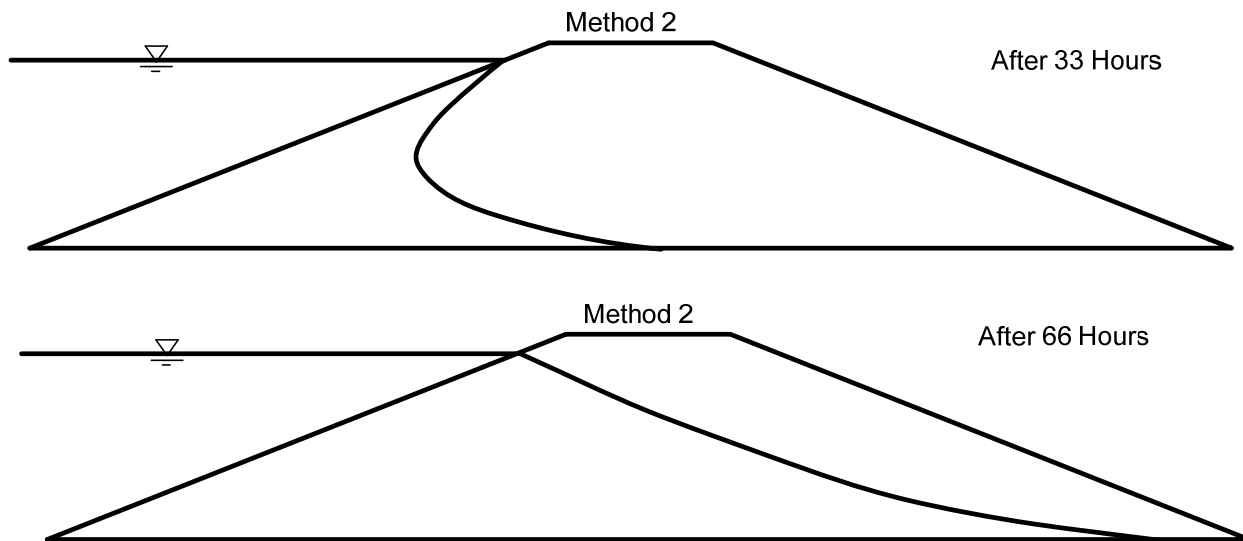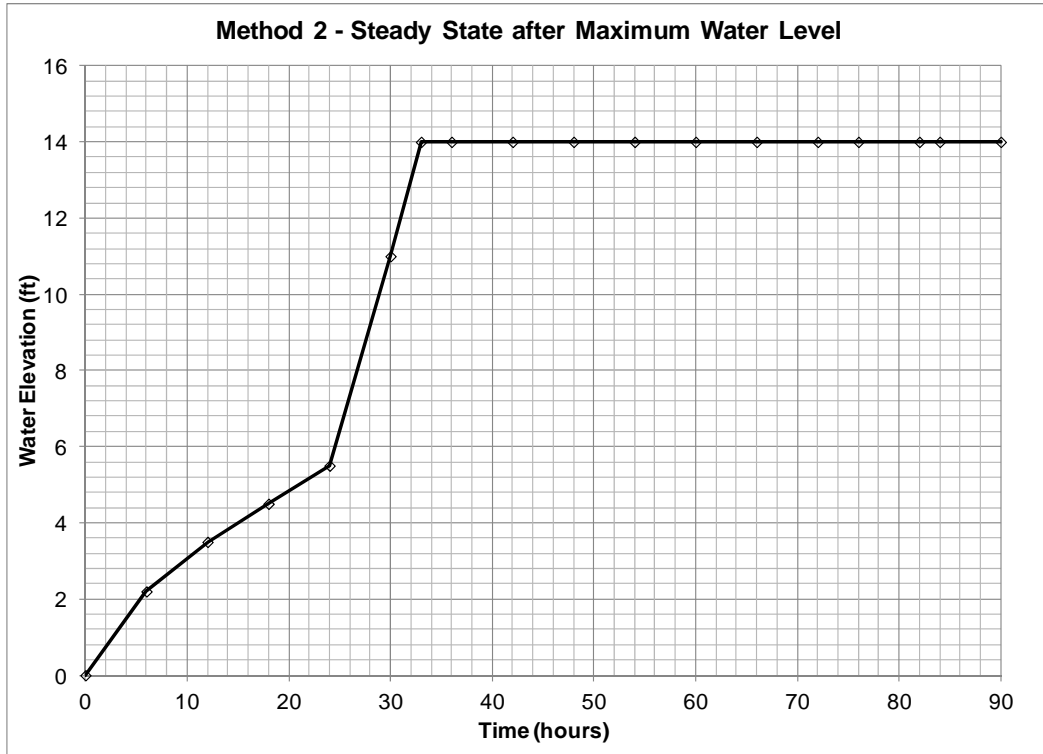
Figure 9-2 – Example 9-1 continued. Computed positions of the phreatic surface when the flood is held constant after the peak

160
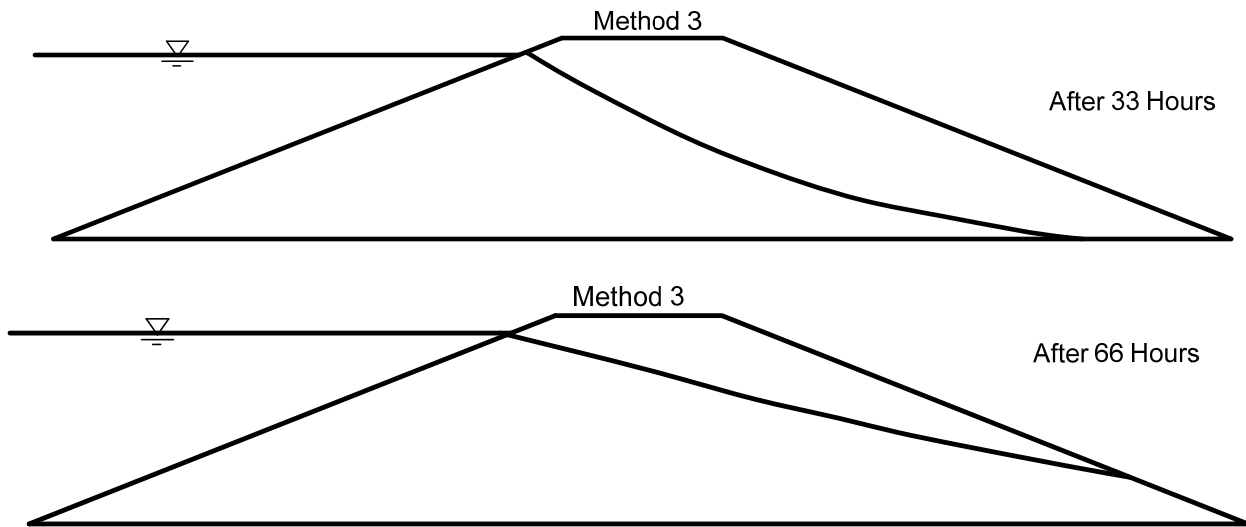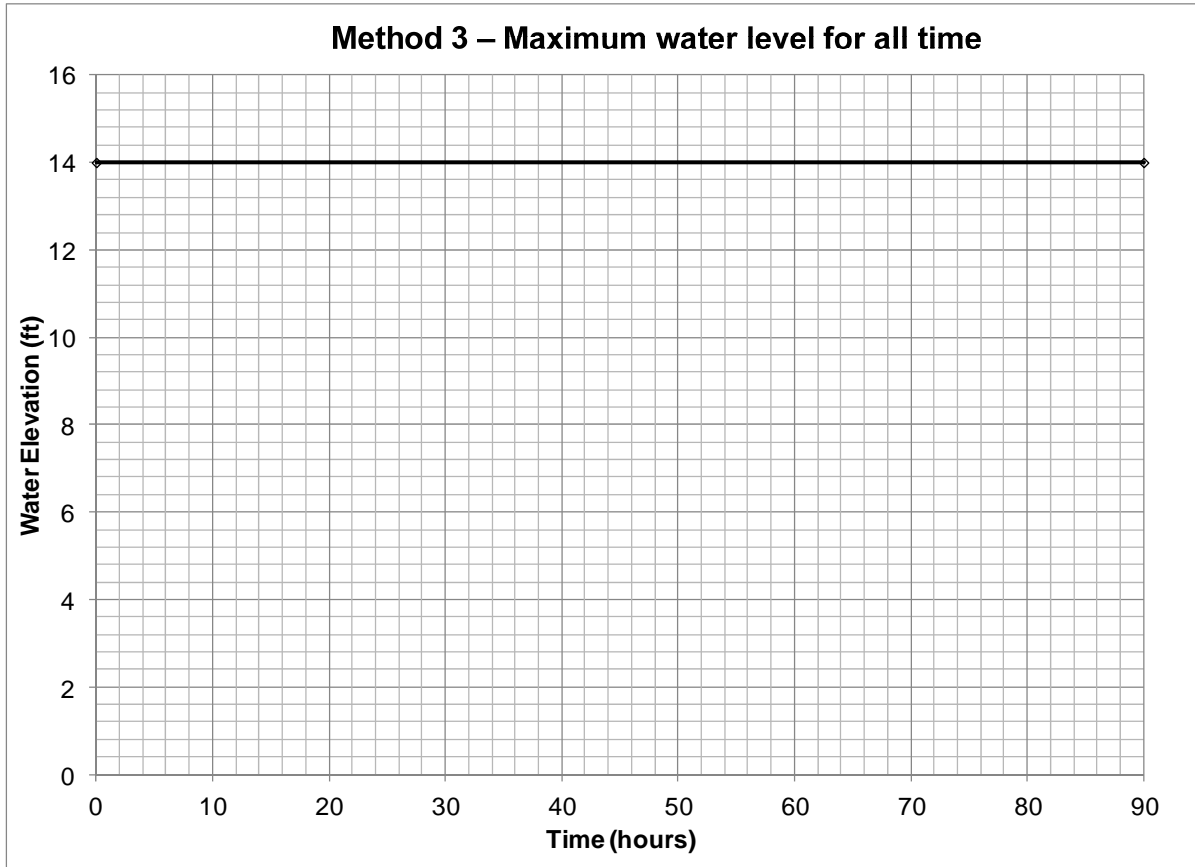
Figure 9-3 – Example 9-1 continued. Computed positions of the phreatic surface when the flood is represented as constant at the peak level

Stability Against Erosion and Piping During a Transient Condition

Pore pressures within a levee and in the levee foundation increase in response to a flood event. As the total head on the riverside of the levee is raised, water flows in the form of underseepage beneath the levee from areas of high head to low head at the landside toe. At the landside toe of the levee and points further away from the river, the underseepage can emerge at the ground surface. If the gradient is high enough, erosion and subsequent piping of the foundation materials can occur. This can cause levee failure as foundation materials are removed and the levee collapses.

During transient seepage, the hydraulic gradients increase in response to the flood event, but remain less than those corresponding to steady state seepage. If a flood event occurs and steady state seepage conditions are not reached before the flood dissipates, the levee will be safer against erosion and piping than if steady state conditions actually develop. Therefore, it is appropriate to analyze flood conditions as transient conditions, because the levee may be safe from erosion and piping even though the steady seepage analysis would indicate that it is not.

Example 9-2

As an example, an analysis was performed for a levee cross section similar to that of the London Avenue Canal in New Orleans, Louisiana. The London Avenue Canal levee sits on marsh deposits with silty sand and sand deposits beneath, as shown in Figure 9-4. The high conductivity of the sand deposits beneath the marsh allows for the development of high hydraulic gradients at the landside toe of the levee quickly in response to a flood event. A steady state and transient seepage analysis of these conditions were conducted assuming that a flood reached the top of the levee fill.

Material	Type	Saturated Conductivity (cm/sec)	Wet Unit Weight (pcf)	c' (psf)	ϕ' (degrees)
Levee Fill	CH	1×10^{-6}	110	0	27
Marsh	OH	1×10^{-5}	80	0	27
Silty Sand	SM	1.5×10^{-4}	120	0	35
Sand	SP	1.5×10^{-2}	115	0	35
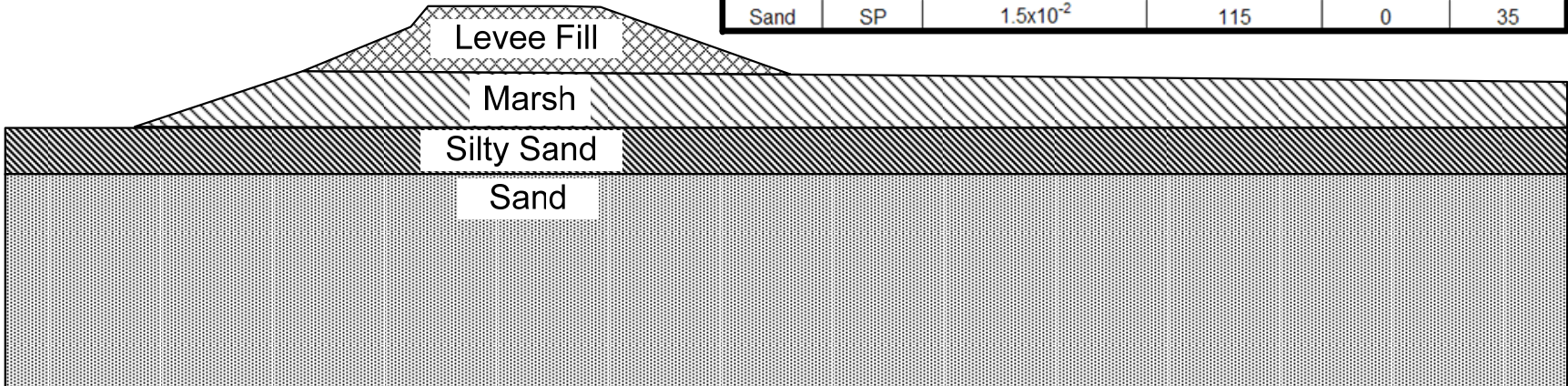
Figure 9-4 – Cross Section for example 9-2

An assumed position of the water table at the base of the levee fill was used to establish the initial conditions for the analysis. Instead of hydrostatic increase of negative pore pressures above the water table, a uniform degree of saturation of 80% was used to represent a simple but realistic initial condition.

The first analysis was performed for steady seepage conditions. The results are shown in Figure 9-6. The pore water pressure at point 1 is 69 psf and the exit gradient at point 2 is 0.11.

A transient seepage analysis was also performed, raising the flood level from the water table from the base of the levee to the top of the levee in one hour, and staying constant at that level for seven days. Results of a transient analysis of these conditions are shown in Figure 9-8. It can be seen that the water pressure remains negative through the entire seven-day period.

Despite the fact that the pore pressures within the levee not reaching steady state conditions, the value of the exit gradient is very near the value of the steady state gradient after only 12 hours of the flood event, as shown in Figure 9-9. The value after 12 hours of the flood event is 0.10, very near the steady state seepage condition of 0.11. Despite the foundation materials being fully saturated, there is a small time lag between the flood and the exit gradient reaching the value of the steady state gradient. This lag time is due to the initial condition of the water table at the base of the levee fill. At the start of the transient seepage analysis, there is vertical flow from the foundation into the levee. This vertical flow requires movement of some water out of the foundation into the unsaturated levee, and creates a time lag between the start of the flood and the formation of the exit gradient.

There are two reasons why in this example the exit gradient nearly reaches the value of the steady state gradient after only a few hours despite the fact that pore pressures within the levee have not reached steady state conditions. Firstly, the initial condition with the water table at the base of the levee corresponds to full saturation in the foundation soils. Since the foundation soils are fully saturated, their hydraulic conductivities are at their maximum values and the pore pressures are positive. Also

164

the sand material in the foundation has a high saturated hydraulic conductivity. Therefore little time is required for the exit gradient to reach a value close to the steady state value.
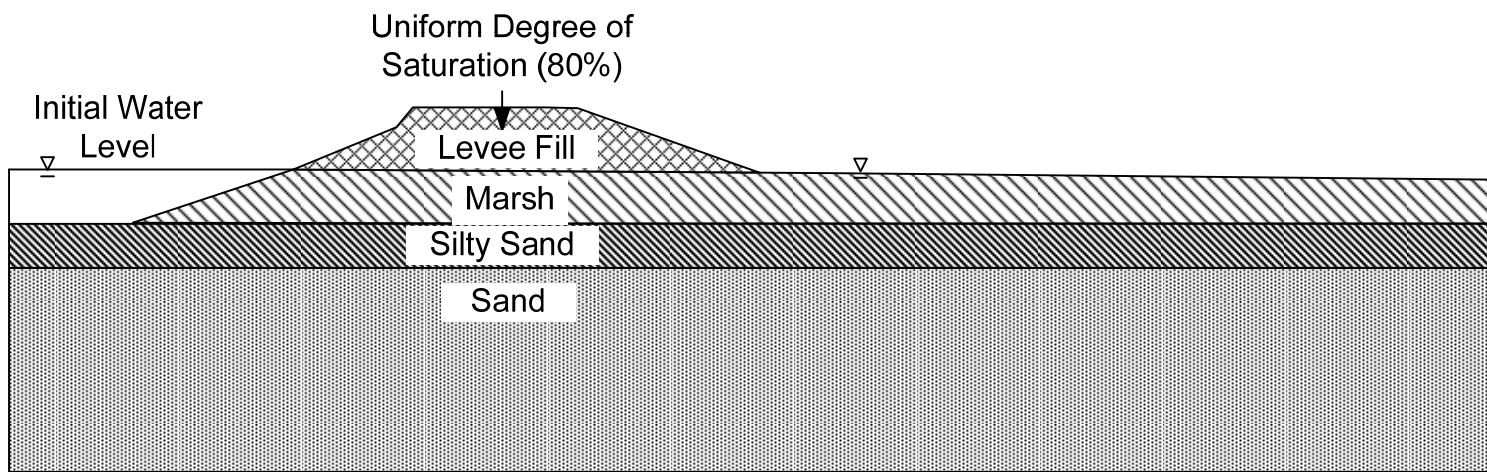
Figure 9-5 – Example 9-2 initial conditions

Pore Pressure = 69 psf

Calculated Gradient = 0.11

Final Water Level

Initial Water Level

1

2
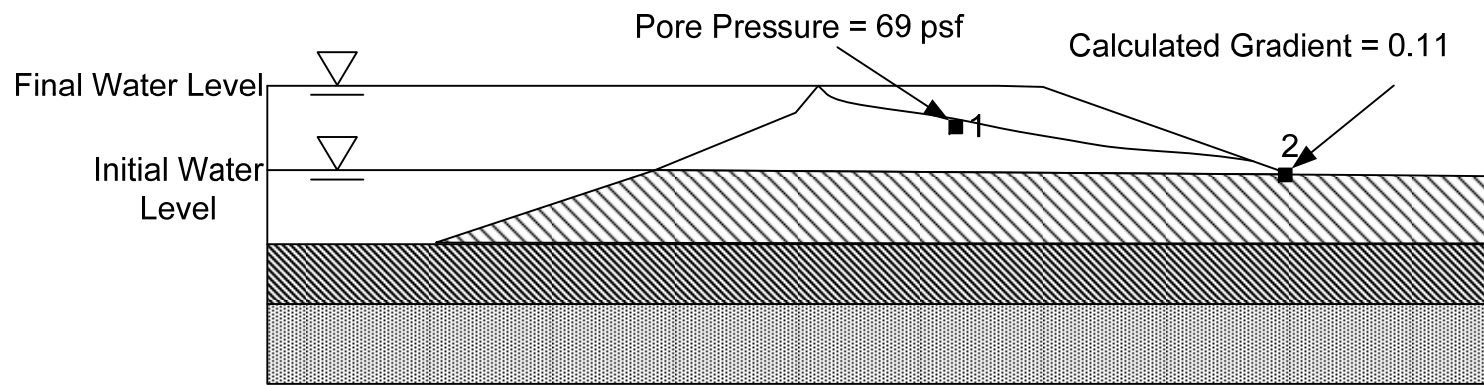
Figure 9-6 – Steady state seepage analysis of example 9-2

Pore Pressure = -59.6 psf

Calculated Gradient = 0.1

Final Water Level

Initial Water Level

1

2
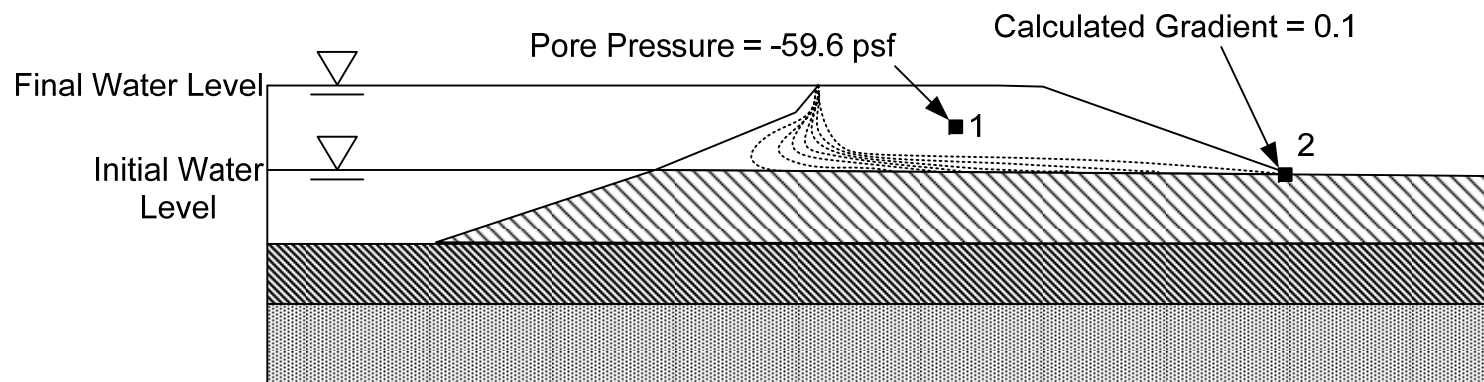
Figure 9-7 – Transient seepage analysis of example 9-2 (dotted lines are lines of zero pressure in one day increments from 1 to 7 days) with calculated pore pressure at Point 1 and exit gradient at Point 2, after 7 days

167
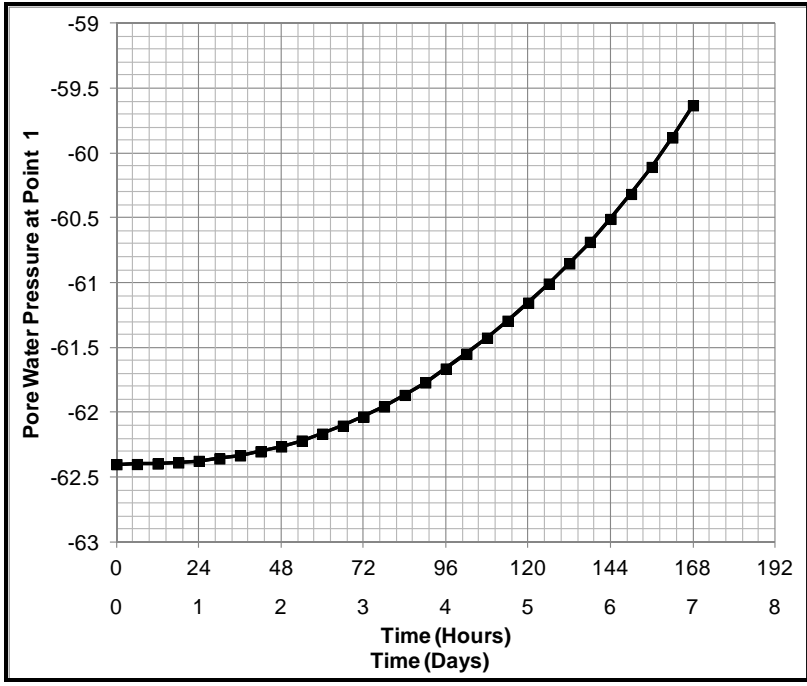
Figure 9-8 – Pore water pressure changes at point 1 in Example 9-2
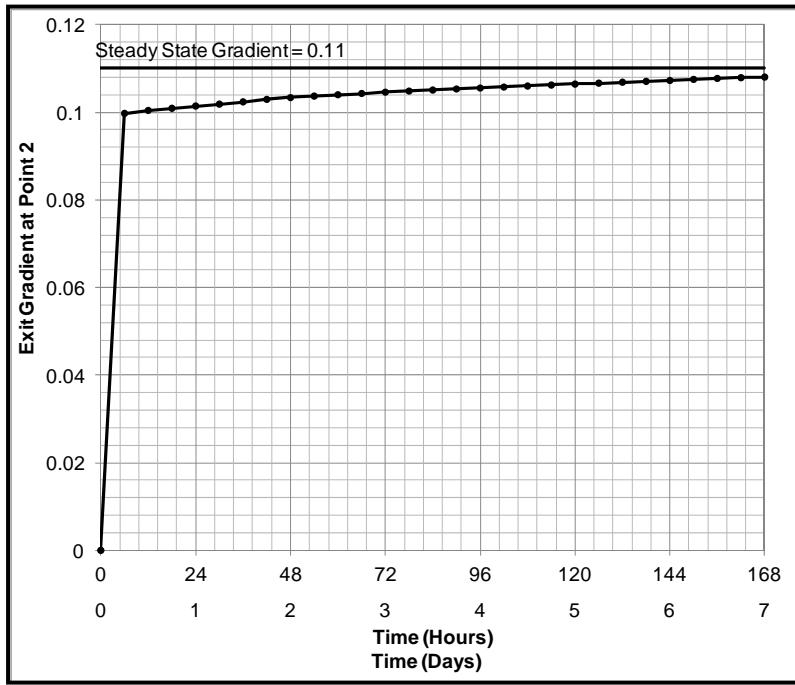
Figure 9-9 – Exit gradient at point 2 for Example 9-2

168

Example 9-3

A cross section similar to the Inner Harbor Navigational Canal in New Orleans is shown in Figure 9-10. This simplification of the IHNC cross section is presented only as an example. The example depicted in Figure 9-10 has a sheet pile wall that extends through the levee fill and stops at the marsh layer. Steady state and transient seepage analyses were performed, with the water level 1 foot below the top of the sheetpile wall. As discussed in Brandon et al. (2008), as the flood level rose against the sheetpile wall, the wall deflected, creating a gap between the wall and soil allowing full hydrostatic pressures to develop against the wall. The gap was not represented in the analyses described here.

The initial conditions for Example 9-3 are shown in Figure 9-11. An initial steady state seepage analysis was run with the canal water level running midway through the sand and upper CH clay layers. Initial pore pressures in this case were defined by a hydrostatic variation above the water table.

Steady state and a transient seepage analyses were conducted assuming a canal water level of 14 feet for the steady seepage analysis, and the flood hydrograph shown in Figure 9-1 for the transient analysis. The 14 foot flood height is 1.5 feet below the top of the sheetpile wall. The results of the steady state seepage analysis are shown in Figure 9-12. The sheet pile wall cuts off a significant amount of seepage. Water emerges on the downstream slope of the levee fill. For the steady state condition, the value of the calculated exit gradient at the toe of the slope is 3.36. The high exit gradient is a result of the low permeability clay layer on top of the higher hydraulic conductivity of the marsh layer. The calculated values of exit gradient for the transient analysis are shown in Figure 9-13. As shown in the figure, the exit gradient responds quickly to the flood hydrograph and almost reaches the steady state value at the peak of the flood. This is because the marsh layer has a high value of hydraulic conductivity as reported by Seed et al. 2009.

Material	Type	Saturated Conductivity (cm/sec)	Wet Unit Weight (pcf)	c (psf)	ϕ' (degrees)
Levee Fill	CH	1×10^{-6}	105	900	0
Marsh	CH	9×10^{-3}	85	0	28
Clay	CI	2×10^{-6}	100	600	0
Clay	CH	2×10^{-6}	95	500	0

Sheetpile

Fill (CH)

Sand

Clay (CH)

Marsh (OH)

Clay (CH)

Clay (CL)
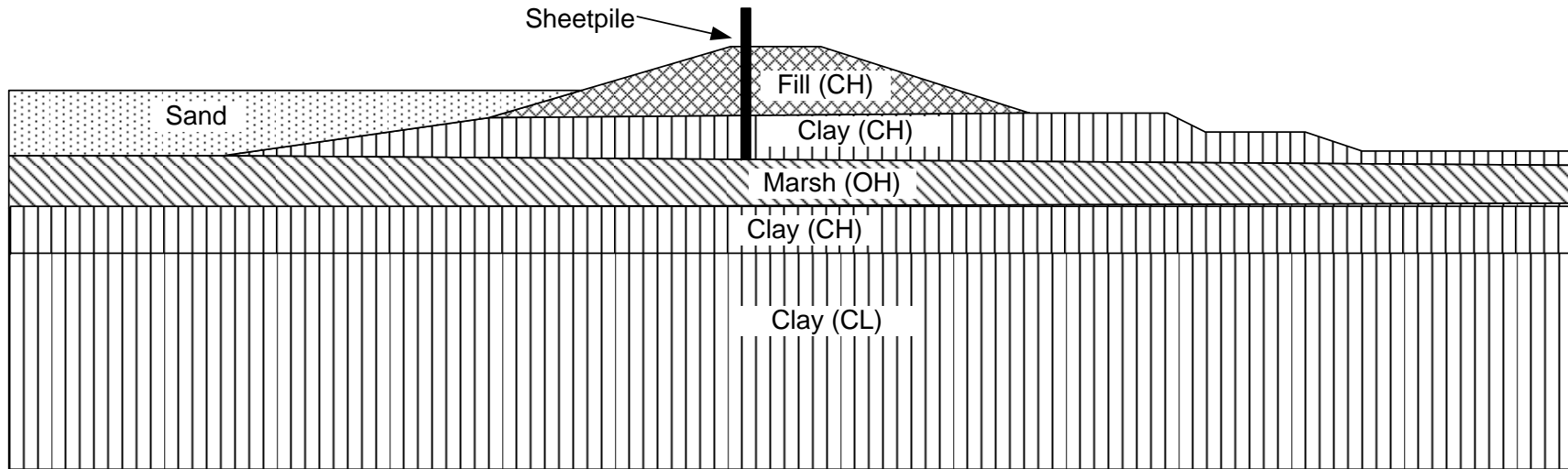
Figure 9-10 – Cross section for Example 9-3
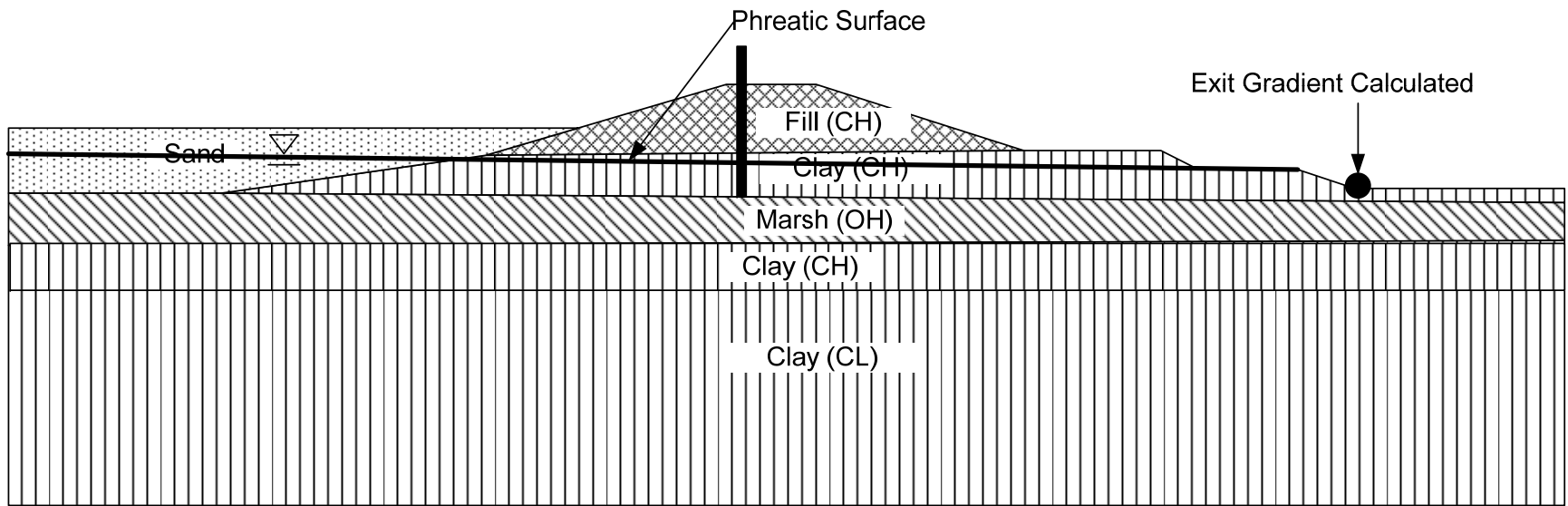
Figure 9-11 – Example 9-3, with the assumed initial position of the phreatic surface
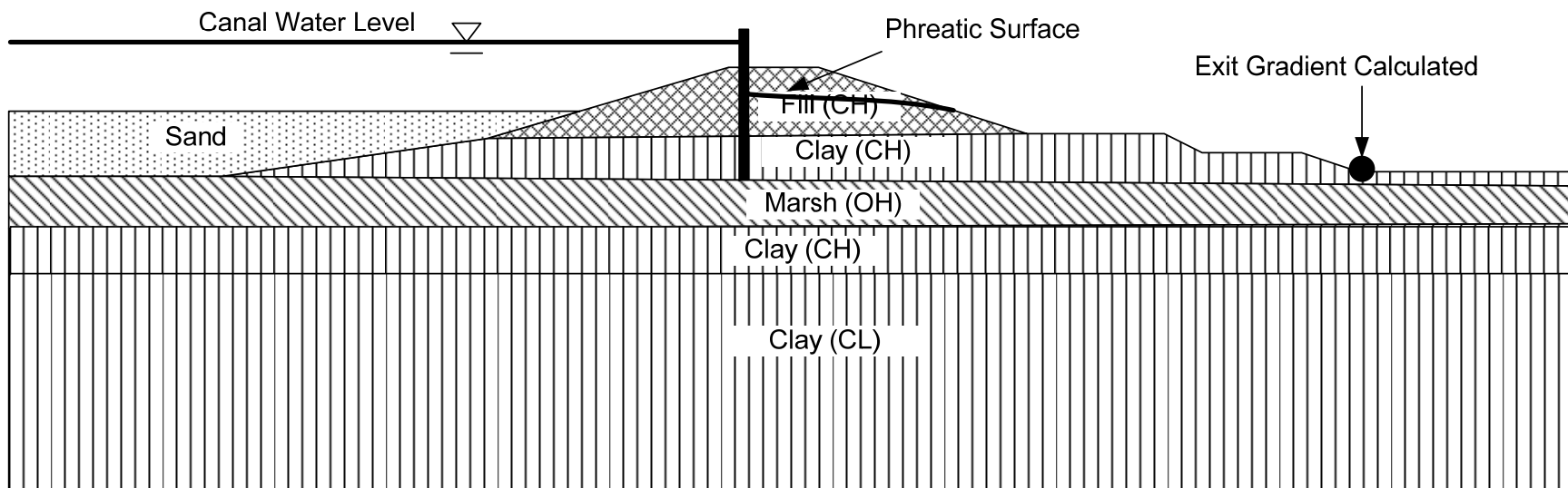
Figure 9-12 – Example 9-3 showing the water level in the canal and the steady state position of the phreatic surface
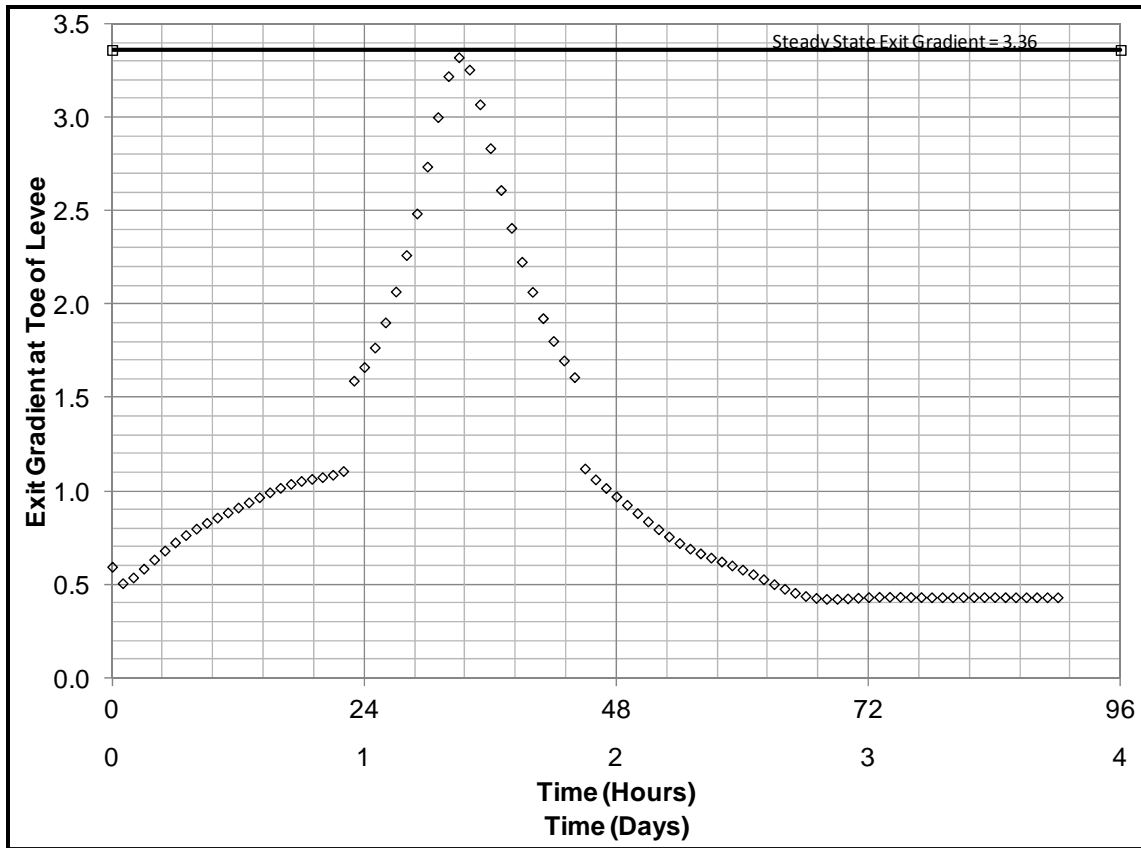
Figure 9-13 – Steady state and transient seepage exit gradients calculated at the toe of the Example 9-3 levee

Example 9-4

A cross section similar to that found at Whittier Narrows Dam in Los Angeles, California is shown in Figure 9-14. This cross section differs from the levees shown previously because it is taller, has a clay core, and the upper stratum is thicker than in the previous examples. In addition, there is not a significant difference in the permeability between the upper and lower substratum. This usually results in less susceptibility to erosion and piping.

Steady state and transient seepage analyses were conducted for the cross section shown in Figure 9-14, with the flood level at the embankment crest. A water table at the base of the dam was assumed for the initial condition in the transient analysis, and the soil suction above the phreatic surface was assumed to vary hydrostatically with elevation.

The maximum calculated value of the exit gradient occurred at the end of the sloping downstream portion of the foundation, as shown in Figure 9-14. The maximum value computed from the steady state analysis is 0.44.

The transient seepage analysis was carried out for 14 days. The variation with time of the calculated exit gradient is shown in Figure 9-15. After 14 days of high water level, the exit gradient had reached a value of 0.38, about 86% of the value calculated in the steady seepage analysis.

Conclusions Regarding Erosion and Piping During Transient Conditions

The examples described in the previous paragraphs support these conclusions regarding transient seepage analyses of erosion and piping.

- Cross sections with subsurface layers that have relatively high values of hydraulic conductivity will develop exit gradients rapidly in response to a flood event.

- Cross sections with a lower conductivity layer on top of a higher conductivity layer develop exit gradients that quickly approach those calculated assuming steady state seepage conditions.
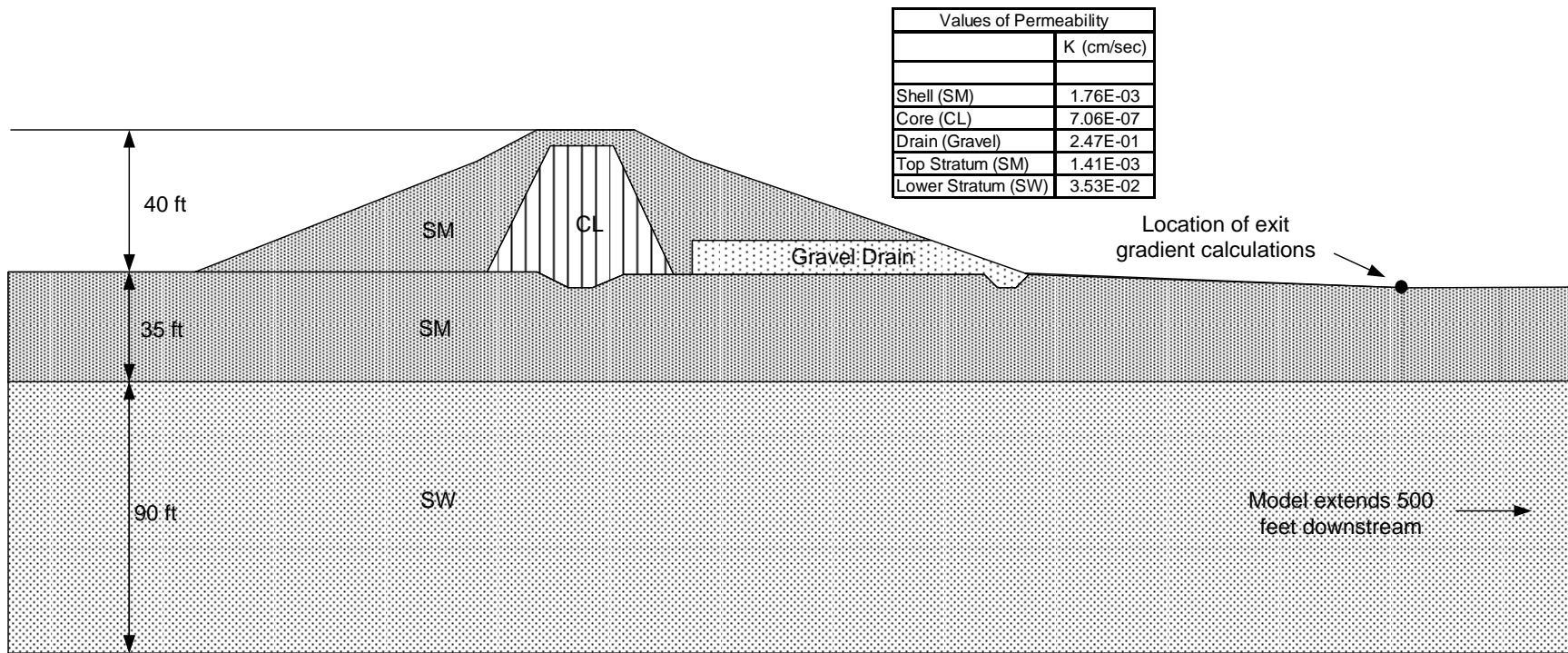
Figure 9-14 – Cross section for example 9-4

Values of Permeability	
	K (cm/sec)
Shell (SM)	1.76E-03
Core (CL)	7.06E-07
Drain (Gravel)	2.47E-01
Top Stratum (SM)	1.41E-03
Lower Stratum (SW)	3.53E-02
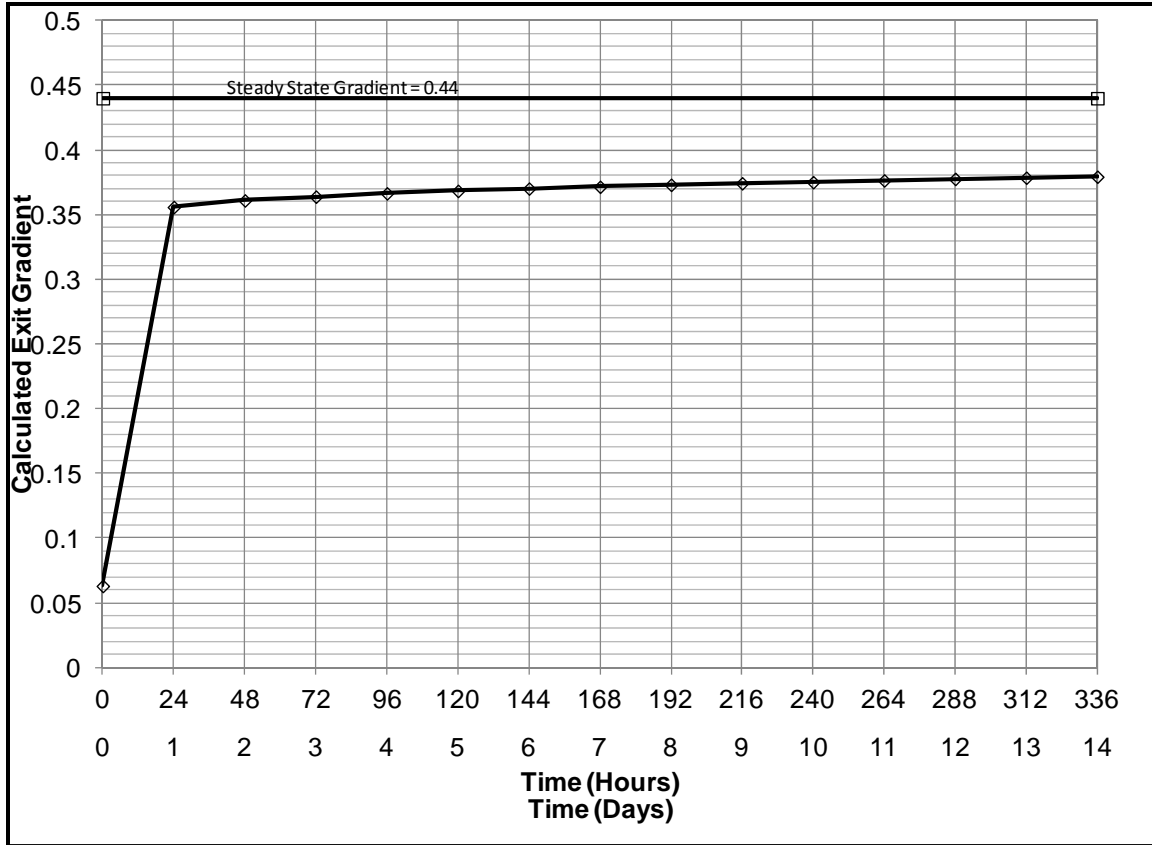
Figure 9-15 – Calculated values of exit gradient at the critical location downstream from the embankment for transient and steady state seepage conditions of example 9-4

Slope Stability

Pore pressures increase in response to a flood event during transient seepage analyses. In effective stress stability analyses, where shear strengths are related to effective stress, the shear strengths decrease with time as pore pressures increase, and the factor of safety decreases. Here an example of a stability analysis is presented with the cross section similar to the London Avenue Canal Levee, as shown in Figure 9-16 (Example 9-5). This factor of safety against slope instability was calculated at each time step of the transient seepage analysis, using the effective stress strength parameters shown in Figure 9-16.

Prior to the transient seepage analysis the same initial conditions for the levee were established as shown in Figure 9-5, with a water table at the base of the levee fill and a uniform degree of saturation of the levee fill materials equal to 80%. Then a flood was initiated as an increase in the canalside water level as shown in the hydrograph of Figure 9-17, where the water level was raised to the top of the levee in one hour. The change in pore water pressures were calculated every six hours in the analysis and for each of these time steps the factor of safety against sliding was calculated.

The results of the analyses are shown in Figure 9-18 after six and 168 hours (7 days) of the flood on the riverside of the levee. After six hours the factor of safety is 1.25 and decreases to 1.15 after 168 hours. The decrease in the factor of safety with time is shown in Figure 9-19. The slope of the decrease in factor of safety with time plot is constant over the seven days of the transient seepage analysis.

Another analysis was conducted to examine the effect on the factor of safety of increasing the hydraulic conductivity of the levee fill material by one order of magnitude. The results of this analysis are shown in Figure 9-20. Due to the higher hydraulic conductivity the phreatic surface has progressed further through the levee fill. The result is an increase in pore pressures for all times in the levee fill.

With higher pore pressures in the levee fill and underlying soils, the calculated factor of safety is lower as shown in Figure 9-20 and Figure 9-21

Material	Type	Saturated Conductivity (cm/sec)	k_v/k_h	Wet Unit Weight	ϕ' (degrees)	c' (psf)
Levee Fill	CH	1×10^{-5}	1	110	28	0
Marsh	OH	1×10^{-5}	0.25	80	27	0
Silty Sand	SM	1.5×10^{-4}	0.33	120	35	0
Sand	SP	1.5×10^{-2}	0.33	115	35	0
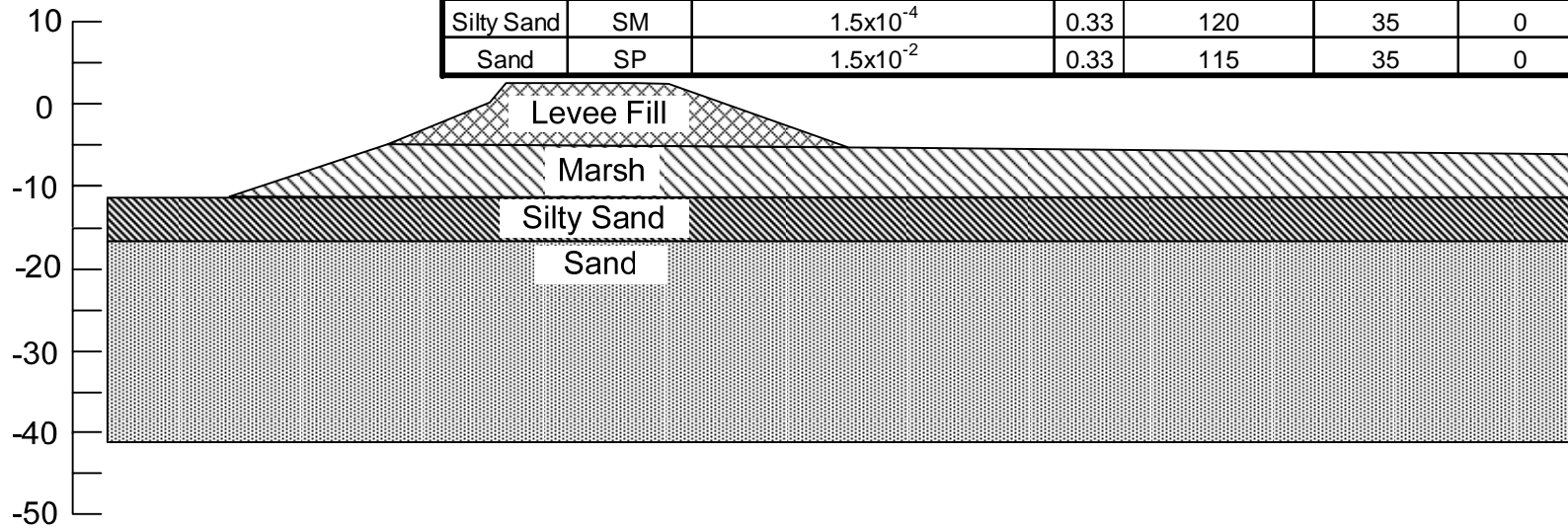
Figure 9-16 – Cross section for example 9-5
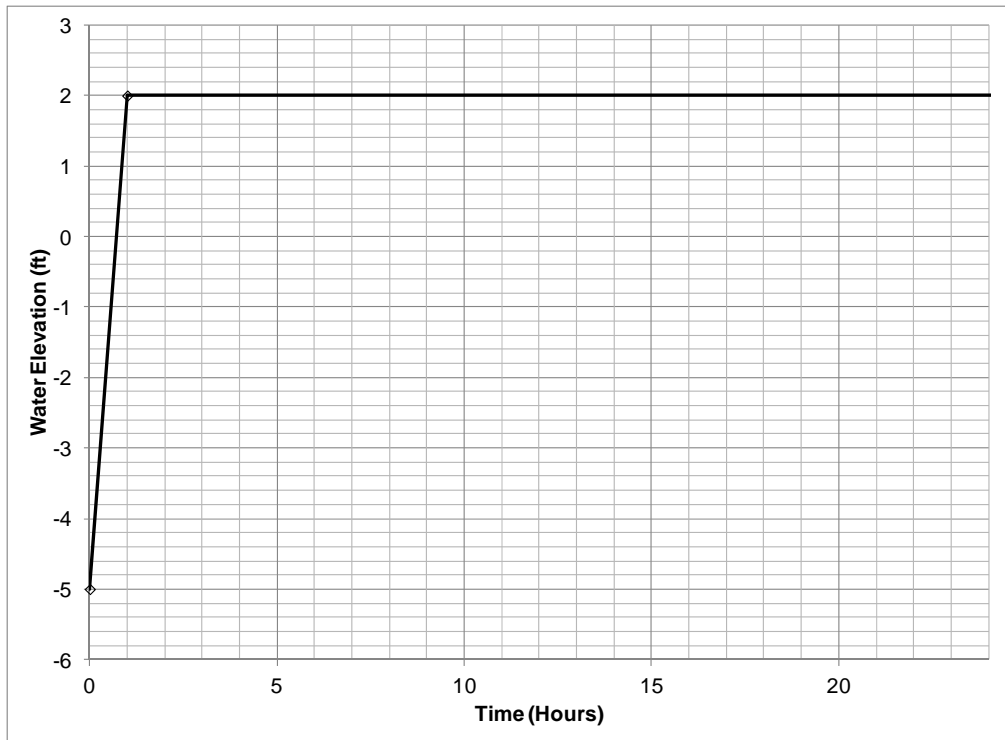
Figure 9-17 – Assumed flood hydrograph for example 9-5
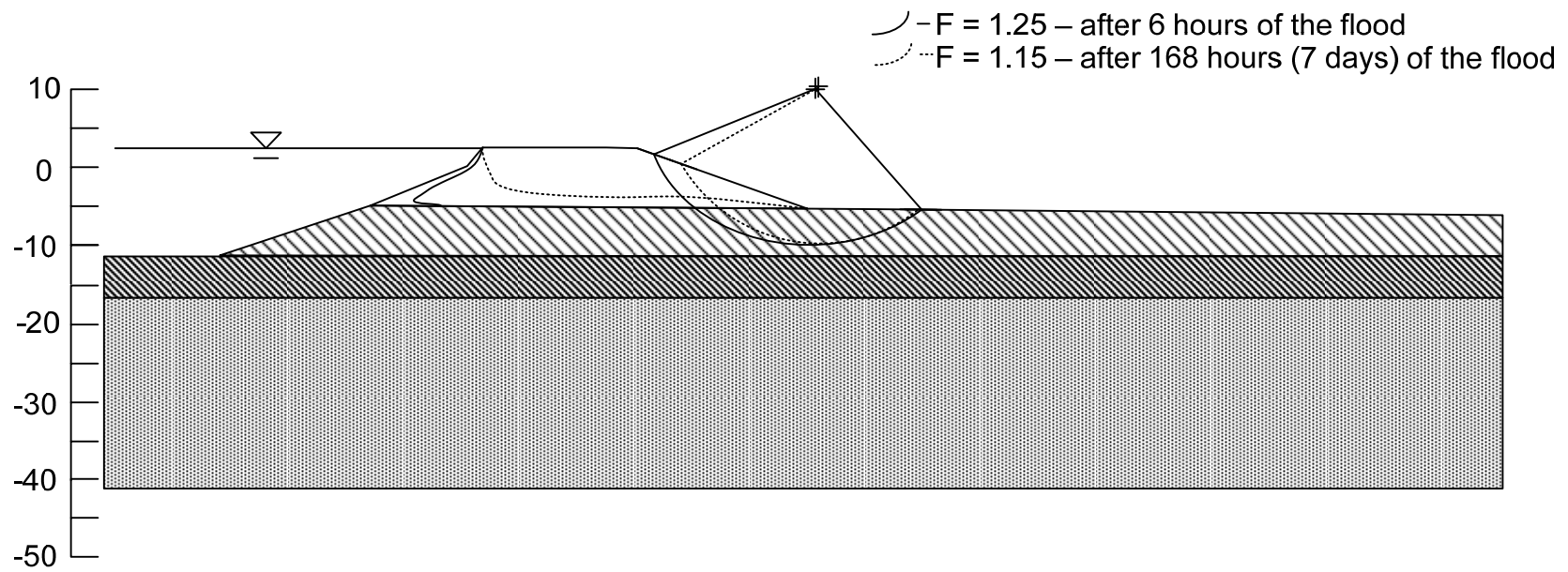
Figure 9-18 – Stability for example 9-5 after 6 and 168 hours of a flood
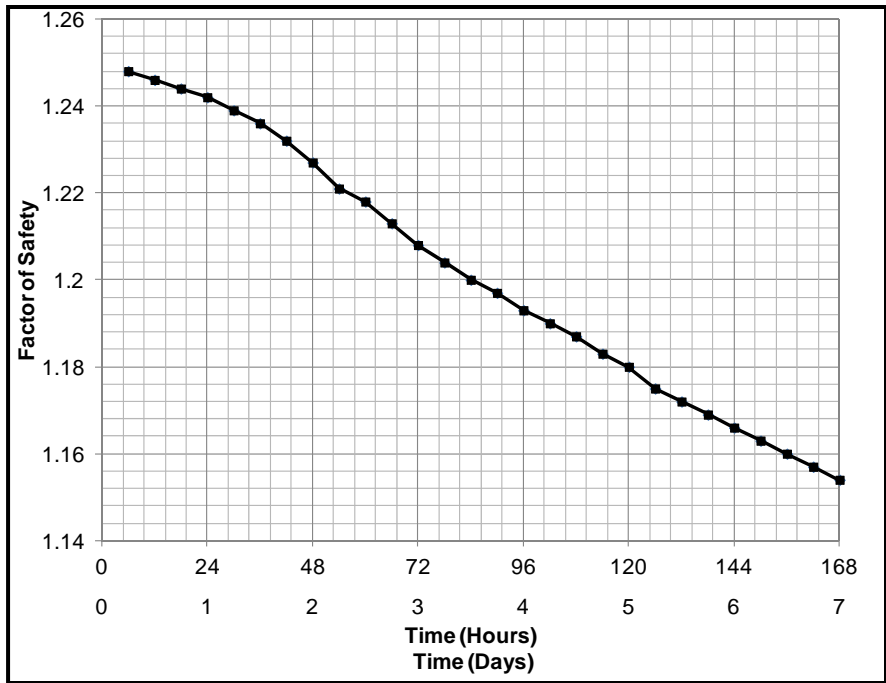
Figure 9-19 – Factor of safety versus time for example 9-5 shown in Figure 9-18
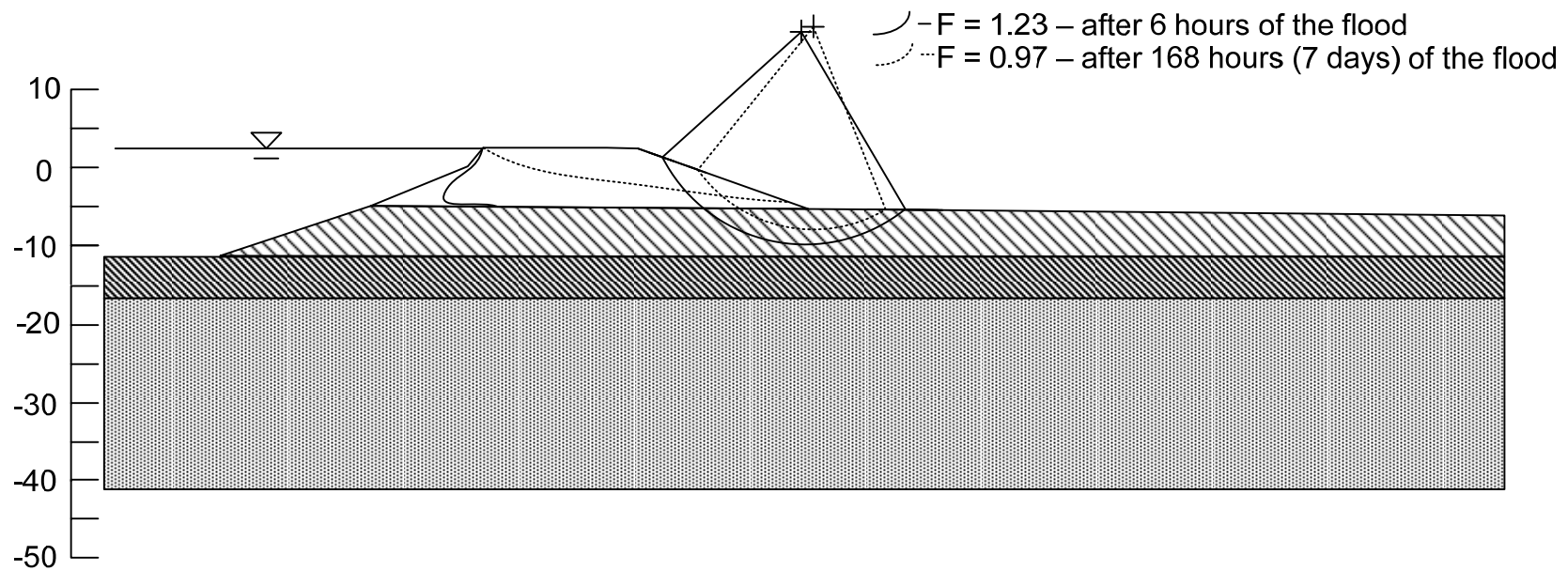
Figure 9-20 – Stability for example 9-5 after 6 and 168 hours of a flood with the hydraulic conductivity of the levee fill increased by 1 order of magnitude
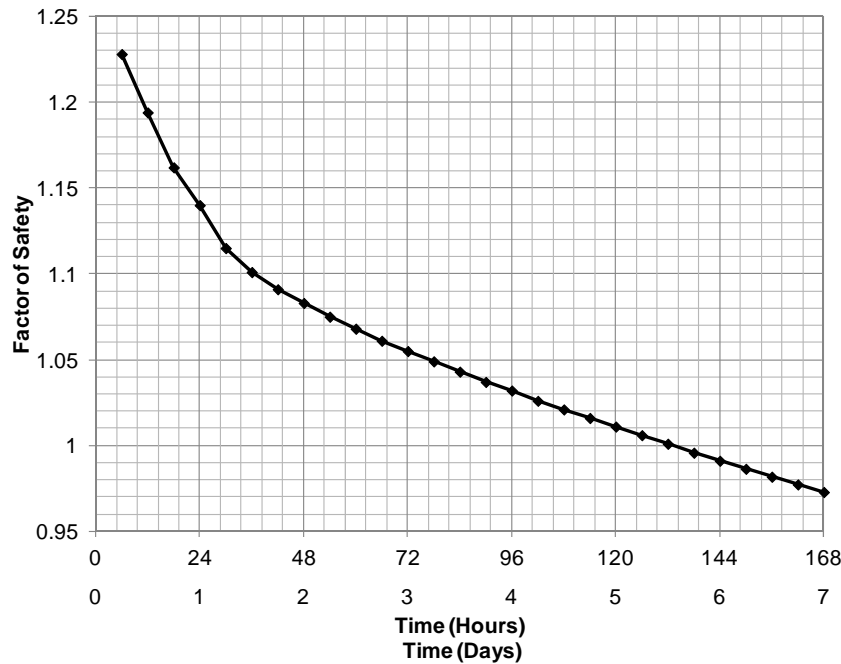
Figure 9-21 – Factor of safety versus time for example 9-5 shown in Figure 9-18 with the hydraulic conductivity of the levee fill increased by 1 order of magnitude

The factor of safety decreases by 21% after seven days of the flood, from 1.23 to 0.97. In addition to the decrease in factor of safety being larger for the higher hydraulic conductivity analysis, the factor of safety decreases more rapidly and the calculations indicate that the levee would become unstable after seven days of a sustained flood level.

These analyses performed using effective stress strength parameters assume the materials are fully drained and that now shear induced pore pressures are generated despite permeability values that indicate that they may behave in an undrained manner.

Soil Suction Effect on Shear strength

A third analysis was conducted to understand the effects soil suction has on the overall factor of safety during a transient seepage analysis. Soil suction increases the shear strength of a soil. An investigation into unsaturated shear strength is beyond the scope of this research. A simple unsaturated shear strength relationship proposed by Vanapalli et al. (1996) has been applied to the unsaturated soils encountered in the

184

levee fill as shown in this example. Vanapalli et al. (1996) related the increase in shear strength of a soil due to soil suction to the soil-water characteristic curve as shown in Eq. 9-1.

$$\tau = c' + (\sigma_n - u_a)\tan\phi' + (u_a - u_w)\left[(\tan\phi')\left(\frac{\theta - \theta_r}{\theta_s - \theta_r}\right)\right]$$

<div align="right">**Eq. 9-1**</div>

Where σ_n is the normal stress (psf), u_a is the air pressure (psf), u_w is the water pressure (psf), θ is the volumetric moisture content (dimensionless), θ_r is the residual volumetric moisture content (dimensionless), and θ_s is the saturated volumetric moisture content (dimensionless).

This equation shows that soil suction $(u_a - u_w)$, will result in an increase in shear strength. The same analysis of the London Avenue Canal levee was performed using this unsaturated shear strength equation for the unsaturated portion of the levee fill materials. The results of this analysis are shown in Figure 9-22. The increase in the factor of safety is due to the shear strength increase provided by the soil suction. The calculated factor of safety after six hours is 1.29 as compared to the value of 1.23 in the analysis where the effect of soil suction on shear strength was not taken into account. The computed factor of safety after 168 hours was 1.08 when the effect of soil suction on shear strength was included, and 0.97 when it was not included.

Conclusions to Slope Stability During a Transient Condition

It was shown that the factor of safety against sliding on the inboard levee slope calculated using effective stress analysis decreases as the pore water pressures increase during flood. The value of saturated hydraulic conductivity has a large effect on the rate at which the factor of safety decreases as the pore pressures change. It was shown that a levee can become unstable after some time during a flood event. If an increase in strength due to soil suction is included, the factor of safety against sliding will be higher than if this increase in strength is ignored.
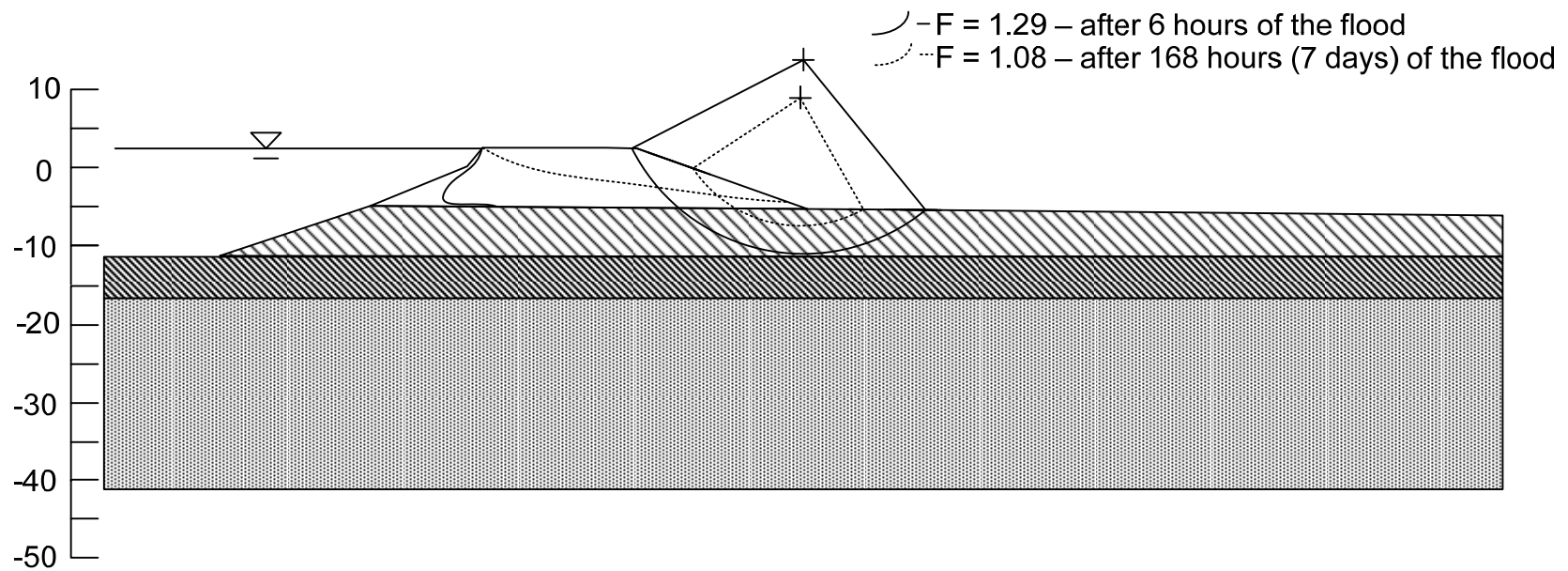
Figure 9-22 – Stability for example 9-5 after 6 and 168 hours of a flood with the hydraulic conductivity of the levee fill increased by 1 order of magnitude and the increase in strength due to soil suction
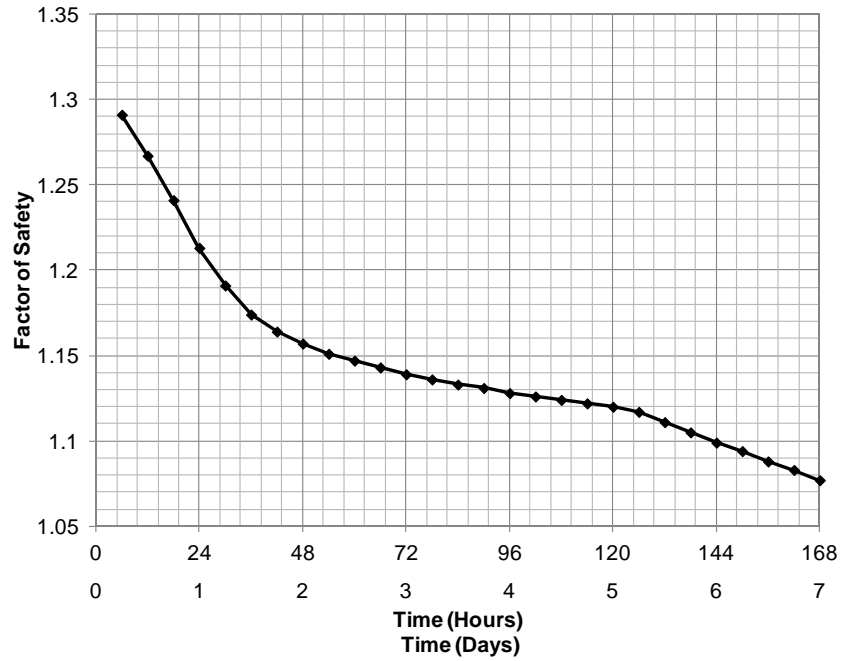
Figure 9-23 – Factor of safety versus time for example 9-5 shown in Figure 9-18 with the hydraulic conductivity of the levee fill increased by 1 order of magnitude and the strength increase due to soil suction

Chapter 10
Summary and Conclusions

The objective of this research was to provide guidance on performing transient seepage analyses through levees. This research has shown that transient seepage analyses are highly dependent on numerical considerations, unsaturated and saturated soil properties and the initial conditions defined before the start of the analysis. It was shown that given the proper amount of information, a meaningful transient seepage analysis can be performed. Rarely is all of the required information available from test results, so properties and initial conditions must be estimated. A method was presented to estimate the soil properties and conditions needed to complete a transient seepage analysis.

Summary of Work Accomplished

The following were accomplished as part of this study on transient seepage analyses through levees:

1. Transient seepage was explained in terms of numerical considerations, soil properties and initial conditions.

2. Numerical models were analyzed using the computer program SEEP/W to illustrate the principles of transient seepage analyses.

3. A review of the literature was conducted to establish both empirical and laboratory methods to estimate or measure unsaturated soil properties.

4. Numerical transient seepage analyses were performed and compared with the results of a half-scale levee constructed and instrumented in a laboratory in Germany.

5. Numerical models were created to illustrate the effects of numerical oscillations and non-convergence on calculated pore pressures and gradients.

6. Numerical models of levees were created to show the significance of soil properties on the outcome of a transient seepage analysis.

7. Factors affecting unsaturated soil properties were defined from the literature.

8. A new method was created for estimating the soil-water characteristic curve based only on the value of saturated hydraulic conductivity.

9. A literature review was conducted surveying initial conditions in terms of pore pressures for unsaturated soils.

10. Examples of transient seepage in two New Orleans levees and a dam in Los Angeles were performed to show applications of the methods developed to field conditions.

Conclusions

Numerical Considerations

1. Numerical oscillations can be avoided if SEEP/W (2007) is used, with 3-node triangles and/or 4-node quadrilaterals. While it might seem logical that higher-order elements would produce more accurate results, the fact is that they produce numerical problems and less accurate results.

2. The position of the line of zero pressure, the phreatic surface, within a levee is not significantly affected by element type, element size or time step magnitude, provided that the sizes of the elements are no more than one-fourth the height of the levee.

3. Smaller elements increase the accuracy with which negative pore pressures within a levee are calculated, but it appears that elements can be as large as one-fourth of the size of the soil region they model without compromising accuracy.

4. Exit gradients should be calculated as the average across the thickness of the capping layer, using elements no larger than one fourth the thickness of the layer. In cases where there is no capping layer, the exit gradient should be calculated for the top foot of the foundation using 0.25-ft elements.

Soil Properties

1. Many studies have been made to measure soil-water characteristic curves and hydraulic conductivity functions for different soils, and a large number of fitting equations have been proposed for use in analyses. It does not appear that any one of the proposed fitting methods is significantly more accurate than the others. Considering the fact that the behavior being modeled is complex, and is affected by many variables, some of which can only be estimated for a particular soil and seepage condition, and considering the fact that even saturated hydraulic conductivity can only be evaluated within one or two orders of magnitude, it appears unlikely that the soil properties required for transient seepage analyses can be estimated with high accuracy, no matter how sophisticated are the fitting relationships that are used.

2. Experimental determination of soil-water characteristic curves and hydraulic conductivity functions is difficult, and the results of such tests involve considerable uncertainty. It is at least as accurate to estimate these functions as it is to try to measure them.

3. A new method that can be used to estimate the soil-water characteristic curve for use in transient seepage analyses of levees has been proposed. The method categorizes soils based on the best estimate of the value of saturated hydraulic conductivity.

Verification of Transient Seepage Analyses

The physical model test performed by Worsching et al. (2006) was replicated numerically using the finite element computer program SEEP/W using reasonable estimates of the soil properties. It was found that the results of the numerical analyses compared well with the experimental measurements. The largest contributing factor to the rate of propagation of the phreatic surface during the transient seepage analysis was the value of saturated hydraulic conductivity.

Initial Conditions

1. A review of measured soil suction profiles shows that values of soil suction measured in the field are smaller than those corresponding to hydrostatic variations of suction with depth. Measured values vary from a minimum value close to zero at 0.5 meter depth in one case, to a maximum of about 85% of the hydrostatic value in another case. Soil suction values are influenced by soil type (generally smaller suctions for coarse-grained soils), rainfall events (generally smaller suctions during and after rainfall), and depth (generally greater variations at depths less than 10 feet).

2. Assuming small values of soil suction results in more rapid movement of the phreatic surface after a rise in water level against a levee, and more rapid development of the steady seepage condition within the levee.

Analysis of Erosion and Piping

1. If the geologic conditions for a levee indicate that erosion and piping may be a problem, i.e. there is a low conductivity layer capping a higher conductivity layer on the inboard side of the levee, the gradients calculated in a transient seepage analysis will change rapidly during a flood event, and quickly approach values calculated using steady state seepage analyses.

2. If the geologic conditions for a levee indicate that erosion and piping is less likely, i.e. there is not a low conductivity capping layer, gradients respond quickly to a flood event but remain significantly less than the values of hydraulic gradient calculated in steady state seepage analyses for a considerable period of time.

Analysis of Stability

1. It is possible for a levee to become unstable after some time in response to a flood event if effective stress analyses are performed.

Recommendations for Further Research

While performing this research on guidance for transient seepage analyses, it became apparent that there are some aspects of research that could be expanded further to benefit engineering practice.

1. More measurements of in situ soil suction at levee sites before and during flood events would be beneficial. These measurements would allow for better understanding of what pore pressures are within the levee prior to the start of a flood event. These measurements could also be used to verify further numerical analyses of transient seepage. They would also provide guidance for how influencing factors such as climate and vegetation affect pore pressures within levees.

2. It would be beneficial to develop a procedure for a *rapid draw-up* analysis, similar to rapid drawdown analysis. With transient seepage analyses, changes in pore pressures within a levee can be calculated in response to a flood. It is still unclear if these pore pressures should be used for an effective stress analysis of levee stability, or if stability at the early stages of floods loading should be analyzed using undrained strengths and total stress methods.

References

Agrawal, G., and Altschaeffl, A. G. (1991). "Effect of water-content variability in design of clay embankments." *Journal of Geotechnical Engineering*, 117(4), 673-683.

Aiban, S. A., Znidarcic, D. (1989). "Evaluation of the flow pump and constant head techniques for permeability measurements." *Geotechnique*, 39(4), 655-665.

Arya, L. M., and Paris, J. F. (1981). "A physicoempirical model to predict the soil moisture characterisitc from particle-size distribution and bulk density data." *Soil Science Society of America Journal*, 45, 1023-1030.

Benson, C. H., and Gribb, M. M. (1997). "Measuring unsaturated hydraulic conductivity in the laboratory and field." *Geotechnical Special Publication 68*, 113-168.

Bicalho, K. V., Znidarcic, D., Ko, H.Y. (2005)."An experimental evaluation of unsaturated hydraulic conductivity functions for a quasi-saturated compacted soil." *Proceedings of International Symposium on Advanced Experimental Unsaturated Soil Mechanics*, Balkema, 325-329.

Bjerrum, L., Huder, J. (1957)."Measurement of the permeability of compacted clays." *Proceedings of the fourth international conference on soil mechanics and foundation engineering*, London, 6-8.

Bulut, R., Lytton, R. L., and Wray, W. K. (2001)."Soil Suction Measurements by Filter Paper." ASCE Geotechnical Special Publication 115, Houston, Texas, USA, p. 14.

Chin, K.-B., Leong, E.-C., and Rahardjo, H. (2010). "A simplified method to estimate the soil-water characteristic curve." *Canadian Geotechnical Journal*, 47, 1382-1400.

Conca, J. L., and Wright, J. V. (1992). "The UFA method for rapid, direct measuremetns of unsaturated transport properties in soil, sediment, and rock." *Australian Journal of Soil Research*, 36, 291-315.

Cosby, B. J., Hornberger, G. M., Clapp, R. B., and Ginn, T. R. (1984). "A Statistical Exploration of the Relationships of Soil Moisture Characteristics to the Physical Properties of Soils." *Water Resour. Res.*, 20(6), 682-690.

Curtis, J. O. (2005). "Electromagnetic Power Attenuation in Soils," Engineer Research and Development Center, Vicksburg, MS, p. 50.

De Jong, R., Campbell, C. A., and Nicholaichuk, W. (1983). "Water Retention Equations and their Relationship to Soil Orgainic Matter and Particle Size Distribuion for Disturbed Samples." *Canadian Journal of Soil Science*, 63(2), 291-302.

Dirksen, C. (2001). "Unsaturated Hydraulic Conductivity." *Soil and Environmental Analysis*, K. A. Smith, Mullins, C.E., ed., Marcel Dekker, Inc.

Fredlund, D. G. (2000). "The 1999 R.M. Hardy Lecture: The Implementation of Unsaturated Soil Mechanics in Geotechnical Egnineering." *Canadian Geotechnical Journal*, 37(5), 963-986.

Fredlund, D. G. (2002)."Use of soil-water characteristic curves in the implementation of unsaturated soil mechanics." *3rd International Conference on Unsaturated Soil Mechanics*, Recife, Brazil, 887-902.

Fredlund, D. G. (2006). "Unsaturated soil mechanics in engineering practice." *Journal of Geotechnical and Geoenvironmental Engineering*, 132(3), 286-321.

Fredlund, D. G., and Houston, S. L. (2009). "Protocol for the assessment of unsaturated soil properties in geotechnical engineering practice." *Canadian Geotechnical Journal*, 46(6), 694-707.

Fredlund, D. G., and Rahardjo, H. (1993). *Soil Mechanics for Unsaturated Soils*, Wiley Inter-Science.

Fredlund, D. G., and Wong, D. K. (1989). "Calibration of Thermal Conductivity Sensors for Measuring Soil Suction." *ASTM Geotechnical Testing Journal*, 12(3), 188-194.

Fredlund, D. G., and Xing, A. (1994). "Equations for the soil-water characteristic curve." *Canadian Geotechnical Journal*, 31(4), 521-532.

Fredlund, D. G., Xing, A., and Huang, S. (1994). "Predicting the permeability function for unsaturated soils using the soil-water characteristic curve." *Canadian Geotechnical Journal*, 31(4), 533-546.

Fredlund, M. D. (1998). "Unsaturated Seepage Modeling Made Easy." *Geotechnical News* (June), 52-59.

Fredlund, M. D., Fredlund, D.G., Wilson, G.W. (1997)."Prediction of the Soil-Water Characteristic Curve from Grain-Size Distribution and Volume-Mass Properties." *3rd Brazilian Symposium on Unsaturated Soils*, Rio de Janeiro, Brazil.

Fredlund, M. D., G.W.; Fredlund, D.G. (1998b)."Estimation of Hydraulic Properties of An Unsaturated Soil Using a Knowledge-Based System." *Proceedings of the Second International Conference on Unsaturated Soils*, Beijing, China.

Garnder, W. (1958). "Mathematics of isothermal water conduction in unsaturated soils." *Highway Research Board Special Report No. 40*, 78-87.

Gasmo, J. M., Rahardjo, H., and Leong, E. C. (2000). "Infiltration effects on stability of a residual soil slope." *Computers and Geotechnics*, 26(2), 145-165.

Gitirana Jr, N., and Fredlund, D. G. (2004). "Soil-water characteristic curve equation with independent properties." *Journal of Geotechnical and Geoenvironmental Engineering*, 130(2), 209-212.

Graham, J., Oswell, J. M., and Gray, M. N. (1992). "The effective stress concept in saturated active clays." *Canadian Geotechnical Journal*, 29, 1033-1043.

Gupta, C. S., Larson, W.E. (1979). "Estimating Soil Water Retention Characteristics from Particle Size Distribution, Organic Matter Percent, and Bulk Density." *Water Resources Management*, 15(6).

Gvirtzman, H., Shalev, E., Dahan, O., and Hatzor, Y. H. (2008). "Large-scale infiltration experiments into unsaturated stratified loess sediments: Monitoring and modeling." *Journal of Hydrology*, 349, 214-229.

Hillel, D. (1971). *Soil and Water*, Academic Press.

Hotes, F. L., Kruse, E. G., Christopher, J. N., Niaz, S., and Robinson, A. R. (1985)."Irrigation Canal Seepage and Its Measurement: State of the Art Review." New York, NY, USA, 93-105.

Houston, W. N., Dye, H. B., Zapata, C. E., Perera, Y. Y., and Harraz, A. (2006)."Determination of SWCC using one point suction measurement and standard curves." *4th International Conference on Unsaturated Soils, April 2, 2006 - April 5, 2006*, Carefree, AZ, United States, 1482-1493.

Hughes, P. N., Glendinning, S., Mendes, J., Parkin, G., Toll, D. G., Gallipoli, D., and Miller, P. (2009). "Full-scale testing to assess climate effects on embankments."

Engineering Sustainability : Proceedings of the Institution of Civil Engineers., 162(2), 67-79.

Johari, A. H., Ghahramani, A. (2006). "Prediction of Soil-Water Characteristic Curve Using Genetic Programming." *Journal of Geotechnical and Geoenvironmental Engineering*, 132(5), 661-665.

Karthikeyan, M., Tan, T. S., and Phoon, K. K. (2001). "Numerical oscillation in seepage analysis of unsaturated soils." *Canadian Geotechnical Journal*, 38(3), 639-651.

Kim, J., Jeong, S., Park, S., and Sharma, J. (2004). "Influence of rainfall-induced wetting on the stability of slopes in weathered soils." *Engineering Geology*, 75, 251-262.

Klute, A. (1972). "The determination of they hydraulic conductivity and diffusivity of unsaturated soils." *Soil Science*, 113(4), 264-276.

Klute, A., Dirksen, C. (1986). "Hydraulic conductivity and diffusivity: laboratory methods." *Methods of Soil Analysis*, A. Klute, ed., Soil Science Society of America.

Kunze, R. J., Graham, K. (1968). "Factors important in the calculation of hydraulic conductivity." *Proceedings of the Soil Science Society of America*, 32, 760-765.

Leij, F. J., Alves, W. J., and Van Genuchten, M. T. (1996). "The UNSODA Unsaturated Soil Hydraulic Database." United State Soil Salinity Laboratory, ed.

Leong, E. C., and Rahardjo, H. (1997a). "Permeability functions for unsaturated soils." *Journal of Geotechnical and Geoenvironmental Engineering*, 123(12), 1118-1126.

Leong, E. C., and Rahardjo, H. (1997b). "Review of soil-water characteristic curve equations." *Journal of Geotechnical and Geoenvironmental Engineering*, 123(12), 1106-1117.

Likos, W. J., Wayllace, A., Lu, N. (2005)."Numerical modeling of constant flow method for measuring unsaturated hydrologic properties." *Proceedings of international symposium on advanced experimental unsaturated soil mechancis*, Balkema, 291-297.

Lins, Y., Schanz, T., and Fredlund, D. G. (2009). "Modified Pressure Plate Apparatus and Column Testing Device for Measuring SWCC of Sand." *Geotechnical Testing Journal*, 32(5), 15.

Lu, N., and Likos, W. J. (2004). *Unsaturated Soil Mechanics*, John Wiley & Sons.

Lu, N., Wayllace, A., Carrera, J., and Likos, W. J. (2004). "Constant flow method for concurrently measuring soil-water characteristic curve and hydraulic conductivity function." *Geotechnical Testing Journal*, 29(3), 12.

Malusis, M. A., Shackelford, C. D., and Olsen, H. W. (2003). "Flow and transport through clay membrane barriers." *Engineering Geology*, 70, 235-248.

Masrouri, F., Bicalho, K. V., and Kawai, K. (2009). "Laboratory Hydraulic Testing in Unsaturated Soils." Laboratory and Field Testing of Unsaturated Soils, 79-92.

McCartney, J. S., and Zorenberg, J. G. (2005)."The centrifuge permeameter for unsaturated soils." *Proceedings of international symposium on advanced experimental unsaturated soil mechanics*, Blakema, 299-304.

Millington, R. J., and Quirk, J. P. (1959). "Permeability of Porous Media." *Nature*, 183, 387-388.

Mualem, Y. (1976). "A new model for predicting the hydraulic conductivity of unsaturated porous media." *Water Resources Research*, 12(3), 513-522.

Mualem, Y. (1986). "Hydraulic conductivity of unsaturated soils: Prediction and formulas." *Methods of Soil Analysis Part I. Physical and Mineralogical Methods*, A. Klute, ed., American Society of Agronomy, Madison.

Nemes, A., Schaap, M. G., Leij, F. J., and Wösten, J. H. M. (2001). "Description of the unsaturated soil hydraulic database UNSODA version 2.0." *Journal of Hydrology*, 251(3-4), 151-162.

Ng, C. W. W., Springman, S. M., and Alonso, E. E. (2008). "Monitoring the performance of unsaturated soil slopes." *Geotechnical and Geological Engineering*, 26, 799-816.

Ng, C. W. W., Zhan, L. T., Bao, C. G., Fredlund, D. G., and Gong, B. W. (2003). "Performance of an unsaturated expansive soil slope subjected to artificial rainfall infiltration." *Geotechnique*, 53, 143-157.

Nimmo, J., Akstin, K., and Mello, K. (1992). "Improved apparatus for measuring hydraulic conductivity at low water content." *Soil Science Society of America Journal*, 56, 1758-1761.

Nimmo, J., Rubin, J., and Hammermeister, D. (1987). "Unsaturated flow in a centrifugal field: measurement of hydraulic conductivity and testing of Darcy's Law." *Water Resources Research*, 23(1), 124-134.

Olsen, H. W., Nichols, R.W., Rice, T.L. (1985). "Low gradient permeability methods in a triaxial system." *Geotechnique*, 35(2), 145-157.

Pachepsky, Y. A., Timlin, D., and Varallyay, G. (1996). "Artificial Neural Networks to Estimate Soil Water Retention from Easily Measurable Data." *Soil Sci. Soc. Am. J.*, 60(3), 727-733.

Perera, Y. Y., Zapata, C. E., Houston, W. N., and Houston, S. L. (2005)."Prediction of the soil-water characteristic curve based on grain-size-distribution and index properties." ASCE Geotechnical Special Publication 130, Reston, VA , 49-60.

Pham, H. Q., and Fredlund, D. G. (2008). "Equations for the entire soil-water characteristic curve of a volume change soil." *Canadian Geotechnical Journal*, 45(4), 443-453.

Pham, H. Q., Fredlund, D. G., and Barbour, S. L. (2005). "A study of hysteresis models for soil-water characteristic curves." *Canadian Geotechnical Journal*, 42(6), 1548-1568.

Phoon, K. K., and Cheng, Y. (2008)."Some numerical considerations in unsaturated slope stability analysis due to rainfall infiltration." *Geotechnial Engineering for Disaster Mitigation and Rehabilitation*, 216-223.

Preko, K., Scheuermann, A., and Wilhelm, H. (2009). "Comparison of invasive and non-invasive electromagnetic methods in soil water content estimation of a dike model." *Journal of Geophysics and Engineering*, 6, 146-161.

Rao, S. M., and Shivananda, P. (2002). "Role of osmotic suction in swelling of salt amended clays." *Canadian Geotechnical Journal*, 42, 1-9.

Rawls, W. J., Brakensiek, D. L., and Saxton, K. E. (1982). "Estimation of Soil Water Properties." *Transactions of the ASAE*, 25(5), 1316-1320.

Rinaldi, M., and Casagli, N. (1999). "Stability of streambanks formed in partially saturated soils and effects of negative pore water pressures: the Sieve River (Italy)." *Geomorphology*, 26(4), 253-277.

Rinaldi, M., Casagli, N., Dapporto, S., and Gargini, A. (2004). "Monitoring and modelling of pore water pressure changes and riverbank stability during flow events." *Earth Surface Processes and Landforms*, 29(2), 237-254.

Rojas, E., and Rojas, F. (2006)."A probabilistic model for the soil-water characteristic curve." ASCE Geotechnial Special Publication 147, Reston, VA, 2453-2464.

Saxton, K. E., Rauls, W.J., Romberger, J.S., and Papendick, R.I. (1986). "Estimating Generalized Soil-Water Characteristics from Texture." *Soil Science Society of America Journal*, 50(4), 1031-1036.

Schaap, M. G., and Leij, F. J. (1998). "Using neural networks to predict soil water retention and soil hydraulic conductivity." *Soil and Tillage Research*, 47(1-2), 37-42.

Schaap, M. G., Leij, F. J., and Van Genuchten, M. T. (2001). "Rosetta: a computer program for estimating soil hydraulic parameters with hierarchical pedotransfer functions." *Journal of Hydrology*, 251(3-4), 163-176.

Sillers, W. S., and Fredlund, D. G. (2001). "Statistical assessment of soil-water characteristic curve models for geotechnical engineering." *Canadian Geotechnical Journal*, 38(6), 1297-1313.

Sillers, W. S., Fredlund, D. G., and Zakerzaheh, N. (2001). "Mathematical attributes of some soil-water characteristic curve models." *Geotechnical and Geological Engineering*, 19(3-4), 243-283.

Springman, S. M., Jommi, C., and Teysseire, P. (2003). "Instabilities on moraine slopes induced by loss of suction: A case history." *Geotechnique*, 53, 3-10.

Tami, D., Rahardjo, H., Leong, E.-C., and Fredlund, D. G. (2004). "Design and laboratory verification of a physical model of sloping capillary barrier." *Canadian Geotechnical Journal*, 41, 814-830.

Tan, T.-S., Phoon, K.-K., and Chong, P.-C. (2004). "Numerical study of finite element method based solutions for propagation of wetting fronts in unsaturated soil." *Journal of Geotechnical and Geoenvironmental Engineering*, 130(3), 254-263.

Terzaghi, K., Peck, R. B., and Mesri, G. (1996). *Soil Mechanics in Engineering Practice*, John Wiley.

Thomas, H. R., and Zhou, Z. (1997). "Minimum time-step size for diffusion problem in FEM analysis." *International Journal for Numerical Methods in Engineering*, 40, 3865-3880.

Tindall, J. A., and Kunkel, J. R. (1999). *Unsaturated Zone Hydrology*, Prentice Hall, New Jersey.

Toll, D. G., Lourenco, S. D. N., Mendes, J., Gallipoli, D., Evans, F. D., Augarde, C. E., Cui, Y. J., Tang, A. M., Rojas, J. C., Pagano, L., Mancuso, C., Zingariello, C., and Tarantino, A. (2011). "Soil suction monitoring for landslides and slopes." *Quarterly Journal of Engineering Geology and Hydrogeology*, 44(Compendex), 23-33.

Tomasella, J., and Hodnett, M. G. (1998). "Estimating Soil Water Retention Characteristics from Limited Data in Brazilian Amazonia." *Soil Science*, 163(3), 190-202.

Trandafir, A. C., Sidle, R. C., Gomi, T., and Kamai, T. (2008). "Monitored and simulated variations in matric suction during rainfall in a residual soil slope." *Environmental Geology*, 55, 951-961.

Tsaparas, I., Rahardjo, H., Toll, D. G., and Leong, E.-C. (2003). "Infiltration characteristics of two instrumented residual soil slopes." *Canadian Geotechnical Journal*, 40, 1012-1032.

Tu, X. B., Kwong, A. K. L., Dai, F. C., Tham, L. G., and Min, H. (2009). "Field monitoring of rainfall infiltration in a loess slope and analysis of failure mechanism of rainfall-induced landslides." *Engineering Geology*, 105(1-2), 134-150.

Tyler, S. W., Wheatcraft, S.W. (1989). "Application of Fractal Mathematics to Soil-Water Retention Estimation." *Soil Science Society of America Journal*, 53(4), 987-996.

Van Genuchten, M. T. (1980). "A Closed-form Equation for Predicting the Hydraulic Conductivity of Unsaturated Soils." *Soil Science Society of America Journal*, 44, 892-898.

Van Genuchten, M. T., Leij, F. J., and Yates, S. R. (1991). "The RETC code for quantifying the hydraulic functions of unsaturated soils." United States Department of Agriculture, ed.

Vanapalli, S. K., and Catana, M. C. (2005)."Estimation of the soil-water characteristic curve of coarse-grained soils using one point measurement and simple properties." *Proceedings of the International Symposium on Advanced Experimental Unsaturated Soil Mechanics*, Trento, Italy, 401-407.

Williams, J. P., Williams, W.T.; Hignett, C.T. (1983). "The influence of texture, structure and clay mineralogy on the soil moisture characteristic." *Australian Journal of Soil Research*, 21, 15-32.

Worsching, H., Becher, R., Schlaeger, S., Bieberstein, A., and Kudella, P. (2006)."Spatial-TDR moisture measurement in a large scale levee model made of loamy soil material." *Proceedings TDR 2006*, Purdue University, West Lafayette, IN, 1-15.

Yang, H., Rahardjo, H., Leong, E.-C., and Fredlund, D. G. (2004). "Factors affecting drying and wetting soil-water characteristic curves of sandy soils." *Canadian Geotechnical Journal*, 41(5), 908-920.

Zapata, C. E. (1999). "Uncertainty in soil-water-characteristic curve and impacts on unsaturated shear strength predictions," Arizonia State Univerisity, Tempe.

Zapata, C. E., Houston, W. N., Houston, S. L., and Walsh, K. D. (2000)."Soil-Water Characteristic Curve Variability." ASCE Geotechnical Special Publication 99, Denver, CO, 84-124.

Appendix A

Figure 3-3   Used with permission

Yang, H., Rahardjo, H., Leong, E.-C., and Fredlund, D. G. (2004). "Factors affecting drying and wetting soil-water characteristic curves of sandy soils." *Canadian Geotechnical Journal*, 41(5), 908-920. Permission attached.

Figure 3-4   Used with permission

Sillers, W. S., and Fredlund, D. G. (2001). "Statistical assessment of soil-water characteristic curve models for geotechnical engineering." *Canadian Geotechnical Journal*, 38(6), 1297-1313. Permission attached.

Figure 3-5   Used with permission

Ng, C., and Pang, Y. (2000). "Experimental Investigations of the Soil-Water Characteristic Curve." *Canadian Geotechnical Journal*, 37(6), 1252-1264. Permission attached.

Figure 3-6   Used with permission

Ng, C., and Pang, Y. (2000). "Experimental Investigations of the Soil-Water Characteristic Curve." *Canadian Geotechnical Journal*, 37(6), 1252-1264. Permission attached.

Figure 3-7   Used with permission

Fredlund, D. G. (2000). "The 1999 R.M. Hardy Lecture: The Implementation of Unsaturated Soil Mechanics in Geotechnical Egnineering." *Canadian Geotechnical Journal*, 37(5), 963-986. Permission attached.

Figure 3-8   Used with permission

Ng, C., and Pang, Y. (2000). "Experimental Investigations of the Soil-Water Characteristic Curve." *Canadian Geotechnical Journal*, 37(6), 1252-1264. Permission attached.

Table 3-2   Used with permission

Fredlund, D. G. (2006). "Unsaturated soil mechanics in engineering practice." *Journal of Geotechnical and Geoenvironmental Engineering*, 132(3), 286-321. Permission attached.

Figure 3-9   Used with permission

Lu, N., and Likos, W. J. (2004). *Unsaturated Soil Mechanics*, John Wiley & Sons. Permission attached.

Figure 3-10   Used with permission

Fredlund, D. G., and Rahardjo, H. (1993). *Soil Mechanics for Unsaturated Soils*, Wiley Inter-Science. Permission attached.

Figure 3-10   Used with permission

Fredlund, D. G., and Rahardjo, H. (1993). *Soil Mechanics for Unsaturated Soils*, Wiley Inter-Science. Permission attached.

Figure 4-3   Used with permission

Tan, T.-S., Phoon, K.-K., and Chong, P.-C. (2004). "Numerical study of finite element method based solutions for propagation of wetting fronts in unsaturated soil." *Journal of Geotechnical and Geoenvironmental Engineering*, 130(3), 254-263. Permission attached.

Figure 6-1   Used with permission

Fredlund, D. G. (2006). "Unsaturated soil mechanics in engineering practice." *Journal of Geotechnical and Geoenvironmental Engineering*, 132(3), 286-321. Permission attached.

Table 6-1   Used with permission

Lins, Y., Schanz, T., and Fredlund, D. G. (2009). "Modified Pressure Plate Apparatus and Column Testing Device for Measuring SWCC of Sand." *Geotechnical Testing Journal*, 32(5), 15. Permission attached.

Figure 6-4   Fair Use

McQueen, I. S., and Miller, R. F. (1974). "Approximating Soil Moisture Characteristics From Limited Data: Empirical Evidence and Tentative Model." *Water Resources Research.*, *10*(3), 521–527. Fair use determination attached.

Table 6-2   Fair Use

Gupta, C. S., Larson, W.E. (1979). "Estimating Soil Water Retention Characteristics from Particle Size Distribution, Organic Matter Percent, and Bulk Density." *Water Resources Management*, 15(6). Fair use determination attached.

Table 6-3   Fair Use

Rawls, W. J., Brakensiek, D. L., and Saxton, K. E. (1982). "Estimation of Soil Water Properties." *Transactions of the ASAE*, 25(5), 1316-1320. Fair use determination attached.

Figure 6-5   Fair Use

De Jong, R., Campbell, C. A., and Nicholaichuk, W. (1983). "Water Retention Equations and their Relationship to Soil Orgainic Matter and Particle Size Distributuion for Disturbed Samples." *Canadian Journal of Soil Science*, 63(2), 291-302. Fair use determination attached.

Figure 6-6   Used with permission

Chin, K.-B., Leong, E.-C., and Rahardjo, H. (2010). "A simplified method to estimate the soil-water characteristic curve." *Canadian Geotechnical Journal*, 47, 1382-1400. Permission attached.

Table 6-4   Fair Use

Tomasella, J., and Hodnett, M. G. (1998). "Estimating Soil Water Retention Characteristics from Limited Data in Brazilian Amazonia." *Soil Science*, 163(3), 190-202. Fair use determination attached.

Figure 6-7   Fair Use

Schaap, M. G., and Leij, F. J. (1998). "Using neural networks to predict soil water retention and soil hydraulic conductivity." *Soil and Tillage Research*, 47(1-2), 37-42. Fair use determination attached.

Table 6-5   Used with permission

Masrouri, F., Bicalho, K. V., and Kawai, K. (2009). "Laboratory Hydraulic Testing in Unsaturated Soils." Laboratory and Field Testing of Unsaturated Soils, 79-92. Permission attached.

Figure 6-8   Used with permission

Benson, C. H., and Gribb, M. M. (1997). "Measuring unsaturated hydraulic conductivity in the laboratory and field." *Geotechnical Special Publication 68*, 113-168. Permission attached.

Figure 6-9   Used with permission

Nimmo, J., Rubin, J., and Hammermeister, D. (1987). "Unsaturated flow in a centrifugal field: measurement of hydraulic conductivity and testing of Darcy's Law." *Water Resources Research*, 23(1), 124-134. Permission attached.

Figure 6-10   Used with permission

Lu, N., and Likos, W. J. (2004). *Unsaturated Soil Mechanics*, John Wiley & Sons. Permission attached.

Figure 6-11   Fair Use

Zapata, C. E., Houston, W. N., Houston, S. L., and Walsh, K. D. (2000)."Soil-Water Characteristic Curve Variability." ASCE Geotechnical Special Publication 99, Denver, CO, 84-124. Fair use determination attached.

Figure 7-1   Used with permission

Fredlund, D. G., and Wong, D. K. (1989). "Calibration of Thermal Conductivity Sensors for Measuring Soil Suction." *ASTM Geotechnical Testing Journal*, 12(3), 188-194. Permission attached.

Figure 7-2   Fair Use

Curtis, J. O. (2005). "Electromagnetic Power Attenuation in Soils," Engineer Research and Development Center, Vicksburg, MS, p. 50. Fair use determination attached.

Table 7-1   Used with permission

Terzaghi, K., Peck, R. B., and Mesri, G. (1996). *Soil Mechanics in Engineering Practice*, John Wiley. Permission attached.

Figure 8-2   Used with permission

Rinaldi, M., Casagli, N., Dapporto, S., and Gargini, A. (2004). "Monitoring and modelling
of pore water pressure changes and riverbank stability during flow events." *Earth
Surface Processes and Landforms*, 29(2), 237-254. Permission attached.

Figure 8-3   Fair Use

Ng, C. W. W., Zhan, L. T., Bao, C. G., Fredlund, D. G., and Gong, B. W. (2003).
"Performance of an unsaturated expansive soil slope subjected to artificial rainfall
infiltration." *Geotechnique*, 53, 143-157. Fair use determination attached.

Figure 8-4   Used with permission

Tu, X. B., Kwong, A. K. L., Dai, F. C., Tham, L. G., and Min, H. (2009). "Field monitoring
of rainfall infiltration in a loess slope and analysis of failure mechanism of rainfall-
induced landslides." *Engineering Geology*, 105(1-2), 134-150. Permission
attached.

Figure 8-5   Used with permission

Li, A. G. T., L.G.; Yue, Z.G.; Lee, C.F.; Law, K.T. (2005). "Comparison of Field and
Laboratory Soil-Water Characteristic Curves." *Journal of Geotechnical and
Geoenvironmental Engineering*, 131(9), 1176-1180. Permission attached.

Figure 8-6   Fair Use

Gofar, N., Lee, L. M., and Kassim, A. (2008). "Response of suction distribution to
rainfall infiltration in soil slope." *Electronic Journal of Geotechnical Engineering*,
13 E. Fair use determination attached.